Evaluation of the geomechanical behavior of fiber-reinforced clay soil

by

Akhila Palat

A thesis submitted in partial fulfillment of the requirements for the degree of

Doctor of Philosophy

In

Geotechnical Engineering

Department of Civil and Environmental Engineering
University of Alberta

Abstract

Adding short discrete fibers is recommended as one potential option for the stabilization of mine fine tailings. Discrete fiber-reinforced composites are also applicable for land reclamation projects including oil sands mine reclamation, landfill liners or final covers and enhancing the strength of subgrades.

This thesis presents a comprehensive study on the role of discrete polymeric fibers in altering the geomechanical behavior of clay soil. The clay soil used in this study is kaolinite clay and polypropylene and nylon fibers are used as reinforcements. The scope of this thesis is to: (1) quantify the influence of changing fiber variables on the undrained geomechanical behavior of the clay soil; (2) determine the role of field placement techniques on the stress-strain behavior and pore pressure response of the fiber-reinforced clay; (3) analyse the fiber-soil interface shear strength; and (4) quantify the amount of tensile stresses mobilized in the fibers when subjected to undrained loading.

The first component of this research included a series of laboratory investigations performed on the fiber-reinforced clay soil to define the response of this composite to undrained loading. The role of different fiber variables (content and length) in influencing the undrained shear strength and pore pressure response of the clay soil was examined. An optimum fiber combination that results in the maximum strength of the composite was proposed based on the lab testing results.

The second stage of this research explored the role of different sample preparation techniques (compaction and hydraulic placement as a slurry) on the undrained stress-strain behavior of fiber-reinforced clay soil. A novel transparent fiber-reinforced clay soil was prepared to analyze the

orientation of fibers within the compacted and slurry samples. Examination of transparent fiber-reinforced clays confirmed the predominant fiber orientation is horizontal in slurry samples and random in samples prepared using the compaction method.

The third component of this thesis investigated the impact of changing fiber types on the geomechanical behavior of the fiber-reinforced clay soil. The fiber-soil interface shear strength was determined using a modified direct shear apparatus. The role of the interface friction angle and mobilized fiber tension in influencing the shear strength of the soil-fiber composite was analysed for samples prepared using the compaction and slurry method.

There exists an important gap in the understanding of fiber-reinforced clays, as no studies were able to quantify the amount of tensile stresses mobilized in the fibers during shearing. The fourth component of this thesis demonstrated the mobilization of tensile stresses within the fibers by performing triaxial extension tests on fiber-reinforced clay composites. The effect of changing fiber variables on the shear strength of the composite was analysed. An empirical model was developed to predict the amount of tensile stresses mobilized in the fibers when the composite is subjected to undrained loading; specifically, how tension in fibers are incorporated into strength and manifest in the mechanism of failure.

The results from this research are anticipated to increase the understanding on the use of discrete fibers for the stabilization of mine fine tailings. This study also comprehends the undrained anisotropic behavior and strength of fibrous organic soils and soils reinforced with elements that act in tension and is expected to have a significant impact on the construction of infrastructure, as implementing this technique of fiber-reinforcement is an option for enhancing the strength of clay soil that is prevalent in Canada.

Preface

This thesis is an original work by Akhila Palat under the supervision of Dr. Michael T Hendry. This is a manuscript-style Ph.D. thesis, with Chapters 3, 4, 5, and 6 intended for publication as peer-reviewed journal articles. Due to the format of the thesis, there are some repetitions among the different manuscripts, and between the manuscripts and other chapters. The conference papers including the work from this thesis are included in the 'References' section of this thesis.

At the time of the publication of this thesis the status of the manuscripts are as follows:

"The effect of polymer fibers on the pore pressure response and undrained shear strength of clay soil" (*Chapter 3*, Manuscript #1). *To be submitted.*

"The effect of sample preparation method on the undrained behavior of fiber-reinforced clay" (*Chapter 4*, Manuscript #2). *To be submitted.*

"Quantification of the effect of fibre polymer type on the undrained behavior and realizable strength of fiber-reinforced clay" (*Chapter 5,* Manuscript #3). *To be submitted.*

"Quantification of undrained behaviour and strength of fiber reinforced clays in extension" (*Chapter 6,* Manuscript #4). *To be submitted.*

All work presented in this thesis has been carried out by Akhila Palat. As supervisor, Dr. Michael T Hendry has reviewed all parts of the work.

To the Almighty

Acknowledgements

I am thankful to all the people who have guided and supported me throughout my Ph.D. journey. First of all, I express my immense gratitude to my advisor Dr. Michael Hendry, for giving me a chance to work in such an interesting field and believing in me during the research work. I also thank him for his excellent guidance and all time valuable support and encouragement. This research would not have been possible without the funding received from Natural Sciences and Engineering Research Council Discovery Grant (#RGPIN-2020-04419) as well as the numerous scholarships provided by the University of Alberta. I also take this opportunity to thank MiniFIBERS. Inc.for supplying fibers for all my laboratory testing.

I would like to extend my gratitude to my supervisory committee Dr. Nicholas Beier and Dr. Lijun Deng for their invaluable technical insight and constant encouragement during my thesis work. I would also like to extent my sincere thanks to Mr. Lucas Duerksen for supporting me throughout my lab works and helping me in completing my experiments on time. Special thanks to my mentors Dr. Ahlam Abdulnabi and Dr. Nathan Deisman for their continuous encouragement throughout my journey.

I am also thankful to my University of Alberta friends for the warmth of their friendship and supportive environment, which has made my journey wonderful. I acknowledge some of my close friends Jen, Vivian, Hasmik, Parisa, Mahya, and Jorge for their role as tension healers and as rich sources of entertainment.

Last but not the least, a big credit of my journey goes to my family for believing in me– my husband Nikhil for motivating me to restart my career as a Ph.D researcher, my daughter Vaidehi, my parents Achuthan Kutty and Sudha for being my backbone, and my in-laws Vijayakumar and Sudha for their constant prayers and support.

Table of Contents

Appendix A: Results from triaxial testing of unreinforced and fiber-reinforced clay soil

Appendix B: Results from direct shear testing of unreinforced and fiber-reinforced clay soil

Appendix C: Additional images from laboratory testing

Appendix D: Visual examination of the fiber-reinforced clay soil

List of Tables

List of Figures

Chapter Seven

Chapter One: Introduction

Current soil behavior models have been developed based on our understanding of particle interactions; much of it is conceptually based on sand and modified to describe the behavior of clayey soils. There are other classes of fibrous and fiber-amended soils, which are not represented well under the current understanding of soil behavior.

Reinforcing the soil by adding short, discrete fibers is one of the potential methods for improving the properties of existing soil. Randomly fiber-reinforced soil has shown an isotropic increase in the shear strength of soil mass without introducing any planes of weakness (Li, 2005). After mixing with the soil, these randomly oriented fibers behave like tension resisting elements and partially withstand the shear stress developed within the soil (Mirzababei et al., 2017). The sudden brittle failure observed in unreinforced clays is transformed to a slow ductile mode of failure by the introduction of fibers (Palat et al., 2019). However, despite its proven record, long history, affordability and ease of construction, this technology has been underutilized (Hatami et al., 2018).

Most of the existing studies are performed on fiber-reinforced sands and a few have been carried out on fiber-reinforced clay soil. This is mainly due to the difficulty in sample preparation and quantifying the pore pressure response and interface shear strength between soil and fibers. Additionally, the models used to describe the mechanical behavior of a soil, more specifically the critical state family of models, assume isotropic elasticity. However, according to Quigley (1980), most postglacial clays are deposited vertically. They are subjected to equal horizontal stress, but the properties do vary from top to bottom and are referred to as transversely isotropic or cross-anisotropic. Studies have been performed in the past to determine the existence of anisotropy in a clay soil but no studies have been attempted until date to evaluate the cross-anisotropic behavior of fiber- reinforced clay soils.

The potential applications of this fiber-reinforced soil composite would be in the stabilization of mine fine tailings, repair of failed slopes, land reclamation projects, and landfill liners or final covers. Other applications include reinforcing the subgrades of roads and highways and increasing the stability of highway embankments. Gregory (2006) discussed the case histories of two large fiber-reinforced soil projects illustrating the potential of using discrete fibers in repairing the failed slopes. These included the President George Bush Turnpike (PGBT) project in Dallas, Texas, United States, and the Lake Ridge parkway slope repair project in the city of Grand Prairie, Texas, United States.

Figure 1.1 shows the photograph of the fiber-reinforced soil construction on the PGBT project and Figure 1.2 shows the fiber-reinforced soil embankment construction in the Lake ridge parkway slope repair project. The slope stability analysis performed as a part of this investigation illustrated that the use of discrete fibers significantly increased the factor of safety of the slope. The construction of PGBT project was completed in late 2004 and the construction of the slope repairs with fiber-reinforced soil for the Lake Ridge parkway was completed in September 2005. According to Gregory (2006), both slopes performed to the expectation, and a number of years are required to evaluate the long-term performance of these slopes.

Figure 1.1: Mixing of fiber-reinforced soil on PGBT project (Gregory, 2006)

Figure 1.2: Fiber-reinforced soil embankment construction – Lake ridge parkway (Gregory, 2006)

The current research program is initiated to evaluate the impact of randomly oriented short, discrete fibers in altering the undrained behavior of fine-grained soils. Kaolinite clay is selected for this study due to their strong interlayer bonding, that do not allow water to break into the pore space between the layers (Salgado, 2011). An extensive laboratory testing is performed to understand the undrained strength, pore pressure response and stiffness of the fiber-reinforced clays and quantify the impact of these tensile elements in contributing to the overall shear strength of the composite. The long-term results are anticipated to be a widely applicable and increased understanding on the addition of discrete polymeric fibers for the stabilization of mine fine tailings, a comprehension of the undrained anisotropic behavior and strength of fibrous and fiber-reinforced soils, and the effect of this behavior on the performance of infrastructure constructed upon these materials.

1.1 Problem Statement

Existing studies on fiber-reinforced soils demonstrated an increase in strength with the addition of fibers. It is hypothesized that these discrete fibers improve the shear strength of the soil by the mobilization of tensile stresses (Michalowski and Cermak 2002, 2003; Li, 2005). However, none of the previous studies on fiber-reinforced soils were able to demonstrate this mobilization of fiber tension during shearing due to the limitations of the traditional triaxial compression testing program. Additionally, the factors influencing the mobilized fiber tension are still unknown and no methodology has been proposed to date to quantify the fiber tension during shearing.

Even though a few studies have been performed to evaluate the response of a compacted fiber-reinforced specimen, very limited data is available on the impact of fibers in influencing the geomechanical behavior of slurry-prepared fine soil. Researchers consider adding discrete fibers as a potential option for improving the mechanical properties of mine fine tailings (Festugato et al. 2013; Festugato et al. 2015; Yi et al. 2015; Consoli et al. 2017; Zheng et al. 2019). Additionally, the technique of fiber reinforcement is also being examined for hydraulic fill during land reclamation. This signifies the necessity to analyze the role of fibers in altering the undrained shear strength and pore water pressure of slurry-prepared fine soil.

Adding fibers to the clay introduces anisotropy. Previous studies on fiber-reinforced sands (Michalowski and Zhao, 1996; Michalowski and Cermak, 2002, 2003) and fibrous peat soils (Yamaguchi et al., 1985; Hendry et al., 2012, 2014) demonstrate that the effect of fibers is maximum when fibers are oriented in the direction of extension. Even though several techniques have been proposed to determine the fiber orientation within the sand, no studies have been done so far to analyze the distribution of fibers within the clay soil and determine the influence of fiber orientation on the shear strength and pore water pressure of the composite.

Although studies have evaluated the behavior of fiber-reinforced clays as a matrix, less attention has been devoted to characterizing the interface parameters between soil and fibers. The amount of tensile stress mobilized in the fibers during shearing is a function of the interface friction angle between fibers and clay and it is important to determine the soil-fiber interface shear strength parameters prior to the application of this composite in the field.

The study proposed in this thesis is the development of a more complete quantification of pore pressure generation, strength and stiffness properties of fiber-reinforced clay soils through laboratory testing. This research evaluated the application of hypotheses made from recent work regarding the anisotropic properties of fibrous peat, which combines the effect of cross-anisotropic stiffness, fiber tension, frictional strength, and principal stress orientation to fiber-reinforced clays. The tensile stresses generated within the fibers were quantified and an empirical model was developed to demonstrate how tension in fibers are incorporated into strength and manifest in the mechanism of failure. This study also explored the potential options to visualize and track the orientation and distribution of fibers within the fiber-reinforced clays.

1.2 Research Objectives

The global objective of this study is to analyse the role of short, discrete, synthetic fibers in altering the geomechanical behavior of a clay soil and evaluate the undrained pore pressure response, shear strength and stiffness properties of this soil-fiber composite through extensive laboratory testing.

The specific research objectives are to:

1. Analyze the role of method of sample preparations (compaction and slurry) in influencing the behavior of fiber-reinforced clay soil.
2. Evaluate the undrained elastic anisotropic response of fiber-reinforced clay soil using the mathematical techniques proposed for describing the anisotropy in a natural clay by Graham and Houlsby (1983) from the results of a series of triaxial tests.
3. Determine the orientation of fibers within the clays and evaluate how that changes with method of preparation/placement.
4. Quantify the distribution of fiber orientation within the clays and the change in orientation during consolidation and compaction.
5. Quantify the fiber-soil interface shear strength.
6. Quantify the tensile stresses generated within the fiber-reinforced clays, analyse how tension in fibers are incorporated into strength, and manifest in the mechanism of failure.

1.3 Scope of Work

One type of clay soil (kaolinite) and two types of polymer fibers, polypropylene (PP) and nylon (PA) are used in this study for preparing the fiber-reinforced composites. Kaolinite clay (EPK Kaolin, Edgar minerals) was used owing to their low activity value resulting in reduced swelling potential. Synthetic fibers (provided by MiniFIBERS Inc., Johnson City, TN, USA) were selected because their properties are controllable and pre-cut fibers can be easily procured from the manufacturer. Consolidated undrained (CU) triaxial tests (compression and extension) were performed to evaluate the role of fibers in influencing the undrained shear strength, induced pore water pressure, yield strength and undrained stiffness of the clay soil. Modified drained direct shear tests evaluated the interface strength properties between the fibers and clay soil. The other variables evaluated in the laboratory-testing program were fiber content, fiber length, fiber alignment, effective confining pressures, and loading path. The study also proposed an optimum fiber combination that results in the maximum strength of the fiber-reinforced clay soil.

Field implementation of this composite is possible either by placing in lifts and compacting (Gregory, 2006) or hydraulically in the form of a fiber-soil slurry. This study explored the two potential options for preparing a fiber-reinforced clay soil namely; (1) compacting the soil and fibers to its optimum moisture content and maximum dry density; and (2) placing hydraulically as a slurry followed by incremental loading. Triaxial samples of fiber-reinforced clay were prepared using both techniques and the impact of sample preparation methods in influencing the undrained shear strength, stiffness, and pore water pressure of the composite was analysed. The laboratory testing results were further evaluated to demonstrate the existence of anisotropy within these fiber-reinforced clay specimens prepared using the compaction and slurry technique.

The mode of failure (bulging response with no distinct shear plane) observed in fiber-reinforced clays during shearing is expected due to the movement of fibers to the potential planes of weakness and distribution of stresses to the surrounding soil mass by means of interface friction. However, these judgements regarding the orientation and movement of fibers within the clay soil is arbitrary and several ambiguities exists about these predictions. Through this research, the feasibly of non-destructive scanning techniques in determining the fiber distribution was analysed and a novel transparent fiber-reinforced soil-surrogate is developed to visualise the distribution of fibers and track their movement during consolidation and compaction.

1.4 Thesis outline

This thesis is prepared in a manuscript-based format and consists of seven chapters including this first introductory chapter and one appendix.

Chapter Two includes a summary of the literature review for all topics discussed in this thesis.

Chapter Three (Manuscript #1) presents the laboratory testing of fiber-reinforced clay soil to evaluate the impact of fibers in altering the geomechanical behavior of a clay soil. The influence of fiber variables such as fiber contents and lengths on the undrained shear strength, induced pore water pressure response, stiffness and yield strength are quantified.

Chapter Four (Manuscript #2) discusses the influence of method of sample preparation on the cross-anisotropic stiffness, induced pore water pressure, mobilized fiber tension, and overall shear strength of the fiber-reinforced composites. A novel transparent fiber-reinforced soil is developed to detect the orientation and movement of fibers within the clay soil.

Chapter Five (Manuscript #3) investigates the impact of changing fiber polymer types in influencing the undrained behavior and strength of fiber-reinforced clay soil. The interface shear strength between the fibers and clay soil is determined by performing a modified direct shear-testing program.

The limitation on the use of CU triaxial compression tests in measuring the impacts of tensile elements within a soil is discussed from *Chapter Three* to *Chapter Five*.

Chapter Six (Manuscript #4) demonstrates the generation of tensile stresses within the fibers by performing a series of triaxial extension tests on the soil-fiber composite. The influence of variables such as loading path, fiber lengths, and fiber alignment on the undrained shear strength, induced pore water pressure and mobilized fiber tension is analyzed. An empirical model is developed to quantify the tensile stresses mobilized in the fibers when subjected to undrained loading and incorporate the contribution of fiber tension into the overall shear strength of the composite.

Chapters Seven provides a summary of the conclusions derived from this research program and recommendations for further research.

Appendix A and *Appendix B* include the data from all triaxial and direct shear tests performed as a part of this research and presented in Chapters 3, 4, 5, and 6. Additional pictures from laboratory testing are presented in *Appendix C*. *Appendix D* includes results from the visual examination of fiber-reinforced soil that are not so successful and hence not included in the dissertation.

Chapter Two: Literature Review

This chapter provides background information and a review of the literature published on topics related to this project. The literature review is divided into six parts:

- Previous studies on fiber-reinforced soils;
- Shear strength of fiber-reinforced soils and fibrous peat;
- A review of the anisotropic soil model developed for a natural clay soil;
- Evaluation of yielding in clay soil;
- Analysis of the interface shear strength; and
- Visualisation techniques in geotechnical engineering.

2.1 Previous studies on fiber-reinforced soil

Several authors have evaluated the potential benefits of adding fibers to reinforce coarse-grained and fine-grained soils (Maher and Woods, 1990; Gray and Ohashi, 1983; Maher and Ho, 1994; Zornberg, 2002; Zornberg and Li, 2003; Li, 2005). Inclusion of randomly distributed fibers increases the shear strength and ductility of the soil. Fibers work in the similar way as planar reinforcements, but have some advantages compared to the fibres that are at a specific alignment or location. The randomly oriented fibers generate isotropic improvement in the strength of a soil and avoid the chance of possible planes of weakness (Maher and Gray, 1990). Maher and Ho (1994) investigated the mechanical properties of kaolinite (Georgia kaolin) fibre-reinforced clay soil and determined that the inclusion of fibers increased the peak compressive strength, ductility, splitting tensile strength, and flexural toughness of kaolinite clay. It was also demonstrated that the fibers increases the peak shear strength and reduces the post-peak reduction in shear strength (Fig. 2.1). This reduction in the post-peak drop was less pronounced for samples with high water contents (wet of optimum) due to the lubricating effect of water resulting in a lower amount of load transfer between the fibers and clay particles. The increase in the peak shear strength is often quantified in terms of an equivalent cohesion and friction angle of the fibre-reinforced soil obtained after testing (Li, 2005). Consolidated undrained (CU) and consolidated drained (CD) triaxial tests showed that the axial deformation of the unreinforced specimen resulted in the development of a failure plane, while the reinforced specimens tended to bulge, indicating an increase in the ductility of the fiber-soil mixture (Freilich and Zornberg, 2010). Nataraj and McManis (1997) showed that the addition of fibers to clay and sand specimens resulted in increased values of the peak friction angle and cohesion. Additionally, these fibers increased the compressive strength and California bearing ratio (CBR) values of the existing soil.

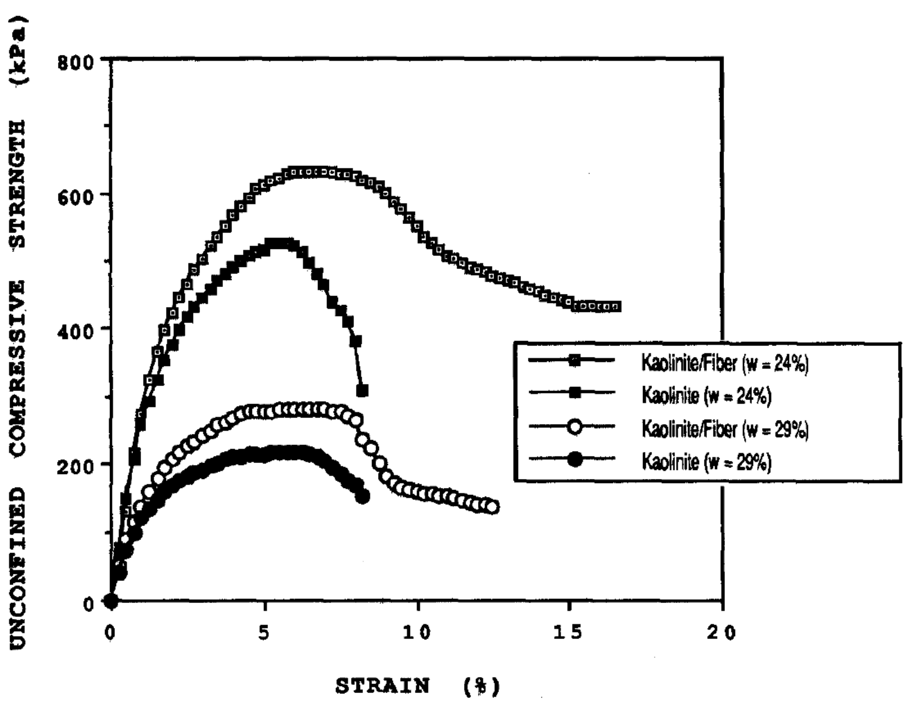

Figure 2.1: Effect of polypropylene fibers in increasing the peak shear strength and reducing the post peak reduction in the shear strength of kaolinite clay at different water contents (Maher and Ho, 1994)

Standard Proctor tests performed on unreinforced and fiber-reinforced samples showed that the addition of fibers do not have any significant effect in the optimum moisture content (OMC) or maximum dry density (MDD) of the soil samples. Fletcher and Humphries (1991) performed compaction tests on silty clay soil specimens reinforced with fibers. They showed that increasing fiber content results in a slight increase in the maximum density and decrease in the optimum water content. Other researchers (Nataraj and McManis, 1997; Al Wahab and Al-Qurna, 1995) also reported similar results.

Zornberg et al., (2004) performed large-scale triaxial tests to characterize the mechanical behavior of tire shred- sand soil composites. The optimum dosage and aspect ratio of tire shreds for mixing with the granular fills were evaluated from these large-scale triaxial tests. The shear strength of the tire shred – sand soil increased with an increase in the tire shred content, up to a maximum of 35%, and then decreased beyond this value. These results suggested the difference in the soil-reinforcement mechanisms that takes place with increase in the tire shred content. Initially tensile forces develop within the tire shreds, leading to increased overall shear strength of the mixture. At higher tire shred contents, shear among the individual tire shreds begin to govern the shear strength of the mixture leading to a reduction in the overall shear strength values. The axial strain at failure for tire shred –sand specimens were higher than unreinforced sand specimens prepared at the same relative density. For the range of aspects ratios used in their study, the shear strength of the tire shred –sand composite increased with an increase in the aspect ratio. The observed increase in the shear strength suggested that, increasing aspect ratio increased the pullout resistance of individual tire shreds, which in turn led to increased tensile forces within the tire shreds ultimately increasing the shear strength of the composite. It was also mentioned that the increase in shear strength with increasing aspect ratio would reach a ceiling for large aspect ratio values due to mixing difficulties. Accordingly, a schematic representation was defined to predict the composite shear strength of the tire shred – sand composites. The composite shear strength involves the contribution of two mechanisms: (*i*) internal shear mechanisms developed among individual tire shreds and sand grains, and (*ii*) reinforcement mechanisms due to tensile forces induced within the tire shreds (Fig. 2.2).

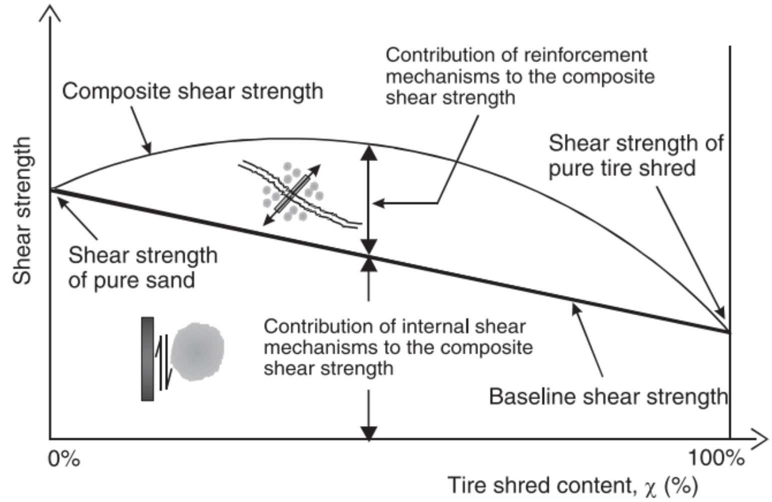

Figure 2.2: Schematic representation of the effect of tire shred content on the shear strength of tire shred – sand mixtures (Zornberg et al., 2004)

Li (2005) performed triaxial compression and triaxial extension tests to evaluate the effect of soil type, soil density and fiber orientation on the shear strength of the composite. A total of 7 soils were used in the experimental testing program, including 2 uniform sands (SP), 2 high-plasticity clays and 3 low-plasticity clays. The shear strength anisotropy introduced with regards to the preferential orientation of the fiber was evaluated in this research. The triaxial testing results were validated with the discrete framework proposed by Zornberg (2002) for the design of fiber-reinforced soil structure. Anagnostopoulos et al., (2013) conducted a series of direct shear tests on fine soil samples with different percentages of fiber and determined that the shear strength of the soil increased up to the optimum dosage of fibers, beyond which it decreased or remained constant. Mirzababei et al., (2017) performed a series of CU triaxial tests on two types of carpet waste fiber-reinforced clay soil. Inclusion of carpet fibers improved the stress strain behavior of the clay soil and this phenomenon was more evident with an increase in fiber content. The author also developed two nonlinear regression models to predict the effective stress ratio and deviator stress of fiber-reinforced clay with limited knowledge of soil properties and less number of testing.

The role of fibers in contributing to the strength of a soil depends on its orientation with respect to the principal axes of deformation of the composite (Diambra et al., 2007). Fibers are in general most influential when oriented in the same direction as tensile strain, whereas the fibers under compression do not contribute any increase to the strength of the composite. Assuming the fiber distribution is anisotropic in the field (due to the compaction energy supplied during the placement), the use of isotropic models will lead to inaccurate predictions of the strength gain attributed to fibers (Michalowski and Cermak, 2002). A few studies were performed to investigate the architecture and orientation of randomly distributed discrete fibers within sand (Michalowski and Zhao, 1996; Michalowski and Cermak, 2002; Michalowski and Cermak, 2003; Diambra et al., 2007; Ibrahim et al., 2012). Michalowski and Cermak (2002) performed CD triaxial compression tests on sand reinforced with three different orientations of fibers namely: random orientation, all fibers in the horizontal direction and all fibers in the vertical direction. During the shearing phase of a triaxial compression test, the maximum extension occurs in the horizontal plane and the greatest strength was observed for samples reinforced with horizontal fibers. For specimens with randomly oriented fibers, one portion of the fibers was subjected to compression and the other portion subjected to extension. Consequently, the overall contribution of fibers to the strength is less than the horizontal fibers with the same concentration. Sample reinforced with vertical fibers had an adverse effect on the stiffness and provided no improvement in the strength. A fiber orientation distribution function ($\rho(\theta)$) was developed as a modelling tool to explain the anisotropic constitutive features of the reinforced sand samples when loaded. This fiber distribution function was then extended to calculate the total volume of fibers intersecting a finite area on a plane cut through the sample (Diambra et al., 2007). The total volume of fibers divided by the volume of a single fiber indicated the number of fibers present in the plane. Freezing and simultaneously cutting the fiber-reinforced sand samples prepared in the lab validated the above method. The average number of fibres were visually counted from an area, compared with the number of horizontal and vertical fibers determined from the analytical solution and a reasonable match was observed. The results indicated that the orientation distribution deviated far from isotropic, with 97% of the fibers oriented at an angle within $\pm\frac{\pi}{4}$ with the horizontal. Since rotation of principal axes of stresses and strains occurs in practise under most types of loading (Arthur et al., 1980), the anisotropic nature of fiber orientation induced by the laboratory and in-situ fabrication processes cannot be ignored (Ibrahim et al., 2012). Extending the above study to samples of fiber-reinforced sand prepared by two different preparation techniques (moist tamping (MT) and moist vibration (MV)) showed that a greater portion of the fibers were oriented near the horizontal plane for MT technique compared to the MV technique. The results from triaxial compression and extension tests performed on these samples demonstrated a marked anisotropic behavior, which supported the anisotropic distribution of fiber orientation, determined using the experimental/analytical procedure developed by Diambra et al., (2007). However, this method of counting the number of number of fibers intersecting a plane is not applicable for smaller diameter fibrillated fibers. Additionally, difficulty arose in counting at higher values of fiber contents (>0.25%) due to the accumulation of fibers in groups (Diambra et al., 2007).

The tensile strength of the soil is assumed merely zero when compared to the compressive strength and shear strength. A desiccation crack appears when the induced tensile stress approaches the soil tensile strength or when the volumetric shrinkage is constrained. (Corte and Higashi, 1960). Researchers proved that the presence of randomly distributed fibers increases the tensile strength of soil (Tang et al., 2007; Ziegler et al., 1998; Consoli et al., 2011). The presence of cracks reduces the mechanical and hydraulic properties of the clay soil and is vital when used in landfill liners, clay slopes, dams, and in the design of geosystems. The presence of cracks also increase the hydraulic conductivity of the soil thereby increasing the chances of failure. Cracks in landfill liners leads to the infiltration of water and generation of waste leachate, which subsequently results in ground and water contamination (Miller et al., 1998). Tang et al., (2007, 2010, and 2012) performed several studies to evaluate the effect of fiber inclusion on the desiccation cracking behavior of fiber-reinforced clay soil. Tang et al., (2012) proved that the addition of polypropylene fibers to the soil matrix improves the bonding strength and restricts the relative movement of the matrix. These discrete fibers act like a three-dimensional mesh to interlock the soil particles and eliminate the stress concentrations during drying. As a result, the fibers will be able to bear some tensile stress and the crack initiation during drying could be decreased. An image processing technique was adopted to analyse the geometrical and morphological characteristics of cracks in unreinforced and fiber-reinforced specimens. Results indicated that fiber addition is an effective option to reduce the amount of desiccation cracks and improve the crack resistance of soil. The increase in bonding strength and friction between fibers and soil particles can subsequently restrict the relative movement of fibers within the soil. As a result, the fibers are capable of withstanding tensile stress and the crack initiation was eliminated. The cracks formed in unreinforced soil samples were wide while relatively narrow cracks were formed in fiber-reinforced specimen. The fibers bear tensile stresses until it gets pulled out from the matrix, thereby increasing the stability of a structure by eliminating a sudden or brittle failure.

2.2 Shear strength of fiber-reinforced soils and fibrous peat

Previous studies on fiber-reinforced soils (Consoli et al., 2007; Palat et al., 2019; Palat and Hendry, 2021) and fibrous peat (Hendry, 2011; Hendry et al., 2012; Hendry et al., 2014) indicated that the specimens exhibited a strain hardening behaviour following an initial elastic response without a clear peak shear stress to define strength. This section of the thesis summarizes the works done in the past to determine the equivalent shear strength of fiber-reinforced soils and fibrous peat samples.

Zornberg (2002) proposed a discrete framework for the limit equilibrium analysis of fiber-reinforced soil by the independent characterization of soils and fibers. The fibers were considered as discrete elements that contribute to the stability by mobilizing tensile stresses along the shear plane. According to this framework, the fiber-induced distributed tension was assumed to act along the failure surface so that the discrete fiber induced tensile contribution could be directly added to the shear strength contribution of the soil (Fig.2.3).

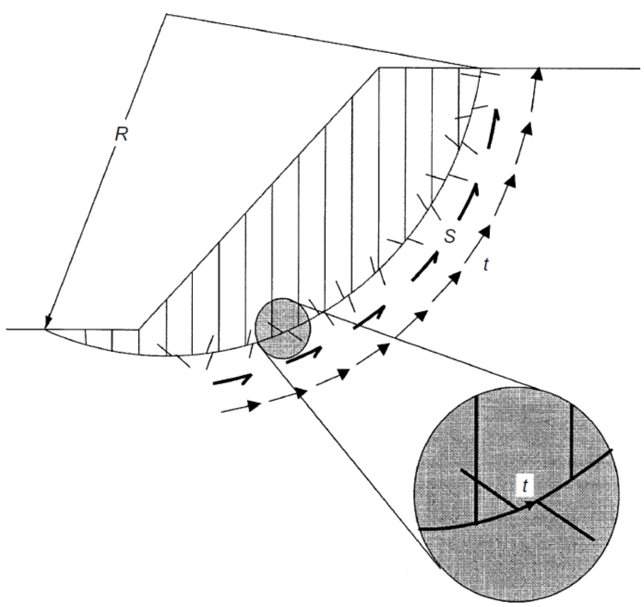

Figure 2.3: Schematic failure surface showing fibre-induced distributed tension parallel to failure plane (Zornberg, 2002)

A critical normal stress ($\sigma_{n,crit}$) was defined as a function of fiber geometry, ultimate tensile strength of the fibers, shear strength of the soil, and interaction coefficients between fibers and soil. If the average normal stress acting on the fibers ($\sigma_{n,ave}$) is less than $\sigma_{n,crit}$, the failure of fiber-reinforced soil is governed by fiber pullout. The fiber pullout is a function of the interface shear strength between fibers and clay, fiber content and the aspect ratio of individual fibers. In these cases, the equivalent shear strength (S_{eq}) of fiber-reinforced composite is the sum of the shear strength of the soil (S) and fiber induced tension where the failure is governed by fiber pullout (t_p). If $\sigma_{n,ave} > \sigma_{n,crit}$, the failure of fiber-reinforced samples are governed by the tensile breakage of fibers which is a function of the ultimate tensile strength of individual fibers. The S_{eq} of fiber-reinforced composite will be the sum of S and fiber induced tension where the failure is governed by tensile breakage (t_t). Accordingly, a bilinear envelope was defined using this discrete framework to represent the S_{eq} of fiber-reinforced composite (Fig.2.4).

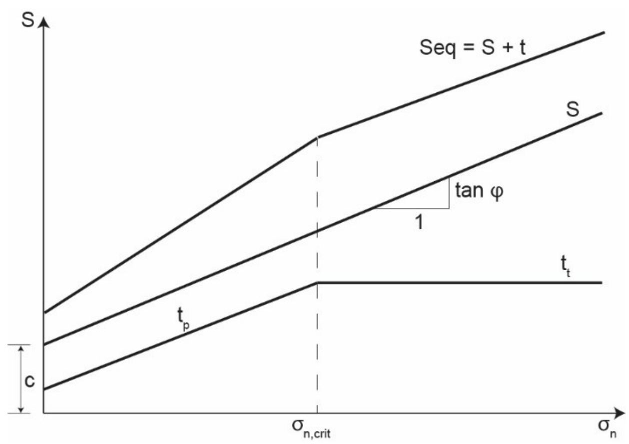

Figure 2.4: Representation of the equivalent shear strength according to the discrete approach (based on Zornberg, 2002)

Consoli et al., (2007) performed CD triaxial tests to evaluate the shear strength behavior of unreinforced and fiber reinforced sand. The fiber-reinforced sand specimen's were experiencing strain hardening until the maximum strain that the apparatus could reach. However, the shear strength envelope for fiber-reinforced sand specimens were taken at 20% shear strain ($\varepsilon_s = \varepsilon_a - \frac{\varepsilon_v}{3}$) where ε_a is the axial strain and ε_v is the volumetric strain. It was shown that the failure envelope of the fiber-reinforced sand tested was independent of the stress path for triaxial compression tests. A bilinear envelope was defined to predict the shear strength behavior of fiber-reinforced sands. Accordingly, the failure of fiber-reinforced sands at lower values of confining pressure could be due to the slippage and yielding of fibers while fiber stretching governed the failure of the composite at higher-pressure part. Consoli et al., (2007) also mentioned that all tests on fiber-reinforced sands experienced strain hardening until the maximum strain the apparatus could reach, and 20% shear strain was picked as a criteria for defining strength as they believed a value of 'strength' has to be defined for this composite at a particular strain.

The fundamental mechanics of fibrous and fiber reinforced soils have shown many similarities to the fibrous peat specimens. The stiffness and strength of peat has shown to be strongly related to the reinforcing effect of the fibres within the peat. Hendry (2011) and Hendry et al., (2012, 2014) undertook a series of investigations in to the fundamental properties that define the response of peat to undrained loading. Following the initial elastic behavior, all samples of fibrous peat showed a gradual transition from a linear elastic to linear strain hardening stress-strain response. The specimens showed no signs of approaching failure and the tests were stopped because of excessive axial compression of the specimen. Hendry et al., (2012) performed CU triaxial compression tests and direct shear tests on remoulded peat and peat fiber specimens to evaluate the shear strength of fibre-reinforced soil. A conceptual model was defined to represent the frictional strength deviator stress (q_{fs}) of fibrous peat using an idealized stress-strain behavior of peat specimens (Fig. 2.5). It was hypothesized in the model that the transition to linear strain hardening response in the stress strain curve is indicative of the shear strength associated with frictional interactions and the linear increase in q during strain hardening is the result of additional shear resistance due to fiber tension. The linear portion of the strain hardening response was then extrapolated to zero axial strain and the q intercept obtained represented the frictional deviatoric yield stress (q_{fs}) associated only with interface friction. A horizontal line through q_{fs} marked the transition from the interface frictional strength to interface frictional strength plus fiber reinforcement.

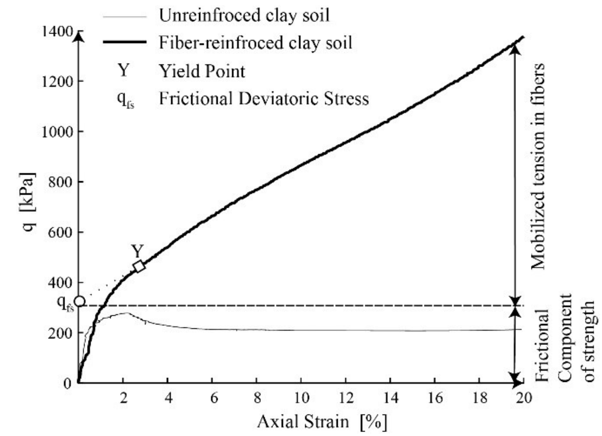

Figure 2.5: Conceptual representation of frictional strength deviatoric stress of fibrous peat (based on Hendry et al., 2012)

Hendry et al., (2014) performed laboratory investigation to evaluate the undrained pore pressure response of peat and compare the fiber-reinforced yield strength between Shelby tube samples of peat from three sites. The yield point in each test was determined based on the hypothesis that the linear strain hardening of peat specimens is solely caused by the tension developed within the fibers and thus the start of linear strain hardening corresponds to the frictional yielding of peat. A single yield line was then plotted by combining the yield points from all sites. The common yield surface demonstrated that the intact peat does not exhibit substantial cohesion. The effective shear strength of fibrous peat was considered as the sum of two components: (1) interface friction between the solid phases of fibers and particles and (2) tension in the fibers that reinforced the peat. The frictional strength is a fundamental property of the surfaces of fibers and particles, whereas the fiber reinforcement component is dependent on the fiber content, fiber aspect ratio and fiber orientation with respect to principal stresses. Based on the conceptual model developed by Hendry et al., (2012), the net effect of peat fiber reinforcement on the strength of foundation soils beneath an embankment was evaluated and was showed that the net effect is dependent on the initial stress state. At lower mean effective stress and higher deviatoric stress, the fibers provide an increased strength caused by fiber reinforcement, whereas at higher mean effective stress and lower deviatoric stress, the net effect of the fibers was detrimental on the shear strength (Hendry et al., 2014).

Yamaguchi et al., (1985) evaluated the undrained shear characteristics of a normally consolidated peat based on the results obtained from undrained triaxial compression and extension tests performed on vertical and horizontal samples of undisturbed peat. The shear strength of fibrous peat was not affected by the magnitude of confining pressure prior to shear or the loading path during shear under undrained compression and extension conditions. The stress- strain plots of peat samples with different orientation of fibers (horizontal (H) and vertical (V)) indicated that the anisotropic behavior of peat specimen remains after isotropic consolidation and is more apparent during the shearing stage. The pore water pressure developed for a V specimen was more than an H specimen as the V specimens takes the form of a fabric with negative dilatancy. The undrained shear strength of fibrous peat specimens were then defined using the deviator stress maximum criteria in accordance with the ASTM standards. However, it was not possible to define the shear strength parameters of H specimens from the extension conditions, as the magnitude of pore water pressure at failure was larger than the axial stress. This behavior was expected due to the contribution of tension in the vegetal fibers to the strength parameters of peat greater than expected with the effect of tension depending on the magnitude of the consolidation pressure.

An investigation into the fundamental mechanics of fibrous and fiber-reinforced soils, with a focus on tensile stresses that occur due to fiber reinforcement, is still missing within the current body of literature. Through this research, the undrained shear strength of unreinforced and fiber-reinforced clay soil is analyzed and the division of strength between the shear strength of the soil matrix and tension within the fibers is quantified. A methodology is developed in *Chapter 6* to quantify the amount of tensile stresses mobilized within the fibers during shearing once the soil and fiber parameters are known.

2.3 A review of the anisotropic soil model developed for a natural clay soil

The purpose of this section is to discuss the mathematical technique proposed by Graham and Houlsby (1983) for describing the pre-yield mechanical properties of natural clay using anisotropic elastic theory and for determining the appropriate material parameters from the triaxial tests data.

The stress strain behavior in a triaxial test is commonly described using the parameters mean effective stress, p' (Eq. 2.1), deviator stress, q (Eq. 2.2), volumetric strain, υ (Eq. 2.3), and shear strain, ε (Eq. 2.4) defined as:

$$p' = \left(\frac{\sigma_{11}' + 2\sigma_{33}'}{3}\right) \tag{2.1}$$

$$q = \sigma_{11}' - \sigma_{33}' \tag{2.2}$$

$$\upsilon = \varepsilon_{11} + 2\,\varepsilon_{33} \tag{2.3}$$

$$\varepsilon = \frac{2\,(\varepsilon_{11} - \varepsilon_{33})}{3} \tag{2.4}$$

where σ_{11}' is the major effective principal stress, σ_{33}' is the minor effective principal stress, ε_{11} is the axial strain and ε_{33} is the lateral strain.

Equation 2.5 represents the stress-strain equation for an isotropic elastic material where the change in υ is represented only as a function of p' and the change in ε is represented solely as a function of q (Wood, 1990). K and G represents the bulk modulus and shear modulus of the material.

$$\begin{bmatrix} \partial p' \\ \partial q \end{bmatrix} = \begin{bmatrix} K & 0 \\ 0 & 3G \end{bmatrix} \begin{bmatrix} \partial \upsilon \\ \partial \mathcal{E} \end{bmatrix} \tag{2.5}$$

Most postglacial clays were deposited vertically and the deformation experienced during and after deposition is one-dimensional (Quigley, 1980). They are subjected to equal horizontal stress and will therefore be expected to have a vertical axis of symmetry. This special form of anisotropy is refereed to as transversely isotropic or cross - anisotropic (Wood, 1990). According to Graham and Houlsby (1983), if a triaxial test is performed on a cross-anisotropic material, the matrix in Eq. 2.5 can be modified as in Eq. 2.6. The parameters $K^*$and G^* have been introduced to emphasize that the material is no longer isotropic. J is the parameter showing the cross dependence of ε on

p' and υ on q. The parameters K^*, G^*, and J are the three parameters required for describing a transversely isotropic (cross-anisotropic) material in a triaxial test.

$$\begin{bmatrix} \partial p' \\ \partial q \end{bmatrix} = \begin{bmatrix} K^* & J \\ J & 3G^* \end{bmatrix} \begin{bmatrix} \partial \upsilon \\ \partial \mathcal{E} \end{bmatrix} \tag{2.6}$$

For an isotropic material, the stiffness matrix can be expressed as in Eq. 2.7 or more conveniently as in Eq. 2.8.

$$\begin{bmatrix} \partial\, \sigma'_{11} \\ \partial \sigma'_{22} \\ \partial \sigma'_{33} \end{bmatrix} = \left[\frac{E}{(1+\upsilon)(1-2\upsilon)}\right] \begin{bmatrix} 1-\upsilon & \upsilon & \upsilon \\ \upsilon & 1-\upsilon & \upsilon \\ \upsilon & \upsilon & 1-\upsilon \end{bmatrix} \begin{bmatrix} \partial \varepsilon_{11} \\ \partial \varepsilon_{22} \\ \partial \varepsilon_{33} \end{bmatrix} \tag{2.7}$$

$$\begin{bmatrix} \partial\, \sigma'_{11} \\ \partial \sigma'_{22} \\ \partial \sigma'_{33} \end{bmatrix} = \begin{bmatrix} A & B & B \\ B & A & B \\ B & B & A \end{bmatrix} \begin{bmatrix} \partial \varepsilon_{11} \\ \partial \varepsilon_{22} \\ \partial \varepsilon_{33} \end{bmatrix} \tag{2.8}$$

To introduce anisotropy in Eq. 2.8, the stiffness coefficients in the horizontal direction are multiplied by an anisotropy factor α as in Eq. 2.9. A and B are replaced by A^* and B^* to emphasis their change in use. The second and third columns of Eq. 2.9 are multiplied by a factor α to introduce symmetry (Eq. 2.10).

$$\begin{bmatrix} \partial\, \sigma'_{11} \\ \partial \sigma'_{22} \\ \partial \sigma'_{33} \end{bmatrix} = \begin{bmatrix} A^* & B^* & B^* \\ \alpha B^* & \alpha A^* & \alpha B^* \\ \alpha B^* & \alpha B^* & \alpha A^* \end{bmatrix} \begin{bmatrix} \partial \varepsilon_{11} \\ \partial \varepsilon_{22} \\ \partial \varepsilon_{33} \end{bmatrix} \tag{2.9}$$

$$\begin{bmatrix} \partial\, \sigma'_{11} \\ \partial \sigma'_{22} \\ \partial \sigma'_{33} \end{bmatrix} = \begin{bmatrix} A^* & \alpha B^* & \alpha B^* \\ \alpha B^* & \alpha^2 A^* & \alpha^2 B^* \\ \alpha B^* & \alpha^2 B^* & \alpha^2 A^* \end{bmatrix} \begin{bmatrix} \partial \varepsilon_{11} \\ \partial \varepsilon_{22} \\ \partial \varepsilon_{33} \end{bmatrix} \tag{2.10}$$

Solving Eq. 2.6 results in a redundancy with two equations having three unknowns and the principle of least squares (the error in calculated and measured volumetric strain) was adopted to solve these equations. Accordingly, the stiffness coefficients for a transversely isotropic material (K^*, G^* and J) can be related to A^*, B^* and α as in Eq. 2.11 – 2.13.

$$A^* = K^* + \frac{4}{3} G^* + \frac{4}{3} J \tag{2.11}$$

$$B^* = \frac{K^* + \frac{4}{3} G^* + \frac{4}{3} J}{\alpha} \tag{2.12}$$

$$\alpha = \frac{\sqrt{9}\left(K^* - \frac{2}{3} G^* + \frac{1}{J}\right)^2 + 8\,(3\,K^*G^* - J^2) - \left(K^* - \frac{2}{3} G^* + \frac{1}{3} J\right)}{2A^*} \tag{2.13}$$

If the value of α is greater than 1, the material is assumed to be stiffer horizontally. If the value of α is less than 1, the material is stiffer vertically and if α is equal to 1, the material is isotropic.

The modified Poisson's ratio (ϑ^*) and modified modulus of elasticity (E^*) for a cross-anisotropic material is expressed in Eq. 2.14 and Eq. 2.15 respectively.

$$\upsilon^* = \frac{B^*}{(A^* + B^*)} \tag{2.14}$$

$$E^* = \frac{(1 + \upsilon^*)(1 - 2\upsilon^*)}{(1 - \upsilon^*)} A^* \tag{2.15}$$

<u>Implications of anisotropy from triaxial testing</u>

1. For any isotropic consolidation test, the ratio of $\delta\upsilon$ to $\delta\varepsilon_{11}$ is equal to 3. If the soil is anisotropic, this value depends on α and υ^* as expressed in Eq. 2.16.

$$\frac{\delta\upsilon}{\delta\varepsilon_{11}} = \left(\frac{\delta\varepsilon_{11} + \delta\varepsilon_{22} + \delta\varepsilon_{33}}{\delta\varepsilon_{11}}\right) = \frac{(2 + \alpha^2) - 2\upsilon^*(1 + 2\alpha)}{(\alpha^2 - 2\alpha\upsilon^*)} \tag{2.16}$$

2. The stress-strain relationship for a transversely isotropic material is expressed in Eq. 2.6. In an undrained triaxial test, $\partial v = 0$ so that the slope of the effective stress path can be expressed as in Eq. 2.17.

$$\frac{\delta q}{\delta p'} = \frac{3G^*}{J} \tag{2.17}$$

J is the parameter that expresses the cross dependence of $\partial \varepsilon$ on p' and ∂v on q. For an isotropic material, the value of J is zero and the above equation results in an effective stress path with a constant mean effective stress. Any deviation of the stress path from vertical indicates anisotropy in the material.

Graham et al., (1983) used these constitutive relationships to predict the stresses before failure in Winnipeg clay and proved that the anisotropic model using K^*, G^* and J gave better predictions of volume and shear strains in a triaxial test that the simple isotropic model using only G and K.

To date, no studies have been attempted to evaluate the cross-anisotropic behavior of fiber-reinforced soils. Through this research, the mathematical methods proposed by Graham and Houlsby (1983) are employed along with the results from triaxial testing to evaluate the extent of anisotropy exhibited by fiber-reinforced kaolinite clay soil. The role of method of sample preparation in influencing the stiffness anisotropy is also discussed in *Chapter 4*.

2.4 Evaluation of yielding in clay soil

The irrecoverable permanent extensions that remain under zero load are plastic deformations, which defines new reference states from which subsequent elastic response are measured (provided the past maximum load be not exceeded). The departure from stiff elastic response that occurs, as reloading proceeds beyond the past maximum load is called yielding and the past maximum load becomes the current yield point for the soil (Wood, 1990). The concept of yielding had proved useful in understanding soft clay behavior beneath embankments and slopes (Graham et al., 1983)

Studies on yielding of a wide variety of natural clays have shown that substantial linear stress-strain behavior is exhibited at stresses, which do not cause yielding (Baracos et al., 1980; Noonan, 1980; Lew, 1981 and Graham et al., 1983). The yield locus in a triaxial test is a section bounding all elastically attainable states for the soil with one particular history (Wood, 1990). The yield envelope is identified by joining the points at which yielding is identified, inside which the strains, strain rates, and pore water pressure are low and outside which all these parameters are much larger (Baracos et al., 1980).

Graham et al., (1983) showed that if test results are examined using suitable stress-strain parameters, a linear behavior was observed over a significant range of stresses from the reconsolidation stress towards yielding. Stresses that pass beyond the initial yield locus produce larger strains and higher pore water pressures, slower excess pore water dissipation and higher creep rates (Graham and Houlsby, 1983). Previous field loading tests and laboratory studies of natural clay soil indicated that the strains are mainly recoverable within the elastic region (Pappin and Brown, 1980). It is thus reasonable to characterize many lightly over consolidated clays as linearly elastic in that part of the stress space within the yield locus.

Studies performed to identify yielding in a natural clay, considered the yield stresses as the intersection of straight approximations of the initial stiff section and the subsequent more flexible response to applied stresses (Graham et al., 1983). Previous researchers used a variety of stress-strain relationships to examine this bi-linear response, which could be used to distinguish pre-limit-state from post-limit-state behaviour (Noonan, 1980; Lew, 1981 and Graham et al., 1983) such as:

(1) Major effective principal stress (σ_1') versus axial strain (ε_1),
(2) p' versus volumetric strain (υ),
(3) q versus shear strain (ε),
(4) Minor effective principal stress (σ_3') versus radial strain (ε_3) and
(5) Energy absorbed per unit volume (W) versus length of the stress strain vector (LSSV) as sample move towards yielding.

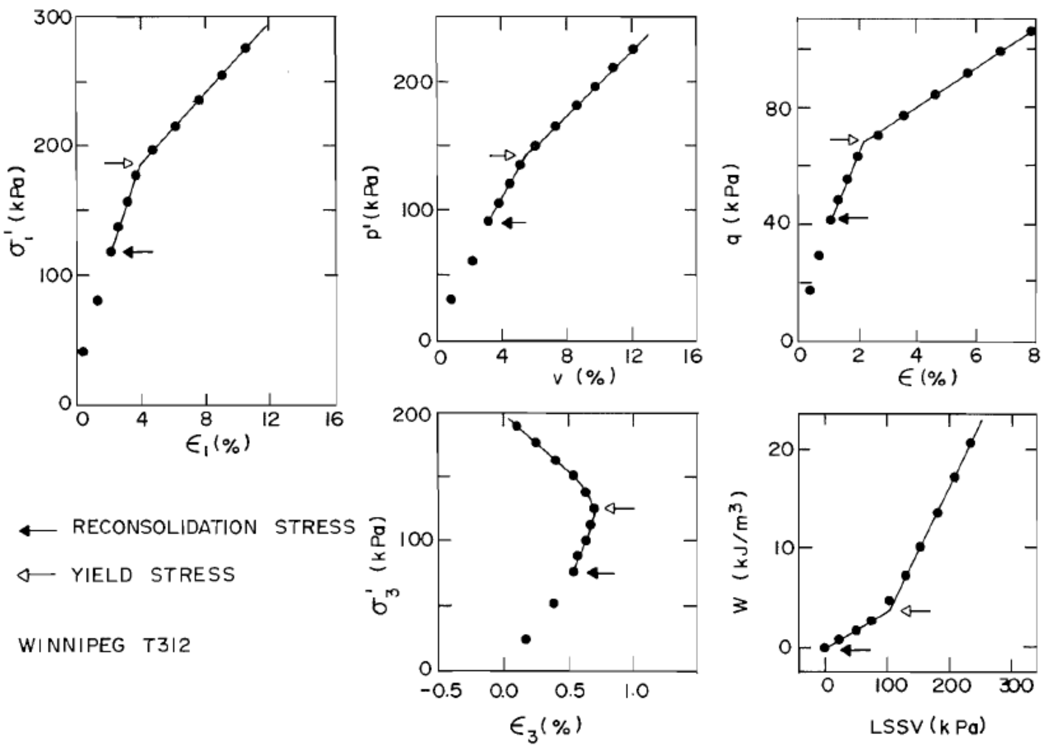

Figure 2.6: Yielding identified from various stress-strain criteria (Graham et al., 1983)

Yield points were identified in all five graphs as shown in Fig. 2.6. The stresses and energies at yield were converted to a common stress variable p' for comparison purposes. A significant level of agreement was observed in all five values of p' and the average values were used for defining the yield envelope of the clay soil. The yield envelopes were observed to increase in size in terms of stresses and decrease in terms of specific volumes as the pre-consolidation pressures increase. Normalizing the yield stresses with the pre-consolidation pressures, the yield envelopes (obtained for different depths in the soil) reduced to a single well-defined envelope and the critical state line became a series of closely spaced points (Graham et al., 1983).

Even though, extensive studies have been directed to the yielding of natural clay soil, the determination of yield stresses in fiber-reinforced clay is still missing within the current body of literature. This study adopts the bilinear technique proposed by Graham et al., (1983) for the identification of yield stresses in fiber-reinforced clays. The role of method of sample preparation and changing fiber polymer types in altering the yield strength of the composite is also analyzed.

2.5 Analysis of the interface shear strength

Understanding the interface shear strength between fibers and clay is critical for comprehending the geomechanical behavior of the fiber-reinforced clay soil. Several authors have attempted to investigate the interface properties between geosynthetics and clay soil, but a very few studies have been directed to the investigation of interface shear strength parameters between fibers and clay. A summary of the studies performed in the past to evaluate the interface strength parameters between geosynthetic and soil and between fibers and soil are included in this section.

2.5.1 Soil – geosynthetic interface shear strength

The two common tests for analysing the interface strength parameters between a soil and geosynthetic are the modified direct shear test and the pullout test. These tests involve placing a geosynthetic between the required soils and moving the assembly at a constant rate of displacement. In the direct shear box, the topsoil layer is moved relative to the clamped geosynthetic, on the other hand, in the pullout test, the geosynthetic be moved relative to the soil. This principle difference in the two test methods mobilize contrasting mechanisms at the soil-geosynthetic interface. In direct shear tests, the primary mechanism is the mobilized interface friction and the goal is to characterize the interface shear strength between soil and geosynthetic. However, in the pullout test, due to movement of the geosynthetic relative to the soil, tensile stresses are developed in the geosynthetics (Gupta, 2014).

Shi and Wang (2013) performed a series of pullout tests to characterize the interface parameters between geogrid and soil. Different reinforcement mechanisms were investigated, analyzed and compared. Studies indicated that the pullout resistance of uniaxial geogrid is mainly due to the geogrid-soil interface friction effect, while that of biaxial geogrid is primarily achieved from geogrid-soil enchasing force. Attempts were also made to modify the conventional direct shear apparatus to perform pullout tests on geosynthetics. Costalonga (1988) introduced modifications in all four features that comprise a direct shear box namely, reaction frame, box, horizontal loading system and vertical loading system. A slot was introduced in the front and back plates to take the geogrid instrumentation out of the box. A horizontal loading system was used to determine the pullout force and to apply the pull out force at a constant rate according to the drainage conditions. The vertical loading system used consisted of prismatic elements forming a pyramid shaped loading head to evenly distribute concentrated loads. Ball bearings were used in between the contact of steel bars to eliminate shear and torsion.

Prashanth et al. (2016) performed pullout tests using a modified direct shear apparatus to measure the interaction parameters between soil and geosynthetic. A conventional direct shear test setup was modified by replacing the test box with a pullout box and providing a horizontal slot on the front face through which the geosynthetic can be taken out. The effect of normal stress values and geosynthetic types on the soil–geosynthetic interaction parameters were discussed. It was also confirmed that the interaction parameters are highly sensitive to the normal stress and the surface roughness nature of geosynthetic materials. Altay et al., (2019) used a special cap to pull the geogrid through the clay soil. The pullout tests results and the direct shear test results were compared and it was found that the interface interaction between clay and geogrid was more resistive than clay-clay.

2.5.2 Soil – fiber interface shear strength

Although considerable research has been devoted to the investigation of fiber-reinforced soil as a matrix, less attention has been directed to characterize the interface parameters between soil and fibers (Ammar et al., 2019). This is mainly because the discrete fibers used for reinforcement are thin and their distribution within the soil is random and complicate (Tang et al., 2010).

Tang et al., (2010) performed single fiber pullout tests to evaluate the interfacial strength properties of polypropylene fiber –reinforced soil. Their results showed that the interfacial mechanical behavior is highly influenced by the normal stress value as well as other factors such as the effective interface contact area, fiber surface roughness, and soil compositions.

Ammar et al., (2019), evaluated the interface response between hemp fibers and natural clay by fixing the clay specimen in the upper part of the shear box and shearing against individual hemp fibers of width 2-3 mm glued onto a steel plate on the lower part of the shear box (Fig. 2.7). These fibers were glued in an orientation in line with the relative displacement between two boxes. To understand the interface behavior between hemp fibers and clay, both drained and undrained direct shear tests were performed in their study. Their studies indicated that only drained interface strength can be reliably measured from a small-scale laboratory direct shear testing due to the partial drainage conditions at the interface. The fibers were efficient in mobilizing the shear strength of clay soil. The drained effective interface resistance between hemp fibers and clay was characterized by an interface friction angle between 22.5 and 23.7º from the direct shear tests.

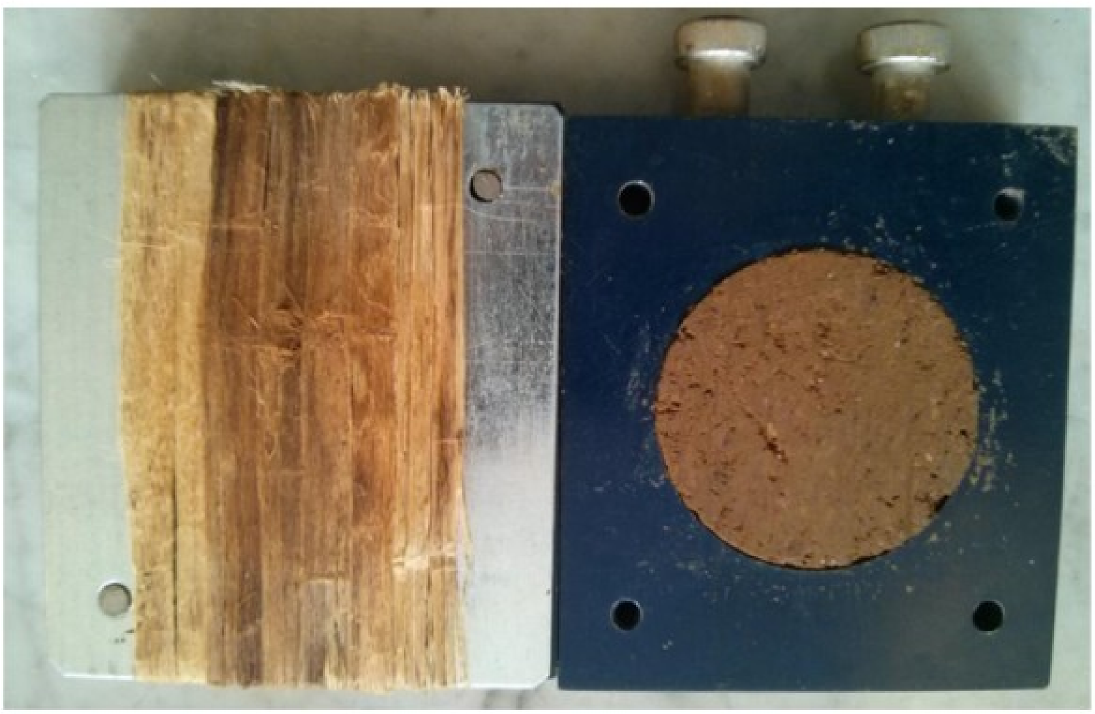

Figure 2.7: Direct shear mold with clay in the upper half and hemp glued to a steel plate on the lower half (Ammar et al., 2019)

As detailed in the literature review, only a few studies have focused on investigating the interface shear strength parameters between fibers and clay soil. However, the amount of tensile stress mobilized in the fibers during shearing is a function of the interface friction angle between fibers and soil (*Chapter Six*, Manuscript #4). This research adopts the modified direct shear testing method to evaluate the interface shear strength between the fibers and clay soil. The impact of the interface friction angle and mobilized fiber tension on the shear strength and pore water pressure of the fiber-reinforced clay soil are also analyzed.

2.6 Visualisation techniques in geotechnical engineering

This section of the thesis discusses the techniques adopted in the past for visualizing the internal structure of the soil.

2.6.1 X-Ray Computed Tomography (CT)

X-Ray Computed Tomography (CT) is a non-destructive and non-invasive technique employed for the three-dimensional examination of soil (Taina et al., 2007). CT imaging has been applied to a variety of geological materials with most of its applications limited to mineral soils and rock, while application to peat and fibrous soil being exceedingly rare (Quinton et al., 2009). Due to the strong contrast of soil pores and associated solids, the discrimination of pores was relatively simple in CT imagery and helped in the quantification of pore networks. Pierret et al., (1999) used X-Ray CT to characterize root network of chestnut and maple trees in sandy soils impregnated with resin. Their results proved that X-ray CT is a valuable tool to obtain an in situ view of the overall morphology of the root network. X-Ray CT images on peat soil helped in the characterization of volumetric content and moisture distribution within the peat samples (Quinton et al., 2009).

The CT technique was extended to develop a three-dimensional description of the fiber architecture in fiber-reinforced sand soils (Soriano et al., 2017). The study used denser fluorocarbon fibers (specific gravity of 1.7 g/cc) to facilitate the detection of fibers from the other phases in the matrix. The fibers appeared in the images as grey colors and were clearly distinguishable from the white grained sand matrix and black pores. A 3D median filter to obtain smoother grey levels first filtered the initial image. An intensity threshold then applied to these images followed by one cycle of morphological erosion to select only the fibers. The final trinarised image was produced by the superposition of the threshold grain phase to the fiber map (Fig. 2.8a). The skeletonization procedure generated the 3D representation of the entire fiber network within the sample (Fig. 2.8b). The test results proved that fiber orientation deviates considerable from being isotropic with majority of the fibers oriented at angle intervals close to the horizontal.

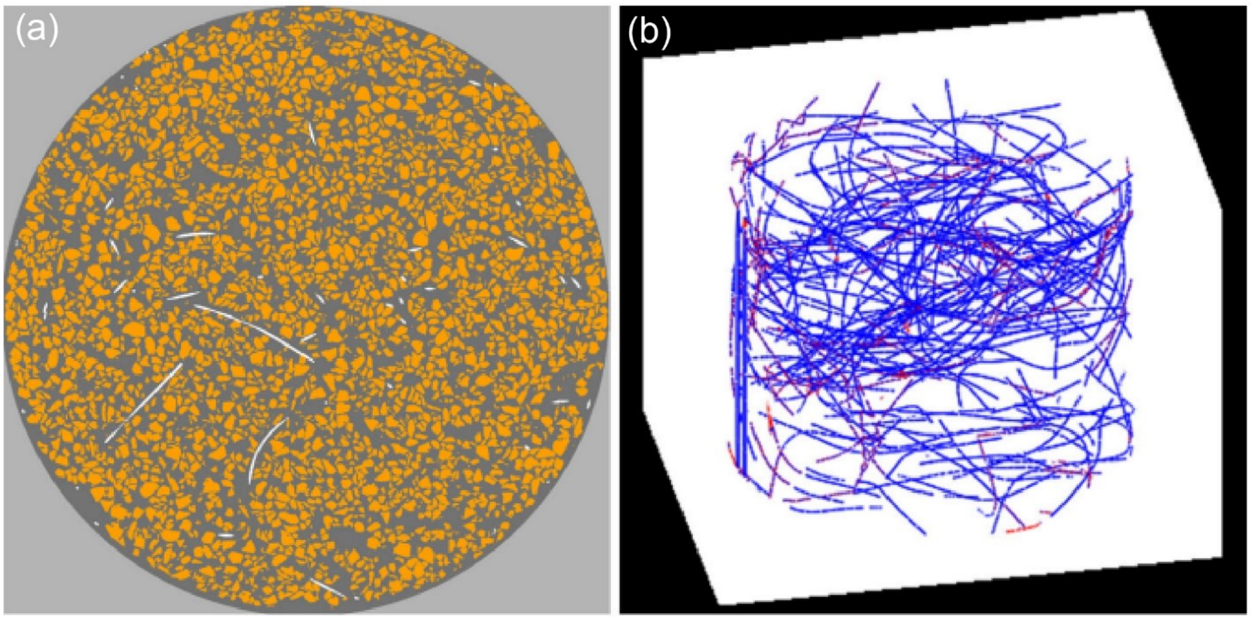

Figure 2.8. Procedure adopted for the 3D representation of fiber network: (a) Final output of the trinarised horizontal image, (b) Skeletonized fiber network within the sample (Soriano et al., 2017)

Nguyen and Indraratna (2019) executed a testing program to evaluate the clogging and discharge capacity of natural fiber drains using micro CT scanning followed by a series of image processing techniques. The variation in the X-ray energy absorption of different materials results in different gray scales such as the more solid the object, the brighter the area will be. The grayscale CT images were initially binarized followed by thresholding to reduce the noise in the image. The objects in the image (pores, fibers and soil fiber drains) were separated and analyzed individually using a logical algorithm. The drains were finally reconstructed in three dimensions based on series of single CT projection images at different angles.

One common problem in the analysis of Computerized Tomography scanned images is the existence of artefacts in the X-Ray CT imagery namely, ring artefacts, beam hardening artefacts, and star artefacts. Ring artefacts are caused by the inhomogeneity of the detector, star artefacts due to the presence of very dense inclusions in the sample and beam hardening artefacts due to preferential absorption of low X-Ray energies during scanning (Taina et al., 2007). In addition to the above-mentioned artefacts, there is also a probability of density discrimination obstruction, signal depreciation, and an increase in the acquisition time to occur while scanning the samples.

2.6.2 Transparent Soil

The refractive index of a transparent material is the ratio of the speed at which a light wave travels through a material compared to the speed of light traveling through a vacuum (Tipler, 1999). When light travels from one medium to another of differing refractive index, one part of the light will be reflected, and the remainder will enter the second medium. The closer the refractive indexes between two mediums, the lesser refraction will occur. When the refractive indexes of both mediums are matched, the reflection will be eliminated, and the two mediums will appear homogeneous as light travels through both mediums without interruption. Transparent soil is prepared when a soil is saturated with a fluid of matched refractive index. Due to the similar refractive index values, the soil/fluid combination appears homogeneous to light and becomes transparent. At degrees of saturation less than 100%, the transparency is diminished as air enters the pore space and becomes visible. (Peters et al., 2011). The clarity of transparent soil depends on the perfect matching of the refractive indices of soil and pore fluid, and the absence of entrapped air and impurities. (Iskander, 2010).

To date, three families of transparent materials have been developed for modelling sand and clay. This includes amorphous silica powder to model the geotechnical properties of natural clays, transparent silica gels to model sand, and aquabeads for representing the flow in soils (Iskander, 2010). Most researchers have adopted amorphous silica powder for the development of transparent clay soil. This is mainly due to the hygroscopic nature of the silica powder, thereby adsorbing pore fluid and displacing air. The large surface area of amorphous silica powder resembles a clay soil (Iskander, 2010). Iskander et al., (2002) developed transparent clays by consolidating suspensions of amorphous silica in a pore fluid with a matching refractive index. Four different silica with different median aggregate size and two different combinations of pore fluids were adopted. A variety of conventional triaxial tests, consolidation, and permeability tests were performed under normally consolidated and over consolidated conditions to evaluate the shear-strength, pore-pressure, volume-change, and permeability characteristics of transparent clays. The results from their experimental testing demonstrated the feasibility of using customized transparent materials to exhibit shear strength, pore pressure, volume change, and permeability characteristics consistent with the behavior of natural clays.

Iskander and Liu (2010) analysed the effect of soil structure interaction in transparent synthetic soils by adopting a system consisting of a laser source and a line-generating lens. A set-up of model footing with a transparent soil model, laser source, sheet generator lens, and a digital camera was developed. The footing was then pushed into the model using a set-up ensuring that loading is axial and a DIC algorithm was developed to obtain the displacement field. The calculated movements were consistent with the classical bearing capacity theory and a wedge failure was clearly visible beneath the footing. Liu and Iskander (2010) presented a technology for measuring spatial deformations within a transparent soil model, with high resolution and non intrusively. The 3D deformation field under a model footing was explored using the proposed technology in order to illustrate its benefits. The tests showed satisfactory results and proved that transparent soil could be used to model natural soil.

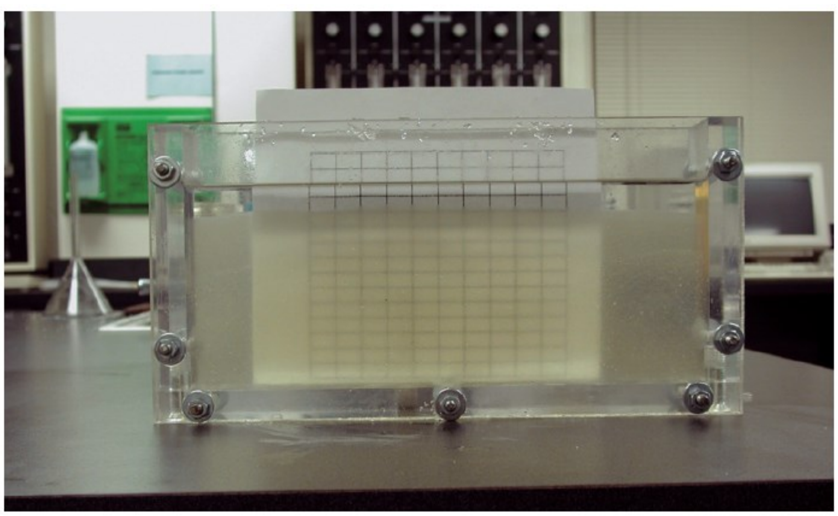

Figure 2.9: Target viewed through a 2-inch thick transparent soil model (Liu and Iskander, 2010)

Several studies have been performed in the University of Sheffield on enhancing the accuracy and precision of transparent synthetic soil modelling. Kelly (2014) utilized the principle of transparent soil and laser aided imaging to evaluate the deformation and failure behavior of stone column foundations. However, this research was performed on a small scale and prototype stress levels were not provided using a geotechnical centrifuge. Black (2012) used the transparent synthetic soil in conjunction with laser aided Particle Image Velocimetry (PIV) to establish soil-pile interaction behavior during installation. A series of centrifuge tests were performed to examine the influence of driving shoe and surface ribs on the installation displacement behavior during press-in of a tubular pile. Black (2015) performed centrifuge tests on transparent soils to address the concerns aroused on the impact of scale and stress levels in the previously reported works. This study outlined the development of an improved testing methodology where transparent soil in conjunction with laser aided imaging are translated to the centrifuge, thus benefiting from the elevated stress conditions provided when testing models in the high gravitation acceleration field but also offering higher measurement resolution capabilities associated with the laser aided DIC.

Ni et al., (2010) developed a small-scale physical modelling method to study the movement of clay during pile installation. The clay was replaced using a mixture of amorphous silica and mineral oil. Bathurst and Ezzein (2015, 2017) worked on the development of a new transparent granular soil that could be used for geotechnical laboratory-scale modeling purposes. The sand consists of fused quartz particles in combination with a mixture of two mineral oils. The author also worked on identifying geogrid - sand interaction by performing laboratory pullout tests. The results demonstrated the utility of an experimental methodology using transparent fused quartz material as a successful analog to a natural sand soil for the investigation of granular soil–geogrid interaction. Bathurst and Ezzein (2015) performed a series of geogrid pullout tests in a novel large pullout box with a transparent granular soil. The test apparatus and methodology allowed the entire geogrid specimen to be visible through the bottom of the box. Specimen displacements were computed from image analysis of pictures taken through the transparent bottom of the pullout box during each test. Bathurst and Ezzein (2017) also performed an experiment to investigate the load transfer between a typical extensible geogrid material and sand during pullout test under different normal stresses. A transparent granular soil was used so that the relative movement of the geogrid specimen and target soil particles could be tracked during pullout of reinforcement specimens in a large pullout box. Their results demonstrated the utility of the experimental methodology using the transparent fused quartz material as a successful analog to a natural sand soil for the investigation of granular soil–geogrid interaction. Ferreira and Zornberg (2015) evaluated the effect of soil-structure interaction in geogrid reinforced earth structures. The feasibility of adopting transparent soil as a surrogate for sands in pullout test was assessed. Costa et al., (2016) performed a study on reduced-scale geosynthetic-reinforced walls using a 15 g-ton geotechnical centrifuge available at the University of Colorado at Boulder. Centrifuge models were built using nonwoven fabrics as reinforcement elements and Monterey No. 30 sand as backfill. Digital image analysis techniques were used to quantify the internal displacements within the reinforced zone.

Initial studies performed in this research demonstrated that the geomechanical behavior of the fiber-reinforced clay soil is dependent on the method of sample preparation as well as the orientation of fibers within the soil (*Chapter Four*, Manuscript #2). No methodology has been developed so far to characterize the distribution of fibers within clay soil. This thesis discusses the limitations of the existing visual examination techniques in determining the evolution of fibers within the clay soil as well as develops a novel transparent fiber-reinforced soil to track the fiber orientation.

Chapter Three: The effect of polymer fibers on the pore pressure response and undrained shear strength of clay soil

Contribution of the Ph.D. candidate

All work presented in this chapter has been carried out by the Ph.D. candidate., which includes review of the literature, preparation of testing specimens, design of the experimental program, execution of the experiments, analysis and discussion of the results and writing of the text.

As supervisor, Dr. M. T. Hendry has reviewed all parts of the work. This chapter will be submitted with the following citation:

Palat, A., and Hendry, M.T. (2022) 'The effect of polymer fibers on the pore pressure response and undrained shear strength of clay soil'.

Contribution of this chapter to the overall study

The findings of this chapter addresses the global objective of analysing the role of short, discrete, synthetic fibers in altering the geomechanical behavior of a clay soil and evaluate the strength and stiffness properties of the composite through laboratory testing. A methodology is developed to prepare cylindrical samples of fiber-reinforced clay soil for triaxial testing by the application of heavier compaction energy (as such the laboratory testing results from this study are only applicable for composites prepared using the compaction method). The challenges encountered while mixing polymer fibers with the clay soil are discussed and the steps taken to overcome these challenges are also mentioned. The effect of increasing fiber content and fiber length on the undrained shear strength and induced pore water pressure is analysed and an optimum fiber combination in terms of content and length is determined. This study further evaluates the role of discrete fibers in altering the undrained stiffness and yield points of a clay soil. The limitations of traditional triaxial compression tests in bringing the fiber-reinforced clay samples to failure and determining the strength of this composite material is also discussed in this chapter.

Abstract

Existing models of soil behavior have been developed based on the understanding of interaction between particles, much of which is conceptually based on sand and modified to describe the behavior of clayey soils. However, for other classes of fibrous soils and soils amended with fibers, these models do not accurately represent soil behavior. This paper reports on investigations conducted to determine the geomechanical properties of fiber-reinforced clay soils and to understand the impact of adding fibers. The impact of fiber on the undrained shear strength and induced pore water pressure response of the clay soil is examined with consolidated undrained triaxial compression testing. Three values of fiber content (1, 2, and 3%) and three fiber lengths (6, 18, and 48 mm) were tested. Samples of fiber-reinforced clay showed a tendency to bulge without developing a distinct shear plane; this behavior is expected due to the movement of fibers to the potential planes of weakness and mobilization of tensile stresses within the fibers. The deviator stress and maximum pore water pressure increased up to a fiber content of 2% and then declined. For the range of fibers used in this study, the deviator stress and maximum pore pressure increased with increasing fiber length. The role of polymer fibers in altering the yield point of a clay soil is evaluated and an analysis of the dependence of the yield point on different fiber variables is also performed. The results of this research have applications with respect to estimating the undrained behavior and shear strength of fibrous organic soils and soils reinforced with elements that act in tension.

3.1 Introduction

The inclusion of fibers can improve the response of soil under both static and dynamic loading conditions (Maher and Woods 1990; Gray and Ohashi 1983; Maher and Ho 1994; Zornberg 2002; Zornberg and Li 2003; Li 2005; Anagnostopoulos et al. 2013). Adding discrete fibers increases the peak shear strength and ductility of cohesionless soil (Maher and Gray 1990). The primary response of fibers to shear deformation is the generation of tensile stresses within the fibers, resulting in increased strength and stiffness of the composite (Hendry 2011). These fibers behave as tension-resisting elements and partially withstand the shear stress developed within the soil (Mirzababaei et al. 2018). The contribution of fibers to the strength of a soil depends on their orientation with respect to the principal axis of deformation (Diambra et al. 2007). Fibers are, in general, most influential if the orientation of the major (compressive) principal stress is perpendicular to the plane of predominant fiber orientation (Michalowski and Cermak 2002; Hendry 2011; Hendry et al. 2012, 2013). Prediction of failure in fiber-reinforced sand resulted in a bilinear failure envelope with fiber stretching and slippage observed in the lower pressure part and tensile yielding governing the failure in the higher-pressure part (Consoli et al. 2007). Zornberg (2002) proposed a discrete framework for the design of a fiber-reinforced soil structure in which the equivalent shear strength of the fiber-reinforced soil is predicted by the independent characterization of soil and fiber properties. Li (2005) used this framework and validated the results with triaxial tests performed on fiber-reinforced composites. These studies (Zornberg 2002; Li 2005) demonstrate the mobilization of fiber-induced tension requires a relatively high strain level, often beyond the peak for unreinforced soil. Li (2005) pointed out the difficulties in quantifying fiber-clay interactions. Indeed, most studies to date have been performed on fiber-reinforced sand, with very few focusing on fiber-reinforced clay soil. This is mainly due to challenges related to sample preparation and the difficulty quantifying pore water pressure and interface shear strength between the soil and the fibers.

The concept of yielding has proven useful for understanding the behavior of clay soil beneath embankments and slopes (Graham et al. 1983). For a natural clay soil, yield stresses have been interpreted from a variety of stress-strain relationships using a bilinear plotting technique and identifying the intersection of the projections of the linear sections; specifically, a series of stress paths were chosen to explore the limit state stresses in various regions of the stress space and a tentative yield envelope was drawn by connecting these points (Baracos et al. 1980; Noonan 1980; Lew 1981). Even though extensive studies have explored the yielding of natural clay soil, a determination of yield stresses in fiber-reinforced clay is still lacking.

This paper presents a comprehensive study on the impact of fibers with respect to altering the geomechanical behavior of clay soil. The influence of variables such as fiber content and length on the undrained shear strength, induced pore water pressure response, and stiffness is quantified. The role of fibers in altering the yield point of a clay soil is evaluated and an analysis of the dependence of the yield point on different fiber variables is conducted. Beyond uses as a ground modification technique, fiber-reinforced clay soil can also be used in several other applications such as stabilization of mine fine tailings, oil sands mining reclamation including tailings ponds, evapotranspiration covers, and low-permeable landfill liners. Other applications include repairing failed slopes, reinforcing the subgrades of roads and highways, and increasing the stability of highway embankments.

3.2 Materials and Methods

3.2.1 Materials

The clay soil adopted in this study was 'EPK Kaolin' manufactured by Edgar Minerals Inc. This study evaluates the behavior of fibers when mixed with a fine-grained soil of known material properties. Kaolinite clay was adopted because it is a neutral material without any unique behavior and the material properties can be easily determined from basic laboratory testing. Laboratory testing of the soil indicated a specific gravity of 2.45, liquid limit of 58%, plastic limit of 42%, and plasticity index value of 16%. Standard Proctor tests resulted in an optimum moisture content (OMC) of 28% and maximum dry density (MDD) of 1500 kg/m^3 (1.5 g/cm^3). The reinforcements used were pre-cut polypropylene (PP) fibers supplied by MiniFIBERS Inc. (Johnson City, TN, USA). Table 3.1 summarizes the physical characteristics of the PP fibers.

3.2.2 Sample preparation

One of the most challenging aspects of this study was the preparation of uniformly fiber-distributed samples for triaxial testing. The challenges faced during sample preparation and the steps taken to prepare consistent samples are described in Palat et al. (2019). To prepare unreinforced specimens, the required quantity of dry kaolinite clay was mixed with de-aired, distilled water at OMC in a mechanical mixer. The fiber-reinforced soil samples were prepared as two lots. Lot 1 was prepared by mixing half of the soil and half of the water using the mixer. Lot 2 was prepared by mixing the remaining half of the soil, half of the water, and the fibers using the same mixer. The mixing speed and time were the same for both lots. Lots 1 and 2 were subsequently mixed together by hand (Fig. 3.1a). This method of preparing fiber-reinforced samples (as two separate lots followed by mixing) was selected to avoid the entangling of PP fibers as they come into contact with water (Roustaei et al. 2015). The unreinforced and fiber-reinforced soils were sealed and stored in a moisture room for 48 hours, after which the test samples were prepared in a split mold (50 mm diameter × 100 mm high) as five equal layers each followed by subsequent compaction. Care was taken to ensure the compaction energy was consistent across all prepared samples. An arbor press was used to compact all samples and the number of blows was restricted to 15 per layer (Palat et al. 2019). Note that the results of this laboratory testing are only applicable to fiber-reinforced clay samples prepared using this compaction method. Figure 3.1b shows a fiber-reinforced specimen prepared using this method.

Table 3.1. Physical properties of the synthetic fibers used in the study (Technical data sheet, Minifibers, Inc)

Properties	PP
Length (mm)	6, 18, 48
Thickness (mm)	0.035
Specific gravity	0.91
Tensile Modulus (GPa)	0.4
Moisture Absorption (%)	< 1

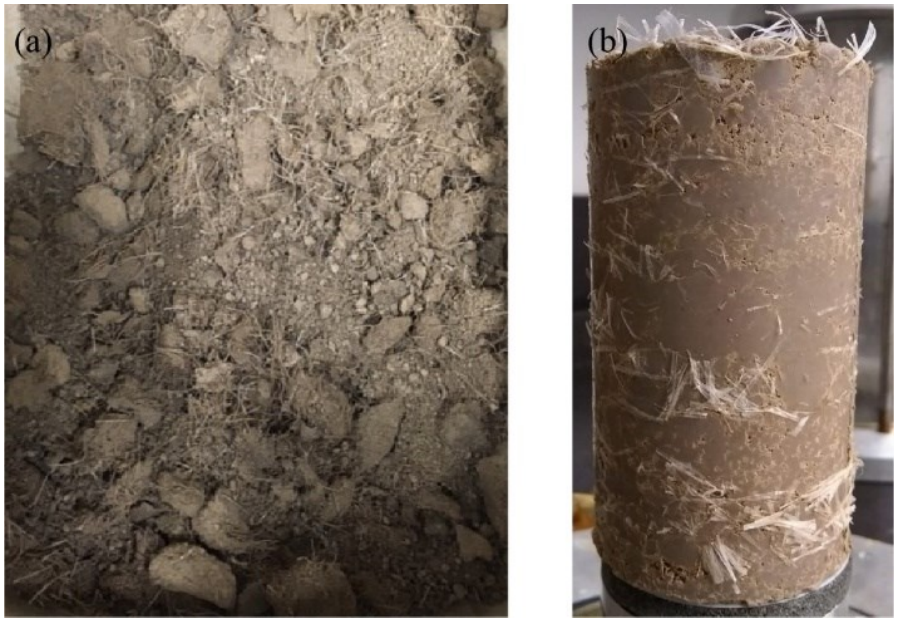

Figure 3.1. (a) Prepared fiber-reinforced soil lot, (b) fiber -reinforced sample used for testing (Fiber content: 2 %; Fiber length: 18 mm; Fiber type: PP).

3.2.3 Testing Method

Specimen strength was determined by performing traditional isotropic consolidated undrained (CU) triaxial tests, in accordance with ASTM D4767-11 (2020). A Humboldt HM-5020 load frame with a capacity of 15 kN was used for the testing. The axial load was measured by a load cell (Model 75/1508, Sensotec) with a capacity of 4.5 kN and accuracy of 0.14%. The vertical displacement of the sample was measured using a linear potentiometer (LP) (Model TR-50, Novotechnik) with a maximum travel length of 50 mm, linearity of ± 0.075%, and repeatability of ± 0.002 mm. A pressure panel was used to control the cell and back pressure applied to the sample. The pore water pressure developed within the specimen was measured by connecting a transducer to the base of the cell. The volume change in the sample during the consolidation phase was measured by attaching an automatic volume change device to the back pressure line of the triaxial chamber. Small strain on-sample transducers were not employed in this testing, which limits the ability to use the test results to interpret soil behavior at strains less than 0.5% (Jardine et al. 1985). However, previous studies on fiber-reinforced clay soil by Li (2005) show the loads resisted by fibers are only substantial at higher strain levels.

Prior to testing, the samples were saturated by applying a back pressure of 390 kPa and a cell pressure slightly greater than the back pressure until a B value greater than 0.97 was achieved. The specimen was then consolidated by maintaining the difference between the cell pressure and back pressure at a value equal to the desired effective stress. Following consolidation, shearing was initiated on the samples, the rate of which was determined based on the consolidation curves. The testing was continued until an axial strain of 20% was achieved.

3.2.4 Scope of the testing program

Six series of CU triaxial tests were conducted as a part of this investigation as outlined in Table 3.2. Each series included testing the samples for three different values of effective confining stresses (p_o'; 50, 100, and 200 kPa). Experimental studies were performed with two varying parameters: (a) fiber content (1, 2, or 3%) and (b) fiber length (6, 18, or 48 mm). Tests were also performed on samples reinforced with 0.5% by weight of fibers; however, no significant improvement in strength or pore pressure values were achieved and therefore these test results are not included herein.

Corrections for filter paper strips and rubber membranes were not considered when calculating the deviator stress, as vertical filter paper strips were not used and the rubber membrane correction factor did not exceed 5%. CU triaxial test results are presented in terms of effective stress paths (ESPs) in deviator stress (q) versus mean effective stress (p'), q versus axial strain (ε_a), and induced pore water pressure (Δu) versus ε_a.

3.3 Results and Discussions

3.3.1 Effect of fiber inclusion

The effect of fiber inclusion was visually observed in all reinforced samples after shearing. Specifically, the unreinforced clay samples failed at lower values of ε_a by developing a well-defined failure plane (Fig. 3.2a). However, no visible failure plane was observed in the fiber-reinforced specimens, which showed a tendency to bulge (Fig. 3.2b). The testing was stopped once an ε_a of 20% was reached even though no failure was observed. This change in mode of failure could be visualized due to the movement of fibers to the potential plane of weakness and mobilization of tension in them in the direction of expansive strain. It is also an indication that the ductility of the clay soil was improved by the inclusion of randomly oriented fibers.

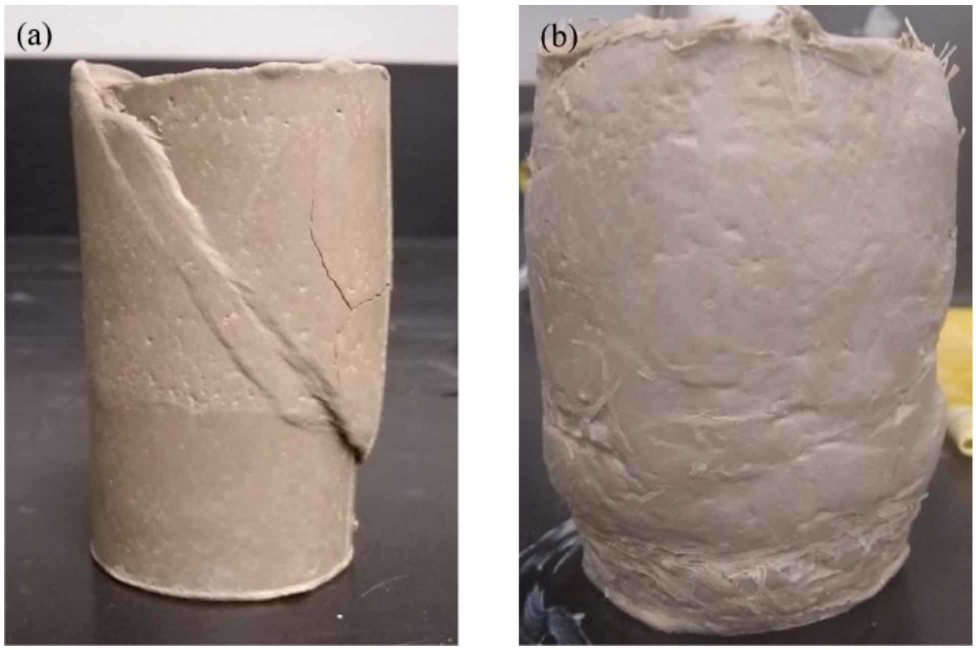

Figure 3.2. Deformation pattern in samples after failure (a) unreinforced sample, (b) fiber-reinforced sample (fiber content: 2 %; fiber length: 18 mm; fiber type: PP).

3.3.2 Effect of fiber content

The effect of fiber content was determined on fiber-reinforced clay samples prepared with three values of PP fiber content (1, 2, or 3%) with a constant fiber length of 18 mm (Table 3.2). With increasing fiber content, the maximum deviator stress (q_{max}) and maximum induced pore water pressure (Δu_{max}) increased to reach their maximum values at 2%, followed by a decline (Fig. 3.3b and c). This reduction in strength beyond 2% could be due to the tendency of fibers to cluster inside the soil sample rather than distribute uniformly. A similar trend was also observed in the shear strength response of fiber-reinforced sand (Zornberg et al. 2004). This behavior could be due to the different types of soil reinforcement mechanisms developed within the composite. Initially, tensile forces develop in the fibers leading to an increased overall shear strength of the matrix. At higher values of fiber content (greater than 2%), shear among individual fibers becomes the governing factor, leading to a reduction in the shear strength and pore pressure values.

The ESPs indicate a strain hardening response, with the maximum q value observed for the 2% fiber-reinforced samples (Fig. 3.3a). However, none trace the path of the tension cut-off line, which indicates the maximum tension has not been mobilized in the fibers. The deviation of the ESP from vertical could be due to anisotropy in the fiber-reinforced samples and the quasi-overconsolidated response due to the higher compaction energy applied during sample preparation.

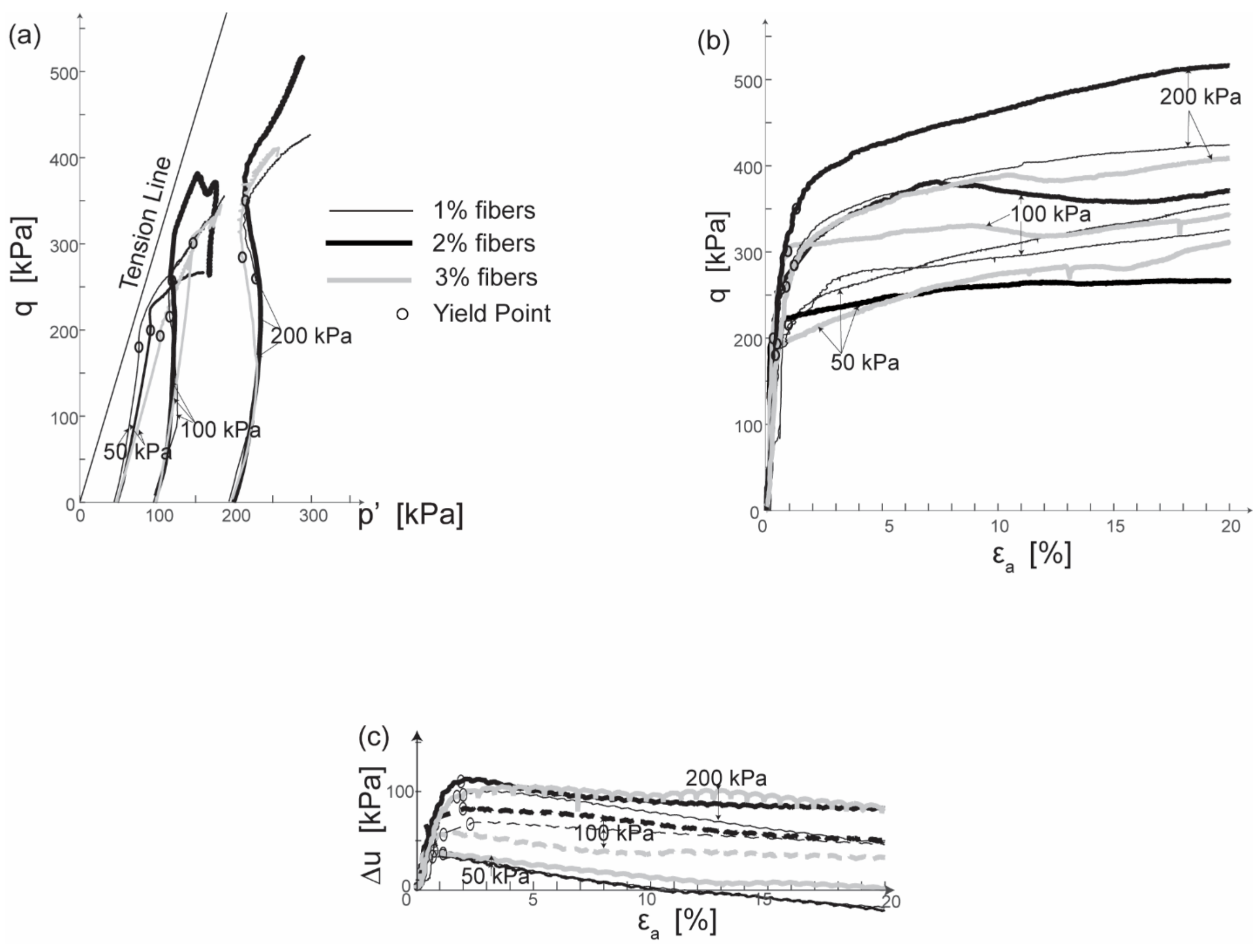

Figure 3.3 Comparison of CU laboratory testing results from kaolinite soil specimens reinforced with three fiber contents (fiber length: 18 mm; fiber type: PP) presented in (a) q versus p' space (b) q versus ε_a space, and (c) Δu versus ε_a space, at three values of p_o'.

3.3.3 Effect of fiber length

The effect of fiber length was determined on fiber-reinforced clay samples prepared with three different lengths of PP fibers (6, 18, or 48 mm) with a constant fiber content of 2% (Table 3.2). For the range of fiber lengths adopted in this study, q_{max} and Δu_{max} increased with increasing fiber length at all values of p'_o (Fig. 3.4b and c). This trend could be due to the greater area of contact between fibers and soil leading to an increase in the frictional component of shear strength. Additionally, increasing the fiber length improves the pullout resistance of individual fibers. This in turn leads to the mobilization of tensile forces within the fibers, which would also contribute to the overall shear strength of the matrix (Zornberg et al. 2004). Overall, the results demonstrate the optimal fiber length for use in practice is beyond the range of lengths tested herein.

For samples reinforced with 48 mm fibers and tested at a p'_o of 200 kPa, a q_{max} value of 1400 kPa was observed at 20% ε_a (Fig. 3.4b). The value of Δu developed in the composite at the end of shearing is almost equal to the p'_o applied (Fig. 3.4c). Yet, the specimens did not show any signs of failure, indicating the increase in q is solely due to the increase in tension mobilized in the fibers (Hendry et al. 2012). Additionally, the ESP corresponding to the strain-hardening portion follows the trace of tension cut-off line (Fig. 3.4a). This indicates the maximum tensile force was mobilized in fibers at higher values of p'_o. The deviation of the ESP to the left indicates an increased stiffness of the composite in the horizontal direction (Hendry et al. 2012). Undrained triaxial compression tests on fibrous peat specimens demonstrated pore pressure values higher than the applied effective confining pressures and this behavior was tied to the anisotropic nature of peat specimens with higher stiffness in the horizontal direction (Acharya et al. 2018). However, an examination of the samples after failure shows no tendency of the fibers to break. The tensile modulus of the PP fibers is 0.4 GPa (Table 3.1). These observations indicate the fibers are highly extensible and the force required to break them was not reached during the triaxial testing.

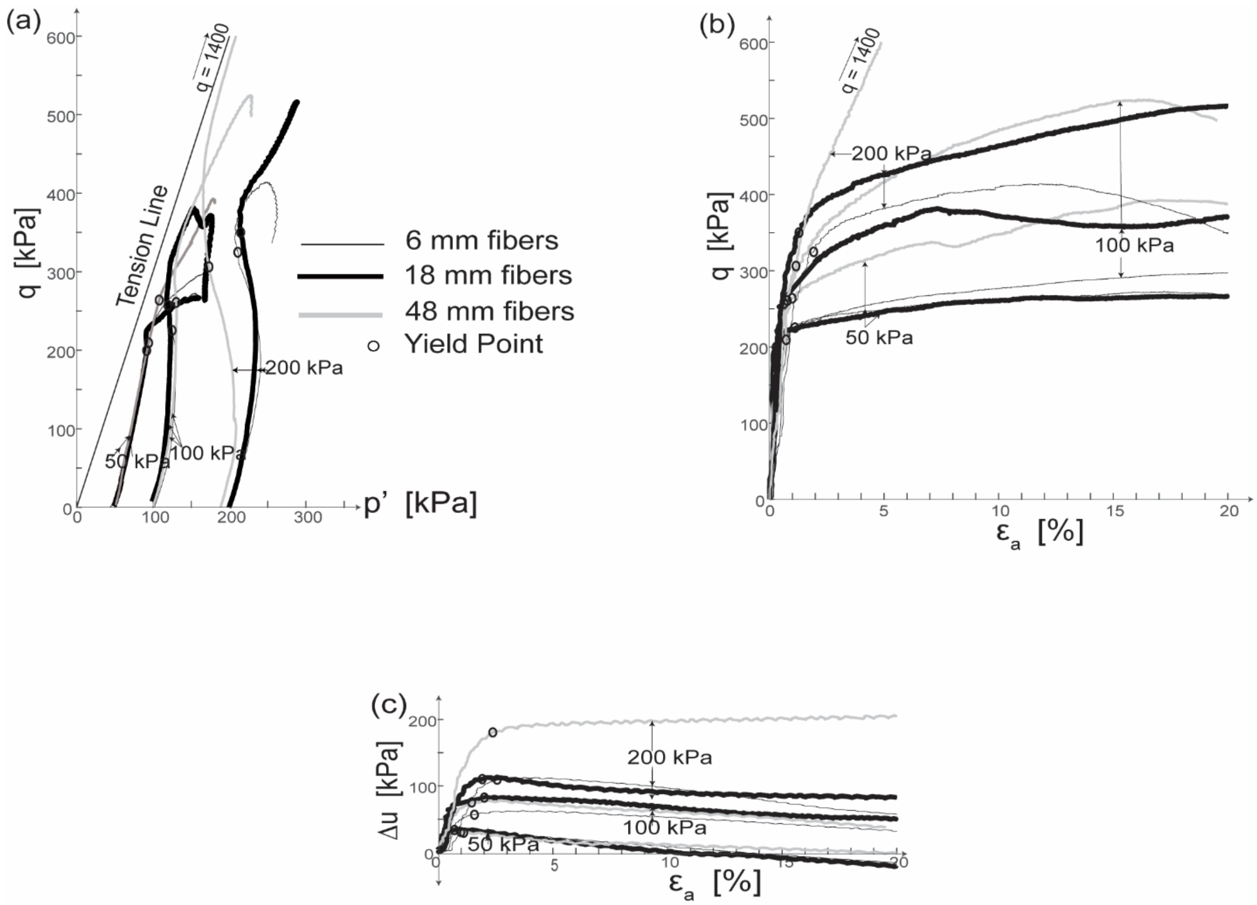

Figure 3.4. Comparison of CU laboratory testing results from kaolinite soil specimens reinforced with three fiber lengths (fiber content: 2%; fiber type: PP) presented in (a) q versus p' space (b) q versus ε_a space, and (c) Δu versus ε_a space, at three values of p'_o.

3.3.4 Modulus of elasticity

In triaxial tests on intact samples of low-plasticity clay, the strains deduced from external measurements of deflection were higher than the strains measured locally on the sample (Jardine et al. 1984). Hence, external measurements of strain gave a linear stress-strain behavior whereas measurements from on-sample transducers showed a much stiffer non-linear response (Jardine et al. 1985). Additionally, the stiffness values measured from high-quality *in situ* tests and field measurements converged within the range measured from the on-sample transducers. However, a close agreement was observed between the strain values measured using the external transducers and those measured locally on the sample beyond an ε_a of 0.5% (Jardine et al. 1985).

Table 3.2. Summary of the CU triaxial tests performed on unreinforced and fiber-reinforced kaolinite clay soil along with the variation of secant modulus ($E_{u\,(1)}$) .

Fiber Type	Fiber Content [%]	Fiber length [mm]	p'_o [kPa]	q at 1% ε_a [kPa]	$E_{u\,(1)}$ [kPa]
PP	0	0	50 100 200	249 247 240	249 247 240
PP	1	18	50 100 200	210 215 274	210 216 274
PP	2	18	50 100 200	223 276 324	223 276 324
PP	3	18	50 100 200	198 306 264	198 302 264
PP	2	6	50 100 200	224 222 236	224 222 236
PP	2	48	50 100 200	265 287 295	265 288 295

Because on-sample transducers were not employed in this study, the role of fibers in altering the stiffness of clay soil was analyzed by calculating the undrained secant modulus at an ε_a of 1% ($E_{u\,(1)}$). $E_{u\,(1)}$ represents the slope of a q versus ε_a plot from 0 to the q value obtained at 1% ε_a. The use of $E_{u\,(1)}$ in this study does not mean the soil behavior is elastic within this range, and is only used as a convenient measure of soil stiffness (Jardine et al. 1984, 1985). Table 3.2 summarizes the $E_{u\,(1)}$ values obtained for unreinforced and fiber-reinforced samples at three values of p'_o; the variation is plotted in Fig. 3.5. The secant modulus can also be used to predict the movement of the soil due to the first application of load (Briaud 2001).

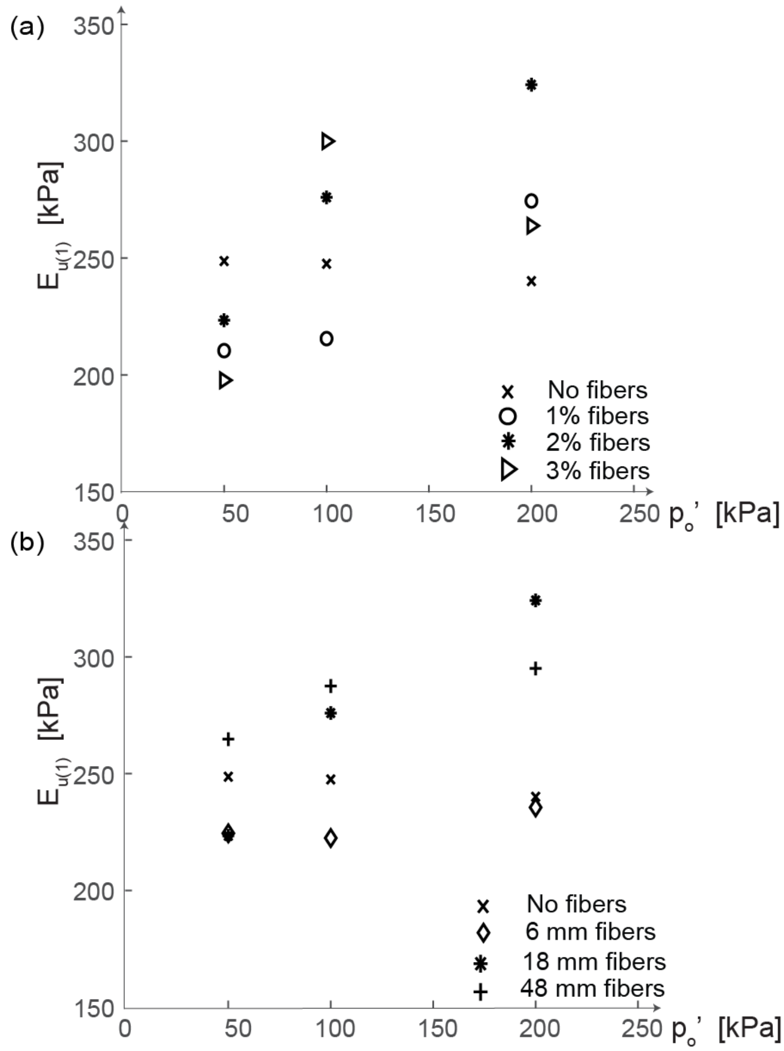

Figure 3.5. Variation of the secant modulus ($E_{u\,(1)}$) calculated at 1% ε_a versus p_o' for fiber-reinforced samples as obtained from the results of CU triaxial testing presented for the variation of (a) Fiber content (Fiber length: 18 mm, Fiber type: PP) and (b) Fiber length (Fiber content: 2%, Fiber type: PP).

For all fiber-reinforced composites, the $E_{u\,(1)}$ increased with increasing confining pressure. A similar behavior was observed for tests on remoulded peat fiber specimens (Hendry et al. 2012) and was expected due to the greater amount of tension mobilized in the fibers at higher p_o' values, which produces a greater contribution to the stiffness of the composite. However, changing the fiber variables (content and length) did not play a notable role in terms of impacting the stiffness of the clay soil. This emphasizes the fact that the fibers are only engaged at higher values of ε_a and do not impact the small strain stiffness of the clay soil. Previous studies on fiber-reinforced sand and fibrous peat indicate the reinforcing effect of fibers is maximized when the major principal stress is perpendicular to the axis of the plane of predominant fiber orientation (Michalowski and Cermak 2002; Hendry et al. 2014). For all tests performed in this study, the major principal stress is in the vertical direction. We speculate some amount of ε_a is required for the fibers to reorient in the horizontal direction during shearing and contribute to the stiffness of the clay soil.

3.3.5 Determination of the yield point

Yielding is defined as a marked change in the stiffness of the clay skeleton at its preconsolidation pressure (Baracos et al. 1980). Yield stresses are in general considered as the intersection of straight approximations of the initial stiff section and the subsequent more flexible response to applied stresses (Graham and Houlsby 1983; Graham et al. 1983). A variety of stress-strain relationships have been used to examine this bi-linear response and could be used to distinguish pre-limit-state from post-limit-state behaviour (Noonan 1980; Lew 1981; Graham et al. 1983). A similar approach was followed in this research to identify the yield stresses in samples of unreinforced and fiber-reinforced clay soil (Fig. 3.6). Because only undrained compression tests were performed in this investigation, the yield points were interpreted by plotting q versus ε_a, major effective principal stress (σ_1') versus ε_a, minor effective principal stress (σ_3') versus radial strain (ε_r), and Δu versus ε_a. The stresses and pore water pressure at yield (as obtained from the figures) were then converted to a common stress variable, mean effective stress (p'), for comparison purposes (Table 3.3). A significant level of agreement was observed in all four values of p', which confirms the concept of yield is applicable for fiber-reinforced soil composites.

The unreinforced samples showed an additional change in the stiffness at stresses lower than the yield stress. Similar behavior was also observed while determining the limit state surface of the lacustrine clay underlying Winnipeg, which was expected due to the marked anisotropy and non-homogeneity of the deposit (Baracos et al. 1980; Noonan 1980). In this case, the quasi-overconsolidated behavior observed in the compacted clay is another factor contributing to the observation of signs of yielding prior to the principal yielding.

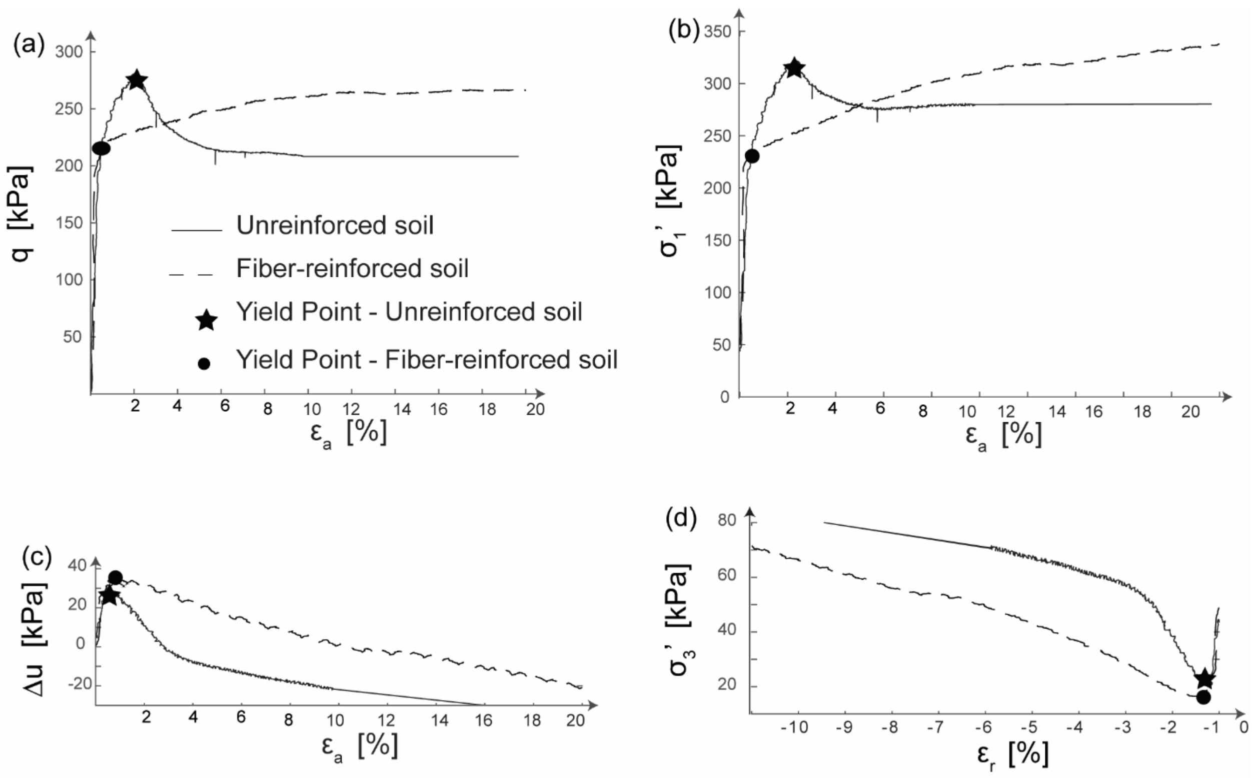

Figure 3.6. Bilinear technique adopted for the determination of yield stresses in unreinforced and fiber reinforced (fiber content: 2%, fiber length: 18 mm, fiber type: PP) samples at a p_o' of 50 kPa: (a) q versus ε_a, (b) σ_1' versus ε_a, (c) Δu versus ε_a, (d) σ_3' versus ε_r.

Figures 3.3 and 3.4 indicate the yield points observed for unreinforced and fiber-reinforced soil composites in the q versus p' , q versus ε_a, and Δu versus ε_a stress spaces. The yielding behavior is observed at lower values of ε_a (<2.5%) for all samples. The deviator stress at yield (q_Y) align at one point when samples are tested at a p_o' of 50 kPa (except for the soil composites with 48 mm fibers). However, more scatter is observed in the data points at higher values of p_o', with the maximum value of q_Y observed in the samples reinforced with 48 mm fibers followed by 18 mm fibers, both at a fiber content of 2%. This behavior ties back to the optimum fiber content and length in a clay soil determined based on the stress and pore pressure response. An increase in q_Y suggests the irrecoverable plastic strain only starts to develop in the composite at higher values of q. The fibers do not play a significant role in altering the mean effective stress at yield (p_Y') of a clay soil. Nevertheless, a reduction is observed in p'_Y for samples containing 48 mm fibers when tested at a p'_o of 200 kPa. This reduction in p'_Y can be attributed to the increased Δu value observed during tests with higher values of p'_o.

Table 3.3. Determination of yield stresses from different yield criteria in unreinforced and fiber-reinforced samples

Fiber Content [%]	Fiber Length [mm]	p'_o [kPa]	q versus ε_a [kPa]	σ'_1 versus ε_a [kPa]	Δu versus ε_a [kPa]	σ'_3 versus ε_r [kPa]
0	0	50	131	133	98	93
		100	166	168	135	133
		200	274	274	190	190
1	18	50	83	76	79	76
		100	116	120	117	120
		200	215	226	214	226
2	18	50	91	91	91	91
		100	119	120	123	120
		200	215	223	215	217
3	18	50	104	103	105	103
		100	147	146	146	145
		200	211	216	209	208
2	6	50	95	89	94	93
		100	125	128	122	126
		200	211	221	208	211
2	48	50	108	108	108	101
		100	130	130	132	129
		200	173	178	167	166

Note: The yield stresses presented in this table have been converted to a common stress variable p' *[kPa] for comparison purposes*

3.3.6 Shear strength of fiber-reinforced samples

The unreinforced clay samples developed a well-defined failure plane and demonstrated a strain weakening behavior after the attainment of peak deviator stress. For those samples, failure was defined corresponding to the maximum deviator stress attained in accordance with the ASTM guidelines. Figure 7 plots the relationship between mean effective stress ($p'_f = \left(\frac{\sigma'_1+2\sigma'_3}{3}\right)_f$) and deviator stress at failure ($q_f = (\sigma_1 - \sigma_3)_f$) for unreinforced samples. M_{cu} and k_{cu} are the slope and Y-axis intercept of the strength line, respectively. For a triaxial compression test, the effective angle of shearing resistance ϕ' and the cohesion intercept c' can be estimated using Eqs. (1) and (2) (Wood 1990):

$$\phi' = \sin^{-1}\left(\frac{3M_{cu}}{6 + M_{cu}}\right) \tag{3.1}$$

$$c' = k_{cu}\left(\frac{3 - \sin\phi'}{6\cos\phi'}\right) \tag{3.2}$$

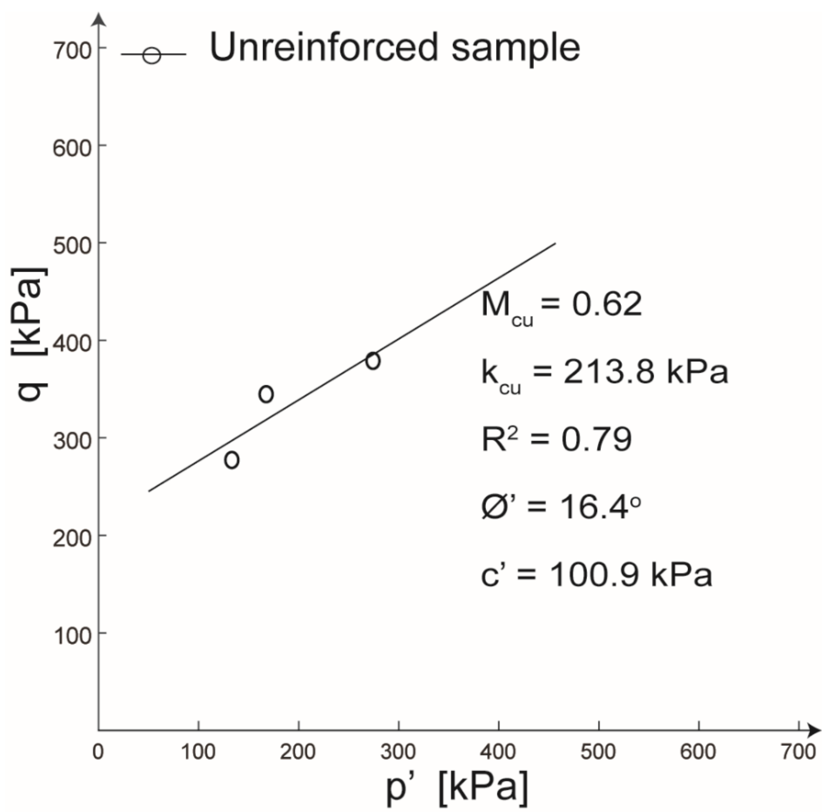

Figure 3.7. Strength line connecting the peak stress points developed in the unreinforced clay soil.

The unreinforced kaolinite clay samples resulted in a c' of 100 kPa and ϕ' of 16.4°. However, the samples of fiber-reinforced clay exhibited a strain hardening behavior (past the yield point) with no signs of failure when tested up to an ε_a of 20%. Hence, it was not possible to define 'strength' for this class of material within the tested range of p_o'. This change of behavior in fiber-reinforced samples could be due to the additional shearing resistance developed in the composite because of the tension mobilized in the fibers. A similar response was observed in samples of fibrous peat, where specimens showed no signs of failure with a gradual transition from linear elastic to linear strain-hardening stress-strain response when loaded (Hendry et al. 2012). This linear increase in q during strain hardening is the result of additional shear resistance due to fiber tension (Hendry et al. 2012).

The findings signify the limitation of triaxial compression tests to define the shear strength of fiber-reinforced clay samples when tested at p_o' values ≤ 200 kPa. It is recommended to perform more tests at wider ranges of p_o' and along varying stress paths to more completely define the shear strength behavior of fiber-reinforced clay soil.

3.4 Conclusions

This study varied confining pressure, fiber content, and fiber lengths in a testing program designed to investigate the geomechanical behavior of compacted fiber-reinforced clay soil, with special emphasis on the effective stress response, stiffness parameters, and yielding behavior. The chapter also proposes an effective method for preparing a uniform and homogeneous fiber-reinforced specimen for triaxial testing. The major observations from this study are summarized below:

- Unreinforced clay samples exhibited a well-defined failure plane and demonstrated a strain weakening behavior after the attainment of peak deviator stress. However, reinforced samples tended to bulge without any evidence of failure plane. This indicates the addition of fibers improved the ductility of the clay soil. Resistance to cracking potential accompanies an improvement in the ductility and would be beneficial when using this composite as a landfill liner or evapotranspiration cover.

- q_{max} and Δu_{max} increased with increasing fiber content, up to an optimum amount of 2%. At greater fiber contents, the fibers tended to cluster inside the soil rather than distribute uniformly. The shear among the individual fibers became the dominating mechanism and the contribution of mobilized fiber tension to the overall shear strength of the composite declined.

- For the range of fiber lengths used in this study, q_{max} and Δu_{max} increased with increasing fiber length. This is due to the greater contact area between fibers and soil, resulting in a higher interface shear strength and a greater amount of tension mobilized in longer fibers. This indicates the optimal fiber length for use in practice is beyond the range of lengths tested herein.

- The role of fibers in altering the stiffness of clay soil was analyzed by calculating the undrained secant modulus at an ε_a of 1% ($E_{u\,(1)}$). For all fiber-reinforced composites, the $E_{u\,(1)}$ increased with increasing p_o' due to the greater amount of tension mobilized in the fibers at higher p_o' values. Changing the fiber variables did not impact the small strain stiffness of the clay soil as the fibers are only engaged at higher values of ε_a.

- The bilinear technique for determining the yield point demonstrated the concept of yield is applicable for this composite material. Adding fibers increased the value of q_Y, with the maximum increase observed in samples with a 2% content of 48 mm fibers. However, the fibers do not play a significant role in altering the p_Y' value of a clay soil.

- Samples of unreinforced kaolinite clay samples demonstrated a c' of 100 kPa and ϕ' of 16.4°. However, the samples of fiber-reinforced clay exhibited a strain hardening behavior with no signs of failure when tested up to an ε_a of 20%. Hence, it was not possible to define 'strength' for this class of material. This signifies the need to perform more tests at wider ranges of p_o' and along varying stress paths to better define the shear strength behavior of fiber-reinforced clay soil.

3.5 Data Availability Statement

Some or all data, models, or code that support the findings of this study are available from the corresponding author upon reasonable request.

3.6 Acknowledgement

This research was funded by a Natural Sciences and Engineering Research Council Discovery Grant (#RGPIN-2020-04419). The authors also thank MiniFIBERS. Inc. for supplying the fibers for triaxial testing.

3.7 References

Acharya, M.P., Hendry, M.T., and Martin, C.D. 2018. “Creep behaviour of intact and remoulded fibrous peat.” Acta Geotechnica 13(2), p399-417, doi: 10.1007/s11440-017-0545-1.

Anagnostopoulos, C.A., Tzetzis, D., and Berketis, K. 2013. “Shear strength behavior of polypropylene fiber reinforced cohesive soil.” Geomechanics and Geoengineering, 9(3), p241-251, doi:10.1080/17486025.2013.804213.

ASTM D4767-11. 2020. Standard Test Method for Consolidated Undrained Triaxial Compression Test for Cohesive Soils. ASTM International, West Conshohocken, PA, 2020, www.astm.org.

Baracos, A., Graham, J., and Domaschuk, L. 1980. “Yielding and rupture in a lacustrine clay.” Canadian Geotechnical Journal, 17 (4), doi: 10.1139/t80-063.

Briaud, J. L. 2001. “Introduction to Soil Moduli.” Geotechnical News, BiTech Publishers Ltd, Richmond, B.C, Canada, geotechnicalnews@bitech.ca.

Consoli, N.C., Heineck, K.S., Casagrande, M. D. T., and Coop, M.R. 2007. “Shear strength behavior of fiber-reinforced sand considering triaxial tests under distinct stress paths.” Journal of Geotechnical and Geoenvironmental Engineering, 133(11),p1466-1469.

Diambra, A., Russel, A.R., Ibrahim, E., and Wood, D.M. 2007. “Determination of fiber orientation distribution in reinforced sands.” Geotechnique, 57(7), p623–628, doi: 10.1680/geot.2007.57.7.623.

Graham, J., Noonan, M.L., and Lew, K.V. 1983. “Yield states and stress-strain relationships in a natural plastic clay.” Canadian Geotechnical Journal, 20(3), p502-516, doi: 10.1139/t83-058.

Graham, J., and Houlsby, G.T. 1983. “Anisotropic elasticity of a natural clay.” Geotechnique, 33(2), p165-180.

Gray, D.H., and Ohashi, H. 1983. “Mechanics of fiber reinforcement in sand.” Journal of Geotechnical Engineering, 109(3), p335-353.

Hendry, M.T. 2011. “The geomechanical behaviour of peat foundations below rail-track structures.” PhD thesis, University of Saskatchewan.

Hendry, M.T., Sharma, J.S., Martin, C.D., and Barbour, S.L. 2012. “Effect of fibre content and structure on anisotropic elastic stiffness and shear strength of peat.” Canadian Geotechnical Journal, 49, p403–415.

Hendry, M.T., Martin, C.D., and Barbour, S.L. 2013. “The measurement of the cyclic 563 response of railway embankments and underlying soft peat foundations to heavy axle 564 loads.” Canadian Geotechnical Journal, 50(5), p467-480.

Hendry, M.T., Barbour, S.L., and Martin, C.D. 2014. “Evaluation of the effect of fibre reinforcement on the anisotropic undrained stiffness and strength of peat.” Journal of Geotechnical and Geoenvironmental Engineering, 140(9).

Jardine, R. J., Symes, M. J. and Burland, J. B. 1984. “The measurement of soil stiffness in the triaxial apparatus.” Geotechnique, 34 (3), p323-340.

Jardine, R. J., Fourie, A., Maswoswe, J. and Burland, J. B. 1985. “Field and laboratory measurements of soil stiffness.” In Proceedings of the eleventh international conference on soil mechanics and foundation engineering, San Francisco, CA, 12-16 August 1985.

Lew, K. V. 1981. “Yielding criteria and limit state in a Winnipeg clay.” M.Sc. Thesis, University of Manitoba, Winnipeg, MB.

Li, C. 2005. “Mechanical response of fiber-reinforced soil.” Ph.D. thesis, University of Texas at Austin, Austin, TX.

Maher, M.H., and Woods, R.D. 1990. “Dynamic response of sand reinforced with randomly distributed fibers.” Journal of Geotechnical Engineering, 116(7), https://doi.org/10.1061/(ASCE)0733-9410(1990)116:7(1116).

Maher, M.H., and Gray, D. H. 1990. “Static response of sand reinforced with randomly distributed fibers.” Journal of Geotechnical Engineering, 116(11), p1661-1677.

Maher, M.H., and Ho, Y.C. 1994. “Mechanical properties of kaolinite/fiber soil composite.” Journal of Geotechnical Engineering, 120(8), p1381-1393.

Michalowski, R.L., and Čermák, J. 2002. “Strength anisotropy of fiber-reinforced sand.” Computers and Geotechnics, 29(4), p279–299, doi: 10.1016/S0266-352X(01)00032-5.

Mirzababaei, M., Arulrajah, A., Haque, A., Nimbalkar, S. and Mohajerani, A. 2018. “Effect of fiber reinforcement on shear strength and void ratio of soft clay.” Geosynthetics International, 25(4), p471-480, doi:10.1680/jgein.18.00023.

Noonan, M. L. 1980. “Limit state studies in Winnipeg clays.” M.Sc. Thesis, University of Manitoba, Winnipeg, MB.

Palat, A., Hendry, M.T., and Roustaei, M. 2019. “Effect of fiber content on the mechanical behavior of fiber-reinforced clay.” In Proceedings of the 72nd Canadian Geotechnical Society Annual Conference, GeoStJohns 2019, St. John’s, NF, 29 September - 2 October 2019.

Roustaei, M., Eslami, A., and Ghazavi, M. 2015. “Effects of freeze–thaw cycles on a fiber-reinforced fine grained soil in relation to geotechnical parameters.” Cold Regions Science and Technology 120, p127-137.

Wood, D.M. 1990. Soil Behavior and Critical State Soil Mechanics, Cambridge University Press. ISBN 0-521-33249-4.

Zornberg, J.G. 2002. “Discrete framework for limit equilibrium analysis of fibre-reinforced soil.” Geotechnique, 52(8), p593–604.

Zornberg, J.G., and Li, C. 2003. “Design of fiber-reinforced soil.” In Proceedings of the Twelfth Panamerican Conference of Soil Mechanics and Geotechnical Engineering, Cambridge, MA, June 22-26, Vol. 2, pp. 2193-2200.

Zornberg, J. G., Cabral, A, R., and Viratjandr, C. 2004. “Behavior of tire shred- sand mixtures.” Canadian Geotechnical Journal, 41(2), p227-241.

Chapter Four: The effect of sample preparation method on the undrained behavior of fiber-reinforced clay

Contribution of the Ph.D. candidate

All work presented in this chapter has been carried out by the Ph.D. candidate., which includes review of the literature, preparation of testing specimens, design of the experimental program, execution of the experiments, analysis and discussion of the results and writing of the text.

As supervisor, Dr. M. T. Hendry has reviewed all parts of the work. This chapter will be submitted with the following citation:

Palat, A., and Hendry, M.T. (2022) 'The effect of sample preparation method on the undrained behavior of fiber-reinforced clay'.

Contribution of this chapter to the overall study

Considering the challenges encountered while preparing a fiber-reinforced clay soil using the compaction method and the restrictions for fibers to mobilize tension within the compacted samples (*Manuscript #1*), a new methodology is developed in this chapter to prepare fiber-reinforced clay soils for triaxial testing. A fiber-soil slurry is prepared by mixing the soil and fibers with a bulk volume of water. Samples for triaxial testing are later extracted by consolidating the slurry to the required confining pressure. This chapter further aims at investigating the specific objectives 2, 3, 4, and 5 outlined in the 'Introduction' section of this thesis. The role of method of sample preparations in influencing the behavior of fiber-reinforced clay soil is determined. A novel fiber-reinforced transparent soil is developed to visualize the orientation of fibers within the clays and track their movement during consolidation and compaction. The anisotropic properties of fiber-reinforced clay soil is analysed and the extent of cross-anisotropy exhibited by this composite is quantified.

Abstract

Reinforcing soil by adding distinct fibers is a means to enhance soil strength. This paper investigates the role of sample preparation method on the undrained behavior of fiber-reinforced clay soil. Samples of fiber-reinforced clay were prepared using two techniques: compacting to its optimum moisture content and hydraulic placement as a slurry. Both compacted and slurry samples were subjected to a program of consolidated undrained triaxial compression testing. All fiber-reinforced samples showed a tendency to bulge without a distinct shear plane, with a greater amount of bulging observed in slurry samples. This is attributed to the increased freedom of fibers in slurry samples to move and mobilize tensile stresses. A novel transparent fiber-reinforced clay soil was prepared to analyze the orientation of fibers within the compacted and slurry samples. The normalized probability distribution chart of fiber inclination confirmed the predominant fiber orientation is horizontal in slurry samples but random in samples prepared using the compaction method. The extent of anisotropy in the soil-fiber composites was evaluated using the measured pore pressure response during undrained loading. Slurry samples got stiffer in the horizontal direction during shearing due to the increased amount of tension mobilized in the horizontally oriented fibers. The value of the anisotropic pore pressure parameter, a, exceeded the limiting ranges proposed for a natural clay soil; hence, the equation developed for estimating the stiffness ratio is not applicable for this material. Slurry samples demonstrated a greater rate of increase in pore pressure during shearing compared to the compacted samples. The shear strength of a fiber-reinforced clay soil is a combination of the strength due to the interaction between clay particles, frictional interaction between the clay and fibers, and tensile strength mobilized in the fibers. The

limitations of traditional triaxial compression tests for predicting the strength of fiber-reinforced composites are also discussed.

4.1 Introduction

The advantages of adding randomly oriented discrete fibers to increase the strength and stability of a soil are well established (Maher and Woods, 1990; Gray and Ohashi, 1983; Maher and Ho, 1994; Zornberg, 2002; Zornberg and Li, 2003; Li, 2005). Maher and Ho (1994) investigated the mechanical properties of fiber-reinforced clay soil and determined that the inclusion of fibers increased the peak compressive strength and ductility of the composite. Zornberg (2002) proposed a discrete framework for the design of fiber-reinforced soil slopes, where the equivalent shear strength of fiber-reinforced soil is predicted by the independent characterization of soil and fiber properties. Li (2005) performed triaxial compression and extension tests on fiber-reinforced soil to evaluate the effect of soil type, soil density, and fiber orientation on the shear strength of the composite. Axial loading of fiber-reinforced clay soil results in an overall bulging with no evident failure plane (Freilich et al., 2010; Palat et al., 2019), which indicates an improvement in the ductility of the composite. Triaxial testing of fiber-reinforced soil has demonstrated that the fibers do not play a role in improving the geomechanical behavior of soil at lower values of axial strain and some amount of deformation is required to engage the fibers before the strengthening effect can be utilized (Kumar et al., 2006; Li, 2005; Palat et al., 2019). Fiber-reinforced clay soil can be used in several applications, such as evapotranspiration covers, oil sands mining reclamation including tailings ponds, low-permeability landfill liners, repair of failed slopes, reinforcing the subgrades of roads and highways, and increasing the stability of highway embankments. Even though many studies have been performed on fiber-reinforced sand, studies on fiber-reinforced clay soil are limited.

A few studies have been performed to investigate the orientation of randomly distributed discrete fibers within sand (Michalowski and Zhao, 1996; Michalowski and Cermak, 2002, 2003; Diambra et al., 2007; Ibrahim et al., 2012; Soriano et al., 2017). Michalowski and Cermak (2002) performed consolidated drained triaxial compression tests on sand reinforced with three different orientations of fibers (random, horizontal, vertical), with the greatest strength observed for samples reinforced with horizontal fibers. A fiber orientation distribution function was developed as a modelling tool to explain these anisotropic constitutive features of the reinforced samples when loaded. Extending this work, Michalowski and Cermak (2002) and Diambra et al. (2007) developed a procedure to determine the fiber distribution in reinforced sand samples. Even though extensive studies have focused on the orientation and distribution of fibers within sand, an analysis of the orientation of randomly distributed discrete fibers within a clay soil is still missing within the current body of literature.

According to Hendry (2011), there is a strong similarity between fiber-reinforced soils and peat, where the tensile stresses generated within the fibers cause an increase in the strength of the composite. Hence, the orientation of the fibers plays a crucial role and this reinforcing effect is maximized if the fibers are oriented with the axis/plane of fibers perpendicular to the direction of major principal stress. Several studies have evaluated the anisotropic load-deformation response and the extent of anisotropy exhibited by fibrous peat (Landva and Pheeney, 1980; Yamaguchi et al., 1985; Hendry et al., 2012, 2014). The anisotropic fabric nature was evident when vertical and horizontal samples of fibrous peat were tested under triaxial compression and extension conditions (Yamaguchi et al., 1985). The horizontal samples showed a larger effective angle of shearing resistance and undrained shear strength in the extension tests, while the vertical samples resulted in a higher shear strength in the compression tests. This indicates the stiffest response is observed when the major principal stress is perpendicular to the predominant orientation of fibers.

Transparent synthetic soils can be used to non-intrusively investigate properties such as internal soil deformation and are developed when a soil is saturated with a fluid of matched refractive index. The clarity of transparent soils depends on the perfect matching of the refractive indices of silica and pore fluid as well as the absence of entrapped air and impurities (Iskander et al., 2002). Fumed or amorphous silica powder along with several pore fluid combinations (e.g., white mineral oil and paraffinic solvent, calcium bromide and water) have been used to develop transparent clay soils (Iskander et al., 2002; Ni et al., 2010; Black and Take, 2015). Tests on silica powder confirmed the transparent amorphous silica has shear strength, consolidation, and permeability properties consistent with the macroscopic properties of many natural clays, but not any one clay in particular (Iskander et al., 2002).

In this study, samples of fiber-reinforced clay were prepared using two techniques: (1) compacting the composite to its optimum moisture content, and (2) hydraulic placement as a slurry followed by incremental loading. A novel transparent fiber-reinforced clay was also developed and this soil surrogate used to analyze the orientation of fibers within the fiber-reinforced clays prepared by the compaction and slurry methods. The influence of fiber orientation on cross-anisotropic stiffness, induced pore water pressure, mobilized fiber tension, and overall shear strength of the fiber-reinforced composites is analyzed. The limitation of the triaxial compression testing method in defining the strength of this class of materials is also discussed.

4.2 Materials and Methods

4.2.1 Materials

The clay soil adopted in this study is 'EPK Kaolin' manufactured by Edgar Minerals Inc. Kaolinite clay was selected for this study because it is a commonly available clay mineral. Laboratory testing of the clay soil gave a specific gravity of 2.45, liquid limit of 58%, plastic limit of 42%, and plasticity index value of 16%. Standard Proctor tests resulted in an optimum moisture content (OMC) of 28% and maximum dry density (MDD) of 1.5 g/cm3. The reinforcements used were pre-cut polypropylene (PP) fibers supplied by MiniFIBERS Inc. (Johnson City, TN, USA). Synthetic fibers were selected for this study because their properties are controllable and precut varieties can be easily procured from the manufacturer. Previous works by the authors (Palat et al., 2019; Palat and Hendry, 2021) demonstrate the optimum fiber content and length of PP fibers for mixing with kaolinite clay is 2% and 18 mm, respectively; consequently, these values are used for all tests reported in this paper. These PP fibers had a thickness of 0.035 mm, specific gravity of 0.91, tensile modulus of 0.4 GPa, and moisture absorption capacity less than 1%.

The transparent clay soil was developed using pyrogenic fumed silica (HDK® H20, Wacker Chemie AG, Germany) along with a combination of Purity FG white oil and Paraflex HT4 process oil (Petro Canada). The silica particles were less than 40 μm in size with a density of 2.2 g/cm3. The white oil and process oil had viscosities of 0.15 and 0.037 cm2/s and densities of 0.859 and 0.825 g/cm3, respectively. The silica powder to pore fluid ratio was kept constant at 6:94, and the volumetric proportion of the white oil to process oil was 77:23; these ratios were selected based on the previous studies conducted on transparent clay (Black and Take, 2015; Black, 2015) and considering the transparency of the prepared soil. Pre-cut TenCate - Mirafi RS580i woven geotextiles (made from PP fibers) were used in place of cut PP fibers to reinforce the transparent clay and prevent the colour from PP fibers mixing with the transparent soil.

4.2.2 Sample Preparation

4.2.2.1 Slurry Method

Unreinforced clay samples were prepared by mixing the dry kaolinite clay powder with distilled water using an all-purpose wire whip mixer to form a slurry. The amount of water used was approximately 2.5 times the liquid limit of clay soil (~145 mL). This large quantity of water is required to avoid lumps in the clay soil and ensure the slurry has a flowing consistency. A mixing time of 10 min was sufficient to obtain a homogenous slurry. After mixing, the slurry was slowly poured into a cylindrical mold (150 mm diameter × 700 mm high) in layers to avoid the introduction of any air bubbles. Care was also taken to ensure no segregation while pouring the slurry. The slurry was allowed to self consolidate for 2 weeks at room temperature under the conditions of double drainage, followed by the application of incremental axial load up to a consolidation pressure of 100 kPa. This consolidation pressure was sufficient to obtain cylindrical samples of fiber-reinforced soil for triaxial testing. The block samples were then removed from the mold, covered with cling film, and stored in a moisture room until further testing. This procedure was also adopted for preparing fiber-reinforced slurry samples, the only difference being that the dry kaolinite clay was initially mixed with PP fibers before adding water to avoid the entangling of fibers in the blades of the mixer.

A hollow round steel tube (50 mm diameter ×100 mm long) was pushed into the resulting blocks to obtain samples for triaxial testing. The fibers in the slurry showed a tendency to get carried along and the steel tubes often came out of the block partially filled. A similar behavior was also observed while obtaining Shelby tube sample of peat samples from the site, and this is hypothesized to be caused by the tension developed in the entangled fibers at the base of the sample, the low amount of horizontal stress, and the friction on the inner surface of the Shelby tubes (Hendry et al., 2014). To avoid this behavior, the walls of the steel tube were filed further to make them thin and the inside and outside of the tubes were oiled prior to pushing into the slurry. These procedures ensured the length of the tube samples was consistent with the distance to which the tube was pushed into the slurry. Figure 4.1b shows a slurry-prepared fiber-reinforced clay soil reinforced with 18-mm PP fibers.

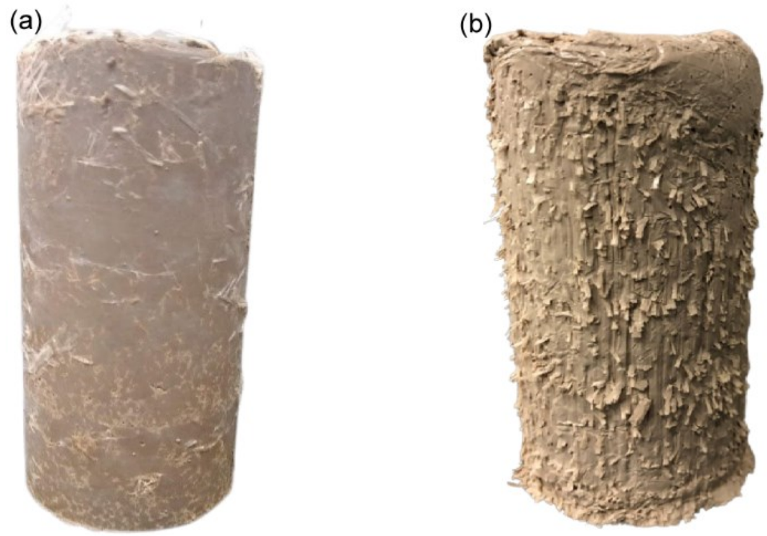

Figure 4.1. Fiber-reinforced samples prepared using the (a) compaction method and (b) slurry method.

The transparent clay slurry was prepared by mixing the white oil and process oil using a hand-held food mixer. Fumed silica powder (6% by weight of the total pore fluid combination) was added to this pore fluid mix and vigorously mixed until a transparent gel formed. The silica-pore fluid mixture was then transferred to a vacuum chamber to de-air the solution, which took between 7 and 9 d. This de-aired mix was then transferred to a glass cylindrical mold and cut geotextiles (2% by weight) were added. Consistent with that described above, this slurry was then allowed to self consolidate for 2 weeks after which a consolidation pressure of 100 kPa was applied. One of the most challenging aspects of this study was to maintain the transparency of the slurry throughout the testing process (Fig. 4.2a, b). The entire testing procedure was conducted in a temperature-controlled room to prevent temperature variations from affecting the transparency. Figure 4.3a shows a geotextile-reinforced transparent clay slurry prepared as a part of this testing process.

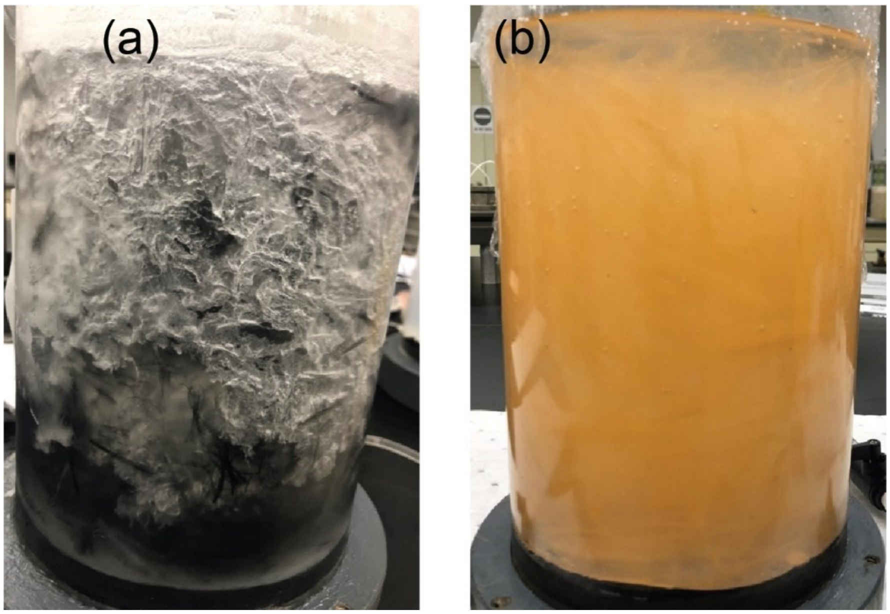

Figure 4.2. Challenges encountered during the preparation of fiber-reinforced transparent soil: (a) intrusion of air bubbles, (b) color from the synthetic fibers mixing with the transparent soil.

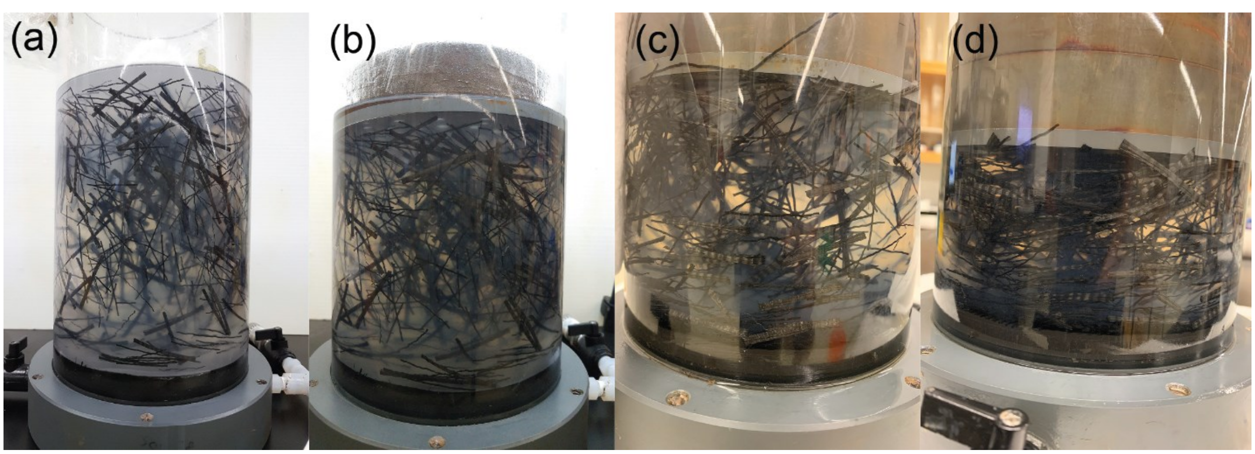

Figure 4.3. Continuous images tracking the consolidation of fiber-reinforced transparent soil slurry captured on day: (a) 1, (b) 20, (c) 30, and (d) 40.

4.2.2.2 Compaction method

Compacted PP fiber-reinforced clay samples were prepared as two lots. Lot 1 was prepared by mixing half of the soil and half of the water using a mixer. Lot 2 was prepared by mixing the remaining half of the soil and water and all of the PP fibers using the same mixer. Lot 1 and 2 were subsequently mixed by hand. The clay-fiber mix was then placed in a split mold, 50 mm in diameter × 100 mm high, as five equal layers, each followed by subsequent compaction. A mechanical press was used to compact all samples and the number of blows was restricted to 15 per layer. The detailed method of preparing compacted fiber-reinforced clay samples and the challenges during sample preparation are discussed in previous works by the authors (Palat et al., 2019; Palat and Hendry, 2021). Figure 4.1(a) shows a clay soil reinforced with 18-mm PP fibers and prepared by the above-mentioned method. The same method was used to prepare compacted samples of transparent soil (Fig. 4.4a).

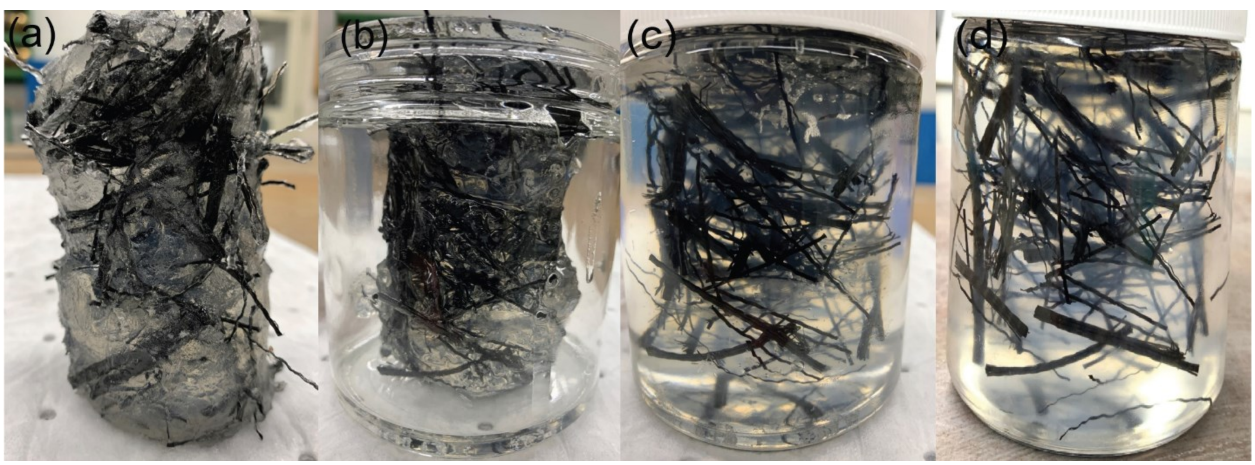

Figure 4.4. Series of steps followed for detecting the orientation of fibers in a compacted fiber-reinforced transparent soil: (a) compacted fiber-reinforced transparent soil prepared, (b) specimen placed in a glass beaker, (c) specimen saturated by pouring a pore fluid combination of matching refractive index from the top, and (d) final image detecting the orientation of fibers within the compacted sample.

4.2.3 Testing Method

Consolidated undrained (CU) triaxial compression tests were performed on samples of fiber-reinforced clay to measure the undrained shear strength and induced pore water pressure developed within the composite. A Humboldt HM-5020 load frame with a capacity of 15 kN was used to perform the tests in accordance with ASTM D4767-11 (2020). Prior to testing, the samples were saturated until a Skempton's B value greater than 0.97 was achieved. The pore water pressure developed within the specimens was measured by connecting a transducer at the base of the cell. Specimens were then consolidated by keeping the difference between cell pressure and back pressure equal to the desired effective stress. Following consolidation, shearing was initiated on the samples, with the rate determined based on ASTM standards: 4% divided by 10 times the time required for 50% of primary consolidation. The axial load was measured by a load cell (Model 75/1508, Sensotec) with a capacity of 4.5 kN and an accuracy of 0.14%. The vertical displacement of the sample was measured using a linear potentiometer (LP) (Model TR-50, Novotechnik) with a maximum travel length of 50 mm, linearity of ± 0.075%, and repeatability of ± 0.002 mm. Small strain on-sample transducers were not employed and this limits the ability of the test results to interpret soil behavior at strains less than 0.5% (Jardine et al., 1985). However, previous studies on fiber-reinforced clay soil by Li (2005) and Palat et al. (2019) show the loads resisted by fibers are only substantial at higher strain levels. The testing was continued until an axial strain of 20% was obtained.

During consolidation of the geotextile-reinforced transparent soil slurry, continuous images were taken with a Canon EOS Rebel T7i digital camera that was triggered every 30 min using the EOS utility software. The images were then processed to track the movement of fibers during the slurry consolidation. A study was performed to quantify the orientation of fibers within the soil samples when prepared using both techniques. Using the polyline angle measurement tool in MATLAB, the inclination of each line in the image was determined by clicking and dragging three polyline vertices. A probability distribution chart was then developed to compare the fiber orientation for samples prepared using each of the two methods. This probability distribution chart was later normalized with the area of the region of interest (Fig. 4.7).

Compacted and slurry samples of kaolinite clay soil reinforced with PP fibers were tested for three values of effective confining stresses (p'_o): 50, 100, and 200 kPa. For the transparent soil, the entire procedure of tracking the fiber orientation during consolidation and compaction was repeated twice to confirm the validity of the testing process.

4.3 Presentation of Results

Figures 4.3a-d track the fiber movement at different intervals during the consolidation of the geotextile-reinforced transparent clay slurry. The fibers were initially oriented randomly when the slurry was poured into the glass mold (Fig. 4.3a). As the soil consolidated on its self-weight, some of the fibers realigned in the horizontal direction. Further, when the slurry was subjected to incremental loading from the top, up to a consolidation pressure of 100 kPa, the majority of the fibers tended to align in the horizontal direction (Fig. 4.3d).

Figure 4.4a shows a compacted geotextile-reinforced transparent soil prepared using the compaction method. Visual observation of the fibers from this specimen was challenging due to the presence of air, which affected the transparency of the specimen. To accentuate the fibers within the sample, the prepared composite was placed in a glass mold (Fig. 4.4b) and a pore fluid combination of matching refractive index was poured from the top (Fig. 4.4c) to saturate the specimen. Figure 4.4d is the final image showing the fiber orientation.

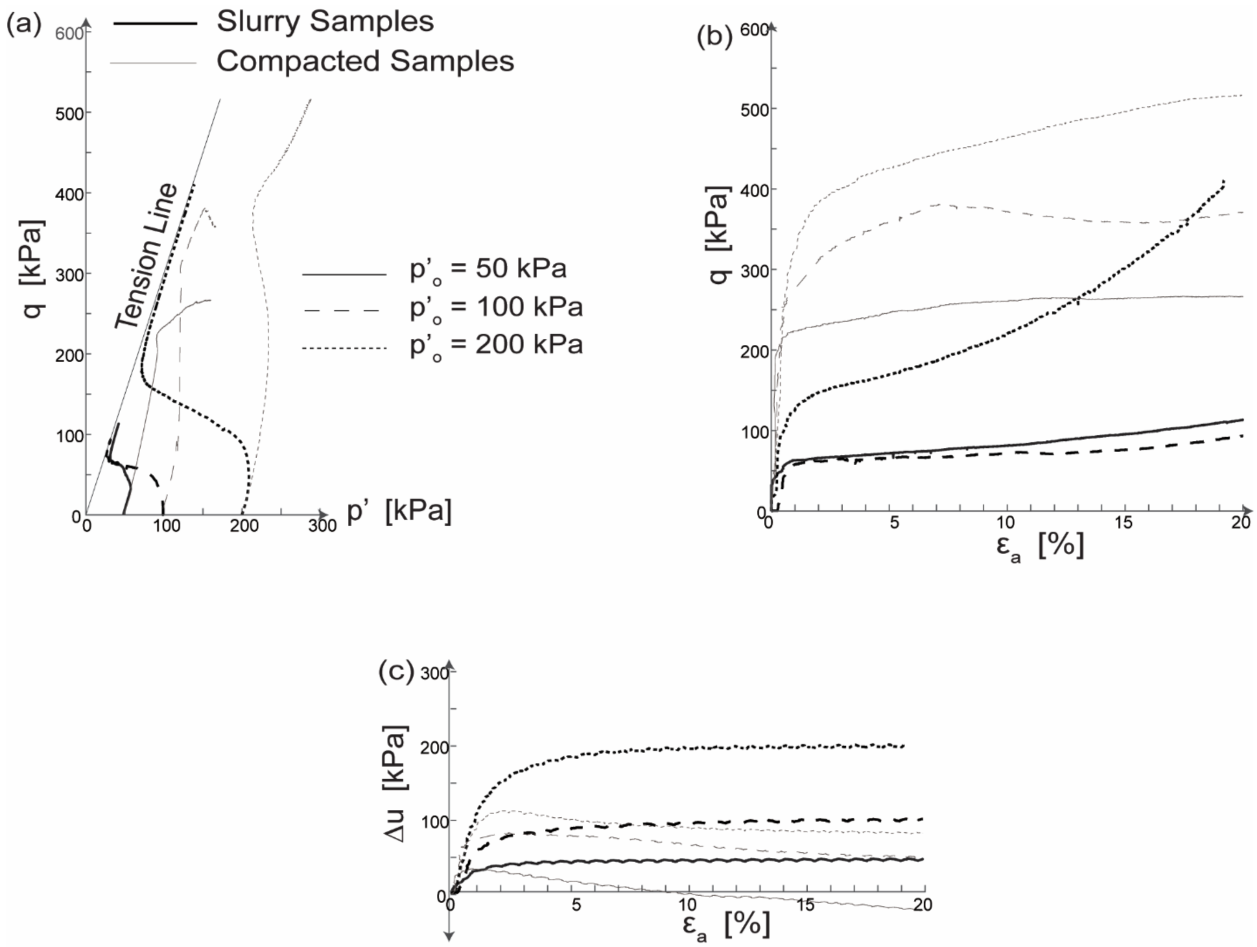

Figure 4.5. Comparison of CU laboratory testing results from compacted and slurry-prepared kaolinite soil specimens reinforced with 18-mm fibers (fiber content: 2%; fiber type: PP) presented in (a) q versus p' space, (b) q versus ε_a space, and (c) Δu versus ε_a space at three values of p'_o.

Figure 4.5 shows the CU triaxial test results for the clay soil reinforced with PP fibers (fiber content: 2%, fiber length: 18 mm) and tested at three values of p'_o. The results are presented in terms of effective stress path (ESP) in deviator stress (q) versus mean effective stress (p') space, q versus axial strain (ε_a), and excess pore water pressure (Δu) versus ε_a. The data in Figure 4.5a indicates an increase in q is accompanied by an increase in p' in the $q - p'$ stress space for all compacted fiber-reinforced samples. Nevertheless, the ESP shows a greater tendency to shift to the left for slurry-prepared specimens, which is due to the increased Δu developed in these samples that leads to a reduction in the p' value. The ESP values of the slurry samples followed the shape of the tension cut-off (TC) line (3:1 slope) at the end of shearing. A similar response was also reported during CU triaxial tests on samples of fibrous peat (Hendry et al., 2012); the potential reasons for this behavior are discussed in a subsequent section. Plots of q versus ε_a for the fiber-reinforced samples (Fig. 4.5b) indicate the initial linear behavior is followed by a strain hardening response, which is expected due to the tension mobilized in the fibers. No visible failure was observed in the fiber-reinforced specimens and the testing was stopped due to excessive axial compression of the specimens (ε_a of 20%). Plots of Δu versus ε_a (Fig. 4.5c) show that, for all compacted specimens, Δu approaches the maximum value (Δu_{max}) at lower values of ε_a followed by a steep reduction. The slurry-prepared samples demonstrate a greater rate of increase of Δu with ε_a, which then remained unchanged after Δu_{max} is attained.

4.4 Discussions

All samples of unreinforced clay failed by forming a well-defined failure plane. The fiber-reinforced specimens showed a tendency to bulge without an evident failure plane when tested up to an ε_a of 20%. This behavior is expected due to the movement of fibers to the potential planes of weakness and mobilization of tensile stresses in them (Palat et al., 2019). Slurry samples (Fig. 4.6b) demonstrated greater bulging compared to the compacted samples (Fig. 4.6a) after failure. When prepared using the slurry technique, there is greater freedom for the fibers to move and mobilize tension in them; in contrast, the higher compaction energy applied during the compaction process suppresses the fibers and they require a substantial amount of ε_a to align perpendicular to the major principal stress and mobilize tension. The authors postulate that the greater amount of bulging observed in fiber-reinforced slurry samples at 20% ε_a could be an indication of the increased tension mobilized in the fibers during shearing.

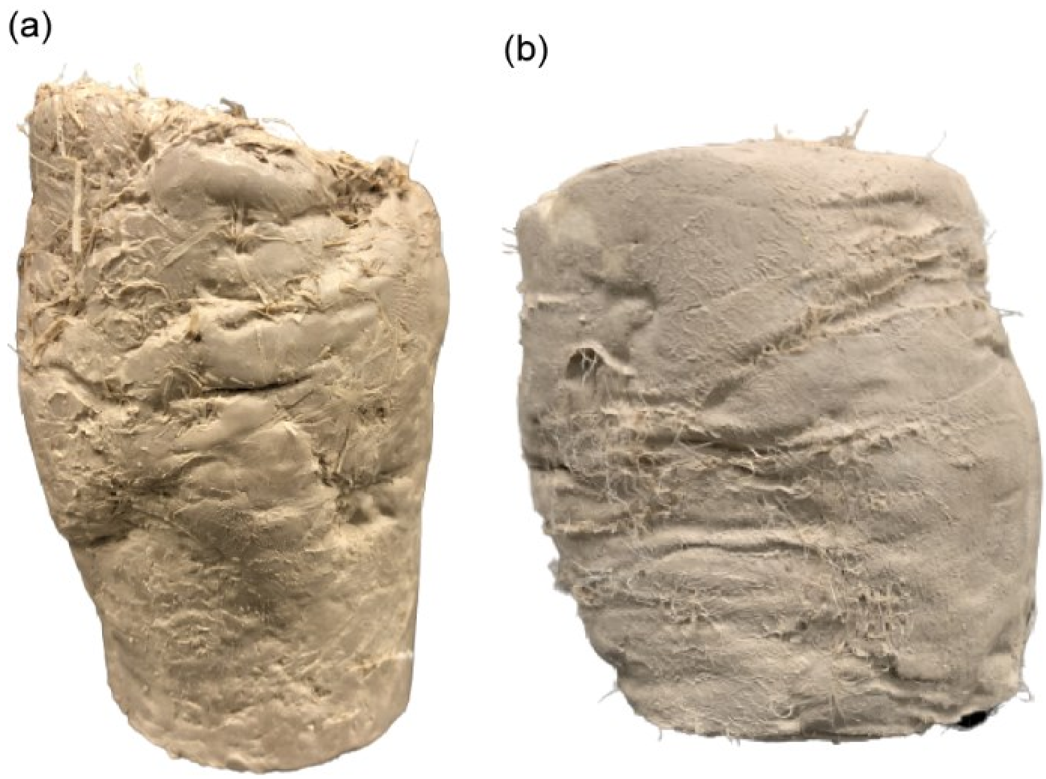

Figure 4.6. Fiber-reinforced samples after failure when prepared using the (a) compaction method and (b) slurry method.

All samples demonstrated an increase in q and Δu with an increase in p'_o. This could be due to the tighter packing of the particles and greater interaction between the clay particles and fibers at higher values of p'_o. In addition, the amount of tension mobilized in the fibers also increases with an increase in p'_o, resulting in an additional increase in the q and Δu values.

4.4.1 Determination of fiber orientation

Visual examination of the consolidated transparent slurry (Fig. 4.3d) and the compacted transparent soil (Fig. 4.4d) shows the fibers are aligned in the horizontal direction at the end of consolidation in the slurry method but in random directions when prepared using the compaction method. The normalized probability distribution chart (Fig. 4.7) indicates that, in a compacted fiber-reinforced specimen, the fibers are inclined at angles varying from 0 to 90° relative to horizontal with a greater likelihood of having fibers inclined at 45° relative to horizontal. However, in slurry samples, the fiber inclination varies from 0 to 40° with a greater probability of having fibers aligned at 20° relative to horizontal. This shift in the normalized probability distribution chart to the left in slurry samples confirms the majority of the fibers are oriented in the horizontal direction using the slurry method but are distributed in random orientation using the compaction method.

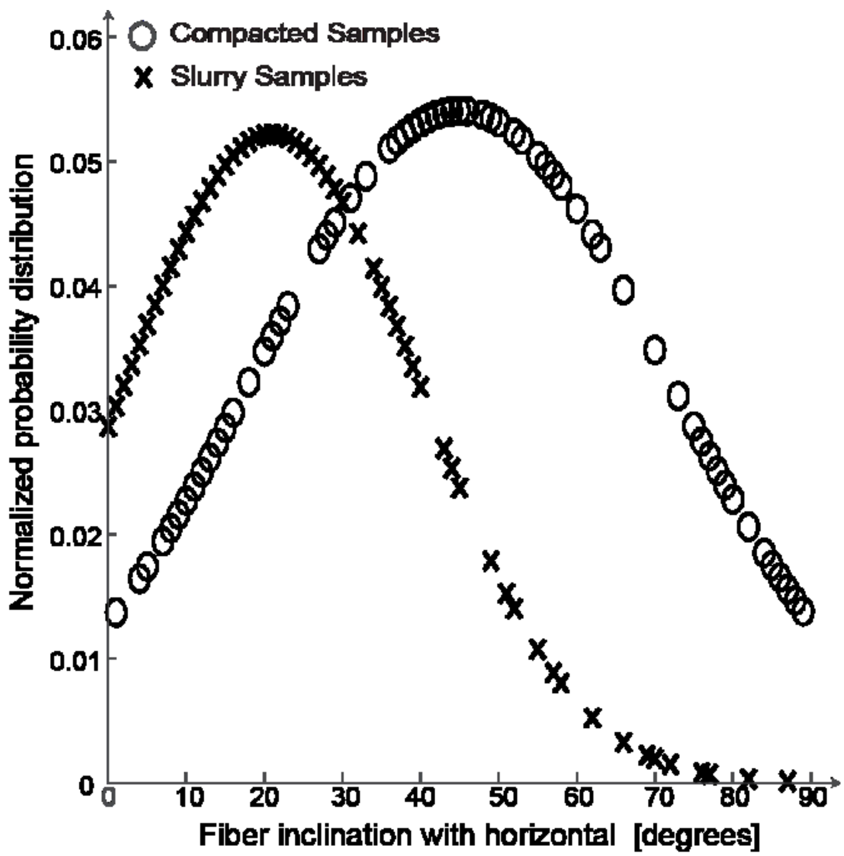

Figure 4.7. Normalized probability distribution of the inclination of fibers with horizontal in compacted and slurry samples.

Previous analyses of the orientation of discrete fibers in fiber-reinforced sand demonstrated a preferred near-horizontal orientation for the fibers. Diambra et al. (2007) analyzed fiber orientation by freezing and cutting the sample followed by visual examination. Their results demonstrated that, of the total amount of fibers mixed with the sand soil, 97% had an orientation that lies within $\pm\ \frac{\pi}{4}$ of the horizontal plane due to the compaction technique used for preparing sand-fiber specimens. However, this method of freezing and cutting the specimen is not applicable for smaller diameter fibrillated fibers as well as for fiber contents > 0.25% (Diambra et al., 2007).

The authors also attempted to use the technique of Computed Tomography (CT) scanning for detecting the fiber orientation in slurry and compacted samples. The soil acted as a very effective shield against X-Ray photons and a little signal penetrated the samples for detection. Besides the fibers had a difficulty in interacting with the X-ray energy making them invisible in the scanned slices. Accordingly, this technique of developing a fiber-reinforced transparent soil is recommended as one of the realizable options for analyzing the fiber orientation in slurry and compacted fiber-reinforced specimens.

4.4.2 Undrained anisotropic response of fiber-reinforced clay

The undrained anisotropic response of fiber-reinforced clay soil was characterized using the measured pore water pressure response resulting from undrained loading. In a CU triaxial test, any increment in the external, total stresses ($\mathit{\Delta} p$ and $\mathit{\Delta} q$) leads to a corresponding change in the effective stresses $\Delta p'$ and $\mathit{\Delta} q$, such that the condition of undrained constant volume is maintained. This change in the mean effective stress $\Delta p'$ is a material response to the change in distortional stress $\mathit{\Delta} q$ (Wood 1990). Hence,

$$\Delta u = \Delta p + a\, \Delta q \,, \tag{4.1}$$

$$\Delta p' = -a\, \Delta q \,, \tag{4.2}$$

The change in pore pressure ($\mathit{\Delta} u$) is linked to the change in the total stresses ($\mathit{\Delta} p$ and $\mathit{\Delta} q$) through a pore pressure parameter a (Eq. 4.1) and the slope of the undrained ESP is equal to $\frac{-1}{a}$ (Eq. 4.2). The response of an isotropic elastic soil specimen subjected to a general triaxial change of effective stress can be expressed using the shear modulus and bulk modulus as in Eq. 4.3.

$$\begin{bmatrix} \Delta\varepsilon_p \\ \Delta\varepsilon_q \end{bmatrix} = \begin{bmatrix} 1/K' & 0 \\ 0 & 1/3G' \end{bmatrix} \begin{bmatrix} \Delta p' \\ \Delta q \end{bmatrix}, \tag{4.3}$$

The off-diagonal zeroes indicate the absence of coupling between volumetric and distortional effects for an isotropic elastic material. A change in mean effective stress (p') produces no distortion ($\delta\varepsilon_q$) and a change in the distortional deviator stress (q) produces no change in volume ($\delta\varepsilon_p$). The condition of zero volumetric strain during the shearing stage of a CU test results in a constant value for the mean effective stress ($\Delta p'$ = 0). The pore pressure developed within the specimen is only a function of the change in the total mean stress (Δp) and the value of a in Eq. 4.1 is zero. Hence, the undrained ESP for an isotropic linear elastic material tends to be vertical (Wood 1990). If the slope of the undrained ESP is positive with a negative a value, this implies an expanding soil that develops negative pore water pressure. For such soils, the Young's modulus in the vertical direction (E_V) is greater than in the horizontal direction (E_H). Similarly, if the slope of the undrained ESP is negative with a positive a value, this implies a contractive soil developing positive pore water pressure with E_H greater than E_V (Hendry et al., 2012). Graham and Houlsby (1983) provide a means to estimate the stiffness ratio $\left(\frac{E_H}{E_V}\right)$ from the slope of the undrained ESP represented by a:

$$a = -\frac{\Delta p'}{\Delta q} = -\frac{2\,(1 - \vartheta^* + \alpha\vartheta^* - \alpha^2)}{3\,(2 - 2\vartheta^* - 4\alpha\vartheta^* + \alpha^2)}, \tag{4.4}$$

where $\alpha^2 = \frac{E_H}{E_V}$ is the cross anisotropy parameter and ϑ^* is a modified Poisson's ratio (Graham and Houlsby, 1983). For a natural clay soil, the value of a spans between $-\frac{1}{3}$ $(E_V \gg E_H)$ and $\frac{2}{3}$ $(E_V \ll E_H)$ (Wood, 1990).

In this paper, the undrained ESPs of fiber-reinforced clay samples (Fig. 4.5a) are evaluated in light of cross-anisotropic elastic behaviour in terms of the pore-water pressure parameter a. Figure 4.8 plots the variation of a with ε_a for slurry and compacted fiber-reinforced samples at three values of p'_o. The secant a values for the fiber-reinforced samples are calculated based on the deviation of the different sections of ESP from vertical (using Eq. 4.2) and plotted against the corresponding value of ε_a.

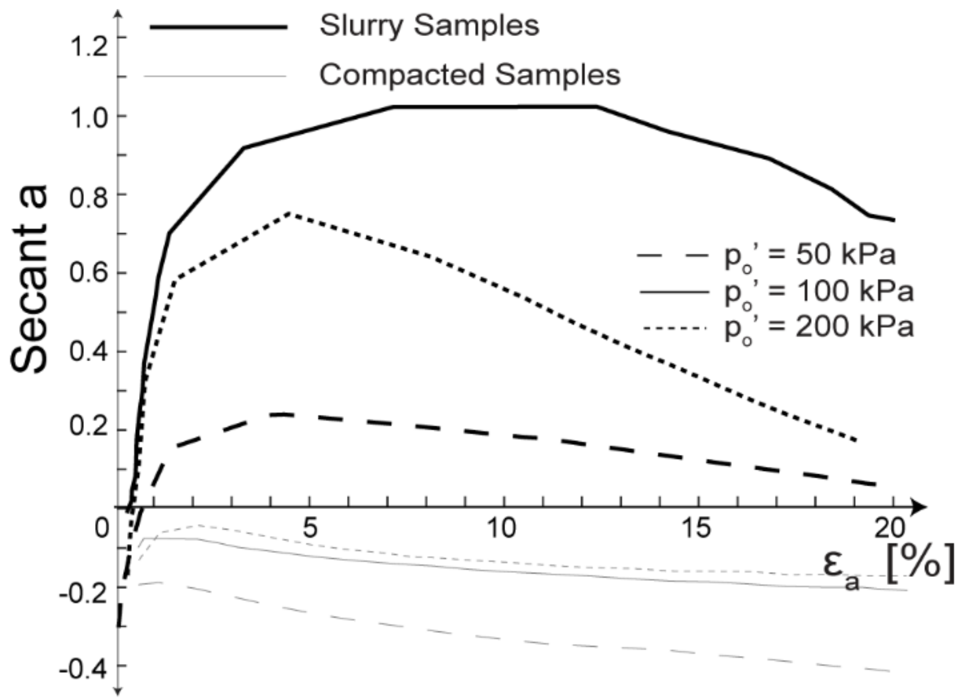

Figure 4.8. Variation of the pore pressure parameter a with ε_a for compacted and slurry-prepared fiber-reinforced clay samples at three values of p_o'.

For all slurry-prepared fiber-reinforced samples, the value of a becomes positive at an ε_a value of less than 1%. The studies on transparent fiber-reinforced clay demonstrate that, when soil samples are prepared using the slurry method, the predominant orientation of fibers is horizontal (Figs. 4.3d and 4.7). Once cylindrical samples are extracted from this slurry using Shelby tubes, the fibers are aligned in the horizontal orientation. For fiber-reinforced soils, the stiffest response is observed when the major principal stress is perpendicular to the predominant orientation of fibers (Yamaguchi et al., 1985). In a triaxial compression test, the major principal stress is vertical and the stiffest response is observed for samples reinforced with horizontal fibers. Consequently, tensile stresses start mobilizing in the fibers as soon as the samples are subjected to shearing, increasing the overall horizontal stiffness of the composite. A similar behavior was also observed in Shelby tube samples of fibrous peat; the *in situ* cross-anisotropic structure was due to the tension mobilized in the fibers resulting in an increased E_H over E_V (Hendry et al., 2012).

The a value for the slurry-prepared fiber-reinforced clay ranges between $-⅓$ and 1 with the maximum value observed at a p'_o of 100 kPa. This observed maximum value of a exceeds the limiting range proposed for a natural clay soil by Graham and Houlsby (1983) and Wood (1990). The deviation from the past literature is attributed to the increased amount of tension mobilized in the fibers during the shearing phase of a triaxial test. The increased tensile stresses in the fibers increase the overall horizontal stiffness of the composite ($E_H \gg E_V$) as well as the a value beyond the previous values stated for a natural clay soil. Accordingly, the equations developed for estimating the stiffness ratio (Eq. 4.4) are not applicable for this class of material.

The a value in the compacted fiber-reinforced clay varied from $-\frac{1}{2}$ to $-\frac{1}{25}$ and remains negative through the shearing stage. Figures 4.4d and 4.7 confirm that, when fiber-reinforced clay soil is prepared using the compaction method, the fibers are oriented in horizontal, vertical, and random orientations, with the majority inclined at an angle of 45° relative to horizontal. It requires a significant amount of ε_a for the fibers to reorient to the horizontal direction (perpendicular to the major principal stress) and mobilize tension therein. This subsequently limits the overall horizontal stiffness of the compacted fiber-reinforced samples.

4.4.3 Effect on induced pore water pressure

Figure 4.5c shows the influence of sample preparation techniques on the pore water pressure developed within the fiber-reinforced clay samples. For compacted samples, Δu approaches the maximum value (Δu_{max}) at lower values of ε_a followed by a steep reduction at all values of p'_o. This heavily overconsolidated behavior in compacted samples is due to the higher compaction energy supplied during sample preparation process.

In contrast, the slurry samples demonstrated a greater rate of increase of Δu with ε_a. The Δu values developed at the end of shearing are equal to the p'_o at which the sample is sheared, and then remain unchanged after the attainment of Δu_{max}. This behavior of the slurry samples is attributed to the increased amount of tension mobilized in the fibers, resulting in an increase in the induced pore water pressure developed within the fiber-reinforced samples. Once the value of Δu is equal to the applied p'_o , the minor effective principal stress (σ'_3) is zero and the ESP approaches the TC line. This behavior is similar to that observed in fibrous peat specimens (Hendry et al., 2012). The absence of failure in the fiber-reinforced samples indicates the increase in q during strain hardening is solely due to the tension mobilized in the fibers (Hendry et al., 2012).

4.4.4 Shear strength of fiber-reinforced samples

The shear strength of a fiber-reinforced soil is the sum of three components, namely the strength developed due to the: (1) interaction between clay particles, (2) interphase friction between clay particles and fibers, and (3) tension mobilized in the fibers. The geomechanical behavior of fiber-reinforced clay samples shares many similarities with that observed in fibrous peat specimens. For both composites, plastic yielding occurs without the development of a failure plane and the stress-strain response shows a gradual transition to a linear strain hardening beyond the initial linear elastic behavior. In addition, the slope of the strain hardening response is strongly dependent on the p'_o at which the specimens are sheared. Using the conceptual model developed for fibrous peat specimens by Hendry et al. (2012), it can be hypothesized that the transition to linear strain hardening response is indicative of the shear strength associated with frictional interactions, and the linear increase in q during strain hardening is the result of the additional shear resistance due to fiber tension. Furthermore, their subsequent paper (Hendry et al., 2014) states that the frictional strength is a fundamental property of the surface of the fibers and particles, whereas the fiber-reinforcement component is dependent on the fiber content, fiber aspect ratio, and fiber orientation with respect to the principal stresses.

Attempts have been made in this paper to quantify the effect of fiber reinforcement on the overall shear strength of the soil-fiber composite. The results indicate the fibers are highly influential when tested at higher values of p'_o. Figure 4.9 plots the ESP, q versus ε_a and Δu versus ε_a for unreinforced and fiber-reinforced samples (compacted and slurry) at a p'_o of 200 kPa. In general, the samples prepared using the slurry technique returned a lower value of q compared to those using the compaction method for a given value of p'_o. In the compaction method, the fiber-reinforced composites are prepared at a water content ranging from 27 – 29% and density values ranging from 1.7 to 2.0 g/cm^3. The water content of the slurry samples after consolidation was between 43 – 46.5%, with density values ranging from 1.4 to 1.62 g/cm^3. The higher density values of compacted samples suggest the clay particles and fibers are tightly packed when prepared using the compaction technique compared to the slurry method. In addition, the compacted samples demonstrated a quasi-overconsolidated behavior due to this higher compaction energy supplied during sample preparation. The authors speculate the tight packing, higher density, and overconsolidation would have contributed to the higher q in the compacted vs. slurry samples.

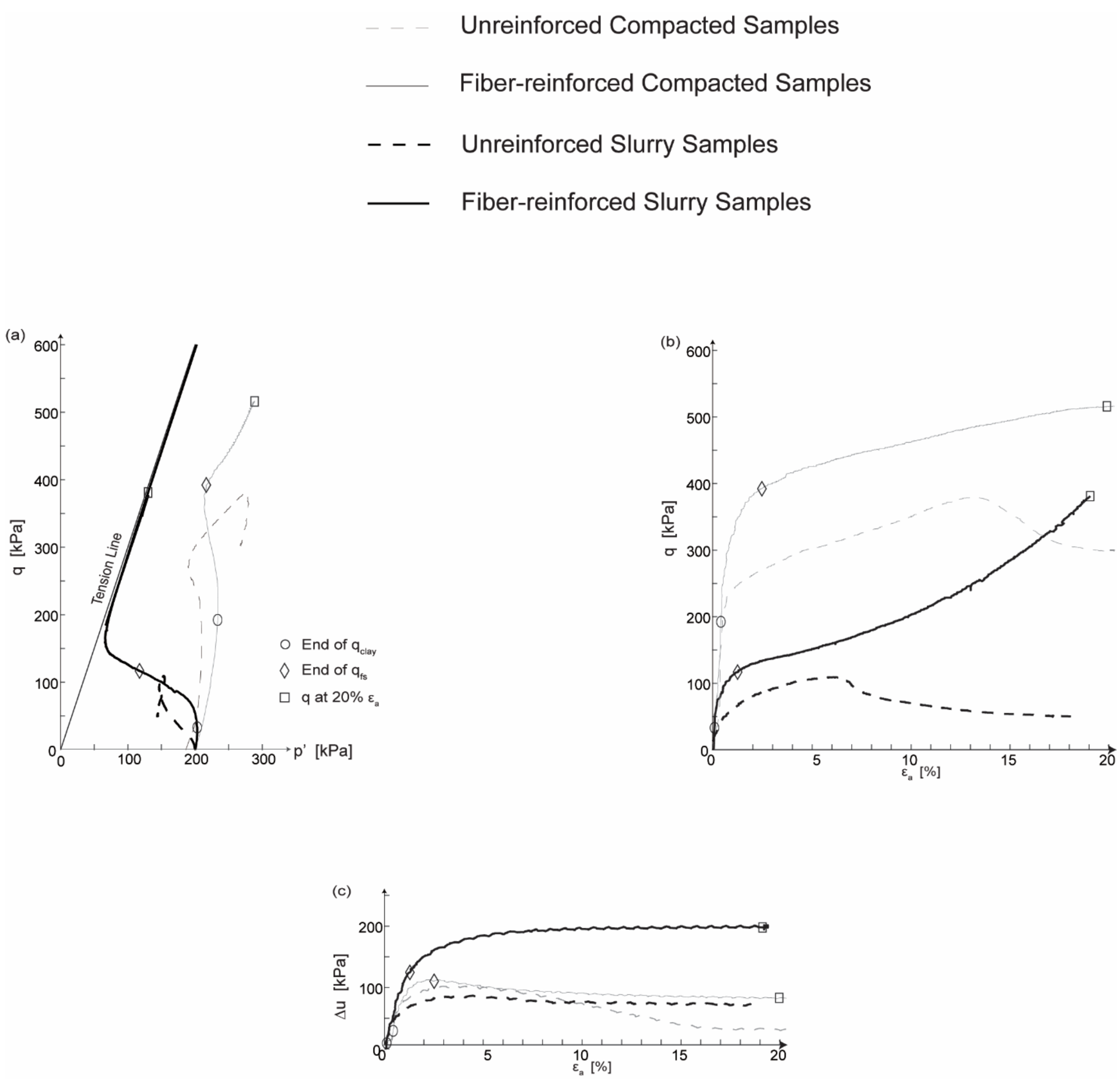

Figure 4.9. Comparison of CU laboratory testing results for unreinforced and fiber-reinforced (fiber content: 2%; fiber type: PP; fiber length: 18 mm) compacted and slurry-prepared specimens tested at a p'_o of 200 kPa presented in (a) q versus p' space, (b) q versus ε_a space, and (c) Δu versus ε_a space.

The initial portion of the q versus ε_a curves are similar for both unreinforced and fiber-reinforced composites (Fig. 4.9b). This indicates any initial increase observed in q is only due to the interaction between clay particles (q_{clay}), and some amount of ε_a is required to engage the fibers (Palat et al., 2019). From the q - ε_a plots of the unreinforced clay, the q_{clay} is estimated at 29 kPa in the slurry samples and 192.3 kPa in the compacted samples. The higher interaction between the clay particles when prepared using the compaction method is due to the tight packing and higher density of the compacted specimens.

The transition to linear strain hardening is indicative of the shear strength, attributed to frictional interaction between clay particles and fibers. The value of q derived from frictional interactions (q_{fs}) is 87.7 kPa in slurry samples and 136.8 kPa in compacted samples. As the fiber type is the same in both cases (resulting in same interface shear strength between fibers and clay), this increase in q in the compacted samples is associated with their tight packing and higher density.

The slope of the strain hardening portion of the q - ε_a curve is indicative of the tensile stress mobilized in the fibers when sheared up to 20% ε_a. The contribution of mobilized fiber tension to the overall shear strength ($q_{tension}$) is 264.3 kPa in slurry samples and 123.8 kPa in compacted samples. The contribution of fiber tension to the overall shear strength doubles when samples are prepared using the slurry method. As the fiber content and aspect ratio are the same, this increase in the fiber reinforcement component in the slurry samples is attributed to the difference in the orientation of fibers with respect to the principal stresses (i.e., more are aligned in the horizontal direction in the slurry samples). The overall contribution of a randomly oriented fiber reinforced composite is less than the soil reinforced with horizontal fibers of same concentration (Michalowski and Cermak, 2002). The random orientation of the fibers in compacted samples limits the potential for the fibers to mobilize tensile stresses and contribute to the shear strength of the composite.

To summarize, any initial increase in q observed at lower values of $\varepsilon_a < 1\%$ is due to the interaction between clay particles (q_{clay}). The q_{clay} depends on the dry density and water content of the prepared samples as well as the p'_o at which the sample is sheared. The transition from initial elastic to the linear strain hardening response is due to the frictional interactions between the clay particles and fibers (q_{fs}). This increase in the deviator stress due to the frictional interaction (q_{fs}) is a function of the interphase shear strength between the fibers and clay particles, p'_o, dry density, and water content of the composite. Any further increase in q characterized by the slope of the strain hardening is an estimation of the tensile stresses mobilized in the fibers. The contribution of fiber tension to the overall shear strength ($q_{tension}$) is primarily dependent on the orientation of fibers with respect to the principal stresses. The value of $q_{tension}$ is maximized when the predominant fiber orientation is perpendicular to the major principal stress. The value of $q_{tension}$ is also dependent on the fiber content, fiber length, and the p'_o at which the sample is sheared.

4.4.5 Limitations of the testing method

The amount of tension mobilized in the fibers increases when samples are prepared using the slurry method compared to the compaction method. This is associated with the predominant horizontal orientation of fibers in slurry samples. The increase in fiber tension is further supported by an increase in the Δu value as well as the deviation of the ESP to the left, indicating an increase in the overall E_H. The ESP shifts to the left, approaches the TC line, and later follows this line (Fig. 4.5a). The TC line defines a limiting condition in the triaxial compression test at which the soil is supposed to carry the condition of zero effective radial stress (Wood, 1990). Any stress state in excess of this line is solely due to the tension mobilized in the fibers. Once the ESP for slurry-prepared fiber-reinforced samples approaches the TC line, Δu is equal to the applied p'_o and the minor effective principal stress (σ'_3) is zero. For the Δu to increase beyond this value, the condition of $\sigma'_3 < 0$ ($\Delta u > \sigma_3 = \sigma_{cell}$) must be satisfied; however, this is not possible by performing an undrained triaxial compression test. This curtails the ability of fibers to mobilize the maximum amount of tension, which subsequently limits the shear strength measured from the triaxial compression testing method.

Furthermore, all samples of fiber-reinforced clay exhibited a linear strain hardening behavior without a peak shear stress that can be considered as the strength of the composite. These findings further stress the limitation of triaxial compression tests to define the shear strength of fiber-reinforced clay samples when tested at p_o' values ≤ 200 kPa.

4.5 Conclusions

The research presented in this chapter investigated the role of sample preparation techniques in altering the undrained behavior of a fiber-reinforced clay soil. Specifically, the compaction method and hydraulic-based slurry method were evaluated in terms of their influence on the cross-anisotropic stiffness, induced pore water pressure, and undrained shear strength of soil-fiber composites. A novel transparent fiber-reinforced clay soil was developed and used to analyze the fiber orientation in the prepared composites. The major observations from this study are summarized below:

- All samples of fiber-reinforced clay exhibited a strain hardening behavior and bulging response (with no evidence of failure plane) when tested up to 20% ε_a. Slurry samples showed a greater amount of bulging compared to compacted samples. This increased bulging could be due to the greater freedom for the fibers to move and mobilize tension when prepared using the slurry method.

- Examination of transparent fiber-reinforced clays confirmed the predominant fiber orientation is horizontal in samples prepared using the slurry method and is random in samples prepared using the compaction method. The normalized probability distribution function developed based on the results from the polyline angle measurement tool in MATLAB confirmed that the fibers in slurry samples are aligned at angles varying from 0 to 40° relative to horizontal with a greater likelihood of having fibers oriented at 20° relative to horizontal. In compacted samples, the fibers are inclined at angles varying from 0 to 90° with a greater probability of 45° inclination relative to horizontal.

- The undrained ESP for fiber-reinforced clays was evaluated based on the measured pore pressure response during undrained loading. For all slurry samples, the value of the pore-water pressure parameter a became positive at ε_a values less than 1%. This is due to the increased tension mobilized in horizontally oriented fibers, leading to an increase in the overall horizontal stiffness of the composite. For the compacted samples, the value of a remained negative throughout the sharing stage.

- The a value ranges between $-\frac{1}{3}$ and 1 in slurry-prepared samples and between $-\frac{1}{2}$ and $-\frac{1}{25}$ in compacted samples. These values exceed the limiting ranges proposed for a natural clay soil and, consequently, the equations developed by Graham and Houlsby (1983) for estimating the stiffness ratio are not applicable for this composite.

- For all compacted specimens, Δu approaches its maximum value (Δu_{max}) at lower values of ε_a, followed by a steep reduction due to the higher compaction energy supplied during sample preparation. In contrast, all slurry samples demonstrated a greater rate of increase of Δu with ε_a, and the Δu values at the end of shearing were equal to the p'_o at which the sample was sheared. This response in slurry samples is associated with the increased amount of tension mobilized in the horizontally oriented fibers.

- The shear strength of a fiber-reinforced clay soil is a combination of the strength developed due to the frictional interaction between clay particles (q_{clay}), interaction between clay particles and fibers (q_{fs}), and tensile stresses mobilized in the fibers ($q_{tension}$). The q_{clay} depends on the density and water content of the composite as well as the value of p'_o. The q_{fs} is a function of the interphase shear strength between fibers and clay particles, p'_o at which the specimen in sheared, and density and water content of the composite. The $q_{tension}$ primarily depends on the orientation of fibers with respect to the principal stresses. It is also a function of the fiber content, length, and p'_o value.

- Triaxial compression tests are limited with respect to their ability to quantify the maximum tension mobilized in the fibers as the condition of $\sigma'_3 < 0$ cannot be satisfied, which subsequently limits the shear strength measured from this test. In addition, none of these tests were able to result in a tensile stress state and it was not possible to define the strength for this class of material. This signifies the need to perform more tests along varying stress paths to better define the shear strength of fiber-reinforced clay soil.

4.6 Acknowledgement

This research is funded by Dr. Hendry's Natural Sciences and Engineering Research Council Discovery Grant (#RGPIN-2020-04419). The authors also like to thank MiniFIBERS. Inc, for supplying the fibers for triaxial testing.

4.7 References

ASTM D4767-11 (2020). Standard Test Method for Consolidated Undrained Triaxial Compression Test for Cohesive Soils. ASTM International, West Conshohocken, PA, 2020, www.astm.org.

Black, J.A., and Take, W.A. (2015) 'Quantification of optical clarity of transparent soil using the modulation transfer function', Geotechnical Testing Journal, 38(5), p588–602, doi: 10.1520/GTJ20140216. ISSN 0149-6115.

Black, J.A. (2015) 'Centrifuge Modelling With Transparent Soil and Laser Aided Imaging', Geotechnical Testing Journal, 38(5), p631–644, doi: 10.1520/GTJ20140231. ISSN 0149-6115.

Diambra, A., Russel, A.R., Ibrahim, E., and Wood, D.M. (2007) 'Determination of fiber orientation distribution in reinforced sands', Geotechnique 57(7), p623–628, doi: 10.1680/geot.2007.57.7.623.

Freilich, B., Li, C., and Zornberg, J.G. (2010) 'Effective shear strength of fiber-reinforced clays', In Proceedings of the 9th International Conference on Geosynthetics, 9ICG, Guarujá, Brazil, May, Vol. 4, p1997-2000.

Graham, J., and Houlsby, G.T. (1983) ‘Anisotropic elasticity of a natural clay’, Geotechnique 33(2), p165-180.

Gray, D.H., and Ohashi, H. (1983) ‘Mechanics of fiber reinforcement in sand’, Journal of Geotechnical Engineering 109(3), p335-353.

Hendry, M.T. (2011) ‘The geomechanical behaviour of peat foundations below rail-track structures’, PhD thesis, University of Saskatchewan.

Hendry, M.T., Sharma, J.S., Martin, C.D., and Barbour, S.L. (2012) ‘Effect of fibre content and structure on anisotropic elastic stiffness and shear strength of peat’, Canadian Geotechnical Journal 49, p403–415.

Hendry, M.T., Barbour, S.L., and Martin, C.D. (2014) ‘Evaluation of the effect of fibre reinforcement on the anisotropic undrained stiffness and strength of peat’, Journal of Geotechnical and Geoenvironmental Engineering 140(9).

Ibrahim, E., Diambra, A., Russel, A.R., and Wood, D.M. (2012) ‘Assessment of laboratory sample preparation for fibre reinforced sands’, Geotextiles and Geomembranes 34, p69-79.

Iskander, M., Liu, J., and Sadek, S. (2002) ‘Transparent amorphous silica to model clay’, Journal of Geotechnical and Geoenvironmental Engineering 128(3), doi:10.1061/ (ASCE)1090-241(2002)128:3(262).

Jardine, R.J., Fourie, A., Maswoswe, J., and Burland, J.B. (1985) ‘Field and laboratory measurements of soil stiffness’, In Proceedings of the 11th international conference on soil mechanics and foundation engineering, San Francisco. 12 August - 16 August 1985.

Kumar, A., Walia, B.S., and Mohan, J. (2006). ‘Compressive strength of fiber reinforced highly compressible clay’, Construction and Building Materials 20(10), p1063–1068.

Landva, A.O., and Pheeney, P.E. (1980) ‘Peat fabric and structure’, Canadian Geotechnical Journal 17(3), p416-435, doi: 10.1139/t80-048.

Li, C. (2005). ‘Mechanical response of fiber-reinforced soil’, Ph.D. thesis, University of Texas at Austin.

Maher, M.H., and Woods, R.D. (1990) ‘Dynamic response of sand reinforced with randomly distributed fibers’, Journal of Geotechnical Engineering 116(7), https://doi.org/10.1061/(ASCE)0733-9410(1990)116:7(1116).

Maher, M.H., and Ho, Y.C. (1994) ‘Mechanical properties of kaolinite/fiber soil composite’, Journal of Geotechnical Engineering 120(8), p1381-1393.

Michalowski, R.L., and Zhao, A. (1996) ‘Failure of fiber-reinforced granular soils’, Journal of Geotechnical and Geoenvironmental Engineering 122(3), p226–234.

Michalowski, R.L., and Čermák, J. (2002) ‘Strength anisotropy of fiber-reinforced sand’, Computers and Geotechnics 29(4), p279–299, doi:10.1016/S0266-352X(01)00032-5.

Michalowski, R.L., and Čermák, J. (2003) ‘Triaxial compression of sand reinforced with fibers’, Journal of Geotechnical and Geoenvironmental Engineering 129(2), p125–136, doi:10.1061/(ASCE)1090-0241(2003)129:2(125).

Ni, Q., Hird, C., and Guymer, I. (2010) ‘Physical modeling of pile penetration in clay using transparent soil and particle image velocimetry’, Geotechnique 60(2), p121–132.

Palat, A., Hendry, M.T., and Roustaei, M. (2019) ‘Effect of fiber content on the mechanical behavior of fiber-reinforced clay’, In Proceedings of the 72nd Canadian Geotechnical Society Annual Conference, GeoStJohns 2019, St. John’s, Newfoundland. 29 September - 2 October 2019.

Palat, A., and Hendry, M.T. (2021) ‘Evaluation of the geomechanical behavior of fiber-reinforced clay soil’, In Proceedings of the 74th Canadian Geotechnical Society Annual Conference and the 14th Joint CGS/IAH-CNC Groundwater Conference, GeoNiagara 2021, Niagara Falls, Ontario. 26 September - 29 September 2021.

Soriano, I., Ibraim, E., Ando, E., Diambra, A., and Laurencin, T. (2017) ‘3D fibre architecture of fibre-reinforced sand’, Granular Matter 19(4).

Wood, D.M. (1990) ‘Soil Behavior and Critical State Soil Mechanics’, Cambridge University Press. ISBN 0-521-33249-4.

Wood, D. M., and Graham, J. (1990) ‘Anisotropic elasticity and yielding of a natural plastic clay’, International Journal of Plasticity 6, p377-388.

Yamaguchi, H., Ohira, Y., Kogure, K., and Mori, S. (1985) 'Undrained shear characteristics of normally consolidated peat under triaxial compression and extension conditions,' Soils and Foundations 3, p1–18, doi:10.3208/sandf1972.25.3_1.

Zornberg, J.G. (2002) 'Discrete framework for limit equilibrium analysis of fibre-reinforced soil', Geotechnique 52(8), p593–604.

Zornberg, J.G., and Li, C. (2003) 'Design of fiber-reinforced soil', In Proceedings of the Twelfth Panamerican Conference of Soil Mechanics and Geotechnical Engineering, Cambridge, Massachusetts, June 22-26 Vol. 2, pp. 2193-2200.

Chapter Five: Quantification of the effect of fibre polymer type on the undrained behavior and realizable strength of fiber-reinforced clay

---

Contribution of the Ph.D. candidate

All work presented in this chapter has been carried out by the Ph.D. candidate., which includes review of the literature, preparation of testing specimens, design of the experimental program, execution of the experiments, analysis and discussion of the results and writing of the text.

As supervisor, Dr. M. T. Hendry has reviewed all parts of the work. This chapter will be submitted with the following citation:

Palat, A., and Hendry, M.T. (2022) 'Quantification of the effect of fibre polymer type on the undrained behavior and realizable strength of fiber-reinforced clay'.

Contribution of this chapter to the overall study

The purpose of this study is to evaluate the effect of changing fiber polymer types on the undrained shear strength and induced pore water pressure developed in the composite when prepared using the compaction and slurry methods presented in *Chapter 4* (Manuscript #2). Through this study, the fiber-soil interface shear strength is determined using a specially designed modified direct shear testing apparatus (specific objective #6). The following manuscript further provides an explanation of the predominant factor contributing to the shear strength of the fiber-reinforced composites when prepared using compaction method and slurry method based on the probability distribution of fiber orientation within the clay soil determined in Chapter 4. The effect of changing fiber types and method of sample preparation on the yield surface of fiber-reinforced clays is analysed ad the yield strength of this composite is determined. The findings from this study further stresses the results obtained from *Chapter 3* (Manuscript #1) and *Chapter 4* (Manuscript #2) stating the limitations of a triaxial compression testing program in quantifying the tensile strength of the fibers within the clay soil.

Abstract

Reinforcement by adding short, discrete fibers is a potential method for improving the strength and stability of an existing soil. This study investigates the impact of different fiber polymer types on the undrained behavior and strength of fiber-reinforced clay soils. Samples of fiber-reinforced clay were prepared using two techniques (compaction method and hydraulic-based slurry method) and reinforced with two types of fibers: polypropylene (PP) and nylon (PA). The fiber-reinforced clays were subjected to consolidated undrained triaxial compression testing to measure the undrained stress-strain response and induced pore water pressure developed within the composites. PA fiber-reinforced clay soil demonstrated an increase in the undrained shear strength when prepared using the compaction method. For slurry-prepared samples, higher values of pore water pressure and strength were observed in PP fiber-reinforced clay soil. A modified direct shear test was performed to measure the interface shear strength between the two fiber types and clay soil. PA fibers had a higher interface friction angle with the clay soil (ϕ_i' = 31.5°) than the PP fibers (ϕ_i' = 22°). When fiber-reinforced clays are prepared using the compaction method, the fibers are oriented randomly and the major contribution to strength comes from the frictional interaction between the fibers and the clay soil. Considering the predominant horizontal orientation of fibers within slurry samples, the increase in strength is primarily due to the tensile stresses mobilized in the fibers. Samples of unreinforced compacted kaolinite clay samples demonstrated higher values of shear strength than slurry-prepared unreinforced samples. However, both PP and PA fiber-

reinforced clay samples (compacted and slurry) exhibited a strain hardening behavior with no signs of failure when tested up to an axial strain of 20%. A common yield line was defined to compare the yield strength of soil-fiber composites, with compacted samples of fiber-reinforced clay demonstrating higher yield strength compared to slurry samples.

5.1 Introduction

Adding short, discrete fibers as reinforcement is one potential option for improving the strength and stability of existing soil. Maher and Ho (1994) demonstrate the inclusion of randomly distributed fibers increases the peak compressive strength, ductility, splitting tensile strength, and flexural toughness of kaolinite clay soil. Studies by Estabragh et al. (2011) on nylon fiber-reinforced clay establish that fibers restrain the volumetric dilation of the soil, leading to an increase in the excess pore water pressure during undrained shearing. Plé and Lê (2011) performed direct tensile tests and triaxial compression tests on polypropylene (PP) fiber-reinforced clay soil. Their results show the initial stiffness, ductility, strength, and hydraulic conductivity of clay soil improves with the inclusion of fibers. Li (2005) states that fiber inclusions improve the post-peak behavior of soil, with mobilization of fiber tension occurring at a strain level higher than the peak strength of unreinforced soil. Mirzababaei et al. (2018) investigated the shear strength of expansive clay soil reinforced with PP fibers by performing a series of multi-stage reverse direct shear tests. Their findings demonstrate the technique of fiber reinforcement is more applicable in areas with low to moderate normal effective stresses. Palat et al. (2019) performed triaxial compression tests on samples of fiber-reinforced clay and demonstrate the unreinforced clay soil failed by forming a well-defined failure plane, while fiber-reinforced samples showed a tendency to bulge due to the movement of fibers to potential planes of weakness and mobilization of tensile stresses. The potential applications of this composite would be in the stabilization of mine fine tailings, oil sands mining reclamation including tailings ponds, evapotranspiration covers, and low-permeability landfill liners.

Zornberg (2002) developed a discrete framework for the limit equilibrium analysis of fiber-reinforced soils by considering fibers as discrete elements mobilizing tensile stresses along the shear plane. According to the framework, the equivalent shear strength of fiber-reinforced soil is the sum of the shear strength of unreinforced soil and fiber-induced distributed tension. If the average normal stress acting on the fibers is less than a critical value of normal stress, the fiber-induced distributed tension is governed by the fiber content, length, and interface shear strength of individual fibers. If the average normal stress acting on the fibers is greater than a critical value of normal stress, the fiber-induced distributed tension is a function of fiber content and the tensile strength of the individual fibers.

Determining the interface shear strength between fibers and clay particles is critical for understanding the geomechanical behavior of fiber-reinforced clay soils. Several authors have attempted to investigate the interface properties between geosynthetics and clay soil (Chai and Saito, 2016; Ellithy and Gabr, 2000; Ferreira et al., 2015), but very few studies have investigated interface shear strength parameters between fibers and clay. Tang et al. (2010) performed single fiber pullout tests to evaluate the interfacial strength properties of PP fiber-reinforced soil. Their results show the interfacial mechanical behavior is highly influenced by the normal stress value as well as other factors, such as the effective interface contact area, fiber surface roughness, and soil composition. Ammar et al. (2019) evaluated the interface response between hemp fibers and natural clay and show the fibers are efficient at mobilizing the shear strength of clay soil. Their studies indicate that drained interface strength is the only parameter that can be reliably measured from small-scale laboratory direct shear testing due to the partial drainage conditions at the interface. Although considerable research has been devoted to the investigation of fiber-reinforced soil as a matrix, less attention has been directed to characterize the interface parameters between soil and fibers (Ammar et al., 2019). Additionally, no studies have been performed to date to quantify the interface characteristics between polymer fibers and clay soil. This is mainly because the discrete fibers used for reinforcement are thin and their distribution within the soil is random and complicated (Tang et al., 2010).

The objective of this research was to determine the impact of different fiber polymer types on the undrained behavior and strength of fiber-reinforced clay soils. Samples of fiber-reinforced clay were prepared using two techniques (compaction method and hydraulic-based slurry method) and reinforced with two fiber types (PP and nylon (polyamide, PA)). The study further evaluated the interface shear strength between the fibers and clay soil. This paper discusses the impact of the interface friction angle and mobilized fiber tension on the undrained shear strength, induced pore water pressure, and yield strength of the fiber-reinforced clay soils.

5.2 Materials and methods

The undrained shear strength and induced pore water pressure developed within fiber-reinforced clays were measured by performing consolidated undrained (CU) triaxial compression tests. The clay soil used in this study was kaolinite, a commonly available clay mineral. The inclusion of two types of synthetic fibers, PP and PA, was considered to determine their influence on the shear strength and pore water pressure. The interphase shear strength between these fibers and the clay soil was determined using a modified direct shear testing program.

5.2.1 Materials

The clay soil adopted in this study was 'EPK Kaolin,' manufactured by Edgar Minerals Inc. Laboratory testing of the clay soil indicated a specific gravity of 2.45, liquid limit of 58%, plastic limit of 42%, plasticity index of 16%, optimum moisture content (OMC) of 28%, and maximum dry density (MDD) of 1.5 g/cm^3.

Pre-cut PP and PA fibers were provided by MiniFIBERS Inc. (Johnson City, TN, USA). Previous works by the authors show the optimum fiber content and length of discrete fibers for mixing with the clay soil is 2% and 18 mm (Palat et al., 2019; Palat and Hendry, 2021). For all tests in this study, the fiber content and length were kept constant at these values. The properties of the fibers (as provided by the manufacturer) are given in Table 5.1. For the direct shear tests, sheets of PP fibers (Fig. 5.1a) and reels of uncut nylon yarn (Fig. 5.1b), with the same properties as the pre-cut fibers used in the triaxial testing, were provided by the same manufacturer.

Table 5.1. Physical properties of the synthetic fibers used in the study (Technical data sheet, Minifibers, Inc)

Properties	PP	PA
Length (mm)	18	18
Thickness (mm)	0.035	0.035
Specific gravity	0.91	1.14
Tensile Modulus (GPa)	0.4	0.96
Moisture Absorption (%)	< 1	3.5 -5.0

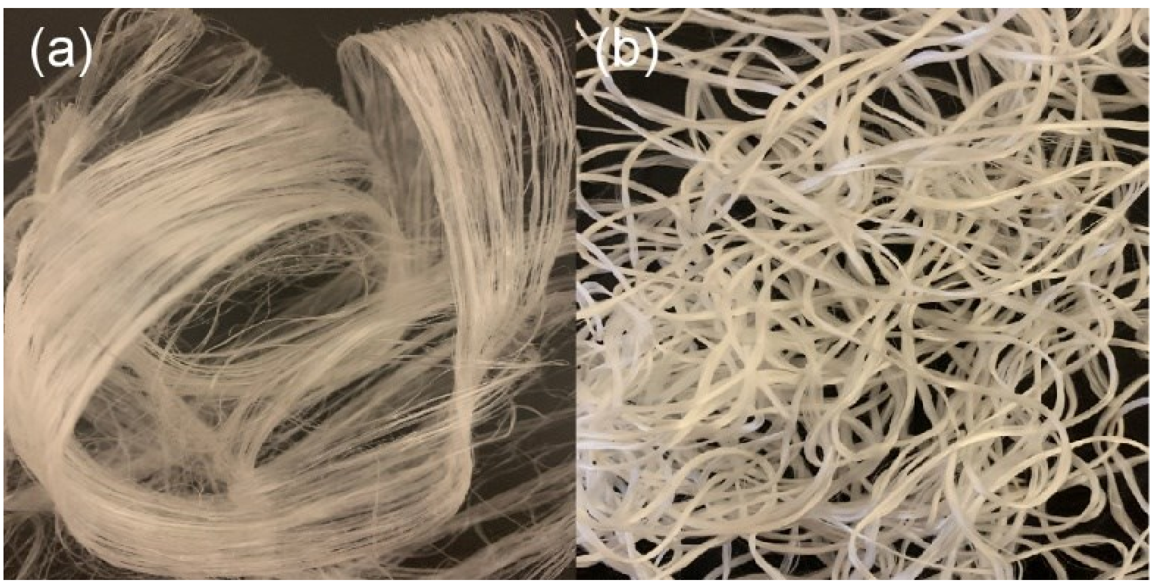

Figure 5.1. Fibers used for direct shear testing: (a) sheets of PP fiber, (b) reels of PA fiber.

5.2.2 Sample Preparation

Two methods were used to prepare fiber-reinforced clay soil for triaxial testing: compacting the soil-fiber composite to its optimum moisture content or hydraulically as a slurry. These two methods are discussed briefly herein; detailed sample preparation steps and challenges encountered while preparing such specimens are discussed in Palat and Hendry (2021).

5.2.2.1 Compaction Method

Standard Proctor tests on fiber-reinforced samples show adding fibers does not alter the OMC of the clay soil. Hence, all compacted fiber-reinforced clays were prepared at a moisture content of 28%. The amount of soil required was back-calculated to target the MDD value of the fiber-reinforced clays as obtained from the Proctor tests. To ensure homogeneity of the prepared specimens, the fiber-reinforced clay soil was prepared as two lots. Lot 1 was prepared by mixing half of the soil with half of the water. Lot 2 was prepared by mixing the other half of soil and water and all of the fibers. Lots 1 and 2 were subsequently mixed by hand and stored in a moisture control room for 48 h. This soil-fiber composite was then placed in a two-part compaction mold (50 mm diameter × 100 mm high) as five equal layers, each compacted with 15 blows using a mechanical press. The compacted samples of fiber-reinforced clay had density values ranging from 1.7 to 2.0 g/cm^3 and a water content of 28%. Figure 5.2a shows a fiber-reinforced clay soil sample prepared using the compaction method.

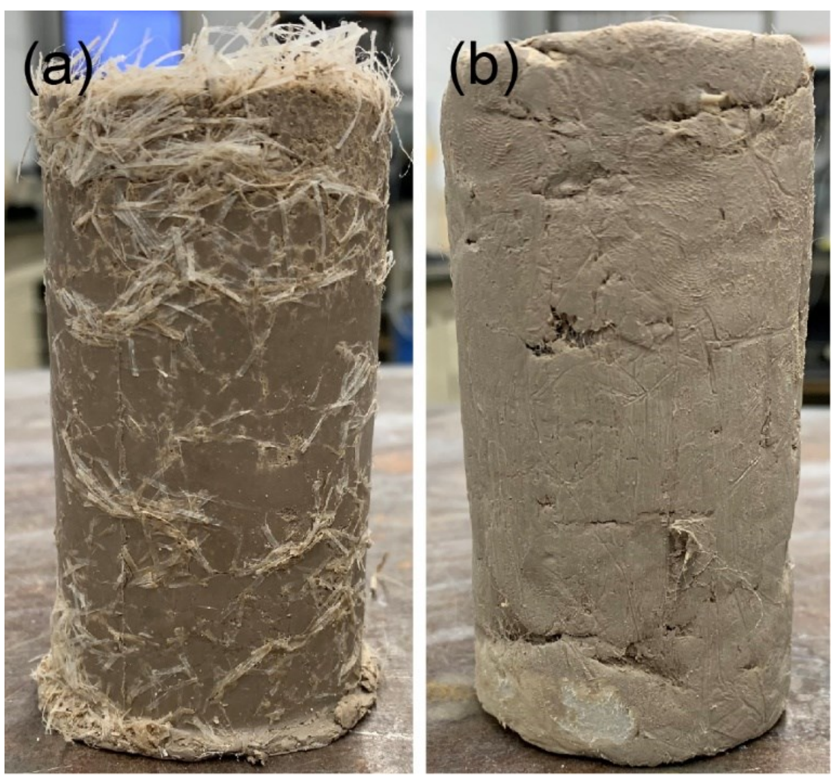

Figure 5.2. Fiber-reinforced samples prepared using the (a) compaction method and (b) slurry method.

5.2.2.2 Slurry method

The soil and fibers were mixed with a bulk volume of water approximately 2.5 times the liquid limit of kaolinite clay (145%). This quantity of water was required to avoid lumps in the kaolinite clay and minimize the amount of air entrapped in the slurry. The soil-fiber slurry was allowed to self consolidate for 14 d under double drainage conditions followed by incremental loading to a consolidation pressure of 100 kPa. Shelby tubes (50 mm diameter × 100 mm high) were pushed into the consolidated soil-fiber block using a mechanical press to obtain cylindrical samples for triaxial testing. The walls of the Shelby tubes were filed thin and oiled inside and outside prior to pushing. These tubes were carefully extracted from the block, and cylindrical samples of fiber-reinforced clay were extruded for triaxial testing. Slurry-prepared fiber-reinforced clay samples had density values ranging from 1.4 to 1.62 g/cm^3 and a water content of 46%. Figure 5.2b shows a fiber-reinforced soil sample prepared using the slurry method.

5.2.3 Laboratory testing methodology

The purpose of the laboratory testing was to quantify the effect of different fiber types on the undrained behavior and strength of fiber-reinforced clay soil. CU triaxial compression tests were performed on compacted and slurry samples of unreinforced and fiber-reinforced (PP or PA) clay to measure the undrained shear strength and induced pore water pressure. Direct shear (DS) tests were preformed by sandwiching sheets of PP and PA fibers between layers of kaolinite clay to determine the interphase shear strength between the fibers and clay soil. All DS tests conducted in this study were consolidated drained tests. The clay soil used in the DS testing program was prepared using the slurry method discussed above.

5.2.3.1 CU Triaxial testing

A Humboldt HM-5020 load frame with a capacity of 15 kN was used to perform the triaxial tests in accordance with ASTM D4767-11 (2020). All CU triaxial test specimens were initially saturated by applying a backpressure of 390 kPa and cell pressure of 400 kPa. Full saturation was confirmed by checking the B-bar value, which was greater than 0.97 for all tests. The time taken to complete full saturation in compacted specimens varied from 4 to 5 d, while in slurry samples full saturation was achieved in less than 2 d. Following saturation, the fiber-reinforced specimens were consolidated to the desired effective stress by adjusting the difference between cell pressure and back pressure to equal to the required confining pressure. Water drained out of the specimen into the automatic volume change device attached to the back pressure line until the pore pressure equalized with the back pressure. The consolidation was assumed complete when no further change was observed in the volume change device reading. The back pressure valve was then closed to prevent any further drainage and ensure the confining pressure remained unchanged. The specimens were then subjected to a displacement-controlled compression, with the rate of shearing determined based on the consolidation curves to allow 95% equalization of pore water pressure throughout shearing. The axial load during shearing was measured by a load cell (Model 75/1508, Sensotec) with a capacity of 4.5 kN, and the vertical displacement of the sample was measured using a linear potentiometer (LP) (Model TR-50, Novotechnik) with a maximum travel length of 50 mm. The pore water pressure developed within the specimen was measured by connecting a transducer to the base of the cell. The shearing was continued until an axial strain of 20% was obtained.

5.2.3.2 Direct Shear tests

The interface shear strength between the fibers and clay soil was measured using a series of drained DS tests partly in accordance with ASTM D5321/D5321M (2021). A circular shear box with a diameter of 63.5 mm was used for all tests. Sheets of PP fibers and reels of PA fibers were laid as sets of parallel strips between the kaolinite clay soil in the upper and lower containers of the DS apparatus. The fibers were placed in line with the relative displacement between two boxes (Ammar et al., 2019). Care was taken to ensure the fiber sheets extended to either side of the clay soil. Each specimen was initially subjected to a vertical compression under the desired normal stress. For normal stress values exceeding 50 kPa, the vertical stress was applied in increments with the first increment not greater than 50 kPa and the successive increment not double the previous load. Each consolidation stage took roughly 4 h to complete, and the completion of consolidation was confirmed once no further change was observed in the vertical displacement value. Following consolidation, shearing was initiated on the samples over the course of 18 h to ensure drained conditions. The shear force was applied using a constant rate of displacement slow enough to dissipate excess pore pressure in the soil. During testing, the shear force was measured by a load cell (Model SBA-1.5K, CAS Corporation), and the shear and vertical displacements within the sample were measured by LPs (Model TR-25, Novotechnik) with a maximum travel length of 25 mm. All tests were continued until the shear force reached a steady state. The specimens were kept submerged in a water bath throughout the testing to prevent drying.

5.2.4 Scope of the testing program

Compacted and slurry-prepared samples of unreinforced and fiber-reinforced (PP or PA) kaolinite clay were subjected to CU triaxial compression tests at three values of effective confining stresses (p'_o): 50, 100, and 200 kPa (18 tests in total). Three series of direct shear tests were performed with: (1) unreinforced clay soil, (2) sheets of PP fibers laid between layers of clay soil, and (3) reels of PA fibers placed between layers of clay soil. Each series included testing for five values of effective normal stress (σ'_N): 50, 100, 200, 300, and 400 kPa (15 tests in total). Large values of σ'_N were used in this study to account for fluctuations in the stress-strain plots when fibers were placed between layers of clay soil.

5.3 Presentation of Results

5.3.1 CU Triaxial test

Figures 5.3 and 5.4 summarize the CU triaxial test results for unreinforced and PP or PA fiber-reinforced clay samples prepared using the compaction method or slurry method and consolidated at three values of p'_o. The results are presented in terms of effective stress paths (ESP) in deviator stress (q) versus mean effective stress (p') space, q versus axial strain (ε_a) plots, and induced pore water pressure (Δu) versus ε_a plots.

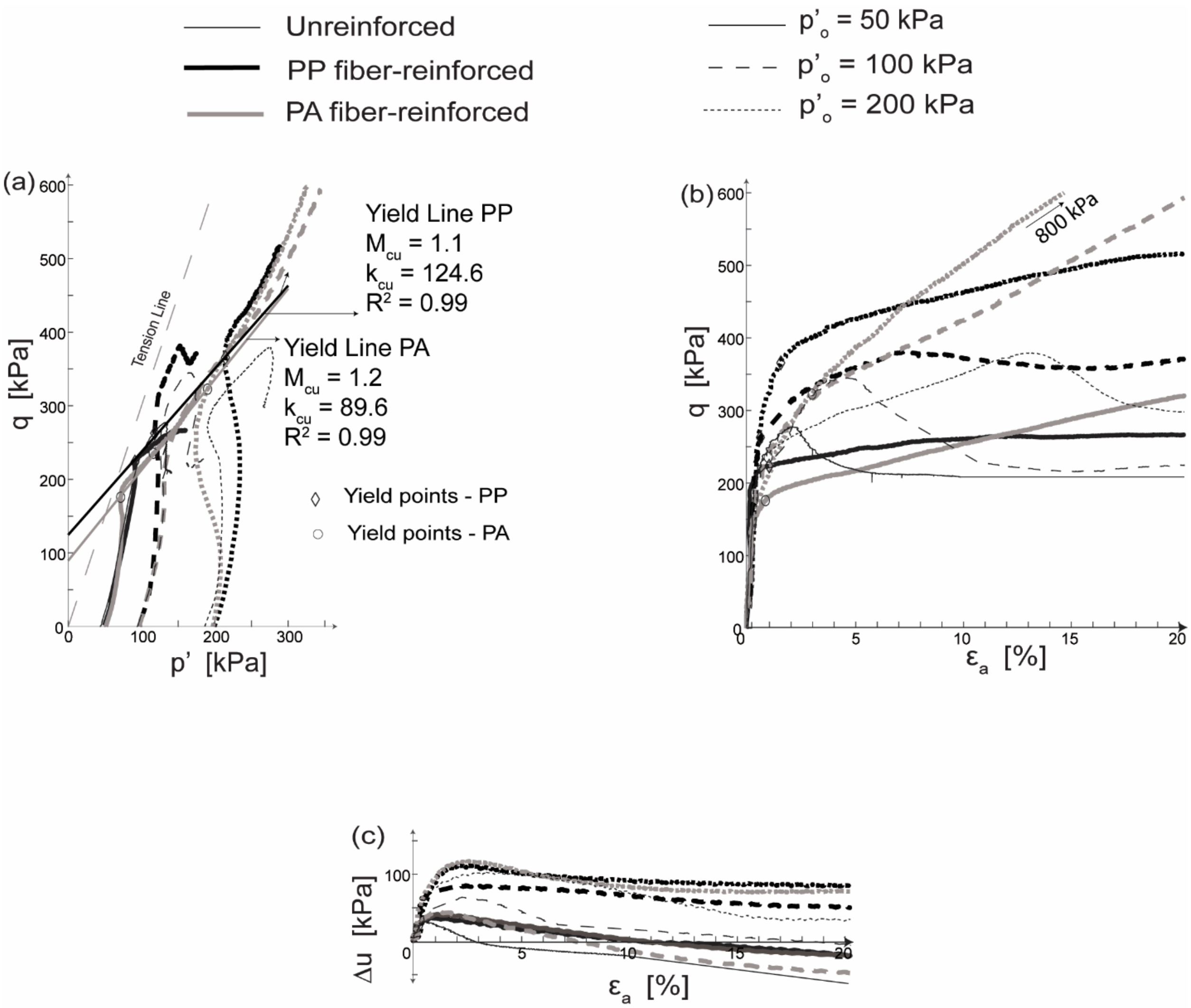

Figure 5.3. Comparison of CU laboratory testing results from compacted unreinforced and fiber-reinforced kaolinite clay specimens reinforced with PP and PA fibers presented in (a) q versus p' space (b) q versus ε_a space, and (c) Δu versus ε_a space, at three values of p'_o.

The effect of different fiber types on the geomechanical behavior of fiber-reinforced clay soil is highly influenced by the method of sample preparation. PP fiber-reinforced samples exhibited higher q and Δu when prepared using the slurry method, while the PA fiber-reinforced composites demonstrated increased strain hardening and higher values of q when prepared using the compaction method. This is attributed to the change in the predominant factors contributing to the shear strength of soil-fiber composites when prepared using the two different methods.

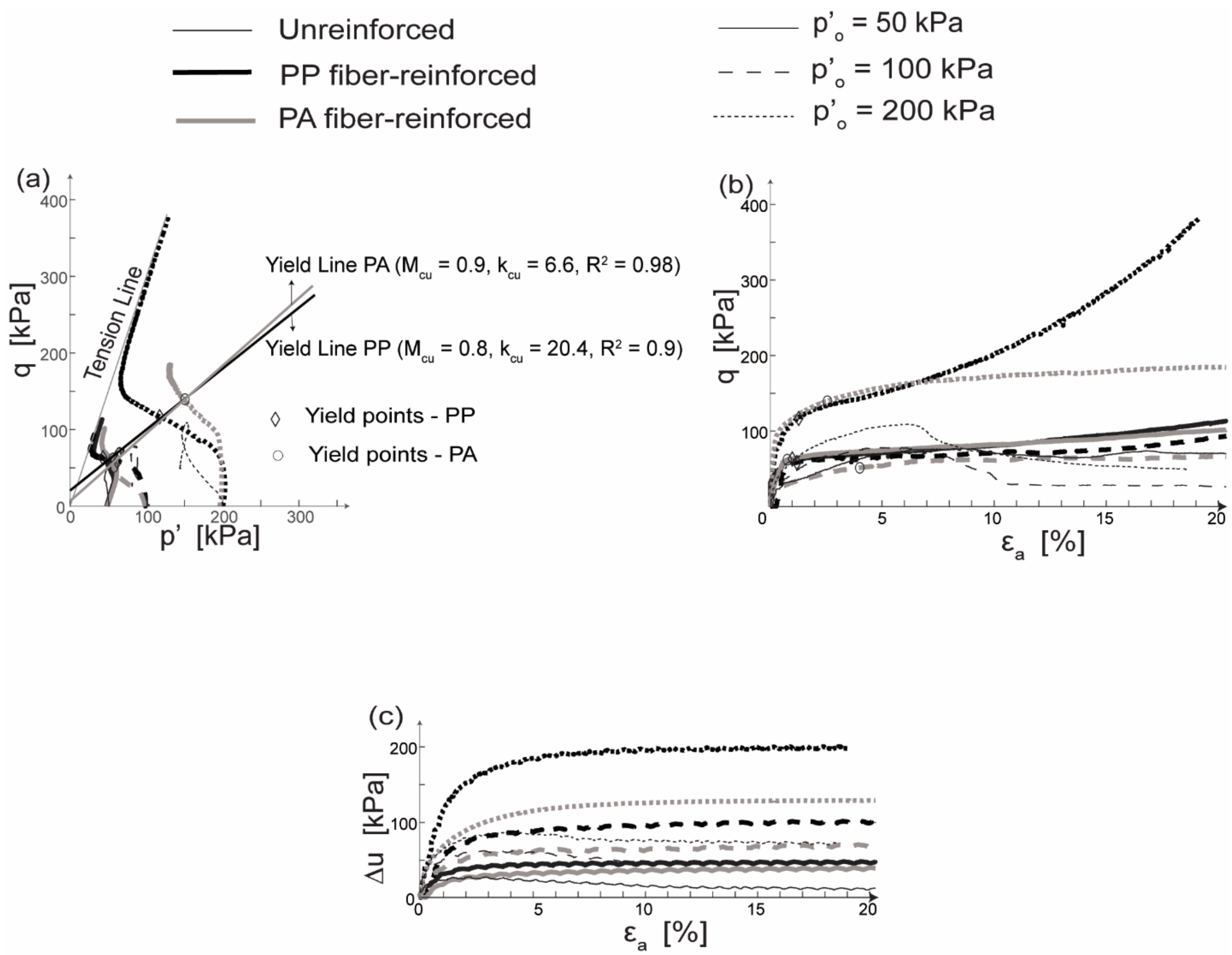

Figure 5.4. Comparison of CU laboratory testing results from slurry prepared unreinforced and fiber-reinforced kaolinite clay specimens reinforced with PP and PA fibers presented in (a) q versus p' space (b) q versus ε_a space, and (c) Δu versus ε_a space, at three values of p'_o.

For all compacted samples, Δu approaches the maximum value (Δu_{max}) at lower values of ε_a followed by a steep reduction at all values of p'_o (Fig. 5.3c). In contrast, the slurry samples demonstrated a greater rate of increase of Δu with ε_a that remained unchanged after the attainment of Δu_{max} (Fig. 5.4c). The ESP for compacted fiber-reinforced samples deviated to the right while shearing (Fig. 5.3a), but for all slurry samples the ESP deviated to the left (Fig. 5.4a).

5.3.2 DS Test results

Figures 5.5a-5.5c plot the shear stress (τ) versus shear displacement (δ_S) from the DS tests on unreinforced, PP fiber-reinforced, and PA fiber-reinforced clay soils consolidated at five values of σ'_N varying from 50 to 400 kPa. For all cases, the measured τ increased with increasing σ'_N. Fluctuations were observed in the $\tau - \delta_S$ plots when sheets of fibers were laid between layers of clay soil, and different configurations were attempted to avoid these undulations. The authors speculate these fluctuations were due to irregularities in the fiber surface as parallel layers of fiber sheets were placed between the layers of clay rather than one single sheet of fiber. All series were tested for five values of σ'_N (more data points) to account for the fluctuations in the $\tau - \delta_S$ graphs. For all values of σ'_N, the interface shear strength measured between the PA fibers and clay soil was greater than that observed for the PP fibers. The maximum τ value observed in the $\tau - \delta_S$ plot was considered the ultimate shear stress (τ_{peak}) for that value of σ'_N.

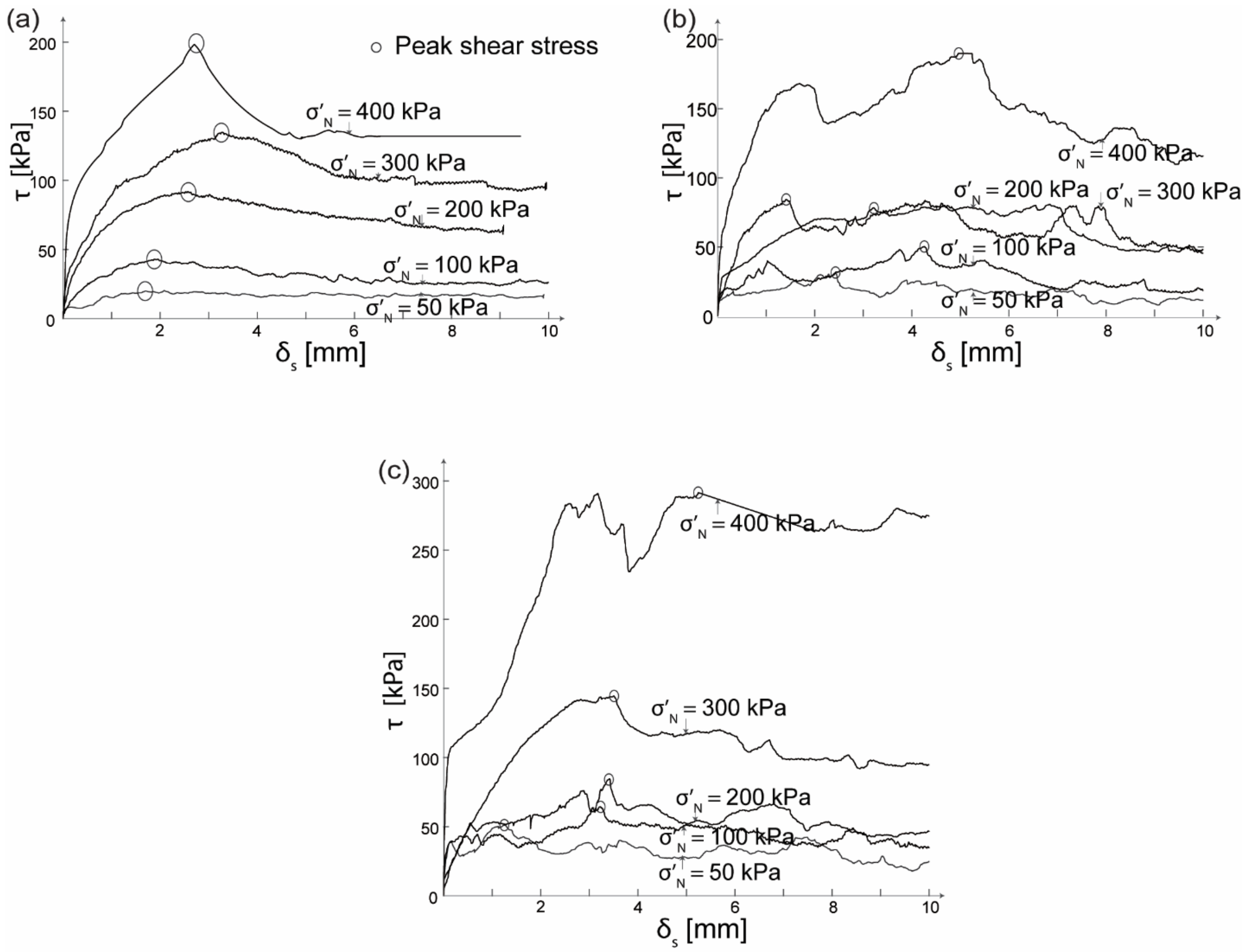

Figure 5.5. Results from DS testing on: (a) unreinforced clay soil; (b) PP fiber-reinforced clay soil; and (c) PA fiber-reinforced clay soil, at five values of normal effective stress (σ_N').

Figure 5.6a plots the τ_{peak} values against σ_N' for the kaolinite clay soil. The clay soil used for direct shear testing was preconsolidated to a pressure of 100 kPa during sample preparation. The reduction observed in the τ values after the attainment of τ_{peak} is expected due to the reduction in the specimen surface area over which the measured shear force is applied, which subsequently reduces the measured τ value (Bareither et al., 2007). Hence, the Mohr Coulomb envelope fit to these points (τ_{peak} versus σ_N') represents the critical state line for the clay soil, defined by a critical state friction angle (ϕ_{CS}') of 25.4°.

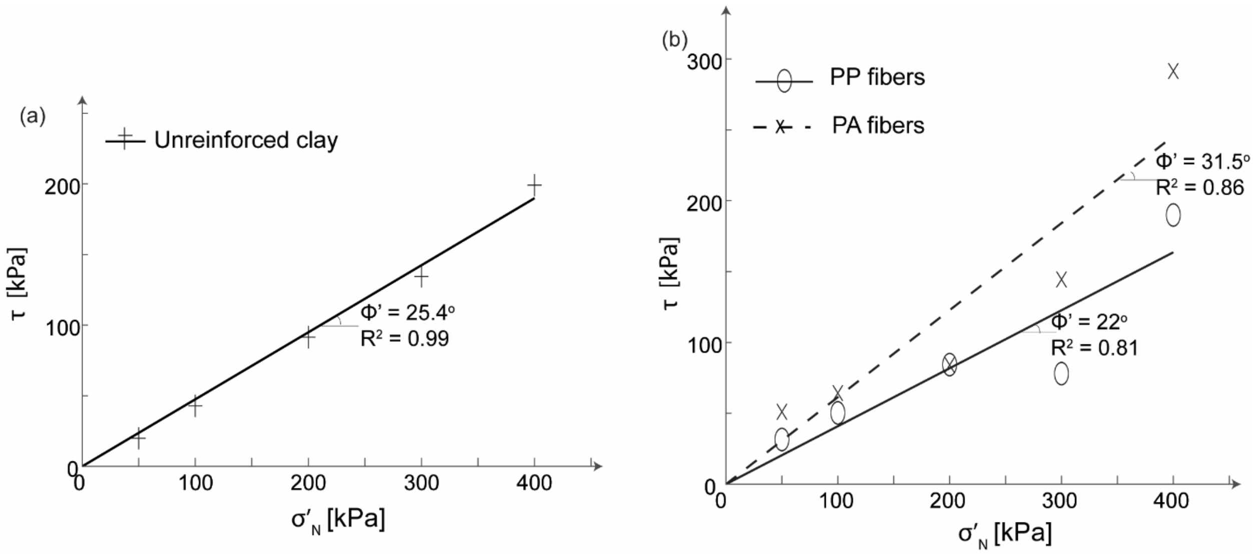

Figure 5.6. Mohr-Coulomb failure envelope for (a) unreinforced clay soil and (b) fiber-reinforced clay soil samples as obtained from DS testing.

Figure 5.6b shows the τ_{peak} values plotted against σ'_N for the PP and PA fiber-clay soils. The fitted Mohr Coulomb envelope passing through the origin resulted in an interface friction angle (ϕ'_i) of 22° between the PP fibers and the clay and 31.5° between the PA fibers and the clay (Fig. 6b). This difference in the ϕ'_i is mainly due to the difference in the affinity of these fibers to water. The moisture absorption capacity of PP fibers is less than 1% while for PA fibers it ranges from 3.5 to 5% (Table 1). PA being hydrophilic has increased bonding with the clay-water mix compared to the hydrophobic PP fibers, resulting in a higher value of interface shear strength. Poor quality of fit (decreased values of correlation coefficients (R^2)) observed in the fitted Mohr Coulomb envelopes of fiber-clay samples is due to the undulations observed in the $\tau - \delta_S$ plots and subsequent errors associated with estimating the τ_{peak} value.

5.4 Discussions

The results from CU triaxial tests show the samples of unreinforced kaolinite clay (compacted and slurry) exhibited a peak value of q (q_{max}) at lower values of ε_a followed by a strain softening response. All fiber-reinforced samples exhibited a strain hardening behavior up to an ε_a of 20% (Figs. 3b and 4b). This indicates an improvement in the ductility of clay soil when fibers are added to the matrix. The increase in the ductility of soil-fiber composites is further supported by the absence of a failure plane in fiber-reinforced clays at the end of shearing (Palat et al., 2019; Palat and Hendry, 2021). The τ between fibers and clay as measured from the DS tests increased with increasing σ_N'. This is attributed to the increased interaction between fibers and clay particles at higher σ_N' values.

5.4.1 Fiber orientation

Figure 5.7 plots the normalized probability distribution of fiber orientation when fiber-reinforced clays are prepared using either a compaction or slurry method. This graph is developed based on previous studies by the authors to analyze the distribution and orientation of fibers in compacted and slurry samples (Palat and Hendry, 2022b). The figure shows the predominant fiber orientation is horizontal in slurry samples, with a greater probability of finding fibers inclined at 20° to the horizontal. However, when prepared using the compaction method the fibers are found in horizontal, vertical, and random orientations with the majority aligned at an inclination of 45° to the horizontal. This shift in the probability distribution chart to the left in the slurry samples is due to the increased tendency of fibers to align in the horizontal direction at the end of consolidation during sample preparation.

Previous studies on fiber-reinforced clays (Palat et al., 2019; Palat and Hendry, 2021) and fibrous peat soils (Hendry et al., 2012, 2013, 2014) show that any increase in the shear strength of fiber-reinforced composites comes from the frictional interaction between fibers and clay particles along with the tensile stresses mobilized in the fibers. The tensile stresses mobilized in the fibers are only dominant if the predominant fiber orientation is perpendicular to the direction of major principal stress (Yamaguchi et al., 1985; Hendry et al., 2012, 2014), which acts in the vertical direction in a triaxial compression test.

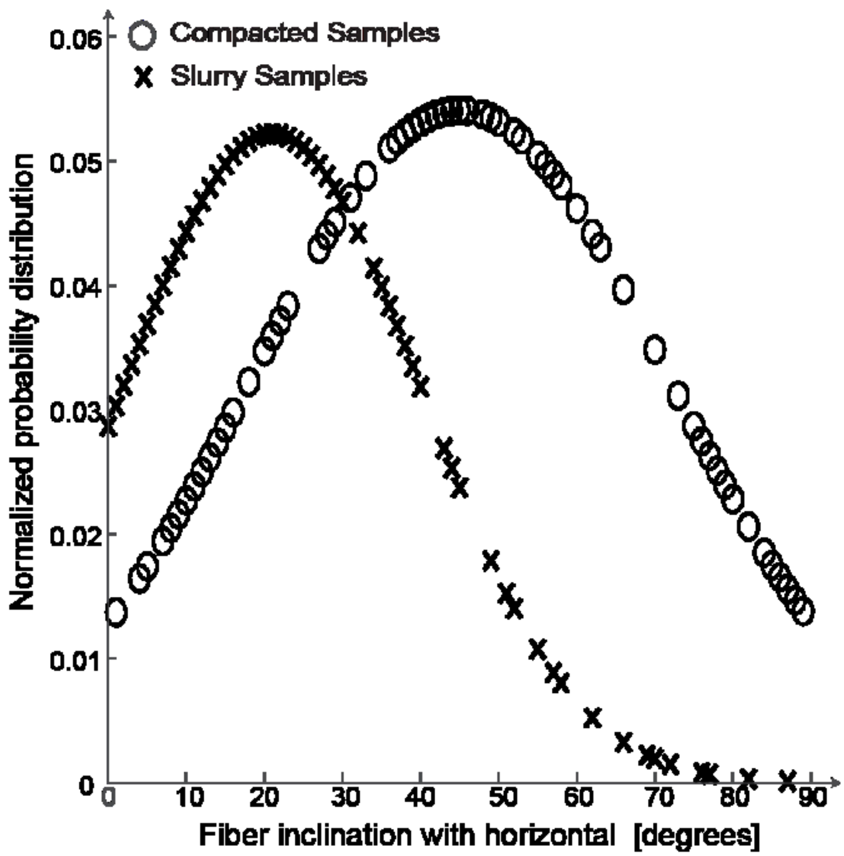

Figure 5.7. Normalized probability distribution of the inclination of fibers with horizontal in compacted and slurry samples.

Considering the horizontal orientation of fibers in slurry samples (Fig. 5.7), the predominant factor contributing to an increase in the q and Δu values while shearing is the tensile stresses mobilized in the fibers. Due to the random fiber orientation in the compacted samples, a significant amount of ε_a is required for the fibers to align in the horizontal direction and mobilize tensile stresses. The increase in the q and Δu values observed in the compacted samples during shearing is primarily due to frictional interaction between fibers and clay particles.

5.4.2 Impact of different fiber types on Δu

The two fiber polymer types (PP or PA) tested had different influences on the Δu developed within the compacted and slurry fiber-reinforced clay soils. For all compacted fiber-reinforced samples, the Δu developed within the specimens approaches Δu_{max} at ε_a values below 2%, followed by a steep reduction (Fig. 3c). This behavior of highly over-consolidated specimens is due to the higher compaction energy supplied during sample preparation. In addition, the ESP deviated to the right with a positive slope throughout shearing (Fig. 3a), indicating an increase in the overall vertical stiffness (E_V) of the composite compared to the horizontal stiffness (E_H) (Hendry et al., 2012). The amount of tension mobilized in randomly oriented fibers when subjected to the triaxial compression test is less, and only the interface shear strength between fibers and clay contributes to an increase in the Δu of the composite. Hence, the maximum Δu is observed for fibers having a higher interface shear strength with the clay soil (PA fibers in this case).

For unreinforced slurry samples, a reduction was observed in the values of Δu after the attainment of Δu_{max}. However, for both PP and PA fiber-reinforced slurry composites, the value of Δu approached Δu_{max} at lower values of ε_a and remained unchanged throughout shearing (Fig. 4c). When slurry-prepared fiber-reinforced samples are subjected to triaxial compression testing, tensile stress mobilizes in the fibers as soon as shearing is initiated. Due to the greater amount of tension mobilized in the PP fibers, higher values of Δu develop in PP fiber-reinforced clay soil. For all values of p_o', the Δu values developed at the end of shearing in slurry PP fiber-reinforced composites is equal to the p_o' at which the sample was consolidated. This greater amount of tension mobilized in the PP fibers compared to the PA fibers is confirmed by the greater deviation of the ESP to the left in PP fiber-reinforced clays, which later follows the tension cut-off line (Fig. 4a). Previous studies on fibrous peat specimens observed Δu values higher than the applied p_o', with this behavior tied to the anisotropic nature of peat specimens with higher stiffness in the horizontal direction (Acharya et al., 2017, 2018).

5.4.3 Shear strength of fiber-reinforced soil

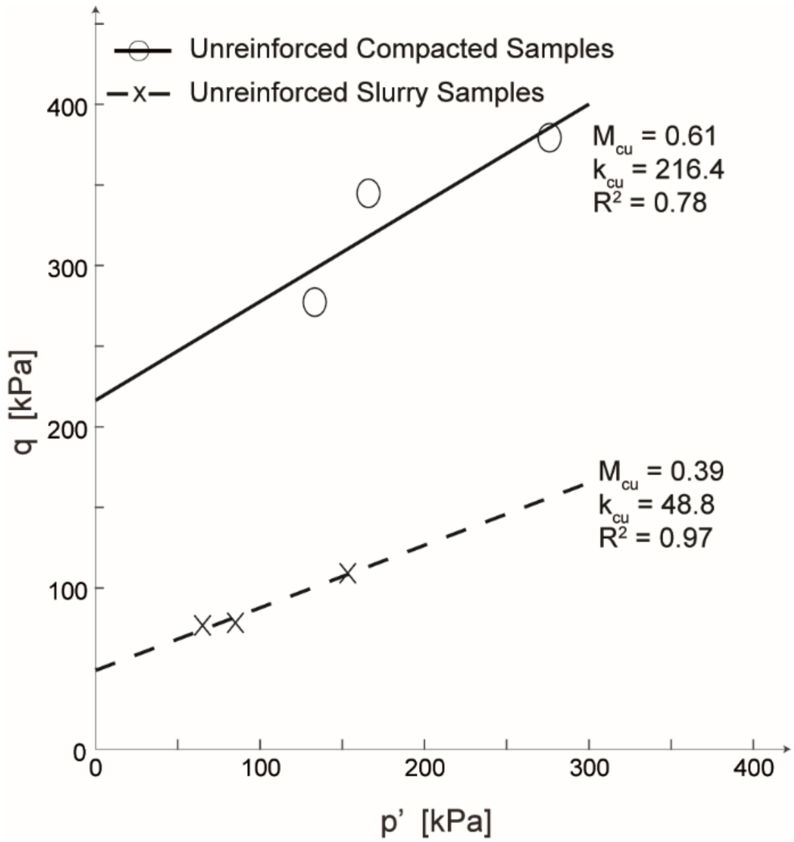

Figure 5.8. Strength line connecting the peak stress points developed in the unreinforced compacted and slurry prepared kaolinite clay soil.

Figure 5.8 plots the relationship between mean effective stress ($p'_f = \left(\frac{\sigma'_1+2\sigma'_3}{3}\right)_f$) and deviator stress at failure ($q_f = (\sigma_1 - \sigma_3)_f$) for compacted and slurry-prepared unreinforced clay soils as determined from CU triaxial compression tests. For all unreinforced samples, failure was defined corresponding to the maximum deviator stress attained in accordance with the ASTM guidelines. M_{cu} and k_{cu} are the slope and y-axis intercept of the strength line, respectively. Using Eqs. (5.1) and (5.2) (Wood, 1990), the cohesion intercept (c') and effective angle of friction (ϕ') for the compacted unreinforced kaolinite clay were determined as 100 kPa and 16°, respectively; for the slurry-prepared unreinforced clay, the corresponding values were 23 kPa and 10.6°.

$$\phi' = \sin^{-1}\left(\frac{3M_{cu}}{6+ M_{cu}}\right) \tag{5.1}$$

$$c' = k_{cu}\left(\frac{3 - \sin\phi'}{6\cos\phi'}\right) \tag{5.2}$$

The compacted samples of fiber-reinforced clay were prepared at a water content of 28% (OMC) and density values ranging from 1.7 to 2.0 g/cm^3. The water content of the slurry samples after consolidation was 46%, with density values ranging from 1.4 to 1.6 g/cm^3. The higher density values of compacted samples suggest the clay particles and fibers are tightly packed when prepared using the compaction technique, leading to an increased contribution from the frictional component of shear strength. Additionally, the compacted samples demonstrated a quasi-over-consolidated behavior due to the higher energy supplied during sample preparation, supported by increased values of c' in the compacted vs. slurry samples.

For both compacted and slurry-prepared samples, the initial portions of the q versus ε_a curves (Figs. 5.3b and 5.4b) for unreinforced as well as PP and PA fiber-reinforced composites are similar. This reaffirms the notion that inclusion of fibers has no effect in terms of altering the undrained shear strength of clay soil at ε_a values less than 1%, with some amount of ε_a required to engage the fibers while shearing.

Compacted PA fiber-reinforced clay soil showed better strain hardening and higher values of q compared to PP fiber-reinforced clay soil (Fig. 3b) at all values of p'_o. A q_{max} value of 800 kPa was observed at 20% ε_a when PA fiber-reinforced samples were tested at a p'_o of 200 kPa. A previous analysis of fiber-reinforced soil by Zornberg (2002) shows that, when the distribution of fibers is random within the soil (compacted samples in this study), the failure in fiber-reinforced composites is governed by fiber pullout and the shear strength of the composite is a function of the interface shear strength between the fibers and clay. The results from DS tests demonstrated the interface shear strength between the PA fibers and clay soil ($\phi'_i = 31.5^o$) is higher compared to PP fibers and clay ($\phi'_i = 22^o$). Consequently, compacted samples of PA fiber-reinforced clay demonstrate higher shear strength in a triaxial tests. However, the $q - \varepsilon_a$ curves of all compacted fiber-reinforced samples exhibit a strain hardening behavior with no identified peak value. Hence, it was not possible to define the shear strength of the compacted fiber-reinforced samples within the tested range of p'_o.

Due to the horizontal orientation of fibers within the slurry samples, the predominant factor contributing to an increase in the undrained shear strength of slurry fiber-reinforced clays is the tensile stresses mobilized in the fibers. A greater amount of tension was mobilized in PP fibers compared to PA fibers, resulting in an increase in the q and Δu values of PP vs. PA fiber-reinforced samples. During shearing, the ESP for PP fiber-reinforced composites demonstrated a greater tendency to deviate to the left, increasing the overall horizontal stiffness of the composite. Once the ESP for PP fiber-reinforced samples approaches the tension cut-off line, Δu is equal to the applied p_o' and the minor effective principal stress (σ_3') is zero. For the Δu to increase beyond this value, the condition of $\sigma_3' < 0$ must be satisfied, which is not possible when performing an undrained triaxial compression test (Palat and Hendry, 2021). This curtails the ability of fibers to mobilize the maximum amount of tension, which subsequently limits the shear strength of slurry-prepared fiber-reinforced samples measured from a triaxial compression test.

5.4.4 Yield Strength of fiber-reinforced clays

Previous researchers have evaluated the yielding behavior of natural clay soil by loading (stress-probing) the sample along a series of stress paths in various regions of the stress space, identifying the yield points and a drawing a tentative yield envelope by connecting these points (Graham et al., 1983; Noonan, 1980; Lew, 1981). The yield envelope bounds all elastically attainable states of stress for the soil with a particular stress history (Wood, 1990). In this study, the unreinforced and fiber-reinforced samples were only subjected to one type of loading condition (increasing the axial stress while keeping the radial stress constant) and the yield stresses were identified as the intersection of straight approximations of the initial stiff section and the subsequent more flexible response to applied stresses (Graham and Houlsby, 1983; Graham et al., 1983). Considering the heavily over-consolidated behavior exhibited by the unreinforced clay soil (q_{max} followed by strain softening), the peak shear strength parameters (Fig. 8) are also a representation of the yield strengths for compacted and slurry-prepared clay soils. These unreinforced samples showed an additional change in the stiffness at stresses lower than the yield stress. Similar behavior was also observed while determining the limit state surface of the lacustrine clay underlying Winnipeg, which was expected due to the marked anisotropy and non-homogeneity of the deposit (Baracos et al., 1980; Noonan, 1980).

The fiber-reinforced clays demonstrate many similarities with fibrous peat soil. The yielding in the laboratory specimens did not result in the development of a failure plane during the CU triaxial compression testing (Hendry et al., 2012). All specimens continued to deform plastically even at ε_a values greater than 20% (Hendry et al., 2012, 2014). The specimen showed a gradual transition from linear elastic to linear strain hardening after yielding (Hendry, 2011). For peat samples, the yield points were determined based on the hypothesis that the linear strain hardening of the q versus ε_a graphs are solely due to the tension mobilized in the fibers and that the onset of strain hardening corresponds to the frictional strength of fiber-reinforced soil (Hendry et al., 2012). Previous works by the authors also determined the yield stresses in samples of fiber-reinforced clay soil using the bilinear technique proposed for a natural clay soil by Graham et al. (1983) and demonstrate the concept of yielding is applicable in fiber-reinforced clays and that the onset of strain hardening corresponds to the yield point in fiber-reinforced clay soil (Palat and Hendry, 2022a).

M_{cu} and k_{cu} are respectively the slope and y-axis intercept of the yield lines for fiber-reinforced clays determined from the yield points shown in Figs. 5.3(a) and 5.4(a). The yield strength parameters, ϕ' and c', estimated using Eqs. 5.1 and 5.2 are presented in Table 5.2. Attempts have been made to define the yield strength of fiber-reinforced clays and determine the influence of yield strength on different fiber types (PP vs. PA) and method of preparation (compaction and slurry).

Initial analysis of the laboratory results indicated PA fiber-reinforced composites demonstrated a greater yield strength than PP fiber-reinforced samples irrespective of the sample preparation technique (Table 5.2). The yield strength of compacted PA fiber-reinforced clays (ϕ'= 31°) was greater than that of compacted PP fiber-reinforced samples (ϕ' = 28°). For slurry-prepared samples, PA fiber-reinforced clays also demonstrated higher yield strength (ϕ'= 23°) compared to PP fiber-reinforced samples (ϕ'= 20°).

Table 5.2. The yield strength properties of PP and PA fiber-reinforced clays prepared by the compaction and slurry method

Fiber type	Method of preparation	M_{CU}	k_{CU} [kPa]	ϕ' (°)	c'(kPa)
PP	Compaction	1.1	124.6	28	59.5
PA	Compaction	1.2	89.6	31	43.2
Common yield line	Compaction	1.2	103.2	30	50
PP	Slurry	0.8	20.4	20	9.6
PA	Slurry	0.9	6.6	23	3.1
Common yield line	Slurry	0.8	13.9	21	6

According to the conceptual model developed by Hendry et al. (2012) for fibrous peat, the transition to linear strain hardening response is indicative of the shear strength associated with frictional interactions, and the linear increase in q during strain hardening is the result of the additional shear resistance due to fiber tension. Previous studies by the authors also show that, in fiber-reinforced clays, any increase in q up to the onset on strain hardening (yield point) is only influenced by the frictional interactions between the fibers and clay particles (Palat and Hendry, 2021). The role of fiber tension is evident after the yield point, i.e., during the linear strain hardening portion of the q - ε_a curve. The higher values of yield strength observed in the PA fiber-reinforced composites can be attributed to the increased ϕ_i' between PA fibers and clay as observed from the DS test results (Fig. 5.6).

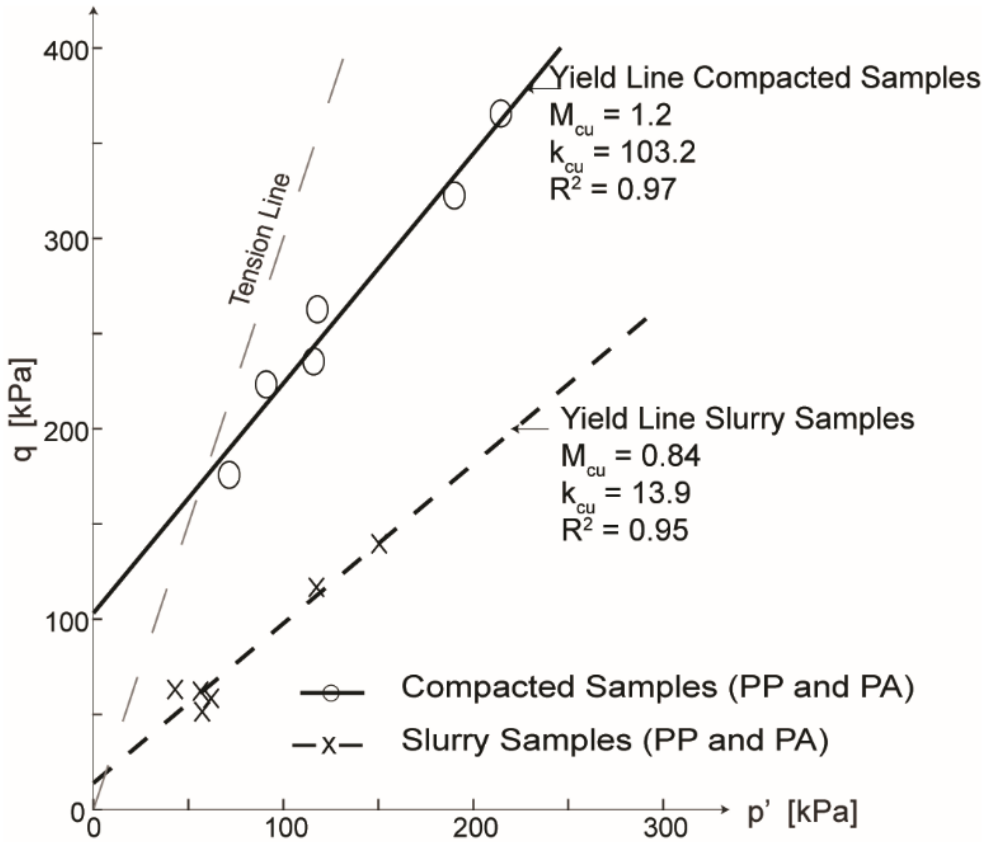

Figure 5.8. Comparison of the yield points for compacted and slurry prepared fiber-reinforced clays as obtained from the CU triaxial tests.

A single yield line is defined for compacted and slurry-prepared fiber-reinforced clays (Fig. 5.9) by combining the yield points of the PP and PA composites. Higher R^2 values indicate the different fiber types have a minimal influence on the yield strength of fiber-reinforced soil and a common yield line can be defined for all samples prepared using one technique. The yield strength primarily depends on the method by which a fiber-reinforced clay sample is prepared. The combined yield lines indicate the compacted fiber-reinforced samples $(\phi' = 30^o)$ demonstrate greater yield strength compared to slurry-prepared samples $(\phi' = 21^o)$. This increased yield strength in compacted samples results from the quasi-over-consolidation that occurs due to the higher compaction energy supplied during sample preparation. The increased density, OMC, and tight packing of the fibers and clay particles also contributed to a higher value of yield strength in compacted fiber-reinforced samples. The high apparent cohesion in compacted samples (c' = 50 kPa) is also attributed to the higher energy supplied during sample preparation. Slurry fiber-reinforced samples demonstrated a low value for effective cohesion (c' = 6 kPa) similar to intact peat specimens (Hendry et al., 2014).

5.5 Conclusions

The research presented in this chapter evaluated the impact of different fiber polymer types on the geomechanical behavior of compacted and slurry-prepared fiber-reinforced clay soils. Two types of fibers (polypropylene and nylon) were used in this study to reinforce the kaolinite clay soil. The undrained shear strength and induced pore water pressure developed within the fiber-reinforced soils was determined by performing CU triaxial compression tests. The interface shear strength between the two fiber types and clay was measured by performing a modified direct shear test. The major observations from this study are summarized below:

- The effect of different fiber types on the geomechanical behavior of fiber-reinforced clay soils is highly influenced by the method of sample preparation. Higher undrained shear strength and increased pore water pressure were observed in PA fiber-reinforced clays when prepared using the compaction method and in PP fiber-reinforced clays when prepared using the slurry method.

- Higher interface shear strength was observed between PA fibers and clay soil compared to PP fibers and clay soil. The fitted Mohr Coulomb envelope passing through the origin resulted in a ϕ'_{CS} of 25.4° for the unreinforced clay and ϕ'_i of 22° between PP fibers and clay and 31.5° between PA fibers and clay. The greater ϕ'_i between PA fibers and clay is attributed to the increased moisture absorption capacity and better bonding of PA fibers with the clay soil.

- When fiber-reinforced clays are prepared using the compaction method, the fibers are oriented in random directions with a greater probability of finding fibers inclined at 45o with the horizontal. Any increase in the q and Δu values observed during shearing is primarily due to frictional interaction between fibers and clay particles. Compacted samples of PA fiber-reinforced clay soil exhibited higher q and Δu values in triaxial compression testing due to the greater interface shear strength between the PA fibers and clay compared to the PP fibers and clay.

- In slurry-prepared fiber-reinforced samples, the predominant fiber orientation is horizontal. The dominant factor contributing to an increase in the q and Δu values is the tensile stress mobilized in the fibers during shearing. The higher q and Δu values in slurry-prepared PP fiber-reinforced samples are due to the increased amount of tension mobilized in the PP fibers compared to the PA fibers.

- Samples of unreinforced compacted kaolinite clay samples resulted in a c' of 100 kPa and ϕ' of 16°, while slurry-prepared unreinforced kaolinite clay resulted in a c' of 23 kPa and ϕ' of 10.6°. Both PP and PA fiber-reinforced clay samples (compacted and slurry-prepared) exhibited a strain hardening behavior with no signs of failure when tested up to an ε_a of 20%. Hence, it was not possible to define strength for this class of material. Additionally, none of the tests were able to result in a tensile stress state in slurry samples as the condition of $\sigma_3' < 0$ cannot be satisfied in a triaxial compression test. This indicates the need to perform more tests along varying stress paths to better define the shear strength of fiber-reinforced clay soils.

- For both compacted and slurry-prepared samples, the inclusion of PA fibers resulted in an increase in yield strength due to the high interface shear strength between the PA fibers and clay soil. A common yield line was defined to compare the yield strength of compacted and slurry-prepared soil-fiber composites. Compacted fiber-reinforced clays demonstrated a higher yield strength (c' = 50 kPa, ϕ'= 30°) compared to slurry composites (c' = 6 kPa, ϕ' = 21°). This is expected due to the increased compaction energy supplied during sample preparation, maximum dry density, optimum moisture content, and tight packing of particles in the compacted samples. Slurry-prepared fiber-reinforced samples demonstrated a low value for effective cohesion.

5.6 Acknowledgement

This research is funded by Dr. Hendry's Natural Sciences and Engineering Research Council Discovery Grant (#RGPIN-2020-04419). The authors also like to thank MiniFIBERS. Inc, for supplying the fibers for triaxial testing.

5.7 References

Acharya, M.P., Hendry, M.T., Martin, C.D., 2017. Quantification of the settlement of an embankment constructed on peat due to the expulsion of gases. Int. J. Geomech. 17(3), doi: 10.1061/(ASCE)GM.1943-5622.0000770.

Acharya, M.P., Hendry, M.T., Martin, C.D., 2018. Creep behaviour of intact and remoulded fibrous peat. Acta Geotech. 13(2), 399-417, doi: 10.1007/s11440-017-0545-1.

ASTM D4767-11, 2020. Standard Test Method for Consolidated Undrained Triaxial Compression Test for Cohesive Soils. ASTM International, West Conshohocken, PA, 2020, www.astm.org.

ASTM D5321/D5321M, 2021. Standard Test Method for Determining the Shear Strength of Soil-Geosynthetic and Geosynthetic-Geosynthetic Interfaces by Direct Shear. ASTM International, www.astm.org.

Ammar, A., Najjar, S., Sadek, S., 2019. Mechanics of the interface interaction between hemp fibers and compacted clay. Int. J. Geomech. 19(4), doi: 10.1061/(ASCE)GM.1943-5622.0001368.

Baracos, A., Graham, J., Domaschuk, L., 1980. Yielding and rupture in a lacustrine clay. Can. Geotech. J. 17(4), doi: 10.1139/t80-063.

Bareither, C.A., Benson, C.H., Edil. T. B., 2007. Reproducibility of direct shear tests conducted on granular backfill materials. Geotech. Test. J. 31(1), doi: 10.1520/GTJ100878.

Chai, J.C., Saito, A., 2016. Interface shear strengths between geosynthetics and clayey soils. Int. J. Geosynth. Ground Eng. 2(3), doi:10.1007/s40891-016-0060-8.

Ellithy, G.S., Gabr, M.A., 2000. Compaction moisture effect on geomembrane/clay interface shear strength. Advances in Transportation and Geoenvironmental Systems Using Geosynthetics, Geo-Denver 2000, Denver, Colorado, United States, doi: 10.1061/40515(291)2.

Estabragh, A.R., Bordbar, A.T., Javadi, A.A., 2011. Mechanical behavior of a clay soil reinforced with nylon fibers. Geotech. Geol. Eng. 29(5), 899–908, doi: 10.1007/s10706-011-9427-8.

Ferreira, F.B., Vieira, C.S., Lopes, M.L., 2015. Direct shear behaviour of residual soil–geosynthetic interfaces – influence of soil moisture content, soil density and geosynthetic type. Geosynth. Int. 22(3), 257–272, doi: 10.1680/gein.15.00011.

Graham, J., Houlsby, G.T., 1983. Anisotropic elasticity of a natural clay. Geotechnique, 33(2), p165-180.

Graham, J., Noonan, M.L., Lew, K.V., 1983. Yield states and stress-strain relationships in a natural plastic clay. Can. Geotech. J. 20(3), 502-516, doi: 10.1139/t83-058.

Hendry, M.T., 2011. The geomechanical behaviour of peat foundations below rail-track structures. PhD thesis, University of Saskatchewan.

Hendry, M.T., Sharma, J.S., Martin, C.D., Barbour, S.L., 2012. Effect of fibre content and structure on anisotropic elastic stiffness and shear strength of peat. Can. Geotech. J. 49, 403–415.

Hendry, M.T., Martin, C.D., Barbour, S.L., 2013. The measurement of the cyclic response of railway embankments and underlying soft peat foundations to heavy axle loads. Can. Geotech. J. 50(5), 467-480.

Hendry, M.T., Barbour, S.L., Martin, C.D., 2014. Evaluation of the effect of fibre reinforcement on the anisotropic undrained stiffness and strength of peat. J. Geotech. Geoenviron. Eng. 140(9), doi: 10.1061/(ASCE)GT.1943-5606.0001154.

Lew, K.V., 1981. Yielding criteria and limit state in a Winnipeg clay. M.Sc. Thesis, University of Manitoba, Winnipeg, Manitoba.

Li, C., 2005. Mechanical response of fiber-reinforced soil. Ph.D. thesis, University of Texas at Austin, Austin, TX.

Maher, M.H., Ho, Y.C., 1994. Mechanical properties of kaolinite/fiber soil composite. J. Geotech. Eng. 120(8), 1381-1393.

Mirzababaei, M., Arulrajah, A., Haque, A., Nimbalkar, S., Mohajerani, A., 2018. Effect of fiber reinforcement on shear strength and void ratio of soft clay. Geosynth. Int. 25(4), 471-480, doi:10.1680/jgein.18.00023.

Noonan, M.L., 1980. Limit state studies in Winnipeg clays. M.Sc. Thesis, University of Manitoba, Winnipeg, Manitoba.

Palat, A., Hendry, M.T., 2021. Evaluation of the geomechanical behavior of fiber-reinforced clay soil. In Proceedings of the 74th Canadian Geotechnical Society Annual Conference and the 14th Joint CGS/IAH-CNC Groundwater Conference, GeoNiagara 2021, Niagara Falls, ON, 26 September - 29 September 2021.

Palat, A., Hendry, M.T. 2022a. "Experimental investigation of the effect of polymer fibers on the pore pressure response and undrained shear strength of clay." (To be submitted).

Palat, A., Hendry, M.T. 2022b. "The effect of sample preparation methods on the undrained behavior of fiber reinforced clay." (To be submitted).

Palat, A., Hendry, M.T., Roustaei, M., 2019. Effect of fiber content on the mechanical behavior of fiber-reinforced clay. In Proceedings of the 72nd Canadian Geotechnical Society Annual Conference, GeoStJohns 2019, St. John's, NF, 29 September - 2 October 2019.

Plé, O., Lê, T.N.H., 2011. Effect of polypropylene fiber-reinforcement on the mechanical behavior of silty clay. Geotext. Geomembr. 32, 111-116, doi: 10.1016/j.geotexmem.2011.11.004.

Tang, C.S., Shi, B., Zhao, L.Z., 2010. Interfacial shear strength of fiber reinforced soil. Geotext. Geomembr. 28 (1), 54–62, doi: 10.1016/j.geotexmem.2009.10.001.

Wood, D.M., 1990. Soil Behavior and Critical State Soil Mechanics. Cambridge University Press. ISBN 0-521-33249-4.

Yamaguchi, H., Ohira, Y., Kogure, K., Mori, S., 1985. Undrained shear characteristics of normally consolidated peat under triaxial compression and extension conditions. Soils Found. 3, 1–18, doi:10.3208/sandf1972.25.3_1.

Zornberg, J.G., 2002. Discrete framework for limit equilibrium analysis of fibre-reinforced soil. Geotechnique 52(8), 593–604.

Chapter Six: Quantification of undrained behaviour and strength of fiber reinforced clays in extension

Contribution of the Ph.D. candidate

All work presented in this chapter has been carried out by the Ph.D. candidate., which includes review of the literature, preparation of testing specimens, design of the experimental program, execution of the experiments, analysis and discussion of the results and writing of the text.

As supervisor, Dr. M. T. Hendry has reviewed all parts of the work. This chapter will be submitted with the following citation:

Palat, A., and Hendry, M.T. (2022) ‘Quantification of undrained behaviour and strength of fiber reinforced clays in extension’.

Contribution of this chapter to the overall study

One of the major limitations from the previous studies (Chapter 3, Manuscript #1, Chapter 4, Manuscript #2 and Chapter 5, Manuscript #3) was the inability to demonstrate the mobilization of tensile stresses within the fibers used as a reinforcement in fiber-reinforced clay soil. Any stress state in excess of the tension cut-off line is solely due to the mobilization of tensile stresses within the fibers. For all triaxial compression tests performed in this study, the undrained effective stress path followed the shape of tension cut off line once the pore water pressure developed within the specimen was equal to the effective confining pressure at which the specimen was sheared. The following manuscript is the first comprehensive study performed to demonstrate and quantify the tensile stresses mobilized in the fibers within the fibrous clays during shearing. This was accomplished by performing triaxial extension tests on fiber-reinforced clays where the condition of pore pressure greater than minor principal stress, but less than cell pressure can be satisfied. A further evaluation of the impact of fiber tension on the confining pressure and other fiber variables are preformed and a methodology has been proposed to quantify the tensile stress mobilized within the fibers during shearing.

Abstract

This paper presents the results of an investigation of the undrained geomechanical behavior and strength of fiber-reinforced clay soil. The samples of fiber-reinforced clay are prepared using the slurry method of sample preparation and reinforced with two lengths of fibers: 18 mm and 48 mm. The effect of changing fiber alignment (horizontal and vertical) on the mobilized tensile stresses and overall shear strength of the composite is also determined. Triaxial compression tests imposes a restriction on the amount of tensile stresses mobilized within the fibers as the condition of pore pressure greater than minor principal stress cannot be attained in a compression-testing program. Triaxial extension tests performed on the fiber-reinforced clay samples demonstrated the mobilization of tensile stresses within the fibers by generating stress values beyond the tension cut off line during shearing. Increasing the length of fibers had a beneficial effect on the shear strength of the composite in an extension test, whereas increasing fiber length beyond 18 mm had an adverse effect on the strength of the composite in compression test. This is expected due to the scale effects factor because of the tendency of 48 mm long fibers to be bent and twisted within a 50 mm diameter specimen. A rapid increase in deviator stress was observed at lower values of axial strain for fiber-reinforced clays with vertically oriented fibers due to the increased ability of vertical fibers (aligned perpendicular to the direction of major principal stress) in carrying the axial load during shearing. A methodology is employed to estimate the stress carried by the fibers during loading and unloading and an empirical model is developed to predict the fiber tension once the

applied external stresses and fiber parameters are known. The validation of the developed model with the experimental results gave accurate estimation of the tensile stress mobilized within the fibers subjected to compression and extension loading conditions.

6.1 Introduction

Addition of discrete fibers as reinforcement is considered as one potential option for the stabilization of mine fine tailings. A few researchers have evaluated the benefits of adding synthetic fibers for improving the properties of tailings (Festugato et al. 2013; Festugato et al. 2015; Yi et al. 2015; Consoli et al. 2017; Zheng et al. 2019). The results demonstrated that fibers improved the mechanical strength of tailings by increasing the shear strength and stiffness as well as by reducing the post-peak strength loss. These discrete fibers also contributed to impede crack propagation by mobilizing tensile strength (Yi et al. 2015).

A series of investigations were also undertaken by the authors to evaluate the impact of short, discrete polymer fibers in altering the geomechanical behavior of clay soil (*Chapter 3*, Manuscript #1, *Chapter 4*, Manuscript #2, *Chapter 5*, Manuscript #3). Adding fibers to the clay demonstrated an increase in the undrained shear strength, stiffness and yield strength of the clay soil. However, none of the previous studies on fiber-reinforced soil were able to demonstrate the tensile stresses that occur due to fiber reinforcement and quantify it's the impact on the strength of the soil due to the limitations of the testing methods. Similar findings were also observed on the studies performed on fibrous peat specimens with fundamental mechanics analogous to fiber-reinforced clays (Hendry 2011; Hendry et al. 2012, 2013, 2014).

The focus of this study is to demonstrate the mobilization of tensile stresses within the fibers by performing triaxial extension tests on fiber-reinforced clay soil. The influence of loading path, fiber lengths, fiber alignment, and effective confining pressure on the undrained shear strength, excess pore water pressure and mobilized fiber tension is analyzed. This study further quantifies the tensile stresses generated within fiber-reinforced clays; specifically, how tension in fibers are incorporated into strength and manifest in the mechanism of failure.

6.2 Background

Several authors have evaluated the potential benefits of adding fibers to the soil (Maher and Woods, 1990; Gray and Ohashi 1993; Maher and Ho 1994; Zornberg 2002; Zornberg and Li 2003; Li 2005). Inclusion of randomly distributed fibers increases the peak shear strength and reduces the post peak reduction in shear strength of clay soil (Maher and Ho 1994). Consolidated undrained (CU) and consolidated drained (CD) triaxial tests on fiber-reinforced clays demonstrated that the axial deformation of the unreinforced specimen resulted in the development of a failure plane, while the reinforced specimens tended to bulge indicating an increase in the ductility of the fiber-soil composite (Freilich and Zornberg 2010; Palat et al. 2019; Palat and Hendry 2021). Zornberg (2002) proposed a discrete framework for the limit equilibrium analysis of fiber-reinforced soil by the independent characterization of soil and fibers. This framework considered fibers as discrete elements contributing to the stability of the composite, by mobilizing tensile stresses along the shear plane. Subsequently, the equivalent shear strength of the fiber-reinforced composite was considered as the sum of shear strength of the soil and fiber induced tension, where the failure is governed by fiber pullout or tensile breakage. Consoli et al. (2007) performed consolidated drained triaxial tests to evaluate the shear strength behavior of unreinforced and fiber-reinforced sand. The authors approximated the shear strength envelope for fiber-reinforced sand specimens at a shear strain of 20%. Consoli et al. (2007) also mentioned that all tests on fiber-reinforced sands experienced strain hardening until the maximum strain the apparatus could reach, and 20% shear strain was picked as a criterion for defining strength as they believed a value of 'strength' has to be defined for this composite at a particular strain.

The fundamental mechanics of fiber-reinforced soils have shown many similarities to the fibrous peat specimens. Hendry (2011) and Hendry et al. (2012, 2013, 2014) examined the fundamental properties that define the response of fibrous peat to undrained loading. A laboratory-testing program involving CU triaxial compression tests and direct shear tests was performed to investigate the role of peat fibers in the development of anisotropic stiffness and strength within peat samples. A conceptual model of peat behavior that incorporates the influence of fiber reinforcement was developed and used to interpret the laboratory test results (Hendry et al. 2012, 2014).

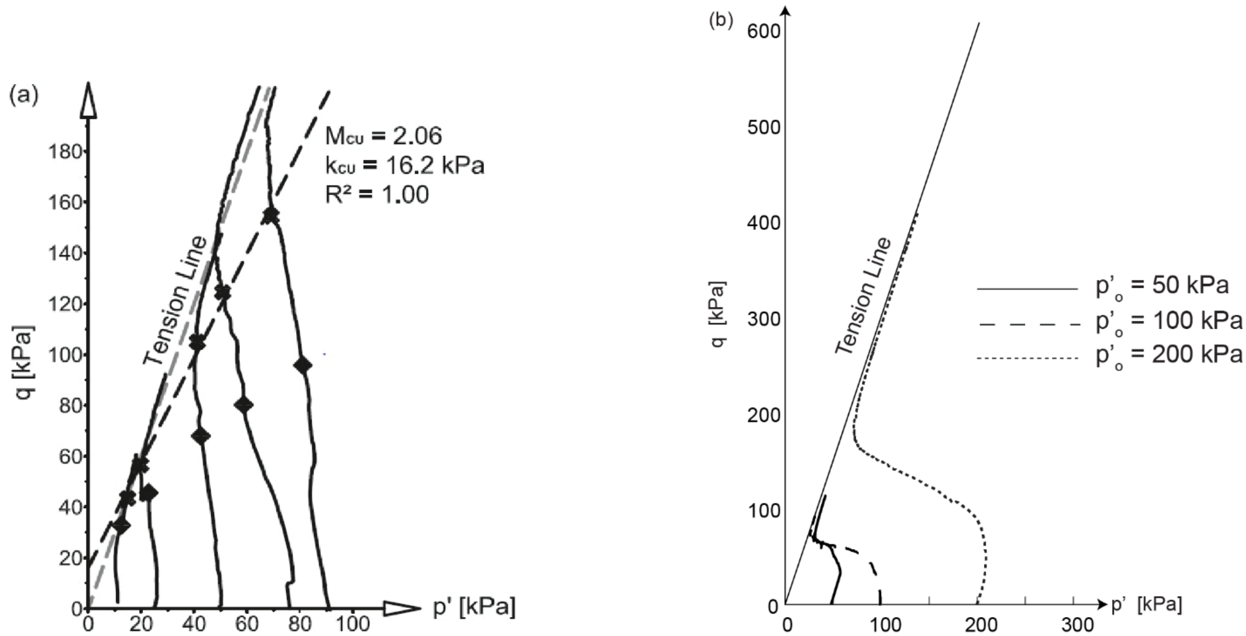

Figure 6.1. Plots demonstrating the ESP for fibrous soils in a triaxial compression test (a) fibrous peat (Hendry et al., 2012), (b) fiber-reinforced clay (Palat and Hendry, 2021).

One common observation from the previous research on fiber-reinforced clays and peat soils was the inability of the samples to develop a distinct shear plane (as it continued to expand radially) and the tests were stopped at an axial strain of 20% at which one could question the validity of further shearing. Additionally, the stress-strain curves for both soil types exhibited a strain hardening behavior without a peak shear stress that can be picked as the strength of the composite. These behaviors were attributed to the development of tensile stresses within the fibers of fiber-reinforced clays and peat. Once the pore water pressure (Δu) developed within the specimen was equal to the effective confining pressure (p_o'), the undrained effective stress paths (ESP) approached the tension cut-off (TC) line (*3:1* slope extending from the origin) and later followed this line (Fig.6.1). The TC line defines a limiting condition in the triaxial compression test where the soil is supposed to carry the condition of zero effective radial stress (Wood 1990). Any stress state in excess of the TC line is solely due to the development of tensile stresses within the fibers. For the ESP to cross the TC line, the Δu developed in the composite has to exceed the p_o'. For Δu to exceed p_o', water has to drain out from the specimen and this condition cannot be achieved by performing an undrained triaxial compression test. This is an observed limitation on the use of CU triaxial compression tests in measuring the impacts of tensile elements within a soil. Attempts have been made in the past to define a strength for fibrous peat based on the onset of yielding within the measured response (Hendry et al. 2012, 2014). These shear strengths are conservative, discount the fiber reinforcement, and are often exceeded in practice without detriment.

The purpose of this study is to manifest the contribution of fiber tension to the shear strength of clay soil by generating stress values beyond the tension cut off line during shearing. The empirical model developed as a part of this research measures the amount of tensile stress mobilized in the fibers once the fiber parameters (fiber content, and length), applied external stresses and the interface friction angle between the fibers and soil are known. The developed model was later validated with the experimental results.

6.3 Materials and Methods

6.3.1 Materials

The kaolinite clay used in this study is 'EPK Kaolin' manufactured by Edgar minerals Inc. Laboratory testing of the clay soil gave a specific gravity of 2.45, liquid limit of 58%, plastic limit of 42%, plasticity index of 16%, optimum moisture content (OMC) of 28%, and maximum dry density (MDD) of 1.5 g/cm^3. The fibers used in this study are pre-cut polypropylene fibers supplied by MiniFIBERS Inc. (Johnson City, TN, USA). These fibers had a thickness of 0.035 mm, specific gravity of 0.91, tensile modulus of 0.4 GPa, and moisture absorption capacity less than 1% (as provided by the manufacturer).

6.3.2 Sample preparation

Samples of fiber-reinforced clay for triaxial testing are prepared using the slurry method of sample preparation discussed in Palat and Hendry (2022b). The required amount of kaolinite clay was mixed with 2% of fibers and 145% of water (2.5 times the liquid limit of clay soil) using a wire whip mechanical mixer. The large amount of water was necessary to avoid the lumps in kaolinite clay and minimize the amount of entrapped air in the slurry. This fiber-soil slurry was poured into a glass cylindrical mold (150 mm diameter × 700 mm high), slowly in layers to avoid segregation. The slurry was allowed to self consolidate for 2 weeks under the conditions of double drainage followed by incremental loading from the top to a consolidation pressure of 100 kPa. After consolidation, shelby tubes (50 mm diameter × 100 mm high) were pushed into the soil-fiber block to extract cylindrical samples for triaxial testing.

Previous works by the authors demonstrated that the fibers within the slurry prepared composites are aligned in the horizontal direction at the end of consolidation (Palat and Hendry 2022b). The technique used for obtaining cylindrical samples with horizontal and vertical fiber orientation is illustrated in Figure 6.2. To obtain samples with horizontal orientation of fibers, the consolidated soil-fiber block was left in the glass mold and shelby tubes were pushed into the slurry block (Fig. 6.2a). On the other hand, to obtain vertically fiber-oriented specimens the consolidated slurry taken out of the glass mold, tilted and placed in a rectangular box. Shelby tubes were then pushed into the soil-fiber block and vertically oriented fiber-reinforced samples were extracted for testing (Fig. 6.2b).

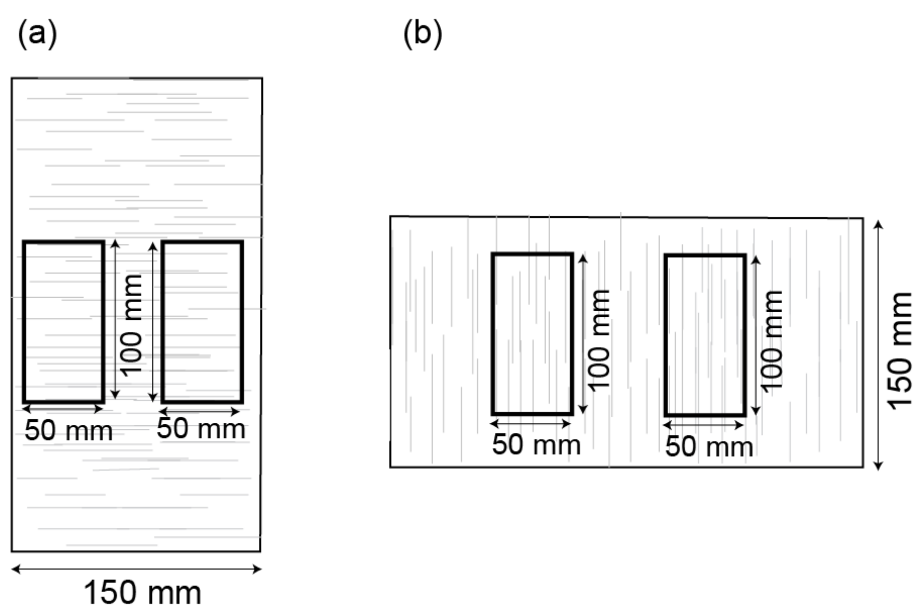

Figure 6.2. Procedure adopted for obtaining fiber-reinforced clay samples with (a) horizontal and (b) vertical alignment of fibers (based on Yamaguchi et al., 1985)

6.3.3 Laboratory testing methodology

CU triaxial extension and compression tests were performed on slurry samples of polypropylene fiber-reinforced clay to measure the undrained shear strength and induced pore water pressure developed within the composites. Both extension and compression tests were continued until an axial strain (ε_a) of 20% was obtained. Previous studies on fiber-reinforced clay soil by Li (2005) and Palat et al. (2019) proved that the load resisted by fibers are only substantial at higher strain levels, hence small strain on-sample transducers were not employed in this testing.

6.3.3.1 CU triaxial extension tests

A Bishop and Wesley stress path triaxial testing system was used to perform triaxial extension tests on fiber-reinforced composites. This testing system was accompanied with a multi channel triaxial control and data acquisition software GEOSYS-Professional, both manufactured by Wille Geotechnik® (Götzenbreite, Germany).The samples were initially saturated by applying a cell pressure of 400 kPa and a backpressure of 390 kPa until Skempton's B parameter was greater than 0.97. The cell and back pressures were applied to the specimen using the automatic electro mechanic volume/pressure controllers (VPC) with a capacity of 2 MPa, volume of 500 ml, and resolution of 0.1 kPa. Following saturation, the samples were consolidated by adjusting the difference between cell pressure and back pressure equal to the desired effective stress. Full consolidation was assumed complete once no further volume change was observed in the back pressure VPC. The specimens were then subjected to a displacement-controlled extension and the rate of shearing was decided based on the consolidation curves. The pore water pressure developed within the specimen was measured using a transducer connected to the base of the cell. Axial load was measured by a submersible load cell with a capacity of 10 kN and accuracy of 0.1%. The vertical displacement during shearing was measured by a linear variable differential transformer (LVDT) with a measuring range of 60 mm and resolution of 0.001 mm.

6.3.3.2 CU triaxial compression tests

A Humboldt HM-5020 load frame with a capacity of 15 kN was used for performing CU triaxial compression tests on fiber-reinforced clay samples, in accordance with ASTM D4767-11 (2020). A pressure panel was used to control the cell and back pressures applied to the sample. The pore water pressure developed within the specimen was measured by connecting a transducer at the base of the cell. The volume change in the sample during the consolidation phase was measured by attaching an automatic volume change device to the back pressure line of the triaxial chamber. The axial load was measured by a load cell (Model 75/1508, Sensotec) with a capacity of 4.5 kN and an accuracy of 0.14%. The vertical displacement of the sample was measured using a linear potentiometer (LP) (Model TR-50, Novotechnik) with a maximum travel length of 50 mm, linearity of ± 0.075%, and repeatability of ± 0.002 mm.

6.3.4 Scope of the testing program

Table 6.1 enlists the five series of CU triaxial tests conducted as a part of this investigation. Each series included testing the fiber-reinforced specimens for three values of p'_o, 50 kPa, 100 kPa, and 200 kPa. The other variables used in the testing program are (1) loading path (compression and extension), (2) fiber lengths (18 mm and 48 mm), and (3) fiber alignment (horizontal and vertical).

Table 6.1. Summary of the CU triaxial tests performed on fiber-reinforced kaolinite clay soil as a part of this investigation

Series	Loading path	Fiber Orientation	Fiber length [mm]	p'_o [kPa]
1	Extension	Horizontal	18	50 100 200
2	Extension	Horizontal	48	50 100 200
3	Extension	Vertical	48	50 100 200
4	Compression	Horizontal	18	50 100 200

5	Compression	Horizontal	48	50 100 200

6.4 Presentation of results

Figures 6.3-6.5 show the CU triaxial test results for clay soil reinforced with PP fibers (fiber content: 2%) and tested at three values of p_o'. The results are presented in terms of ESP in deviator stress (q) versus mean effective stress (p') space, q versus ε_a, and Δu versus ε_a.

The data in Figs. 6.3 and 6.4 demonstrate the influence of loading paths (compression and extension) on the shear strength and Δu of the slurry prepared clay soil reinforced with 18 mm and 48 mm long fibers respectively. In compression tests of 18 mm long fiber-reinforced composites, the ESP approaches the TC line and later follows the line (Fig. 6.3a) once the Δu developed within the composite becomes equal to the p_o' at which the specimen was sheared (Fig. 6.3c). Increasing the fiber length to 48 mm has a detrimental effect on the q and Δu values in compression test (Fig. 6.4b and 6.4c). This is expected due to the increased tendency of the 48 mm long fibers to be bent and twisted inside a 50 mm diameter specimen thereby restricting the amount of tension mobilized in the fibers during shearing. When subjected to extension tests, the amount of tension mobilized in the fibers increases as indicated by the crossing of the ESP beyond the TC line (-2:3 slope extending from the origin) and increase in the value of q during shearing (Figs. 6.3a and 6.4a). The ε_a at which ESP crosses the TC line increases with an increase in p_o' and the probable reasons for this behavior will be discussed in the subsequent sections.

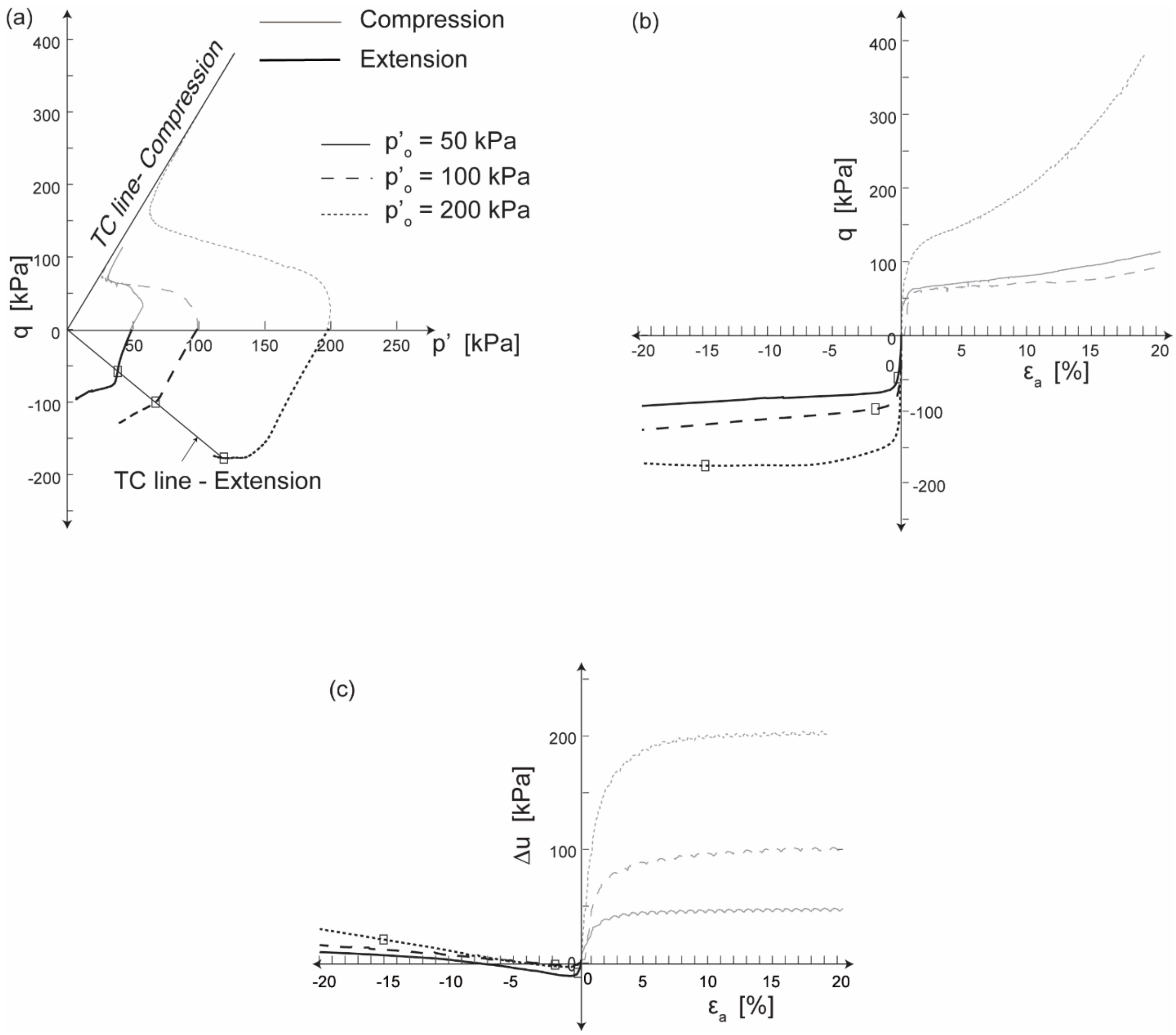

Figure 6.3. Comparison of CU triaxial compression and extension laboratory testing results from slurry-prepared kaolinite soil specimens reinforced with 18-mm fibers (fiber alignment: horizontal) presented in (a) q versus p' space, (b) q versus ε_a space, and (c) Δu versus ε_a space at three values of p'_o.

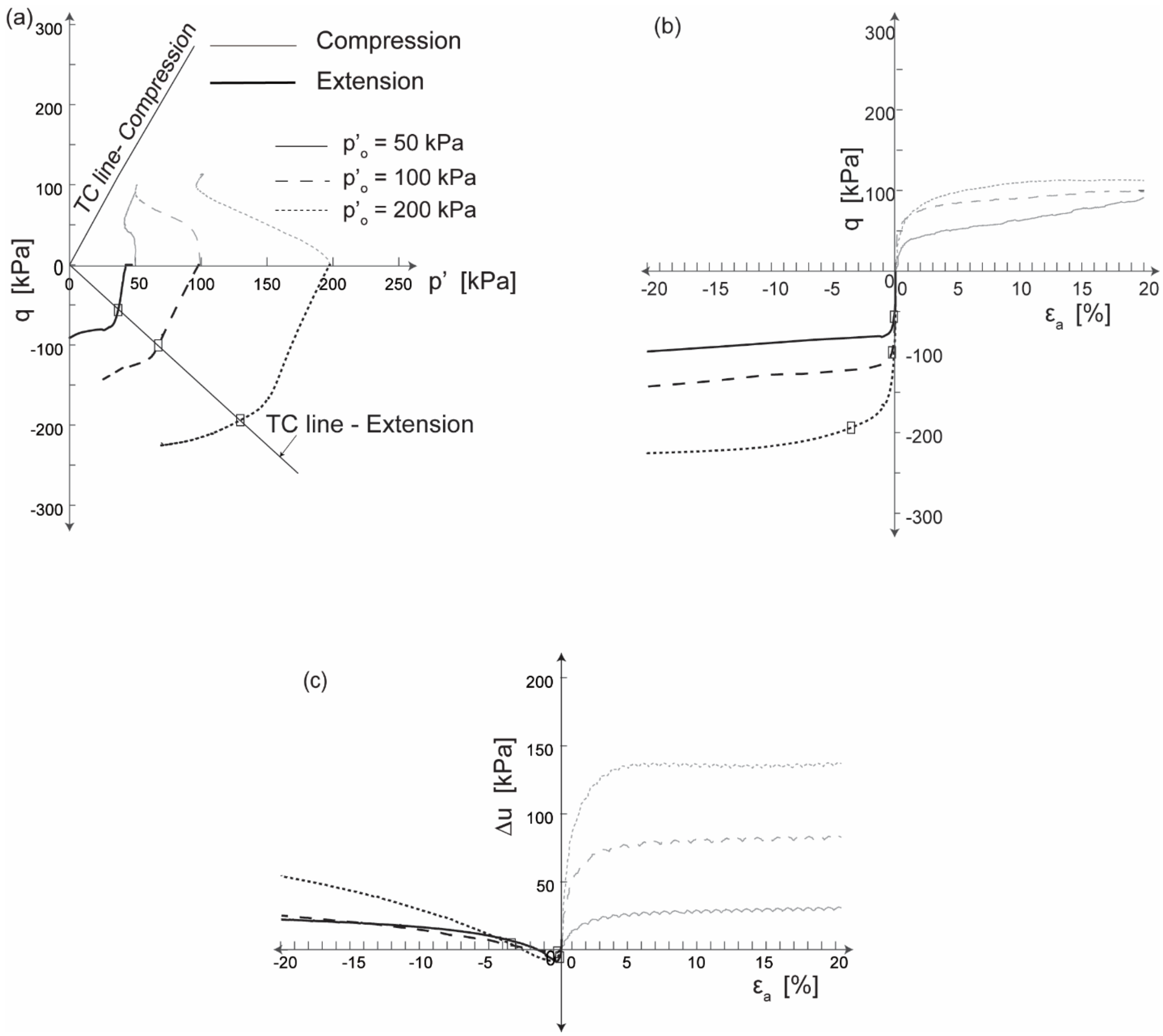

Figure 6.4. Comparison of CU triaxial compression and extension laboratory testing results from slurry-prepared kaolinite soil specimens reinforced with 48-mm fibers (fiber alignment: horizontal) presented in (a) q versus p' space, (b) q versus ε_a space, and (c) Δu versus ε_a space at three values of p_o'.

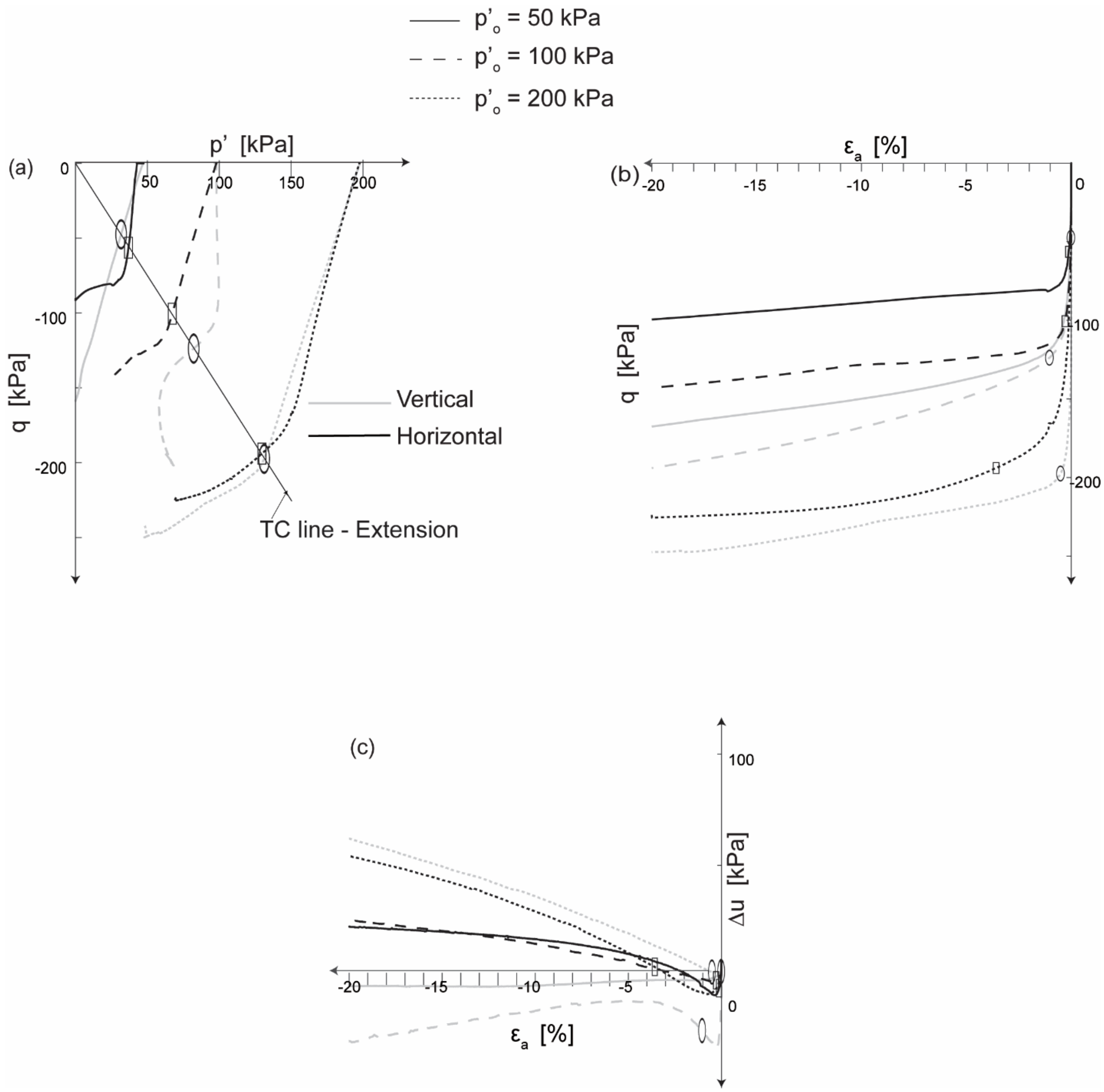

Figure 6.5. Comparison of CU triaxial extension laboratory testing results for slurry prepared kaolinite soil specimens with vertical and horizontal alignment of fibers (fiber length: 48 mm) presented in (a) q versus p' space, (b) q versus ε_a space, and (c) Δu versus ε_a space at three values of p'_o.

The effect of fiber alignment in impacting the q and Δu values of fiber-reinforced clay is shown in Fig. 6.5. The technique used for preparing specimens with horizontal and vertical orientation of fibers is demonstrated in Fig. 6.2. All tests are performed on samples reinforced with 48 mm long fibers and prepared using the slurry method. For all values of p'_o, greater amount of q was developed in vertically oriented fiber-reinforced composites.

6.5 Discussions

Figure 6.6. Slurry prepared fiber-reinforced samples after failure in (a) compression test and (b) extension test.

Slurry fiber-reinforced clays showed a tendency to bulge without an evident failure plane in compression test (Fig. 6.6a). This observed bulging response is expected due to the movement of fibers to the potential planes of weakness and mobilization of tensile stresses within the fibers (Palat et al. 2019). When subjected to compression test, the fibers align in the horizontal direction (perpendicular to the major principal stress, σ_1) and resist the lateral deformation of the soil. Under extension loading conditions, the samples of fiber-reinforced clay demonstrated an increase in length and reduction in diameter at the neck after failure (Fig. 6.6b). The fibers realign in the vertical direction during an extension test (perpendicular to σ_1) and resist the axial stress applied onto the composite.

6.5.1 Effect of loading path

This section of the paper uses the data from Figs. 6.3 and 6.4 to discuss the influence of loading path on the q and Δu values developed within the fiber-reinforced clay soil. This includes triaxial compression and extension tests performed on slurry prepared soil-fiber composites reinforced with two lengths of fibers (18 mm and 48 mm). The fiber orientation is horizontal for all specimens (Fig. 6.2a).

The TC line defines the condition in a triaxial test where the soil is supposed to carry zero effective minor principal stress, σ_3' (Wood 1990). The TC line extending from the origin has a slope of 3:1 in the compression stress space and -2:3 in the extension stress space. Once shearing is initiated on the soil-fiber composite, tensile stress mobilize within the fibers increasing the q and Δu developed in the fiber-reinforced clay soil (Palat and Hendry 2021). When the undrained ESP for the compression and extension tests approaches the TC line, $\sigma_3' = 0.$ For the ESP to cross the TC line, the Δu developed within the composite has to exceed the minor principal stress (σ_3) acting on the specimen. In a triaxial compression test, the σ_3 is the cell pressure (σ_{cell}) and acts in the horizontal direction. On the contrary, the σ_3 in a triaxial extension test is the axial stress (σ_a) and acts in the vertical direction.

For the Δu to exceed the σ_{cell} in a compression test, water has to drain out from the specimen. Thus, the observed behavior was the pore water draining out of the specimen into a void between the membrane and the specimen as a result of $\Delta u > \sigma_{cell}$. This drainage of pore water caused a drained ESP, which follows the *3:1* slope of the total stress path and also the TC line. Thus, these tests were unable to result in a tensile stress state.

The development of tensile stresses within the fibers has been demonstrated by performing a series of triaxial extension tests on fiber-reinforced clays. Any increase in the observed value of q beyond the TC line is only due to the tensile stresses mobilized in the fibers (Figs. 6.3a and 6.4a). This was possible because σ_3 acts in the axial direction for extension tests, and the condition of $\Delta u > \sigma_3$ can be attained while maintaining $\Delta u < \sigma_{cell}$, and thus preventing the drainage out of the specimen. The triaxial extension testing method imposes no restriction of the amount of tension mobilized within the fibers during undrained shearing. Higher values of q was developed at lower values of ε_a due to the increased amount of tensile stresses mobilized in the fibers. The value of ε_a at which ESP crosses the TC line increased with an increase in the p'_o at which the composite is sheared due to the increased interaction between clay particles as well as between clay particles and fibers at higher p'_o value, which subsequently improves the contribution of interface frictional strength to the overall q of fiber-reinforced clays.

6.5.2 Effect of fiber length

The samples of fiber-reinforced clay are prepared using two lengths of fibers, 18 mm and 48 mm and subjected to extension and compression loading conditions (Figs. 6.3 and 6.4). All samples are prepared using the slurry method and the orientation of fibers within the composite is horizontal.

Increasing the length of fiber augments the area of contact between fibers and soil leading to an increase in the interphase frictional component of shear strength. Additionally, increasing the fiber length improves the pullout resistance of individual fibers. This in turn leads to the mobilization of tensile stresses within the fibers, which would also contribute to the overall shear strength of the matrix (Zornberg et al. 2004).

For samples subjected to extension loading conditions, the q and Δu developed within the composite increased with an increase in the length of fibers. On the other hand, greater amount of q and Δu was observed for 18 mm long fiber-reinforced composites subjected to triaxial compression tests. The ESP for 18 mm samples deviated to the left and approached the TC line. Further mobilization of fiber tension was restricted due to the limitations of the triaxial compression-testing program as discussed in the previous section. Increasing the fiber length to 48 mm reduced the q and Δu values developed within the fiber-reinforced clays. The inability of the ESP of 48 mm long fiber-reinforced clays to approach the TC line further states the reduction in the amount of tension mobilized in 48 mm long fibers. This is expected due to the tendency of 48 mm long fibers to bend and twist inside a 50 mm diameter cylindrical sample used for triaxial testing. The bending of the fibers reduces the area of contact with the clay particles as well as limits the amount of tension mobilized. The authors expect these bent 48 mm long fibers to untwine when subjected to extension tests and mobilize tensile stresses.

It is recommended to perform tests on larger diameter samples and confirm the influence of increasing fiber lengths on the q and Δu values developed in fiber-reinforced clays. The authors expect that the boundary restrictions imposed while placing 48 mm long fiber reinforcements within a 50 mm diameter triaxial specimen are not expected to play a role when this composite is used for practical applications on field.

6.5.3 Effect of fiber alignment

Figure 6.5 evaluates the effect of fiber alignment on the q and Δu developed within the fiber-reinforced clay soil. Samples with horizontal and vertical orientation of fibers are prepared using the technique discussed in the sample preparation section of this paper and illustrated in Fig. 6.2. The fiber length is kept constant as 48 mm.

The q - ε_a curves for vertically fiber-oriented composites demonstrated a steep increase in the value of q at ε_a less than 1%. The fibers in vertically oriented fiber-reinforced samples are already aligned perpendicular to the direction of σ_1. As soon as the shearing is initiated (axial unloading), tensile stresses mobilize in the fibers increasing the q of the composite. Those samples with horizontal oriented fibers require some amount of ε_a to align perpendicular to the direction of σ_1 and mobilize tensile stresses. Yamaguchi et al. (1985) observed similar response on extension tests performed on fibrous peat samples. Peat samples with vertical orientation of fibers (referred to H-specimens in Yamaguchi et al. 1985) demonstrated a rapid increase in q for the changes in ε_a at small values of ε_a. The vertically fiber aligned specimens also showed increased value of effective angle of shearing resistance and undrained shear strength in the extension tests. This observed behavior was related to the anisotropic fabric of fibrous peat.

6.5.4 Tensile stresses mobilized within the fibers

This section of the paper summarizes the stresses acting on an unreinforced and fiber-reinforced composite prepared using the slurry method and subjected to triaxial compression and extension test.

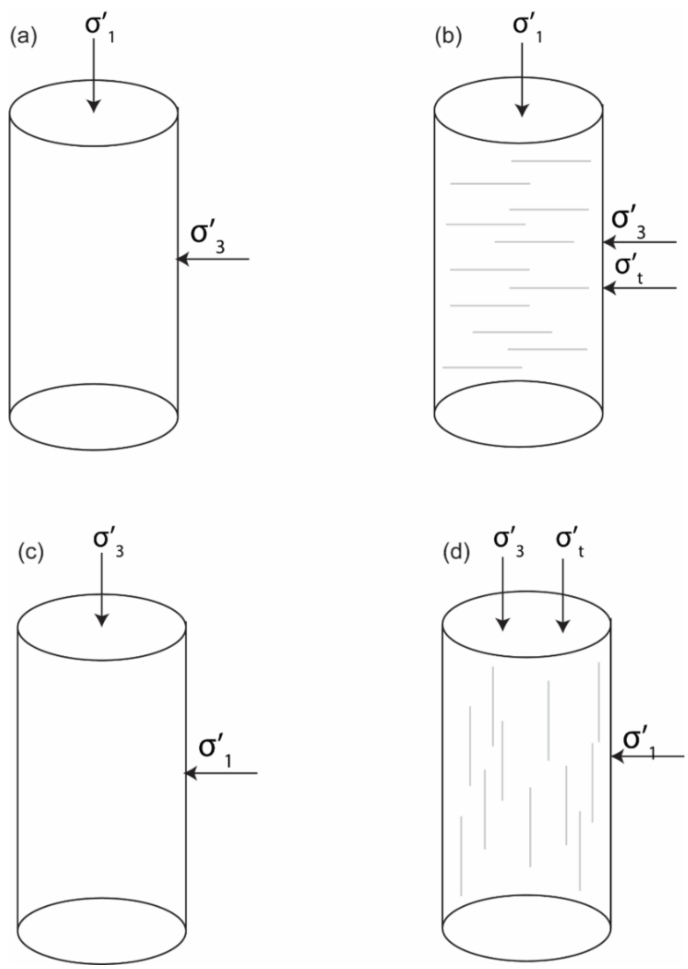

Figure 6.7. Stresses acting on an (a) unreinforced clay subjected to triaxial compression test; (b) fiber-reinforced clay subjected to triaxial compression test; (c) unreinforced clay subjected to triaxial extension test and (d) fiber-reinforced clay subjected to triaxial extension test.

In a triaxial compression test, the effective major principal stress (σ_1') acts in the vertical direction and σ_3' in the horizontal direction (Figs.6.7a and b). An increase in the σ_a during shearing (axial loading) resulted in the shear failure of the unreinforced clay soil (Palat et al. 2019). Additionally, the stress- strain plots demonstrated a peak value of q followed by a post peak response with continued shearing (Palat et al. 2019; Palat and Hendry 2022c). When fiber – reinforced composites were subjected to triaxial compression test, the fibers within the sample aligned in the horizontal direction (perpendicular to σ_1) during shearing and offered lateral resistance to the externally applied σ_a. A bulging response was observed in the composite at the end of shearing (Fig. 6.6a) along with a strain-hardening response of the stress-strain curve (Fig. 6.3b). In a triaxial compression test, σ_t' represents the lateral stress resisted by the fibers during shearing and it acts in the horizontal direction, opposite to the direction of expansive strain (Fig. 6.7b). The values of σ_1' and σ_3' acting on a fiber-reinforced clay soil subjected to a triaxial compression test is given in Eqs. (6.1) and (6.2) respectively where σ_a' and σ_r' denotes the effective axial and radial stress applied on the specimen.

$$\sigma_1' = \sigma_a' + \sigma_r' \tag{6.1}$$

$$\sigma_3' = \sigma_r' + \sigma_t' \tag{6.2}$$

In a triaxial extension test, the σ_1' acts in the horizontal direction and σ_3' acts in the vertical direction (Figs. 6.7c and d). A reduction in the value of σ_a during shearing (axial unloading) resulted in the shear failure of an unreinforced clay soil. When a fiber-reinforced clay soil is subjected to triaxial extension test, the fibers within the clay realign in the vertical direction (perpendicular to σ_1) during shearing, resists the σ_a applied on the soil, thereby restricting the formation of a shear plane (Fig. 6.6b). The σ_t' represents the axial stress resisted by the fibers and acts in the vertical direction, opposite to the direction of expansive strain (Fig. 6.7d). Eqs. (6.3) and (6.4) represents the σ_1' and σ_3' acting on a fiber-reinforced specimen subjected to triaxial extension test.

$$\sigma_1' = \sigma_r' \tag{6.3}$$

$$\sigma_3' = \sigma_r' + \sigma_t' - \sigma_a' \tag{6.4}$$

6.5.5 Quantification of the tensile stresses mobilized in the fibers

As observed in Fig. 6.7, adding fibers to the clay soil alters the σ_3' acting on the specimen (Eqs. (6.2) and (6.4)). The σ_t' mobilized within the fibers acts in the lateral direction in a compression test and in the axial direction in an extension test. The objective of this section is to develop a methodology to estimate the value of σ_t' from the experiments and come up with an empirical model to predict the measured σ_t' as a function of the fiber parameters and external stresses applied on the composite.

6.5.5.1 Estimating σ_t' from the triaxial tests

Landva and La Rochelle (1983) evaluated the shear characteristics of Radforth peats and demonstrated that the peat fibers affect the geotechnical behavior of peat by providing an internal lateral resistance to shear deformations in the triaxial mode of shear. This internal resistance offered by the fibers against deformation was considered as a function of the friction between the fibers (or between the fibers and the matrix) and the tensile strength of the fibers. According to Landva and La Rochelle (1983), even though the resistance induced by the fibers cannot be measured directly in peat specimens, the fiber contribution can be determined from the Mohr's circles if the shear strength without fibers is known.

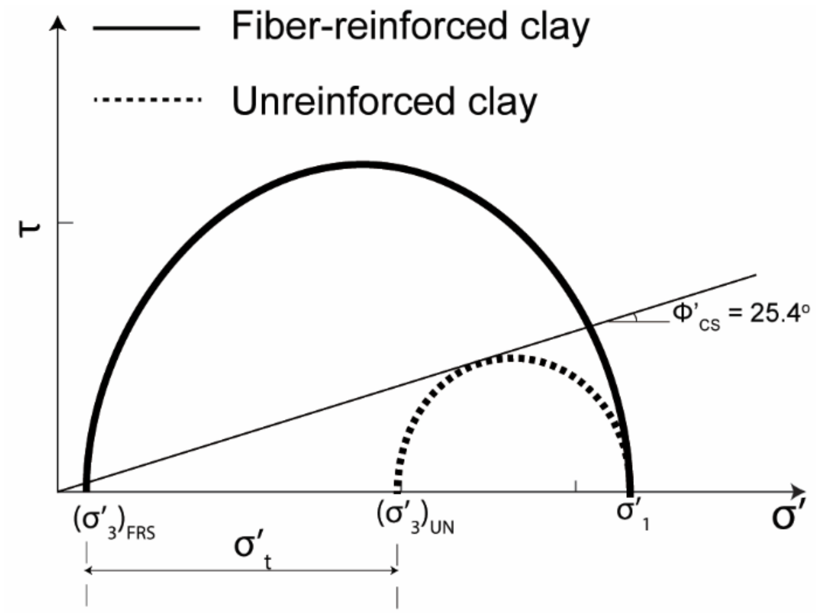

Figure 6.8. Conceptual representation of the stress resisted by the fibers during shearing (based on Landva and La Rochelle, 1983)

Figure 6.8 represents the Mohr's circles for an unreinforced and fiber-reinforced clay soil subjected to the same value of σ_1'. According to the conceptual model developed by Hendry et al. (2012) for fibrous peat, the linear increase in q during strain hardening is the result of the shear resistance due to fiber tension. Hence, during the linear strain hardening response observed in the q versus ε_a curves of fiber-reinforced soil, the clay soil will be at its critical state. Previous studies by the authors have estimated a critical state friction angle (ϕ_{CS}') of 25.4° for the unreinforced clay soil (Palat and Hendry 2022c). The value $(\sigma_3')_{UN}$ can then be estimated from the applied values of σ_1' and the ϕ_{CS}' of the clay soil from Eq. (6.5).

$$(\sigma_3')_{UN} = \frac{\sigma_1'}{\tan^2(45 + \frac{\phi_{CS}'}{2})} \tag{6.5}$$

The resulting shift to the left observed in the Mohr's circle of a fiber-reinforced clay soil corresponds to the resistance offered by the fibers during shearing (σ_t'). This value of σ_t' can then be estimated using Eq. (6.6) where $(\sigma_3')_{FRS}$ corresponds to σ_3' acting on the fiber-reinforced soil as measured from the triaxial test.

$$\sigma_T' = (\sigma_3')_{UN} - (\sigma_3')_{FRS} \tag{6.6}$$

6.5.5.2 Empirical model to predict σ_t' from fiber properties and external stresses

Previous studies on fiber-reinforced sand by Michalowski and Cermak (2002, 2003) demonstrated that the interaction between the fibers – sand interface is predominantly frictional. A failure criterion was subsequently developed for the fiber-reinforced sand by equating the work done by external forces to the internal work dissipation that occurs along the soil-fibers interfaces. The internal work dissipation was assumed to occur during the sliding of the fibers within the matrix (until the fiber stress reaches the yield point) and was only integrated along those fibers in the tensile regime. Additionally, this proposed model by Michalowski and Cermak (2002, 2003) was also sensitive to fiber concentration and fiber aspect ratio.

Following this work by Michalowski and Cermak (2002, 2003), the authors performed triaxial compression tests on clay soil reinforced with varying fiber contents and lengths to determine its influence in contributing to the shear strength of the composite. Figures 6.9a and b plot the variation of q with ε_a for clay soil reinforced with three values of fiber contents and lengths respectively tested at a p_o' of 200 kPa. This value of p_o' was selected because previous studies by the authors demonstrated that the interaction between fibers and clay particles are significant at higher values of p_o' (Palat and Hendry 2022).

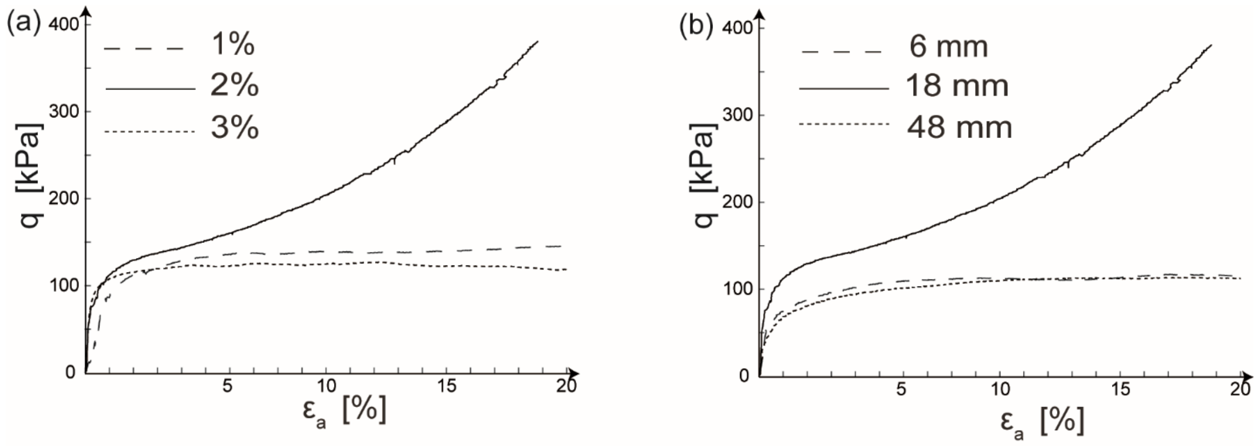

Fig. 6.9. Comparison of CU triaxial compression laboratory testing results for slurry prepared fiber-reinforced clay specimens in the q versus ε_a space for varying (a) fiber contents (fiber length = 18 mm) and (b) fiber lengths (fiber content = 2%) at a p'_o of 200 kPa.

The shear strength of fiber-reinforced clay soil is a function of fiber content where q increases with an increase in the fiber content up to an optimum fiber concentration of 2%, beyond which any increase in the fiber content resulted in a reduction. Similar value of optimum fiber content was also observed in the fiber-reinforced clay soils prepared using the compaction method (Palat and Hendry 2022a) and it is expected due to clustering of fibers within the matrix when the fiber content is increased beyond the optimum amount of 2% such that, the shear among the fibers becomes the dominating factor rather than the tensile stress mobilized in individual fibers (Palat et al. 2019).

Increasing the fiber length from 6 mm to 18 mm increased the shear strength of the composite as greater amount of tensile stresses are mobilized in longer fibers. However, increasing the fiber length to 48 mm demonstrated a reduction in q and this is expected due to the tendency of 48 mm long fibers to bend and entangle within a 50 mm diameter specimen being unable to mobilize tension while shearing. These 48 mm long fibers are expected to untwine in a triaxial extension test where an increase was observed in the q value for the range of fiber lengths used in this study (Figs. 6.3b and 6.4b). Previous studies on compacted fiber reinforced clays by Palat and Hendry (2022) demonstrated an increase in q with an increase in the length of fibers. Studies by Michalowski and Cermak (2003) on fiber-reinforced sands also stated that larger stresses would be induced on longer fibers as the axial stress in the fibers is equal to the integrated shear stress on the fiber-matrix interface.

These observations demonstrate that the amount of σ_T' mobilized within the fibers during shearing is also a function of the effectiveness of fibers in realigning in the direction of extension and contributing to the overall shear strength of the composite. Similar findings were observed from the studies on fiber-reinforced sands where the contribution of fibers to the strength of the soil is dependent on the orientation of fibers within the composite (Michalowski and Cermak 2002). The fibers in the direction of extension contribute most to the strength of the composite, whereas the fibers under compression do not produce an increase in the composite strength (Michalowski and Cermak 2002).

It is further assumed in this model that the interaction between fibers and clay particles is purely frictional where σ_T' is a function of the applied effective stresses as well as the interface friction angle between the fibers and clay soil.

Summarizing these observations, an empirical model (Eq. (6.7)) is developed to predict the σ_T' mobilized within the fibers of fiber-reinforced clay soil from the onset of strain hardening towards the end of shearing.

$$\Delta\sigma_T' = \rho\eta F(\Delta\sigma_1' - \Delta\sigma_3')\tan\phi_i' \tag{6.7}$$

where,

- ρ: fiber content defined as the ratio of the mass of fibers to the mass of clay soil. The ρ values used for the analysis are 0.01, 0.02, and 0.03.
- η: fiber aspect ratio defined as the ratio of fiber length to diameter. The fiber dimeter is kept constant as 0.035 mm for all tests. The η values corresponding to fiber lengths of 6, 18 and 48 mm are 171.4, 514.2, and 1371.4 respectively.
- F : fiber contribution ratio defined as the ratio of the amount of fibers which aligns in the direction of extension and contribute to the shear strength of the composite to the total fiber concentration. Previous experimental results demonstrated that a reduction will be observed in

the F value on increasing ρ and η. The values of F calculated based on the available experimental data are plotted in Fig. 6.10. Intermittent vales within the tested range of fiber contents and fiber lengths can be determined by interpolation.

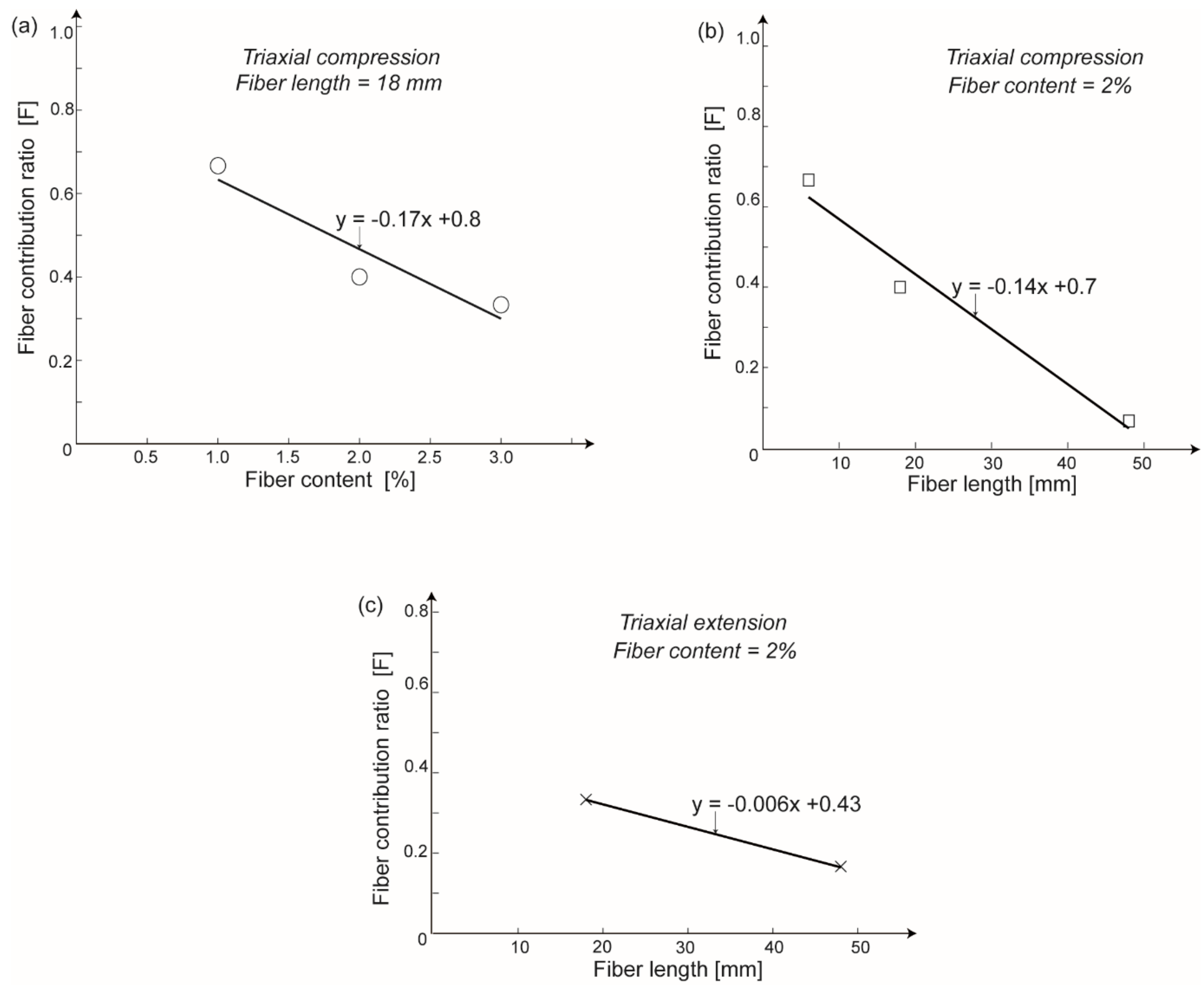

Fig. 6.10. Variation of F with varying (a) fiber contents in compression test with constant fiber length of 18 mm, (b) fiber lengths in compression test with constant fiber content of 2%, and (c) fiber lengths in extension test with constant fiber content of 2%.

- $\Delta\sigma_1'$: change in the effective major principal stress applied on the fiber-reinforced clay soil
- $\Delta\sigma_3'$: change in the effective minor principal stress applied on the fiber-reinforced clay soil

- ϕ_i': interface friction angle between the fibers and clay soil. Modified direct shear tests performed to evaluate the interface shear strength parameters between fibers and clay resulted in a ϕ_i' of 22° between the polypropylene fibers and clay soil (Palat and Hendry 2022c).

6.5.5.3 Comparison of experimental results to model predictions

Figure 6.11 and 6.12 plots the $\Delta\sigma_T'$ measured from the experiment (Eq. 6.5 and Eq. 6.6) versus $(\Delta\sigma_1' - \Delta\sigma_3') \tan\phi_i'$ from the triaxial compression and extension tests performed on fiber-reinforced clay soil as a part of this study. Clay samples reinforced with 18 and 48 mm long fibers were subjected to three values of p_o': 50, 100, and 200 kPa under compression (Figs. 6.11a and b) and extension (Figs. 6.12a and b) loading conditions. Additional compression tests were performed on 1% and 3% fiber reinforced clay soil (Figs. 6.11c and d) and on samples reinforced with 6 mm long fibers (Fig. 6.11e). The values of $\Delta\sigma_T'$ estimated from Eq. 6.7 are also superimposed on each plots for comparison purpose.

A bilinear envelope was observed in the compression tests performed on 2% - 18 mm long fiber-reinforced clay soil while plotting the experimental results showing the variation of $\Delta\sigma_T'$ versus $(\Delta\sigma_1' - \Delta\sigma_3') \tan\phi_i'$. This is expected because once the ESP for these composites approaches the TC line, $\Delta\sigma_3'$ equals zero and any further mobilization of tensile stresses is affected as the condition of $\Delta u > \sigma_3$ cannot be attained in a triaxial compression test (discussed in detail in Section 6.5.1). Hence, only the initial section of the curve, that is $\Delta\sigma_T'$ from the onset of strain hardening till the ESP approaches the TC line ($\Delta\sigma_3' > 0$) is only considered in the validation of the developed model.

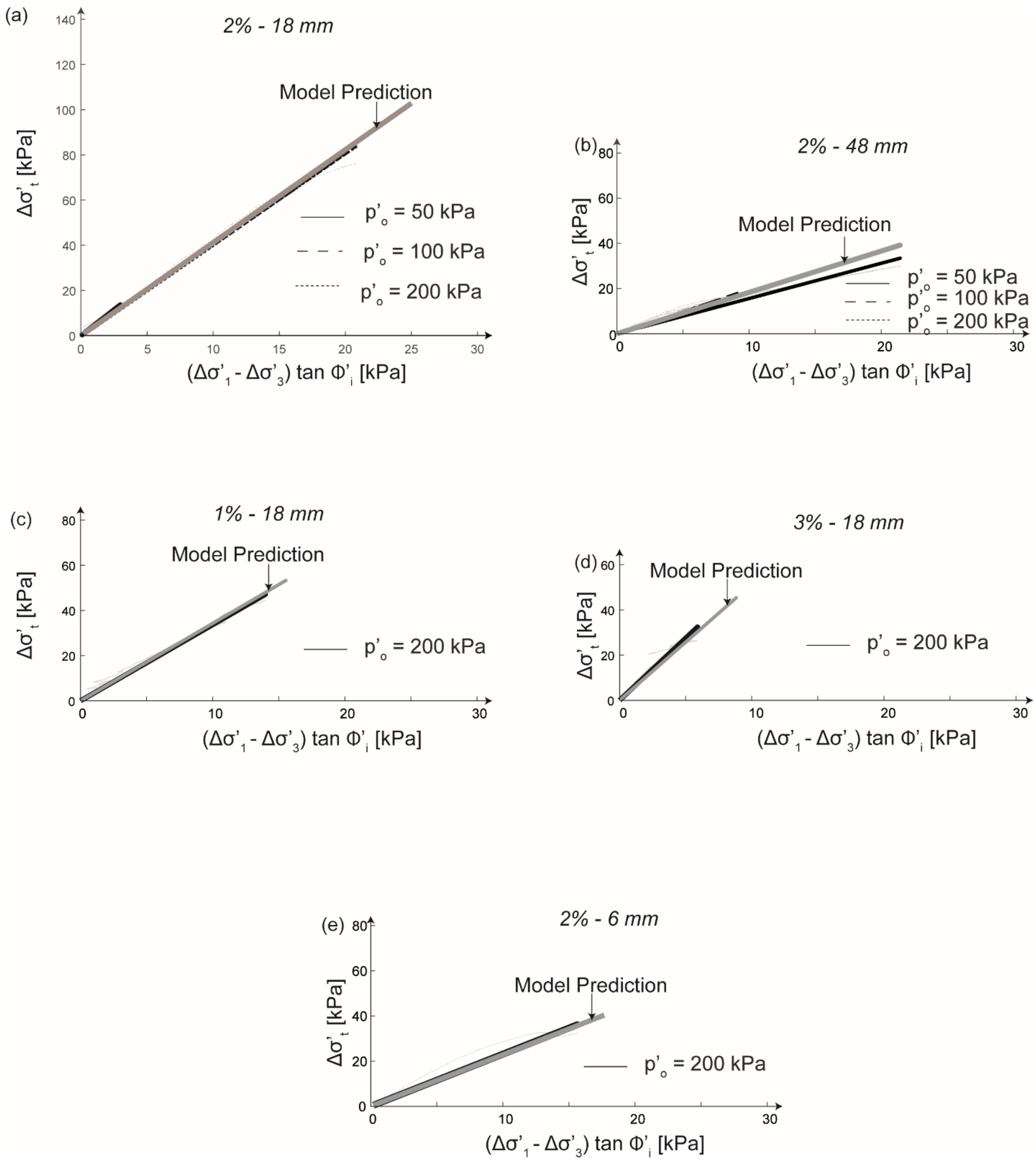

Fig. 6.11. Model predictions and experimental results showing the variation of $\Delta\sigma_T'$ versus $(\Delta\sigma_1' - \Delta\sigma_3')\tan\phi_i'$ in triaxial compression tests performed on (a) 2% - 18 mm, (b) 2% - 48 mm (c) 1% - 18 mm (d) 3% - 18 mm and (e) 2% - 6 mm fiber-reinforced clay soil.

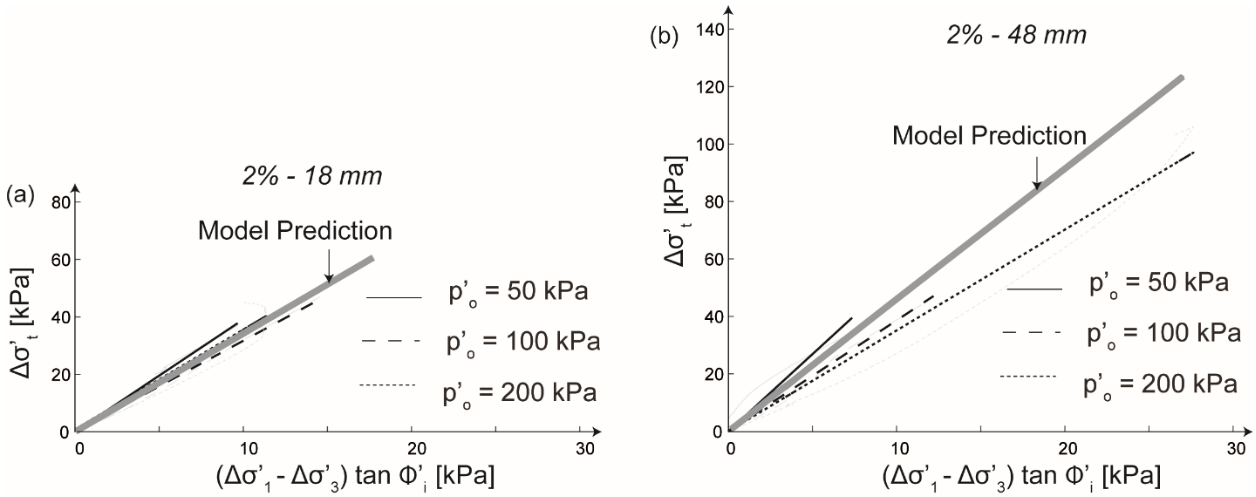

Fig. 6.12. Model predictions and experimental results showing the variation of $\Delta\sigma_T'$ versus $(\Delta\sigma_1' - \Delta\sigma_3')\tan\phi_i'$ in triaxial extension tests performed on (a) 2% - 18 mm and (b) 2% - 48 mm fiber-reinforced clay soil.

The model gave accurate predictions for the σ_T' mobilized within the fibers for all compression and extension tests performed as a part of this study. The scatter observed in the datasets for 48 mm long fiber-reinforced samples (Figs. 6.11b and 6.12b) are expected due to the restrictions imposed by the boundary where 48 mm long fibers will have limited ability to mobilize tension within a 50 mm diameter specimen. The authors recommend testing on larger diameter samples to analyse whether the tensile stress mobilized in the fibers is a function of the specimen diameter. The other limitations of this proposed model are as follows:

- The model is only validated within the range of fiber contents (1% - 3%) and fiber lengths (6 mm – 48 mm) used in this study.
- This model is only applicable for fiber-reinforced clay soil prepared using the slurry method of sample preparation.
- Finally, the model is only validated for clay soil reinforced with polypropylene fibers. The next stage in this study involves evaluating the wide applicability of this proposed model in predicting the tensile stresses that occur due to fiber reinforcement within other fibrous soils such as peat.

6.6 Conclusions

The scope of CU triaxial compression tests are limited with their ability to measure the impacts of tensile elements within a fiber-reinforced soil. The undrained ESP for the soil-fiber composites followed the shape of TC line when Δu was equal to p_o' and no compression tests were able to demonstrate the mobilization of tensile stresses that occur due to fiber reinforcement. The primary objective of this study was to demonstrate the mobilization of tensile stresses within these discrete fibers used as reinforcements in fiber-reinforced clays. The influence of fiber length, fiber alignment, and p_o' on the undrained shear strength and mobilized fiber tension are quantified. An empirical model was then developed to predict the mobilized internal fiber tension as a function of the applied external stresses and fiber parameters.

- Samples of fiber-reinforced clay exhibited a bulging response with no evident shear plane in compression tests. Fiber-reinforced clays subjected to triaxial extension tests demonstrated an increase in length with a reduction of diameter at neck during shearing.

- The TC line defines the condition in a triaxial test where the σ_3' equals zero. Any stress state in excess of the TC line is solely due to the mobilization of tensile stresses within the fibers. Triaxial extension tests performed on fiber-reinforced clays demonstrated the mobilization of tensile stresses within the fibers where the ESP's exhibited values of q in excess of the TC line. This is possible because the condition of $\Delta u > \sigma_3$ can be satisfied in an extension test by maintaining $\Delta u < \sigma_{cell}$ and preventing the drainage from the specimen.

- Increasing the length of fibers from 18 mm to 48 mm had a beneficial effect on the shear strength of the composite in a triaxial extension test. This comes from the greater area of contact of fibers with the clay particles (higher contribution from the interface frictional strength) as well as increased amount of tensile stresses mobilized in longer fibers. In contrast, increasing the fiber length beyond 18 mm had a detrimental effect on the q of the composite in compression test. The authors expect fibers of length 48 mm to bend and twist inside a 50 mm diameter specimen thereby limiting their ability to mobilize tensile stresses during shearing. These fibers are expected to untwine and contribute to the q of the composite under extension loading conditions.

- Triaxial extension tests on vertically aligned fiber-reinforced samples demonstrated a rapid increase in the value of q at lower values of ε_a. The fibers within these samples are already oriented perpendicular to the direction of σ_1, hence tensile stresses mobilize in the fibers as soon as the shearing is initiated. The fibers aligned in the horizontal orientation requires some amount of ε_a to align perpendicular to σ_1 and mobilize tension.

- When a fiber-reinforced clay soil is subjected to triaxial compression test (axial loading), the fibers align in the horizontal direction and offers lateral resistance to the applied external load. Whereas, when subjected to extension loading conditions (axial unloading), the fibers realign in the vertical direction and resist the σ_a applied on the composite. For both loading conditions, the σ_t' acts in the direction opposite to the direction of expansive strain.

- An empirical model was developed to predict the σ_t' mobilized within the fibers under compression and extension loading conditions by assuming that the interactions between fibers and clay are purely frictional. The developed model was also sensitive to fiber content, length, and the effectiveness of the fibers to realign in the direction of extension and mobilize tension during shearing. The model gave accurate predictions to the σ_t' measured from the experiments specifically for 6 mm and 18 mm long fibers. The authors recommend performing more tests on larger diameter samples as well as other fibrous soils such as peat to validate the extended applicability of the model.

6.7 Acknowledgement

This research was funded by a Natural Sciences and Engineering Research Council Discovery Grant (grant no: #RGPIN-2020-04419). The authors also thank MiniFIBERS. Inc. for supplying the fibers for triaxial testing.

6.8 References

ASTM D4767-11. 2020. Standard Test Method for Consolidated Undrained Triaxial Compression Test for Cohesive Soils. ASTM International, West Conshohocken, PA, 2020, www.astm.org.

Consoli, N.C., Heineck, K.S., Casagrande, M. D. T., and Coop, M.R. 2007. "Shear strength behavior of fiber-reinforced sand considering triaxial tests under distinct stress paths." Journal of Geotechnical and Geoenvironmental Engineering, 133(11),p1466-1469.

Consoli, N.C., Nierwinski, H. P., da Silva, A. P., Sosnoski, J. 2017. "Durability and strength of fiber-reinforced compacted gold tailings cement blends." Geotextiles and Geomembranes 45, p98-102, doi: 10.1016/j.geotexmem.2017.01.001.

Festugato, L., Fourie, A., Consoli, N. C. 2013. "Cyclic shear response of fibre-reinforced cemented paste backfill." Geotechnique Letters 3(1), p5–12.

Festugato, L., Consoli, N. C., Fourie, A. 2015. "Cyclic shear behaviour of fibre-reinforced mine tailings." Geosynthetics International, 22(2), p196–206, doi: 10.1680/gein.15.00005.

Freilich, B., Li, C., and Zornberg, J.G. 2010. "Effective shear strength of fiber-reinforced clays." In Proceedings of the 9th International Conference on Geosynthetics, 9ICG, Guarujá, Brazil, May, Vol. 4, p1997-2000.

Gray, D.H., and Ohashi, H. 1983. "Mechanics of fiber reinforcement in sand." Journal of Geotechnical Engineering, 109(3), p335-353.

Hendry, M.T. 2011. "The geomechanical behaviour of peat foundations below rail-track structures." PhD thesis, University of Saskatchewan.

Hendry, M.T., Sharma, J.S., Martin, C.D., and Barbour, S.L. 2012. "Effect of fibre content and structure on anisotropic elastic stiffness and shear strength of peat." Canadian Geotechnical Journal, 49, p403–415.

Hendry, M.T., Martin, C.D., and Barbour, S.L. 2013. “The measurement of the cyclic 563 response of railway embankments and underlying soft peat foundations to heavy axle 564 loads.” Canadian Geotechnical Journal, 50(5), p467-480.

Hendry, M.T., Barbour, S.L., and Martin, C.D. 2014. “Evaluation of the effect of fibre reinforcement on the anisotropic undrained stiffness and strength of peat.” Journal of Geotechnical and Geoenvironmental Engineering, 140(9).

Landva, A.O., and La Rochelle, P. 1983. “Compressibility and shear characteristics of radforth peats.” In Testing of Peats and Organic Soils. ASTM Special Technical Publication, 820, p157-191.

Li, C. 2005. “Mechanical response of fiber-reinforced soil.” Ph.D. thesis, University of Texas at Austin, Austin, TX.

Maher, M.H., and Woods, R.D. 1990. “Dynamic response of sand reinforced with randomly distributed fibers.” Journal of Geotechnical Engineering, 116(7), https://doi.org/10.1061/(ASCE)0733-9410(1990)116:7(1116).

Maher, M.H., and Ho, Y.C. 1994. “Mechanical properties of kaolinite/fiber soil composite.” Journal of Geotechnical Engineering, 120(8), p1381-1393.

Michalowski, R.L., and Čermák, J. 2002. “Strength anisotropy of fiber-reinforced sand.” Computers and Geotechnics, 29(4), p279–299, doi: 10.1016/S0266-352X(01)00032-5.

Michalowski, R.L., and Čermák, J. 2003. “Triaxial compression of sand reinforced with fibers.” Journal of Geotechnical and Geoenvironmental Engineering, 129(2).

Palat, A., Hendry, M.T., and Roustaei, M. 2019. “Effect of fiber content on the mechanical behavior of fiber-reinforced clay.” In Proceedings of the 72nd Canadian Geotechnical Society Annual Conference, GeoStJohns 2019, St. John’s, NF, 29 September - 2 October 2019.

Palat, A., and Hendry, M.T. 2021. “Evaluation of the geomechanical behavior of fiber-reinforced clay soil.” In Proceedings of the 74th Canadian Geotechnical Society Annual Conference and the 14th Joint CGS/IAH-CNC Groundwater Conference, GeoNiagara 2021, Niagara Falls, Ontario. 26 September - 29 September 2021.

Palat, A., and Hendry, M.T. 2022. “Investigation of the behavior of fiber-reinforced clay soil.” In Proceedings of the 20th International Conference on Soil Mechanics and Geotechnical Engineering, ICSMGE 2022, Sydney, Australia. 1 May- 6 May 2022.

Palat, A., Hendry, M.T. 2022a. “Experimental investigation of the effect of polymer fibers on the pore pressure response and undrained shear strength of clay.” *(To be submitted)*.

Palat, A., Hendry, M.T. 2022b. “The effect of sample preparation methods on the undrained behavior of fiber reinforced clay.” *(To be submitted)*.

Palat, A., Hendry, M.T. 2022c. “Quantification of the effect of fiber polymer type on the undrained behavior and realizable strength of fiber-reinforced clay.” *(To be submitted)*.

Wood, D.M. 1990. Soil Behavior and Critical State Soil Mechanics, Cambridge University Press. ISBN 0-521-33249-4.

Yamaguchi, H., Ohira, Y., Kogure, K., and Mori, S. 1985. “Undrained shear characteristics of normally consolidated peat under triaxial compression and extension conditions.” Soils and Foundations 3, p1–18, doi:10.3208/sandf1972.25.3_1.

Yi, X.W., Ma, G.W., Fourie, A. 2015. “Compressive behaviour of fibre-reinforced cemented paste backfill.” Geotextiles and Geomembranes 43, p207-215, doi: 10.1016/j.geotexmem.2015.03.003.

Zheng, B., Zhang, D., Liu, W., Yang, Y., Yang, H. 2019. “Use of basalt fiber-reinforced tailings for improving the stability of tailings dam.” Materials, 12, 1306; doi:10.3390/ma12081306.

Zornberg, J.G. 2002. “Discrete framework for limit equilibrium analysis of fibre-reinforced soil.” Geotechnique, 52(8), p593–604.

Zornberg, J.G., and Li, C. 2003. “Design of fiber-reinforced soil.” In Proceedings of the Twelfth Panamerican Conference of Soil Mechanics and Geotechnical Engineering, Cambridge, MA, June 22-26, Vol. 2, pp. 2193-2200.

Zornberg, J. G., Cabral, A, R., and Viratjandr, C. 2004. “Behavior of tire shred- sand mixtures.” Canadian Geotechnical Journal, 41(2), p227-241.

Chapter Seven: Conclusions and Recommendations

7.1 General Conclusions

Through this study, it is demonstrated that the addition of short, discrete polymer fibers improve the geomechanical behavior of clay soil. The stress-strain curves from triaxial compression and extension tests on unreinforced clay demonstrated a strain weakening behavior after the attainment of maximum deviator stress and all unreinforced samples failed by forming a well-defined failure plane. Fiber-reinforced clay samples exhibited a bulging response in compression tests and an increase in length (with a reduction of diameter at neck) in extension tests, without an evident shear plane under both loading conditions. Additionally, the stress-strain curves for all fiber-reinforced samples demonstrated a strain hardening response without a maximum value of shear stress that can be identified as the strength of the composite. Adding fibers to the clay also increased the undrained shear strength, excess pore water pressure and yield strength of the clay soil.

The research objectives accomplished as a part of this study are as follows:

- Investigated the fundamental mechanics of fiber-reinforced clays with focus on tensile stresses that occur due to fiber reinforcement and its impact on realizable strength.

- Examined the role of fiber variables (fiber content, length, and type) in influencing the undrained shear strength, induced pore water pressure, undrained stiffness, and yield strength of the soil-fiber composite.
- Evaluated the role of method of sample preparations (compaction and slurry) in influencing the goemechanical behavior of fiber-reinforced clay soil.
- Analyzed the extent of anisotropy exhibited in fiber-reinforced clays prepared using two different techniques and the role of fiber orientation in influencing the mobilized tensile stresses and the overall shear strength of the composite.
- Developed a technique to visualize and track the distribution, orientation and movement of fibers within the clay soil.
- Investigated the interface shear strength between fibers and clay soil and discussed the impact of the interface friction angle in influencing the shear strength, pore pressure, and yield strength of fiber-reinforced clay soils.
- Quantified the tensile stresses generated within the fiber-reinforced clays specifically, how tension in fibers are incorporated into the strength.

The following sections provides the major conclusions from the studies conducted as a part of this research:

7.1.1 Shear strength of fiber-reinforced clays

This study evaluated the shear strength of fiber-reinforced clay soil prepared using two techniques – compaction method and slurry method. The other variables included in the laboratory testing program are:

- Effective confining pressures (p'_o) – 50 kPa, 100 kPa, and 200 kPa
- Fiber contents –1%, 2%, and 3%
- Fiber lengths –6 mm, 18 mm, 48 mm
- Fiber types – Polypropylene (PP) and Nylon (PA)
- Loading path – Compression and extension
- Fiber alignment – Horizontal and vertical

The overall shear strength of a fiber –reinforced clay soil is the sum of three parameters: (1) strength due to the interaction between clay particles; (2) strength due to interface frictional interaction between fibers and clay; and (3) mobilized tensile stresses along the fibers. Fibers do not play a greater role in altering the behavior of the clay soil at lower values of axial strain (ε_a) as some amount of ε_a is required to engage the fibers. Any increase in the deviator stress (q) and pore water pressure (Δu) observed at lower ε_a levels are due to the interaction between the clay particles. The increase in the shear strength after the linear elastic region until the onset of strain hardening was observed to be the effect of interface frictional interaction between fibers and clay. The increase in q during the linear strain-hardening portion of the stress-strain curve was due to mobilization of tensile stresses within the fibers.

Effect of p_o'

The values of q and Δu increased with an increase in p_o' for both unreinforced and fiber-reinforced samples. In case of unreinforced samples, the particles get tightly packed at higher p_o'. This increases the bonding and force of attraction among the particles leading to an increase in the strength and pore pressure values. For the fiber-reinforced samples, the increase in q and Δu with p_o' could be due to the contribution of two factors. Firstly, there will be greater interaction between soil particles and fibers leading to an increase in the frictional component of shear strength. Secondly, the amount of tension mobilized in the fibers increases with an increase in p_o' providing additional shearing resistance (Palat and Hendry, 2022).

Effect of fiber content

Triaxial compression tests on compacted and slurry prepared fiber-reinforced samples demonstrated that the shear strength of the composite increased with an increase in fiber content up to 2%, beyond which any further increase in the fiber content resulted in a reduction of strength. This is expected due to the uneven distribution of fibers within the soil when the fiber content is increased beyond the optimum amount of 2%. The fibers are expected to adhere to each other and form lumps rather than connecting the soil particles and improving the bonding. The shear among the individual fibers becomes the dominating factor over the tensile stresses mobilized in individual fibers. This concludes that the optimum fiber content for mixing with the clay soil is

2% irrespective of the method of sample preparation (*Chapter Three*, Manuscript #1, *Chapter Six*, Manuscript #4).

Effect of fiber length

Increasing the length of fibers increases the area of contact between the fibers and clay particles resulting in an increase in the interface frictional component of shear strength. Additionally, the amount of tensile stresses mobilized in the fibers also increases with an increase in fiber length.

For compacted samples subjected to triaxial compression test (*Chapter Three*, Manuscript #1) as well as for slurry samples in triaxial extension tests (*Chapter Six*, Manuscript #4), the shear strength of the soil-fiber composite increased with an increase in the length of the fibers. For 48 mm long fiber-reinforced compacted specimens, a maximum value of q equals 1200 kPa was observed at the end of shearing when subjected to a p'_o of 200 kPa.

However, for slurry prepared fiber-reinforced composites subjected to triaxial compression tests, a reduction was observed in the q and Δu values when the fiber length was increased from 18 mm to 48 mm (*Chapter Six*, Manuscript #4). This is expected due to the increased tendency of the 48 mm long fibers to be bent and twisted when 50 mm diameter shelby tubes are pushed into the soil-fiber block for extracting cylindrical samples for triaxial testing. These bent 48 mm fibers are expected to untwine under extension loading conditions, mobilize tensile stresses and contribute to the overall shear strength of the composite.

It can thus be summarized that, for the range of fiber lengths used in this study, the overall shear strength of the composite increased with an increase in the length of the fibers. The reduction observed for 48 mm long fiber-reinforced slurry samples under compression test is the effect of restrictions imposed by the boundary.

Effect of fiber type

The effect of changing fiber types on the shear strength of fiber-reinforced clays is highly dependent on the method of sample preparation as well as the orientation of fibers within the clay soil. Higher values of q was observed in the PA fiber-reinforced clay soil when prepared using the compaction method whereas in PP fiber-reinforced clays when prepared using the slurry method.

A novel transparent fiber-reinforced clay soil was developed in this research to visualize the orientation of fibers within compacted and slurry prepared composites. Visual examination of the transparent fiber-reinforced clays confirmed the predominant fiber orientation is horizontal in samples prepared using the slurry method and is random in samples prepared using the compaction method (*Chapter Four*, Manuscript #2).

The principal factor contributing to the shear strength of a randomly fiber oriented composite is the interface shear strength between the fibres and clay particles. Modified direct shear tests performed to determine the interface shear strength between fibers and clay (*Chapter Five*, Manuscript #3) gave an interface friction angle (ϕ_i') of 31.5° between PA fibers and clay and 22° between PP fibers and clay. The higher ϕ_i' between PA fibers and clay resulted in higher values of shear strength when discrete PA fibers were used as a reinforcement within the compacted soil-fiber composites. The tensile stresses mobilized in the fibers are dominant when fibers are aligned perpendicular to the direction of major principal stress. In a triaxial compression test, the major principal stress acts in the vertical direction and the maximum amount of tension will be mobilized in the horizontally aligned fibers. Greater amount of tension mobilized in the PP fibers resulted in higher values of q in the slurry prepared PP fiber-reinforced clay soil.

Effect of fiber alignment

The effect of changing fiber alignment on the shear strength of fiber-reinforced clays was determined by performing triaxial extension tests on the composites. Visual examination of the slurry prepared transparent soil demonstrated that the fibers are predominantly oriented in the horizontal direction within the slurry samples. The technique used for preparing slurry fiber-reinforced clays with horizontal and vertical orientation of fibers is illustrated in Fig. 6.2 (*Chapter Six*, Manuscript #4). Changing the fiber alignment was also a deciding factor for the rate at which q increased with increasing ε_a. Higher values of q was observed at lower values of ε_a for those composites with vertical orientation of fibers. The behavior is tied to the difference in orientation of fibers with respect to the major principal stress acting on the composite. The major principal stress acts in the horizontal direction in an extension test and the greater contribution to shear strength comes from samples reinforced with vertically oriented fibers. For fiber-reinforced samples with horizontally oriented fibers, they require some amount of ε_a to align perpendicular to the direction of major principal stress and mobilize tension.

Effect of loading path

Performing a triaxial compression test limits the potential to maximize the shear strength of fiber-reinforced clays and demonstrate the mobilization of tensile stresses within the fibers. The tension cut off (TC) line defines a condition in a triaxial test where the minor effective principal stress is zero. The TC line extending from the origin has a slope of 3:1 in the compression stress space and -2:3 in the extension stress space. Any stress state in excess of the TC line is solely due to the mobilization of tensile stresses within the fibers. When 2% - 18 mm long slurry prepared fiber-reinforced samples were subjected to triaxial compression test, the Δu developed within the composite became equal to the p_o' at which the specimen was sheared, the effective stress path (ESP) approached the TC line and later followed the trace of the TC line. For the ESP to cross the TC line and to demonstrate the mobilization of tensile stress within the fibers, the condition of $\Delta u > \Delta\sigma_3$ $(= \Delta\sigma_{cell})$ has to be satisfied and no tests were able to result in a tensile stress state during compression shearing (*Chapter Four*, Manuscript #2).

The mobilization of tensile stresses within the fibers of fiber-reinforced clays were demonstrated by performing a series of triaxial extension tests on fiber-reinforced clays (*Chapter Six*, Manuscript #4). For all fiber-reinforced samples subjected to triaxial extension tests, the ESP's demonstrated values of q in excess of the TC line and greater amount of fiber tension was observed in composites reinforced with fibers of longer length.

Contribution of mobilized fiber tension to the shear strength of the composite

Samples of unreinforced compacted clay resulted in a c' of 100 kPa and $\phi'$of 16°, while slurry-prepared unreinforced clay resulted in a c' of 23 kPa and ϕ' of 10.6° (*Chapter Five*, Manuscript #3). Considering the strain hardening response of the stress-strain curves (compacted and slurry prepared PP and PA fiber-reinforced composites) without a well-defined peak stress, it was not possible to define the strength for this class of material.

The discrete fibers within the clay soil increased the overall shear strength of the composite by mobilizing tensile stress in the direction opposite to the direction of expansive strain. During the linear strain hardening section of the stress-strain curve, the clay soil will be at its critical state. Consolidated drained direct shear tests on unreinforced clay estimated a critical state friction angle (ϕ'_{CS}) of 25.4° for the unreinforced clay soil. A methodology is demonstrated in this study to determine the magnitude of tensile stress mobilized within the fibers from the Mohr's circles of unreinforced and fiber-reinforced clays once the critical state strength of the clay soil is known (Fig. 6.8, *Chapter Six*, and Manuscript #4).

An empirical model was then developed to predict the fiber tension as a function of the applied external stresses as well as fiber parameters. This model later validated with the experimental results, gave accurate correlations for predicting the tensile stress mobilized within 6 mm and 18 mm long fibers. The scatter observed in predicting the tensile stress within 48 mm long composites are expected due to the restrictions imposed by the boundary. According to the proposed empirical model, the interaction between fibers and clay particles are predominantly frictional in nature where the fiber tension was observed to be a function of the effective stresses acting on the composite as well as the interface friction angle between the fibers and clay soil. The amount of mobilized fiber tension also increased with an increase in the fiber content, fiber length as well as the effectiveness of the fibers to realign in the direction of maximum extension and contribute to the shear strength of the composite during shearing.

7.1.2 Evaluation of the cross-anisotropy

The undrained anisotropic response of compacted and slurry prepared fiber-reinforced clay soil has been characterized using the measured pore water pressure response that resulted from undrained loading (*Chapter Four*, Manuscript #2).

The orientation of fibers within clay soil was highly dependent on the method by which the soil-fiber composite was prepared. Two potential options were explored in this research to prepare fiber-reinforced clay soil for triaxial testing (1) compacting to the maximum density; (2) hydraulically placing as a slurry followed by incremental loading. A novel transparent fiber-reinforced soil was then developed to visualize and track the distribution and orientation of fibers within the compacted and slurry prepared composites (*Chapter Four*, Manuscript #2).

The fibers within a compacted fiber-reinforced clay soil were oriented in random directions due to the higher compaction energy supplied during the sample preparation (Fig. 4d, *Chapter Four*, Manuscript #2). These compacted fiber-reinforced composites demonstrated a quasi over consolidated behavior where the ESP's deviated to the right throughout shearing indicating an increased value of vertical stiffness over horizontal stiffness (*Chapter Three*, Manuscript #1, *Chapter Four*, Manuscript #2). For all compacted fiber-reinforced samples, the a value remained negative (varied from $-\frac{1}{2}$ to $-\frac{1}{25}$) throughout the shearing indicating that more amount of ε_a is required for the fibers to reorient in the horizontal direction during shearing and contribute to the horizontal stiffness of the clay soil.

When a fiber-reinforced composite was prepared using the slurry method, the fibers were initially oriented in random directions when the slurry was prepared and poured into the glass mold (Fig. 3a, *Chapter Four*, and Manuscript #2). At the end of consolidation, the fibers in the slurry developed a tendency to realign in the horizontal direction owing to their self-weight (Fig. 3d, *Chapter Four*, and Manuscript #2). Undrained shearing of these composites demonstrated an increase in the overall horizontal stiffness of the composite where the ESP's deviated to the left, approached the TC line (once Δu was equal to $\Delta\sigma_3$), and later followed the trace of the TC line. The value of pore pressure parameter a became positive at lower values of ε_a (spanned between $-\frac{1}{3}$ and 1) for all slurry samples. The positive value of a as well as the deviation of the ESP to the left confirmed the ability of the horizontally oriented fibers within the slurry samples to mobilize tensile stresses and increase the overall horizontal stiffness of the composite during shearing.

The observed maximum value of a exceeded the limiting ranges proposed for natural clay soil by Graham and Houlsby (1983) and Wood (1990). This deviation from the past literature was attributed to the increased amount of tension mobilized in the fibers during the shearing phase of a triaxial test increasing the overall horizontal stiffness of the composite as well as the a value beyond the previous ranges stated for natural clay soil. Accordingly, the equations developed for estimating the stiffness ratio by Graham and Houlsby (1983) were not applicable for this class of material (*Chapter Four*, Manuscript #2).

7.1.3 Yield strength of fiber-reinforced clays

In this research, the role of fibers in altering the yield point of a clay soil was investigated by using the bilinear technique proposed by Graham et al. (1983). Yield points were approximated as the intersection of straight approximations of the initial stiff section and the subsequent more flexible response to applied stresses. The yield points were interpreted from the plots of q versus ε_a, major effective principal stress (σ_1') versus ε_a, minor effective principal stress (σ_3') versus radial strain (ε_r) and Δu versus ε_a. The stresses and pore water pressure at yield (as obtained from the graphs) were then converted to a common stress variable, mean effective stress (p') for the comparison purpose. A significant level of agreement was observed in all four values of p' and the study confirmed that the concept of yield is applicable for the fiber-reinforced soil composites (*Chapter Three*, Manuscript #1).

Changing the fiber contents and lengths did not play a remarkable role in altering the p' at yield for a clay soil. However, the q observed at yield increased with an inclusion of fibers with a maximum value observed for fiber-reinforced samples prepared at a fiber content of 2% and fiber length of 48 mm. This observation tied back to the optimum fiber content and length determined based on the shear stress and pore pressure response from the lab testing results (*Chapter Three*, Manuscript #1).

Additionally, changing fiber types (PP vs. PA) also had a minimal effect in influencing the yield strength of fiber-reinforced clay soil and a common yield line was defined for the fiber-reinforced composites prepared using the compaction and slurry method of sample preparation (*Chapter Five*, Manuscript #3). Compacted fiber-reinforced clays demonstrated a higher yield strength (c' = 50 kPa, ϕ'= 30°) compared to slurry composites (c' = 6 kPa, ϕ' = 21°). In the compaction method, the fiber-reinforced composites are prepared at a water content of 28% (OMC) and density values ranging from 1.7 to 2.0 g/cm^3. The water content of the slurry samples after consolidation was 46%, with density values ranging from 1.4 to 1.62 g/cm^3. The higher yield strength in compacted samples is expected due to the increased compaction energy supplied during sample preparation, maximum dry density, optimum moisture content, and tight packing of particles (*Chapter Five*, Manuscript #3). Slurry fiber-reinforced samples demonstrated a low value for effective cohesion (c' = 6 kPa) similar to intact peat specimens (Hendry et al., 2014).

7.1.4 Undrained stiffness of the soil-fiber composite

Triaxial compression and extension tests performed on fiber-reinforced clay soil demonstrated that adding fibers did not play a remarkable role in altering the undrained stiffness of a clay soil. This ties back to the observations from previous studies that some amount of ε_a is required to engage the fibers (Li, 2005) and the fibers are unable to alter the geomechanical properties of the soil at lower values of ε_a. The initial portion of the stress-strain curve looked similar for both unreinforced and fiber-reinforced composites irrespective of changing fiber contents, lengths, and types.

However, an increase was observed in the undrained stiffness of both unreinforced and fiber-reinforced composites with an increase in the p'_o at which the sample was sheared. This was attributed to the greater increase in the interaction between clay particles as well as between clay particles and fibers at higher values of p'_o.

7.1.5 Influence on pore water pressure

For all compacted samples in compression tests, the Δu developed within the specimen approached maximum value (Δu_{max}) at lower values of ε_a followed by a steep reduction. This behavior of a heavily over consolidated sample was due to the higher compaction energy imparted during sample preparation. For 48 mm compacted fiber-reinforced samples tested at a p'_o of 200 kPa in compression test, the value of Δu at the end of shearing was equal to the p'_o applied.

Greater amount of Δu was developed in all slurry prepared composites when subjected to compression loading conditions. The value of Δu increased at lower values of ε_a and it remained unchanged throughout the end of shearing. This is attributed to the increased amount of tensile stresses mobilized within the fibers of slurry samples leading to an increase in the Δu values. For 18 mm long slurry prepared composites, the Δu at the end of shearing was equal to the p'_o at which sample was sheared when tested at all values of p'_o. Further mobilization of tensile stresses within the fibers were limited due to inability of Δu to increase beyond the p'_o value as the drainage of water from the sample is prevented in an undrained triaxial test (*Chapter Four*, Manuscript #2).

The role of changing fiber polymer types in influencing Δu is dependent on the method of sample preparation. For sample prepared using the compaction method, greater values of Δu was observed in PA fiber-reinforced composite due to the higher interface shear strength between PA fibers and clay soil. In contrast, greater value of Δu was observed in PP fiber-reinforced composites when prepared using the slurry method. This is expected due to the increased amount of tension mobilized in PP fibers during shearing (*Chapter Five*, Manuscript #3).

7.1.6 Potential applications for the stabilization of mine fine tailings

Accumulation of fines over time has been identified as a reason for the slow rate of reclamation in oil sands. Various tailings treatment methods are adopted to treat the fluid fine tailings and make it ready for reclamation. Reinforcing with discrete fibers can be considered as a potential option for improving the properties of fluid fine tailings.

This research investigates the fundamental mechanism of fine-grained soil reinforced with short, discrete fibers with special emphasis on the undrained stress-strain response, pore water pressure, undrained stiffness, and yield strength of the composite. This effect of altering fiber variables (content, length, type, and alignment) on the undrained behavior of fine-grained soil is evaluated and an empirical model is developed to estimate the contribution of fiber tension to the overall shear strength of the soil.

An evaluation of the fiber orientation within clays indicates that the fibers are oriented in the random direction when mixed hydraulically with a fine-grained soil. These discrete fibers realign in the horizontal direction during self-weight consolidation as well as when subjected to an incremental load from the top.

Reinforcing with discrete fibers improves the geomechanical behavior of fine-grained soil and the major observations from this study are summarised below:

- Adding fibers increases the ductility of the clay soil as indicated by the bulging response (without an evident failure plane) as well as a strain hardening behavior of the stress-strain curve.
- Fibers contribute to the shear strength of fine-grained soil predominantly by the mobilization of tensile stresses during shearing. Fiber mobilized tension is paramount when the orientation of fibers is perpendicular to the direction of major principal stress.
- The optimum fiber content for mixing with fine-grained soil is 2%, beyond which the fibers tend to cluster within the soil reducing the efficiency to mobilize tension.
- Increasing the length of fibers improves the shear strength of the composite as the amount of tensile stress mobilized in the fibers increases with an increase in fiber length. However, the optimal fiber length for use in practise must be selected considering the area of placement, to ensure that no restrictions are imposed by the boundary.
- Tensile stresses mobilize within the horizontally oriented fibers during loading, subsequently increasing the overall horizontal stiffness of the composite over the vertical stiffness. An increase in horizontal stiffness is accompanied by an increase in the pore water pressure during shearing.
- The empirical model developed in Chapter 6 can be used to estimate the amount of effective fiber tension mobilized during shearing once the fiber parameters and applied external stresses are known. The effective fiber tension acts in the horizontal direction during loading providing an added confinement to the applied external stresses. When

subjected to unloading, the effective fiber tension acts in the vertical direction reducing the net axial stress applied on the soil.

The results from this study demonstrates that reinforcing with discrete fibers can be considered as a potential option for stabilizing mine fine tailings as well as for the management of fines to a treated state and ensure the reclamation is performed as quickly as possible.

7.2 Recommendations

The research presented within this thesis is a preliminary investigation of the role of short, discrete, synthetic fibers in altering the geomechanical behavior of clay soil with special emphasis on undrained pore pressure response, shear strength, yield strength, and stiffness of the soil-fiber composite. The following recommendations for additional work will aid in the progression of this program.

7.2.1 Testing for more variables (soil types, fiber types, and testing methods)

All tests in this research are performed on kaolinite clay soil (EPK kaolin manufactured by Edgar minerals). Additionally, this work only investigated two fiber types (PP and PA) to prepare fiber-reinforced clay soil for triaxial testing. The study can be extended to other clay minerals and fiber types (e.g. biodegradable fibers like nanocellulose) to analyse the effect of changing soil and fiber parameters on the geomechanical behavior of fiber-reinforced clay soils.

All tests in this study were consolidated undrained (CU) triaxial tests as the major objective of this research was to quantify the undrained shear strength and induced pore water pressure of the fiber-reinforced clay. No drained tests have been performed as a part of this research. Initial works demonstrated that the bilinear technique for determining the yield point is applicable for this soil - fiber composite (*Chapter Three*, Manuscript #1). It is recommended to perform consolidated drained (CD) triaxial tests on the fiber-reinforced clays along varying stress paths and define the yield points along different regions of the stress space. These yield points can then be combined to define the yield envelope of fiber-reinforced clay soil. A study can also be performed to analyse the influence of fiber contents, lengths, and types in altering the shape and size of the yield envelope.

Additionally, an empirical model has been defined as a part of this study to predict the tensile stress mobilized in the fibers of fiber-reinforced clays subjected to compression and extension shearing. This model demonstrated that mobilized fiber tension is a function of the fiber content, fiber length, the effectiveness of fibers to realign in the direction of extension and mobilize tension, applied effective stresses, and ϕ_i' between fibers and clay. Further recommendations involve performing triaxial compression and extension tests on other fibrous soils such as peat and evaluating the wide applicability of the developed empirical model in predicting the tensile stresses that occur due to fiber reinforcement.

7.2.2 Visualization techniques

Prior to the development of transparent fiber-reinforced soil, other techniques were explored to visualize the distribution of the fibers within the compacted and slurry prepared composites. The fiber-reinforced samples were subjected to the non-destructive computerized tomography (CT) scans and the images were analyzed to examine the orientation of fibers in the specimen. The Toshiba Aquilion One X-Ray CT Scanner available at the research park facility of Alberta Innovates was used for scanning the fiber-reinforced samples. This 320-slice helical scanner had a resolution of 300 micrometers and used an energy of 100 kV for the X-Ray scan beam. Figure 7.1a shows the negative of a Digital Imaging and Communications in Medicine (DICOM) image representing a slice of thickness 300μm as retrieved from the CT scan. Detecting the presence of polypropylene fibers out of the DICOM image was a great challenge owing to the difficulty of fibers in interacting with the X-Ray energy due to their low-density value. Subsequently a program was developed in Matlab by adopting the principle of Canny Edge detection algorithm (Fisher et al. 1996) to detect the lines in each DICOM image. However, the lines in the final image retrieved from Matlab (Fig 7.1b) represented the air and water boundaries, along with the fibers.

The grayscales in the DICOM images reflect the relative linear attenuation coefficient (μ) of the components, which determines the degree to which different components are distinguishable. The value of μ for air and water are -1000 Hounsfield Unit (HU) and 0 HU respectively. By using the software Image J (that is adopted for determining the μ value in a DICOM image), air and water boundaries were filtered out from the eventual Matlab image. Figure 7.1c shows the final output where black lines indicate fibers, pink lines indicate the pore air spaces and blue line shows the pore water spaces. This study is described in detail in Palat and Hendry (2022). However, adopting the technique of CT scanning for detecting the fibers is time consuming, as it is required to apply canny edge detection principle to each individual slice and filter out fibers from the air/water boundaries.

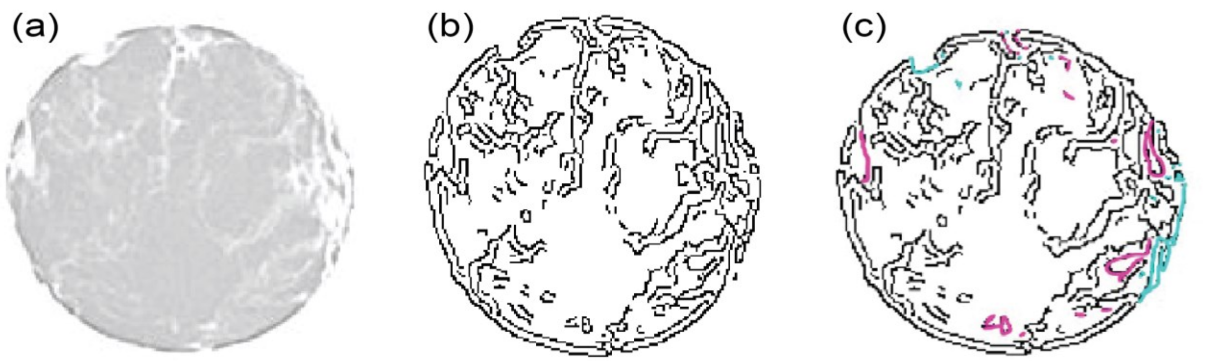

Figure 7.1. Procedure for determining the fibers out of a CT scanned image (a) DICOM slice, (b) final image from Matlab, (c) image after filtering out the fibers from the air and water boundaries.

One major issue in using the technique of CT imaging was the inability of PP fibers to interact with the X-ray energy. It is recommended to increase the density of polypropylene fibers by using an X-Ray contrasting agents such as Omnipaque solution. Omnipaque is an iodine solution used as a contrast enhancement in X-Ray CT imaging for the better visualisation of arteries, veins, and joints. It is recommended to immerse the PP fiber in Omnipaque solution prior to the preparation of fiber-reinforced composites for triaxial testing. Increasing the density of the PP fibers used for testing will enhance their chance of being visible during the CT scanning.

7.2.3 *Implement the fiber-reinforced soil model within a numerical framework*

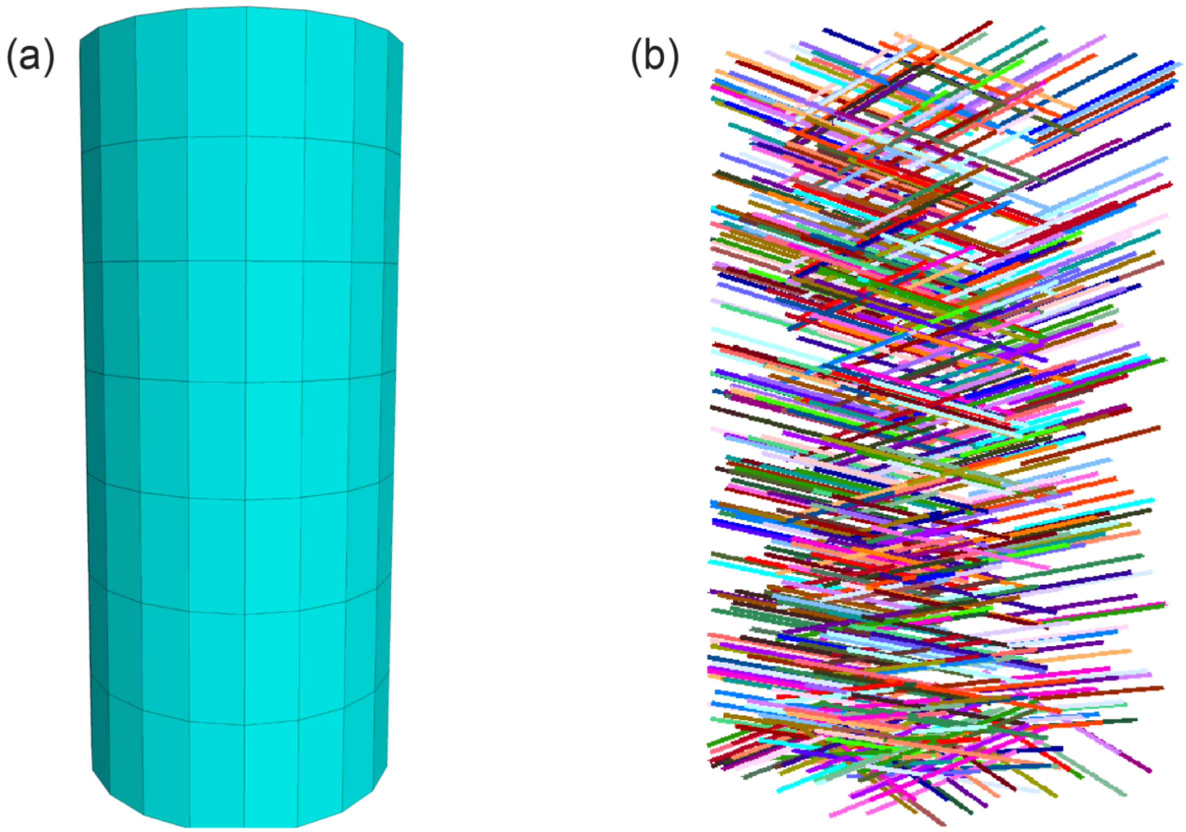

Figure 7.2. Numerical modelling of fiber-reinforced soil in FLAC 3D software (a) Soil specimen can be generated using cylindrical soil elements, (b) Generation of randomly oriented cable elements.

It is recommended to implement this fiber-reinforced soil model within a numerical framework so that the impact of these unique behaviors can be evaluated as per the resulting spatial distribution of stress, pore pressure and yielding beneath structures built upon these materials.

Basic analysis has been performed to evaluate the potential of numerical software in implementing this class of material. The numerical modeling software FLAC 3D was used to model the fiber-reinforced clay soil. Soil specimen was generated using cylindrical soil elements with the x- and z-axes located at the base of the cylinder and the y-axis pointing along the cylinder length (Figure 7.2a). A modified cam clay material model and in-built cable structural elements were used to model the soil and fibers respectively. The mechanical properties of the clay soil was obtained from basic laboratory testing and the cable (fiber) properties were provided by the manufacturer. The coordinates of the nodes and the orientation angle of cable elements were generated randomly using a FISH function to ensure that the fibers are distributed uniformly in the soil (Figure 7.2b). The number of fibers in the sample were back calculated based on the target fiber percentage and weight of the soil (Babu and Chouksey, 2010). A triaxial compression test was simulated by applying a uniform velocity at the top end in the negative y direction and a uniform compressive stress in the radial direction. Other loading conditions were also simulated by initializing the appropriate boundary conditions. The mode of failure, the formation of shear band, and the variation in pore water pressure and deviator stress were evaluated for different percentages, lengths, and orientations of fibers.

7.2.4 Evaluate the bearing capacity mechanism in fiber-reinforced clay soil using a centrifuge-testing program.

The motive of performing centrifuge tests on soil samples is to analyse the role of fibers in changing the mode of failure of clay soil and analyse the stress distribution and displacement pattern around the foundation. Performing centrifuge testing under an increased G (acceleration due to gravity) environment will allow the small-scale models tested over a short period to be representative of large real life structures testes over a long period. Performing centrifuge tests on the transparent fiber-reinforced clay (developed in *Chapter Four*, Manuscript #2) can be used to visualise the bearing capacity failure and track the movement of fibers beneath the foundation.

References

Acharya, M.P., Hendry, M.T., Martin, C.D. (2017) ‘Quantification of the settlement of an embankment constructed on peat due to the expulsion of gases’, Int. J. Geomech. 17(3), doi: 10.1061/(ASCE)GM.1943-5622.0000770.

Acharya, M.P., Hendry, M.T., Martin, C.D. (2018) ‘Creep behaviour of intact and remoulded fibrous peat’, Acta Geotech. 13(2), 399-417, doi: 10.1007/s11440-017-0545-1.

Altay, G., Kayadelen, C., Taskıran, T., and Kaya, Y. Z. (2019) ‘A laboratory study on pull-out resistance of geogrid in clay soil’, Measurement 139, p301-307, doi: 10.1016/j.measurement.2019.02.065.

Al Wahab, R.M., and Al-Qurna, H.H. (1995) ‘Fiber Reinforced Cohesive Soils for Application in Compacted Earth Structures’, In Proceedings of Geosynthetics ’95, IFAI, Vol. 2, Nashville, Tennessee, USA, p433-446.

Ammar, A., Najjar, S., and Sadek, S. (2019) ‘Mechanics of the Interface Interaction between Hemp Fibers and Compacted Clay’, International Journal of Geomechanics 19(4), doi: 10.1061/(ASCE)GM.1943-5622.0001368.

Anagnostopoulos, C, A., Tzetzis, D., and Berketis, K. (2013) ‘Shear strength behavior of polypropylene fiber reinforced cohesive soil’, Geomechanics and Geoengineering 9(3), p241-251, doi:10.1080/17486025.2013.804213.

Arthur, J. R. F., Rodriguez, J. I. C., Dunstan, T., and Chua, K. S. (1980) ‘Principal Stress Rotation: A Missing Parameter’, Journal of the Geotechnical Engineering Division 106 (4), p419-433, doi: 10.1061/AJGEB6.0000946.

ASTM D4767-11 (2020). Standard Test Method for Consolidated Undrained Triaxial Compression Test for Cohesive Soils. ASTM International, West Conshohocken, PA, 2020, www.astm.org.

ASTM D5321/D5321M (2020). Standard Test Method for Determining the Shear Strength of Soil-Geosynthetic and Geosynthetic-Geosynthetic Interfaces by Direct Shear. ASTM International, www.astm.org.

Babu, G. L. S., and Chouksey, S. K. (2010), 'Model for analysis of fiber-reinforced clayey soil', Geomechanics and Geoengineering 5(4), p277–285.

Baracos, A., Graham, J., and Domaschuk, L. (1980) 'Yielding and rupture in a lacustrine clay', Canadian Geotechnical Journal 17 (4), doi: 10.1139/t80-063.

Bareither, C.A., Benson, C.H., Edil. T. B., 2007. Reproducibility of direct shear tests conducted on granular backfill materials. Geotech. Test. J. 31(1), doi: 10.1520/GTJ100878.

Bathurst, R. J., and Ezzein, F. M. (2015) 'Geogrid and Soil Displacement Observations during Pullout Using a Transparent Granular Soil', Geotechnical Testing Journal, 38 (5) p673–685, doi: 10.1520/GTJ20140145. ISSN 0149-6115.

Bathurst, R. J., and Ezzein, F. M. (2017) 'Insights into geogrid–soil interaction using a transparent granular soil', Géotechnique Letters 7, p179–183, doi:10.1680/jgele.16.00191.

Black, J.A. (2012) 'Centrifuge modelling of press-in piling installation', In Proceedings of the International Press-in Association 4th Workshop. Singapore.

Black, J.A. (2015) 'Centrifuge Modelling With Transparent Soil and Laser Aided Imaging', Geotechnical Testing Journal, 38(5), p631–644, doi: 10.1520/GTJ20140231. ISSN 0149-6115.

Black, J.A., and Take, W.A. (2015) 'Quantification of optical clarity of transparent soil using the modulation transfer function', Geotechnical Testing Journal, 38(5), p588–602, doi: 10.1520/GTJ20140216. ISSN 0149-6115.

Briaud, J. L. (2001) 'Introduction to Soil Moduli', Geotechnical News, BiTech Publishers Ltd, Richmond, B.C, Canada, geotechnicalnews@bitech.ca.

Chai, J. C., and Saito, A. (2016) 'Interface Shear Strengths between Geosynthetics and Clayey Soils', International Journal of Geosynthetics and Ground Engineering 2(3), doi:10.1007/s40891-016-0060-8.

Consoli, N.C., Heineck, K.S., Casagrande, M. D. T., and Coop, M.R. (2007) 'Shear strength behavior of fiber-reinforced sand considering triaxial tests under distinct stress paths', Journal of Geotechnical and Geoenvironmental engineering 133(11),p1466-1469.

Consoli, N.C., de Moraes, R.R., Festugato, L. (2011) 'Split tensile strength of monofilament polypropylene fiber-reinforced cemented sandy soils', Journal of Geotechnical and Geoenvironmental Engineering 18 (2), p57-62.

Consoli, N.C., Nierwinski, H. P., da Silva, A. P., Sosnoski, J. (2017) 'Durability and strength of fiber-reinforced compacted gold tailings cement blends', Geotextiles and Geomembranes 45, p98-102, doi: 10.1016/j.geotexmem.2017.01.001.

Corte, A. E., and Higashi, A. (1960) 'Experimental research on desiccation cracks in soil', Research Report 66, U.S. Army Snow, Ice, and Permafrost Research Establishment, Engineer Research and Development Center (U.S.), Wilmette, Illinois.

Costa, C. M. L., Zornberg, J. G., Bueno, B. S., and Costa, Y. D. J. (2016) 'Centrifuge evaluation of the time-dependent behavior of geotextile-reinforced soil walls', Geotextiles and Geomembranes 44(2), p188-200, doi: 10.1016/j.geotexmem.2015.09.001.

Costalonga, M.A. D. R. C. (1988) 'Geogrid pull-out tests in clay' PhD thesis, University of Alberta, doi: 10.7939/r31j97c98.

Diambra, A., Russel, A.R., Ibrahim, E., and Wood, D.M. (2007) 'Determination of fiber orientation distribution in reinforced sands', Geotechnique 57(7), p623–628, doi: 10.1680/geot.2007.57.7.623.

Ellithy, G. S., and Gabr, M. A. (2000) 'Compaction Moisture Effect on Geomembrane/Clay Interface Shear Strength', Advances in Transportation and Geoenvironmental Systems Using Geosynthetics, Geo-Denver 2000, Denver, Colorado, United States, doi: 10.1061/40515(291)2.

Estabragh, A.R., Bordbar, A.T., and Javadi, A. A. (2011) 'Mechanical Behavior of a Clay Soil Reinforced with Nylon Fibers', Geotechnical and Geological Engineering 29 (5), p899–908, doi: 10.1007/s10706-011-9427-8.

Ferreira, F.B., Vieira, C.S., and Lopes, M. L. (2015) 'Direct shear behaviour of residual soil–geosynthetic interfaces – influence of soil moisture content, soil density and geosynthetic type', Geosynthetics International 22(3), p257–272, doi: 10.1680/gein.15.00011.

Ferreira, J. A. Z., and Zornberg, J. G. (2015) 'A Transparent Pullout Testing Device for 3D Evaluation of Soil–Geogrid Interaction', Geotechnical Testing Journal 38 (5) p686–707, doi: 10.1520/GTJ20140198. ISSN 0149-6115.

Festugato, L., Fourie, A., Consoli, N. C. (2013) 'Cyclic shear response of fibre-reinforced cemented paste backfill', Geotechnique Letters 3(1), p5–12.

Festugato, L., Consoli, N. C., Fourie, A. (2015) 'Cyclic shear behaviour of fibre-reinforced mine tailings', Geosynthetics International, 22(2), p196–206, doi: 10.1680/gein.15.00005.

Fisher, R., Perkins, S., Walker, A., and Wolfart, E. (2000) 'Hypermedia Image Processing Reference', Published by J. Wiley & Sons, Ltd.

Fletcher, C.S., and Humphries, W.K. (1991) 'California Bearing Ratio Improvement of Remolded Soils by the Addition of Polypropylene Fiber Reinforcement', In Proceedings of Seventieth Annual Meeting, Transportation Research Board, Washington, DC, USA, p80-86.

Freilich, B., Li, C., and Zornberg, J.G. (2010) 'Effective shear strength of fiber-reinforced clays', In Proceedings of the 9th International Conference on Geosynthetics, 9ICG, Guarujá, Brazil, May, Vol. 4, p1997-2000.

Graham, J., and Houlsby, G.T. (1983) 'Anisotropic elasticity of a natural clay', Geotechnique 33(2), p165-180.

Gray, D.H., and Ohashi, H. (1983) 'Mechanics of fiber reinforcement in sand', Journal of Geotechnical Engineering 109(3), p335-353.

Graham, J., Noonan, M.L., and Lew, K.V. (1983) 'Yield states and stress-strain relationships in a natural plastic clay', Canadian Geotechnical Journal 20(3), p502-516, doi: 10.1139/t83-058.

Gregory, G. H. (2006) 'Shear Strength, Creep and Stability of Fiber-Reinforced Soil Slopes', Ph.D. Dissertation, Oklahoma State University, Stillwater, OK, USA.

Gregory, G.H. (2011) 'Stabilization of Deep Slope Failure with Drilled Shafts: Lake Ridge Parkway Station 248; Grand Prairie, TX, In Proceedings of Geo-Frontiers Congress 2011, March 13-16, 2011 | Dallas, Texas, United States.

Gupta, R., Swan, R. H., and Zornberg, J.G. (2014) 'Laboratory Pullout Equipment for Testing Soil- Geosynthetic Interface for Reinforced Flexible Pavement Design', In Proceedings of the ASCE Geo- Congress 2014, Atlanta, Georgia, Geotechnical Special Publication no. 234, p2543-2557.

Hatami, K., Gregory, G. H., Garland, J., and Gregory,S. (2018) 'Guidelines for the Use of Fiber Reinforced Soil (FRS) in Highway Construction', Technical Report SPTC15.1-24-F, Southern Plains Transportation Center, ODOT MATCHING FUNDS,SP&R 2160.

Hendry, M.T. (2011) 'The geomechanical behaviour of peat foundations below rail-track structures', PhD thesis, University of Saskatchewan.

Hendry, M.T., Sharma, J.S., Martin, C.D., and Barbour, S.L. (2012) 'Effect of fibre content and structure on anisotropic elastic stiffness and shear strength of peat', Canadian Geotechnical Journal 49, p403–415.

Hendry, M.T., Martin, C.D., and Barbour, S.L. (2013) 'The measurement of the cyclic response of railway embankments and underlying soft peat foundations to heavy axle loads', Canadian Geotechnical Journal, 50(5), p467-480.

Hendry, M.T., Barbour, S.L., and Martin, C.D. (2014) 'Evaluation of the effect of fibre reinforcement on the anisotropic undrained stiffness and strength of peat', Journal of Geotechnical and Geoenvironmental Engineering 140(9).

Houlsby, G.T. (1981) 'Study of plasticity theories and their applicability to soils', PhD thesis, University of Cambridge, doi: 10.17863/CAM.14121.

Ibrahim, E., Diambra, A., Russel, A.R., and Wood, D.M. (2012) 'Assessment of laboratory sample preparation for fibre reinforced sands', Geotextiles and Geomembranes 34, p69-79.

Iskander, M., Liu, J., and Sadek, S. (2002) 'Transparent amorphous silica to model clay', Journal of Geotechnical and Geoenvironmental Engineering 128(3), doi:10.1061/ (ASCE)1090-241(2002)128:3(262).

Iskander, M. (2010) ‘Modelling with Transparent Soils Visualizing Soil Structure Interaction and Multi Phase Flow, Non-Intrusively’, Springer Science & Business Media, ISBN: 978-3-642-02501-3.

Iskander, M., and Liu, J. (2010) ‘Spatial Deformation Measurement Using Transparent Soil’, Geotechnical Testing Journal, 33 (4), Paper ID GTJ102745.

Jardine, R. J., Symes, M. J. and Burland, J. B. (1984) ‘The measurement of soil stiffness in the triaxial apparatus’, Geotechnique 34 (3), p323-340.

Jardine, R.J., Fourie, A., Maswoswe, J., and Burland, J.B. (1985) ‘Field and laboratory measurements of soil stiffness’, In Proceedings of the 11th international conference on soil mechanics and foundation engineering, San Francisco. 12 August - 16 August 1985.

Kelly, P. (2014) ‘Soil Structure Interaction and Group Mechanics of Vibrated Stone Column Foundations’, PhD thesis, University of Sheffield.

Kumar, A., Walia, B.S., and Mohan, J. (2006). ‘Compressive strength of fiber reinforced highly compressible clay’, Construction and Building Materials 20(10), p1063–1068.

Landva, A.O., and La Rochelle, P. (1983) ‘Compressibility and shear characteristics of radforth peats’, In Testing of Peats and Organic Soils. ASTM Special Technical Publication, 820, p157-191.

Landva, A.O., and Pheeney, P.E. (1980) ‘Peat fabric and structure’, Canadian Geotechnical Journal 17(3), p416-435, doi: 10.1139/t80-048.

Lew, K. V. (1981) ‘Yielding criteria and limit state in a Winnipeg clay’, M.Sc. Thesis, University of Manitoba, Winnipeg, Manitoba.

Li, C. (2005). ‘Mechanical response of fiber-reinforced soil’, Ph.D. thesis, University of Texas at Austin.

Liu, J., and Iskander, M. (2010) ‘Modelling capacity of transparent soil’, Canadian Geotechnical Journal 47(4), p451-460, doi: 10.1139/t09-116.

Maher, M.H., and Gray, D. H. (1990) ‘Static response of sand reinforced with randomly distributed fibers’, Journal of Geotechnical Engineering 116(11), p1661-1677.

Maher, M.H., and Woods, R.D. (1990) ‘Dynamic response of sand reinforced with randomly distributed fibers’, Journal of Geotechnical Engineering 116(7), https://doi.org/10.1061/(ASCE)0733-9410(1990)116:7(1116).

Maher, M.H., and Ho, Y.C. (1994) ‘Mechanical properties of kaolinite/fiber soil composite’, Journal of Geotechnical Engineering 120(8), p1381-1393.

Michalowski, R.L., and Zhao, A. (1996) ‘Failure of fiber-reinforced granular soils’, Journal of Geotechnical and Geoenvironmental Engineering 122(3), p226–234.

Michalowski, R.L., and Čermák, J. (2002) ‘Strength anisotropy of fiber-reinforced sand’, Computers and Geotechnics 29(4), p279–299, doi:10.1016/S0266-352X(01)00032-5.

Michalowski, R.L., and Čermák, J. (2003) ‘Triaxial compression of sand reinforced with fibers’, Journal of Geotechnical and Geoenvironmental Engineering 129(2), p125–136, doi:10.1061/(ASCE)1090-0241(2003)129:2(125).

Miller, C.J., Mi, H., and Yesiller, N. (1998) ‘Experimental analysis of desiccation crack propagation in clay liners’, Journal of the American Water Resources Association, 34(3), p677–686.

Mirzababaei, M., Mohamed, M., Arulrajah, A., Horpibulsuk, S., and Anggraini, V. (2017) ‘Practical approach to predict the shear strength of fiber-reinforced clay’, Geosynthetics International 25(1), doi: 10.1680/jgein.17.00033.

Mirzababaei, M., Arulrajah, A., Haque, A., Nimbalkar, S. and Mohajerani, A. (2018) ‘Effect of fiber reinforcement on shear strength and void ratio of soft clay’, Geosynthetics International 25(4), p471-480, doi:10.1680/jgein.18.00023.

Nataraj, M.S., and McManis, K.L. (1997) ‘Strength and Deformation Properties of Soils Reinforced With Fibrillated Fibers’, Geosynthetics International 4 (1), p65-79.

Nguyen, T. T., and Indraratna, B. (2019) ‘Micro-CT Scanning to Examine Soil Clogging Behavior of Natural Fiber Drains’, Journal of Geotechnical and Geoenvironmental Engineering 145(9):04019037, doi: 10.1061/(ASCE)GT.1943-5606.0002065.

Noonan, M. L. (1980) ‘Limit state studies in Winnipeg clays’, M.Sc. Thesis, University of Manitoba, Winnipeg, Manitoba.

Ni, Q., Hird, C., and Guymer, I. (2010) ‘Physical modeling of pile penetration in clay using transparent soil and particle image velocimetry’, Geotechnique 60(2), p121–132.

Palat, A., Hendry, M.T., and Roustaei, M. (2019) ‘Effect of fiber content on the mechanical behavior of fiber-reinforced clay’, In Proceedings of the 72nd Canadian Geotechnical Society Annual Conference, GeoStJohns 2019, St. John’s, Newfoundland. 29 September - 2 October 2019.

Palat, A., and Hendry, M.T. (2021) ‘Evaluation of the geomechanical behavior of fiber-reinforced clay soil’, In Proceedings of the 74th Canadian Geotechnical Society Annual Conference and the 14th Joint CGS/IAH-CNC Groundwater Conference, GeoNiagara 2021, Niagara Falls, Ontario. 26 September - 29 September 2021.

Palat, A., and Hendry, M.T. (2022) ‘Investigation of the behavior of fiber-reinforced clay soil’, 20th International Conference on Soil Mechanics and Geotechnical Engineering, ICSMGE 2022, Sydney, Australia,1 -6 May 2022.

Palat, A., Hendry, M.T. (2022a) ‘Experimental investigation of the effect of polymer fibers on the pore pressure response and undrained shear strength of clay’ *(To be submitted)*.

Palat, A., Hendry, M.T. (2022b) ‘The effect of sample preparation methods on the undrained behavior of fiber reinforced clay’ *(To be submitted)*.

Palat, A., Hendry, M.T. (2022c) ‘Quantification of the effect of fiber polymer type on the undrained behavior and realizable strength of fiber-reinforced clay’ (*To be submitted*).

Pappin, J. W., and Brown, S. F. (1980) ‘Resilient stress-strain behaviour of a crushed rock’, In Proceedings of International Symposium on Soils under Cyclic and Transient Loading, Swansea, Wales, p169- 177.

Peters, S. B., Siemens, G., and Take, W. A. (2011) ‘Characterization of Transparent Soil for Unsaturated Applications’, Geotechnical Testing Journal, 34 (5), doi: 10.1520/GTJ103580.

Pierret, A., Capowiez, Y., Moran, C. J., and Kretzschmar, A. (1999) 'X-ray computed tomography to quantify tree rooting sparial distributions', Geoderma 90, p307–326. doi: 10.1016/S0016-7061(98)00136-0.

Plé, O., and Lê, T.N.H. (2011) 'Effect of polypropylene fiber-reinforcement on the mechanical behavior of silty clay', Geotextiles and Geomembranes 32, p111-116, doi: 10.1016/j.geotexmem.2011.11.004.

Prashanth, V., Krishna, A. M., and Dash, S. K. (2016) 'Pullout Tests Using Modified Direct Shear Test Setup for Measuring Soil–Geosynthetic Interaction Parameters', International Journal of Geosynth. and Ground Eng. 2(10), doi:10.1007/s40891-016-0050-x.

Quigley, R, M. (1980) 'Geology, mineralogy and geochemistry of soft soils and their relationship to geotechnical problems', Canadian Geotechnical Journal 17(2), p261-285.

Quinton, W. L., Elliot, T., Price, J. S., Rezanezhad, F., and Heck, R. (2009) 'Measuring physical and hydraulic properties of peat from X-ray tomography', Geoderma 153 (1–2), p269-277, doi: 10.1016/j.geoderma.2009.08.010.

Roscoe, K. H., and Burland, J. B. (1968) 'On the generalized stress-strain behavior of wet clay', Engineering Plasticity, Cambridge University Press, p535-609.

Roustaei, M., Eslami, A., and Ghazavi, M. (2015) 'Effects of freeze–thaw cycles on a fiber-reinforced fine grained soil in relation to geotechnical parameters', Cold Regions Science and Technology 120, p127-137.

Salgado, R. (2011) 'The Engineering of Foundations', Tata McGraw-Hill Edition. ISBN-13: 978-1-25-900226-7.

Schofield, A.N., and Wroth, C. P. (1968) 'Critical State Soil Mechanics', Publisher: London McGraw-Hill, ISBN: 978-0641940484.

Shi, D., and Wang, F. (2013) 'Pull-out Test Studies on the Interface Characteristics between Geogrids and Soils', The electronic journal of geotechnical engineering, EJGE 18.

Soriano, I., Ibraim, E., Ando, E., Diambra, A., and Laurencin, T. (2017) '3D fibre architecture of fibre-reinforced sand', Granular Matter 19(4).

Taina, I. A., Heck, R. J., and Elliot, T. R. (2007) ‘Application of X-ray computed tomography to soil science: A literature review’, Canadian Journal of Soil Science, doi: 10.4141/CJSS06027.

Tang, C.S., Shi, B., Gao, W., Chen, F., and Cai, Y. (2007) ‘Strength and mechanical behavior of short polypropylene fiber reinforced and cement stabilized clayey soil’, Geotextiles and Geomembranes 25, p194–202.

Tang, C.S., Shi, B., and Zhao, L.Z. (2010) ‘Interfacial shear strength of fiber reinforced soil’, Geotextiles and Geomembranes 28 (1), p54–62, doi: 10.1016/j.geotexmem.2009.10.001.

Tang, C.S., Shi, B., Cui, Y. J., Liu, C., and Gu, K. (2012) ‘Desiccation cracking behavior of polypropylene fiber–reinforced clayey soil’ Canadian Geotechnical Journal 49, p1088–1101, doi:10.1139/T2012-067.

Tipler, P. A. (1999) ‘Physics for Engineers and Scientist: Electricity, Magnetism and Light’, 4th Edition, W.H. Freeman and Company, NY, p1041-1042.

Wood, D.M. (1990) ‘Soil Behavior and Critical State Soil Mechanics’, Cambridge University Press. ISBN 0-521-33249-4.

Wood, D. M., and Graham, J. (1990) ‘Anisotropic elasticity and yielding of a natural plastic clay’, International Journal of Plasticity 6, p377-388.

Yamaguchi, H., Ohira, Y., Kogure, K., and Mori, S. (1985) ‘Undrained shear characteristics of normally consolidated peat under triaxial compression and extension conditions,’ Soils and Foundations 3, p1–18, doi:10.3208/sandf1972.25.3_1.

Yi, X.W., Ma, G.W., Fourie, A. (2015) ‘Compressive behaviour of fibre-reinforced cemented paste backfill,’ Geotextiles and Geomembranes 43, p207-215, doi: 10.1016/j.geotexmem.2015.03.003.

Zheng, B., Zhang, D., Liu, W., Yang, Y., Yang, H. (2019) ‘Use of basalt fiber-reinforced tailings for improving the stability of tailings dam,’ Materials, 12, 1306; doi: 10.3390/ma12081306.

Ziegler, S., Leshchinsky, D., Ling, H.I., and Perry, E.B. (1998) ‘Effect of short polymeric fibers on crack development in clays’, Soils and Foundations, 38 (1), p247–253.

Zornberg, J.G. (2002) ‘Discrete framework for limit equilibrium analysis of fibre-reinforced soil’, Geotechnique 52(8), p593–604.

Zornberg, J.G., and Li, C. (2003) ‘Design of fiber-reinforced soil’, In Proceedings of the Twelfth Panamerican Conference of Soil Mechanics and Geotechnical Engineering, Cambridge, Massachusetts, June 22-26 Vol. 2, pp. 2193-2200.

Zornberg, J. G., Cabral, A, R., and Viratjandr, C. (2004) ‘Behavior of tire shred- sand mixtures’, Canadian Geotechnical Journal 41(2), p227-241.

Appendix A: Results from triaxial testing of unreinforced and fiber-reinforced clay soil

This appendix provides a record of the CU triaxial compression and extension testing results for unreinforced and fiber-reinforced samples of kaolinite clay presented in *Chapters 3, 4, 5, and 6* (Manuscripts #1, #2, #3, and #4).

CU triaxial compression testing of unreinforced kaolinite clay specimen at a p'_o of 50 kPa

<u>CU Testing</u>
Specimen type: Reconstituted - compacted
Fiber Content: 0
Fiber length: NA
Fiber type: NA
Trimmed specimen length: 98.9 mm
Specimen diameter: 50.2 mm
Water content: 27.5 %
Dry density: 1.6 g/cm^3

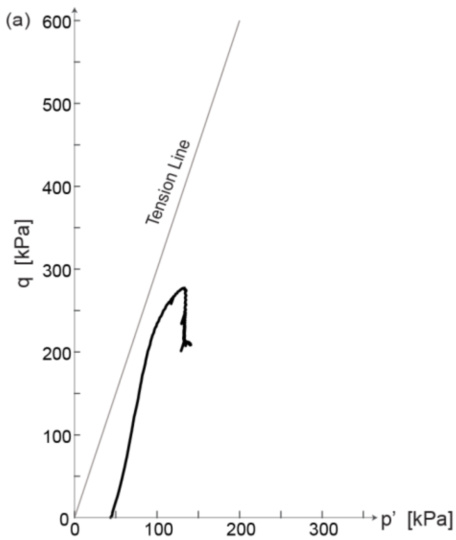

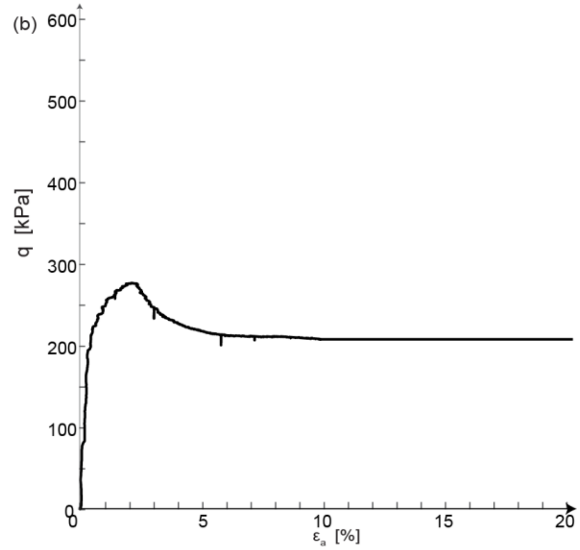

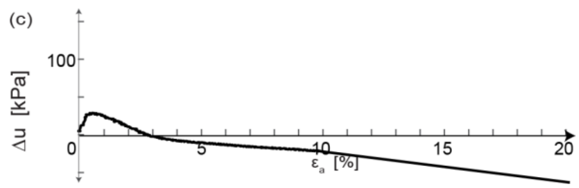

CU triaxial compression testing of unreinforced kaolinite clay specimen at a p'_o of 100 kPa

<u>CU Testing</u>
Specimen type: Reconstituted - compacted
Fiber Content: 0
Fiber length: NA
Fiber type: NA
Trimmed specimen length: 97.5 mm
Specimen diameter: 50.1 mm
Water content: 28 %
Dry density: 1.6 g/cm^3

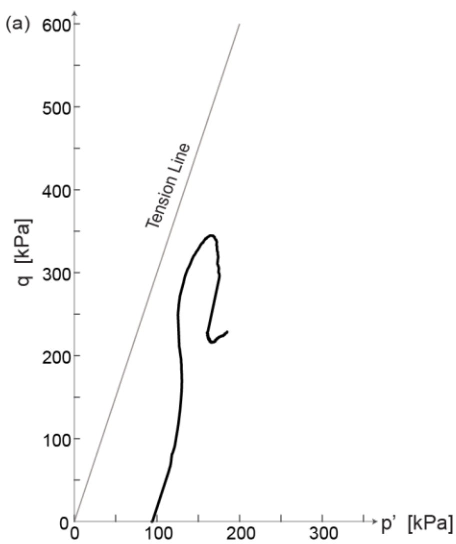

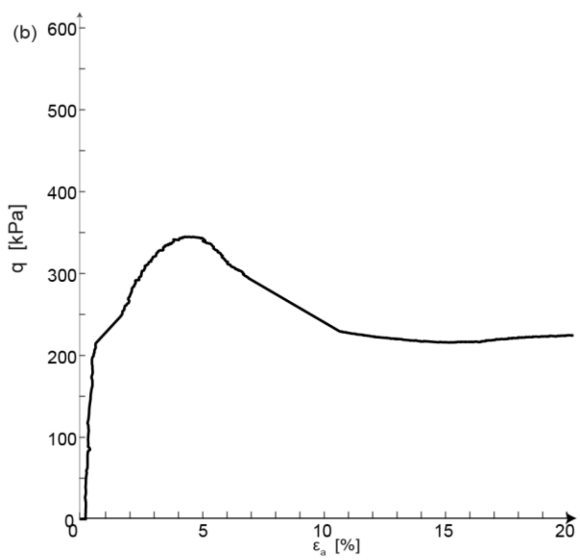

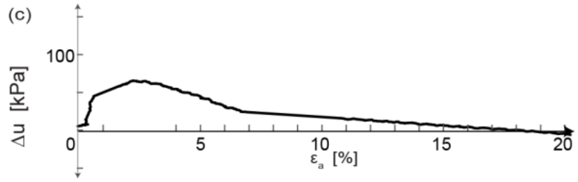

CU triaxial compression testing of unreinforced kaolinite clay specimen at a p'_o of 200 kPa

<u>CU Testing</u>

Specimen type: Reconstituted - compacted

Fiber Content: 0

Fiber length: NA

Fiber type: NA

Trimmed specimen length: 94.5 mm

Specimen diameter: 50.3 mm

Water content: 27.45 %

Dry density: 1.62 g/cm^3

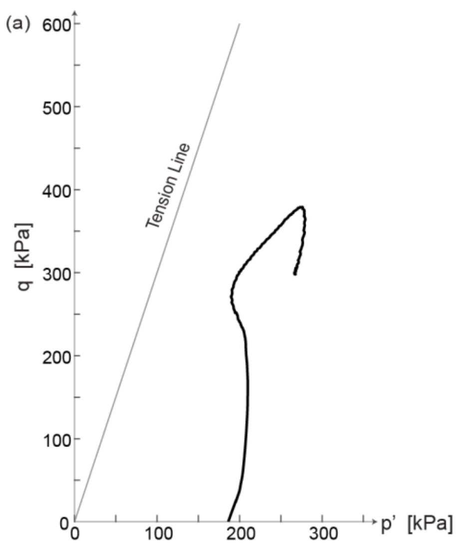

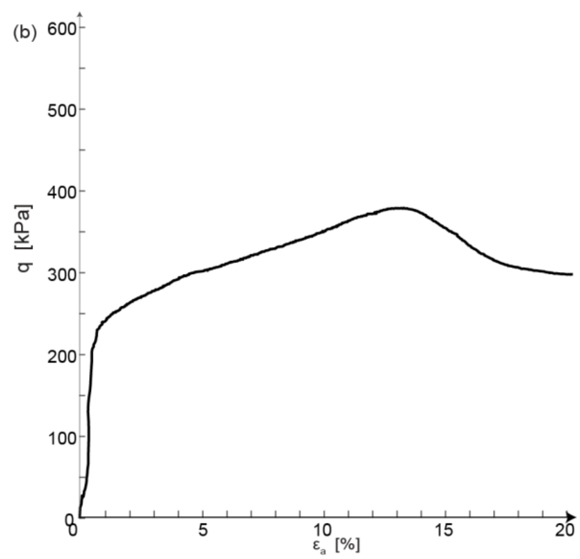

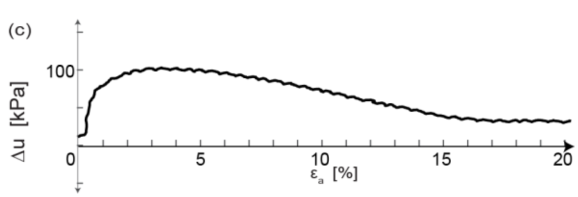

CU triaxial compression testing of fiber-reinforced kaolinite clay specimen at a p'_o of 50 kPa

<u>CU Testing</u>
Specimen type: Reconstituted - compacted
Fiber Content: 1%
Fiber length: 18 mm
Fiber type: PP
Trimmed specimen length: 96.49 mm
Specimen diameter: 50 mm
Water content: 28.9 %
Dry density: 1.74 g/cm^3

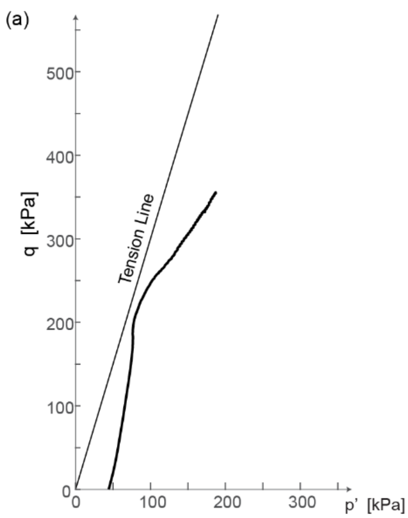

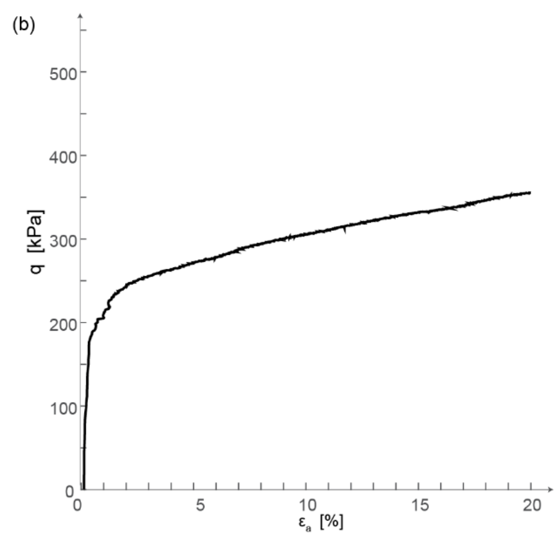

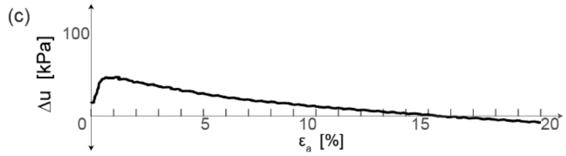

CU triaxial compression testing of fiber-reinforced kaolinite clay specimen at a p'_o of 100 kPa

<u>CU Testing</u>
Specimen type: Reconstituted - compacted
Fiber Content: 1%
Fiber length: 18 mm
Fiber type: PP
Trimmed specimen length: 94.9 mm
Specimen diameter: 49.4 mm
Water content: 27.8 %
Dry density: 1.77 g/cm^3

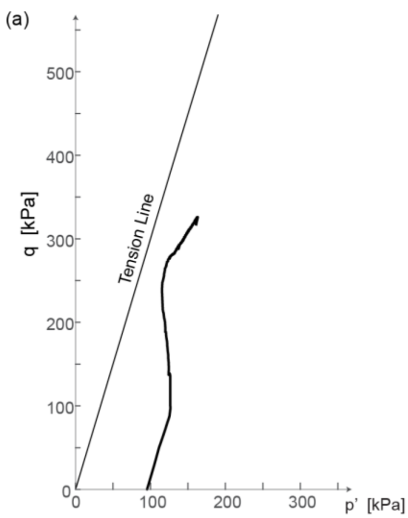

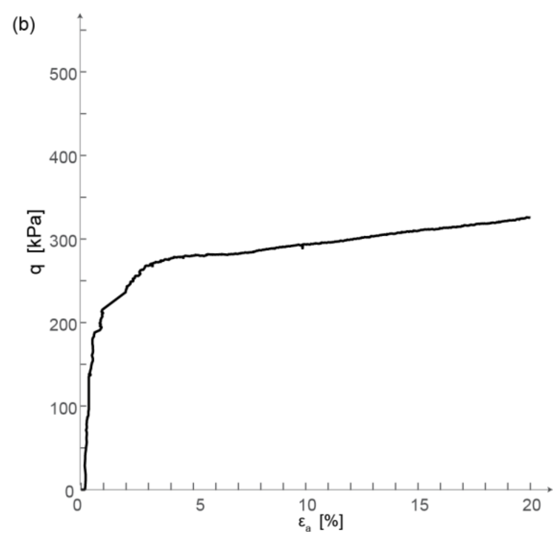

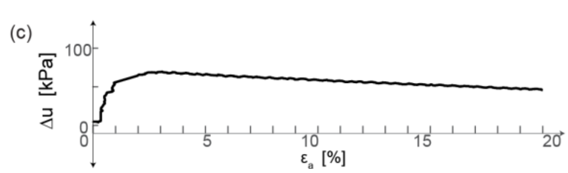

CU triaxial compression testing of fiber-reinforced kaolinite clay specimen at a p_o' of 200 kPa

<u>CU Testing</u>
Specimen type: Reconstituted - compacted
Fiber Content: 1%
Fiber length: 18 mm
Fiber type: PP
Trimmed specimen length: 93 mm
Specimen diameter: 50.34 mm
Water content: 27.9 %
Dry density: 1.75 g/cm^3

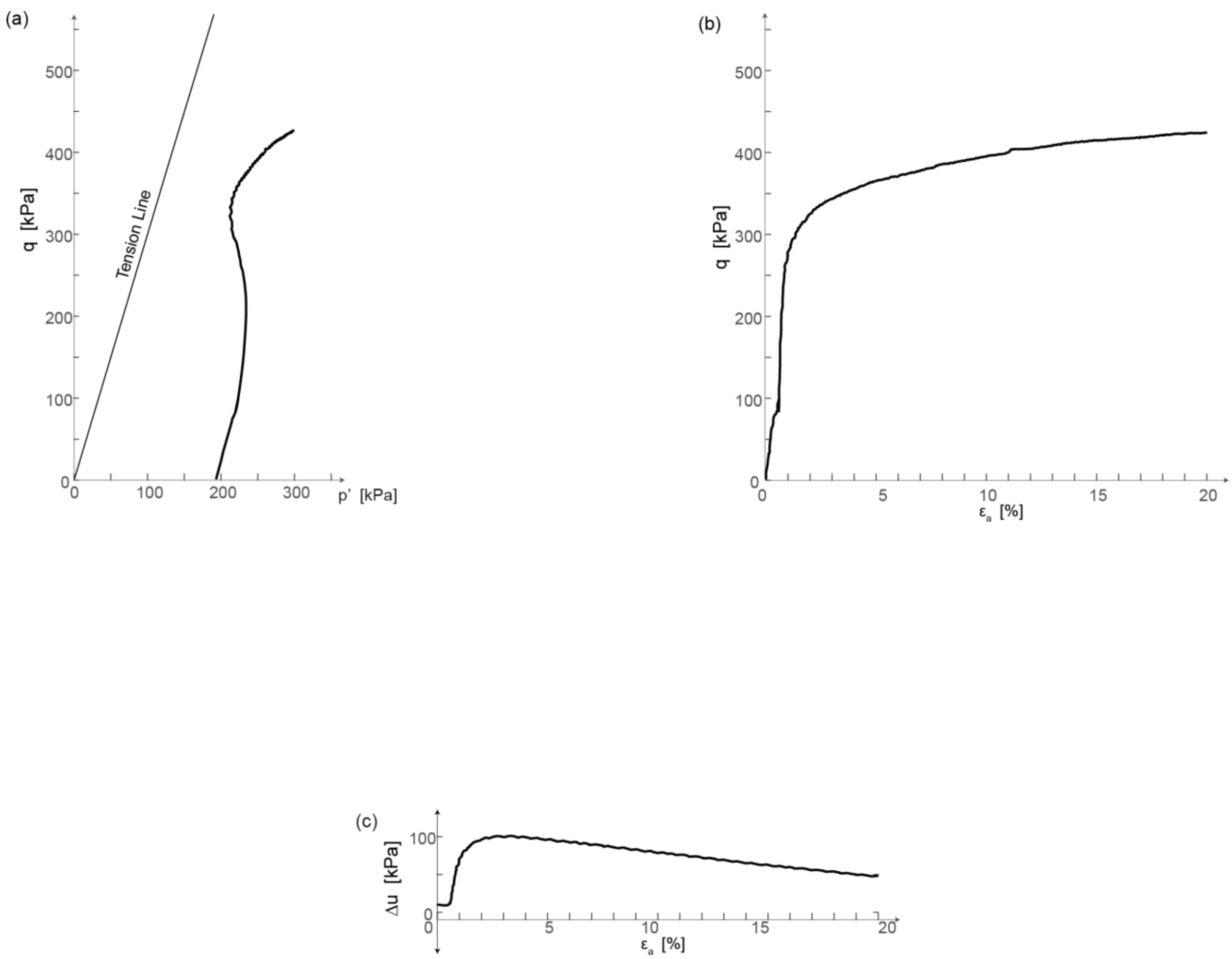

CU triaxial compression testing of fiber-reinforced kaolinite clay specimen at a p'_o of 50 kPa

<u>CU Testing</u>
Specimen type: Reconstituted - compacted
Fiber Content: 2%
Fiber length: 18 mm
Fiber type: PP
Trimmed specimen length: 96.4 mm
Specimen diameter: 50 mm
Water content: 28 %
Dry density: 1.86 g/cm^3

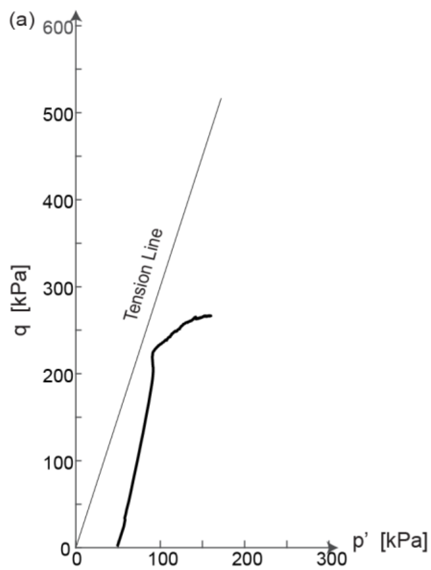

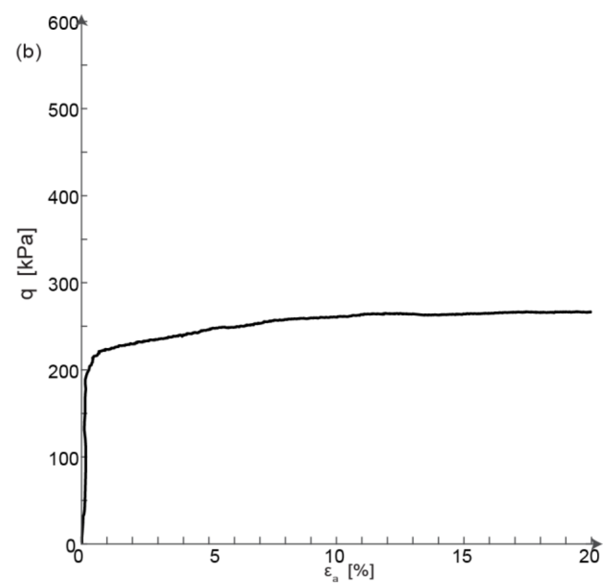

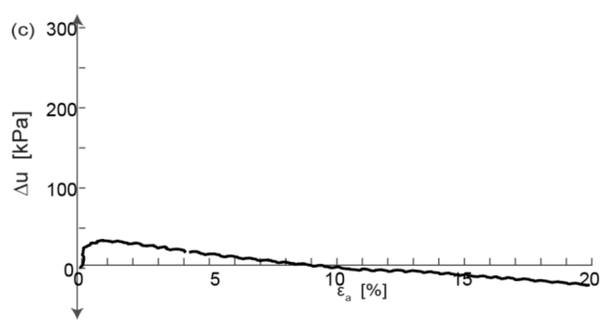

CU triaxial compression testing of fiber-reinforced kaolinite clay specimen at a p'_o of 100 kPa

<u>CU Testing</u>
Specimen type: Reconstituted - compacted
Fiber Content: 2%
Fiber length: 18 mm
Fiber type: PP
Trimmed specimen length: 97.3 mm
Specimen diameter: 49.8 mm
Water content: 28.8 %
Dry density: 1.84 g/cm^3

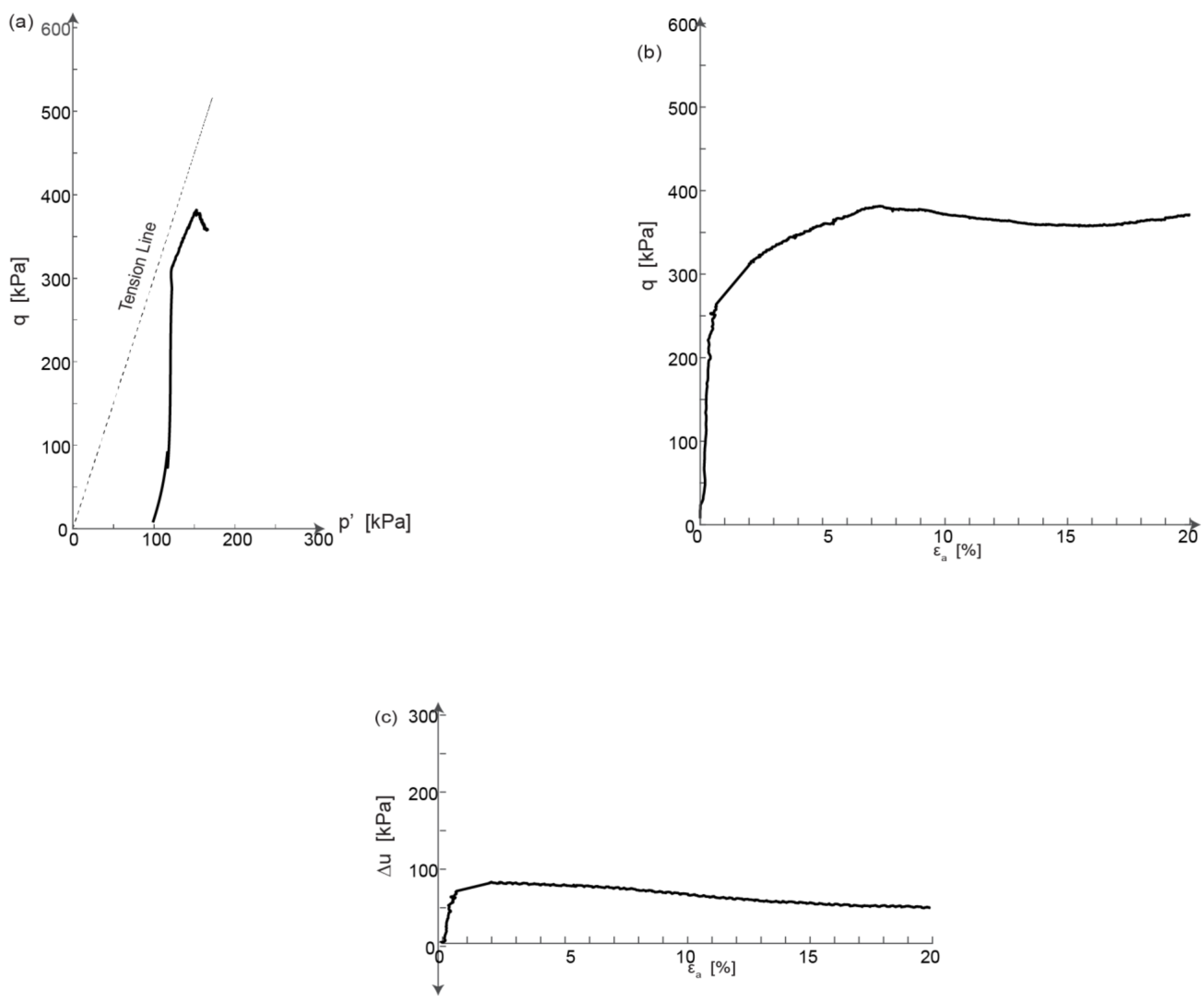

CU triaxial compression testing of fiber-reinforced kaolinite clay specimen at a p'_o of 200 kPa

<u>CU Testing</u>
Specimen type: Reconstituted - compacted
Fiber Content: 2%
Fiber length: 18 mm
Fiber type: PP
Trimmed specimen length: 95.2 mm
Specimen diameter: 50.6 mm
Water content: 28.4 %
Dry density: 1.85 g/cm^3

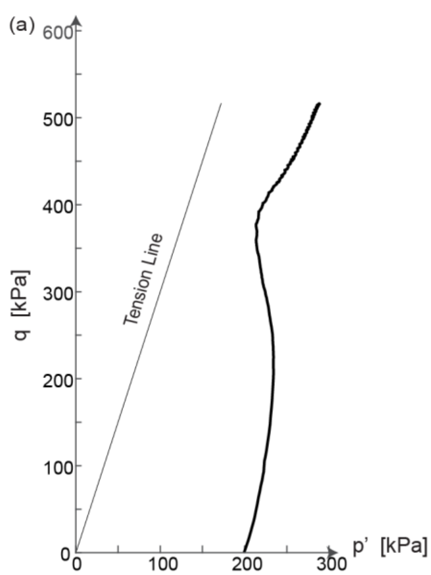

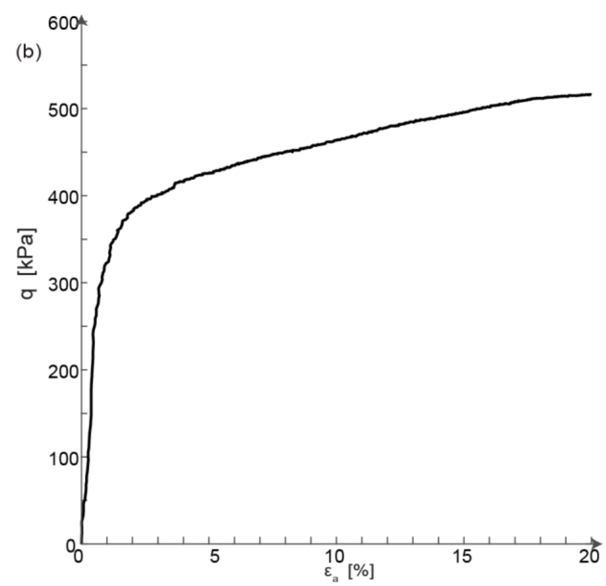

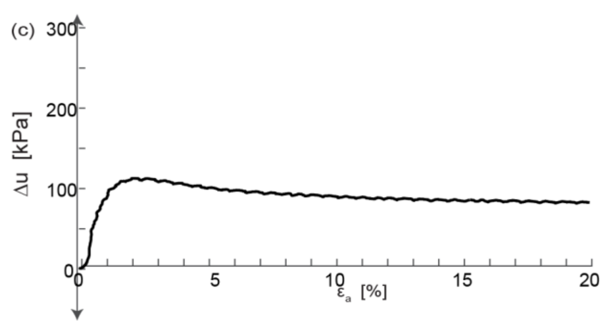

CU triaxial compression testing of fiber-reinforced kaolinite clay specimen at a p_o' of 50 kPa

<u>CU Testing</u>
Specimen type: Reconstituted - compacted
Fiber Content: 3%
Fiber length: 18 mm
Fiber type: PP
Trimmed specimen length: 97 mm
Specimen diameter: 49.7 mm
Water content: 28.6 %
Dry density: 1.92 g/cm^3

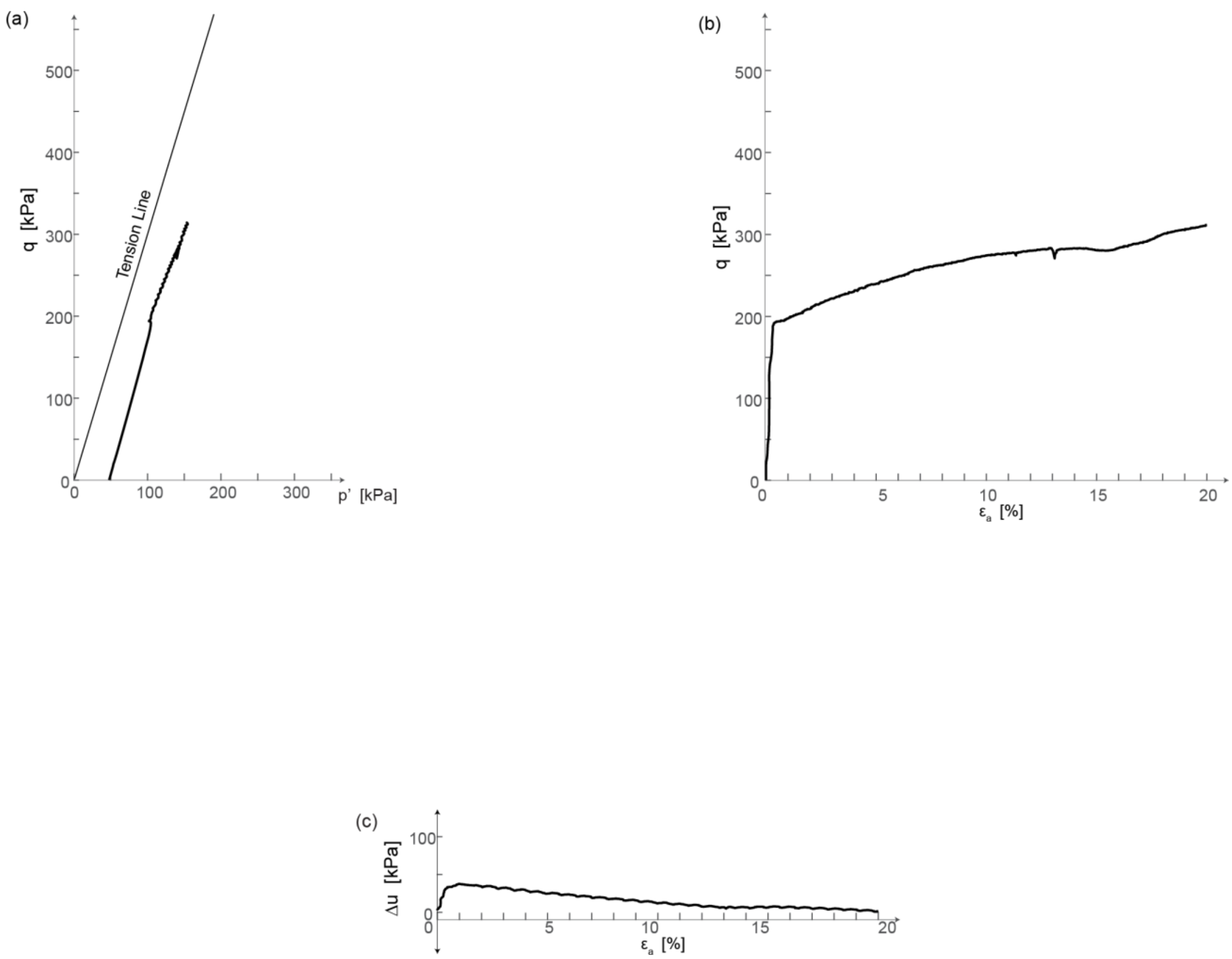

CU triaxial compression testing of fiber-reinforced kaolinite clay specimen at a p'_o of 100 kPa

<u>CU Testing</u>

Specimen type: Reconstituted - compacted
Fiber Content: 3%
Fiber length: 18 mm
Fiber type: PP
Trimmed specimen length: 97.5 mm
Specimen diameter: 49.9 mm
Water content: 27.9 %
Dry density: 1.89 g/cm^3

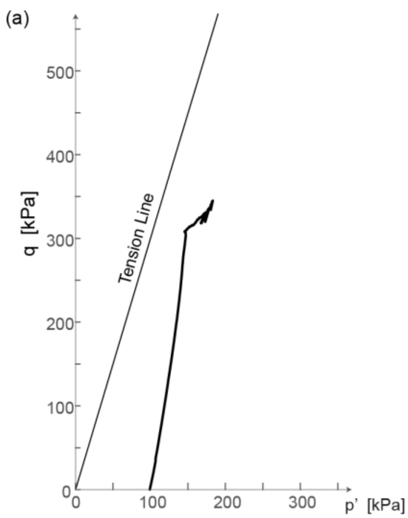

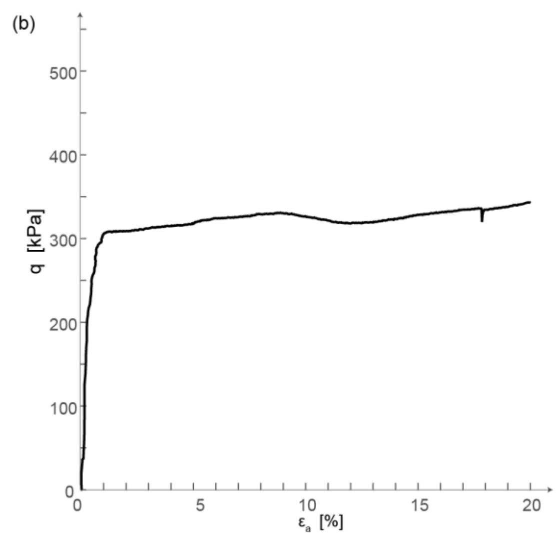

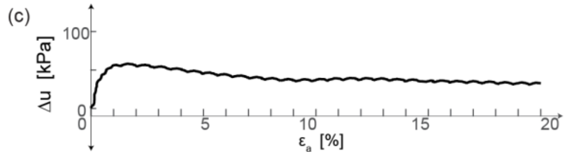

CU triaxial compression testing of fiber-reinforced kaolinite clay specimen at a p_o' of 200 kPa

<u>CU Testing</u>
Specimen type: Reconstituted - compacted
Fiber Content: 3%
Fiber length: 18 mm
Fiber type: PP
Trimmed specimen length: 100.16 mm
Specimen diameter: 50.5 mm
Water content: 29 %
Dry density: 1.92 g/cm^3

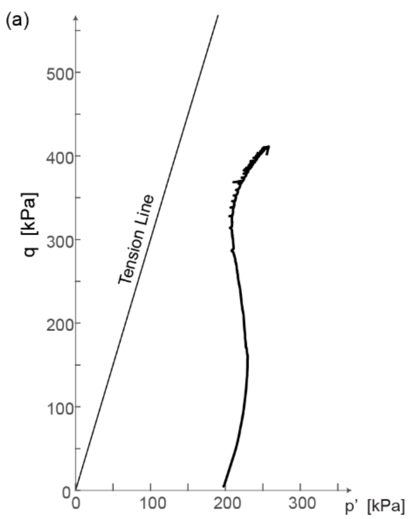

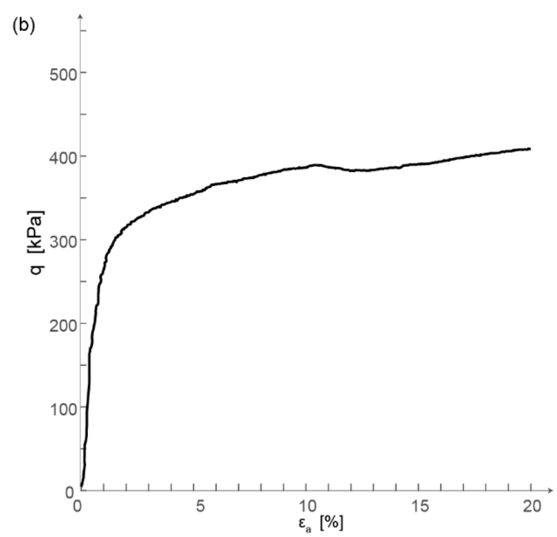

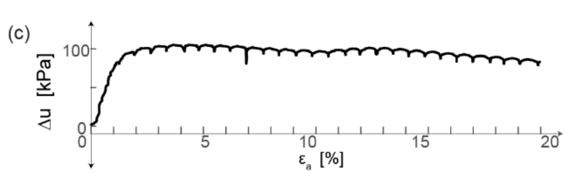

CU triaxial compression testing of fiber-reinforced kaolinite clay specimen at a p'_o of 50 kPa

<u>CU Testing</u>
Specimen type: Reconstituted - compacted
Fiber Content: 2%
Fiber length: 6 mm
Fiber type: PP
Trimmed specimen length: 94.8 mm
Specimen diameter: 50.3 mm
Water content: 27.2 %
Dry density: 1.72 g/cm^3

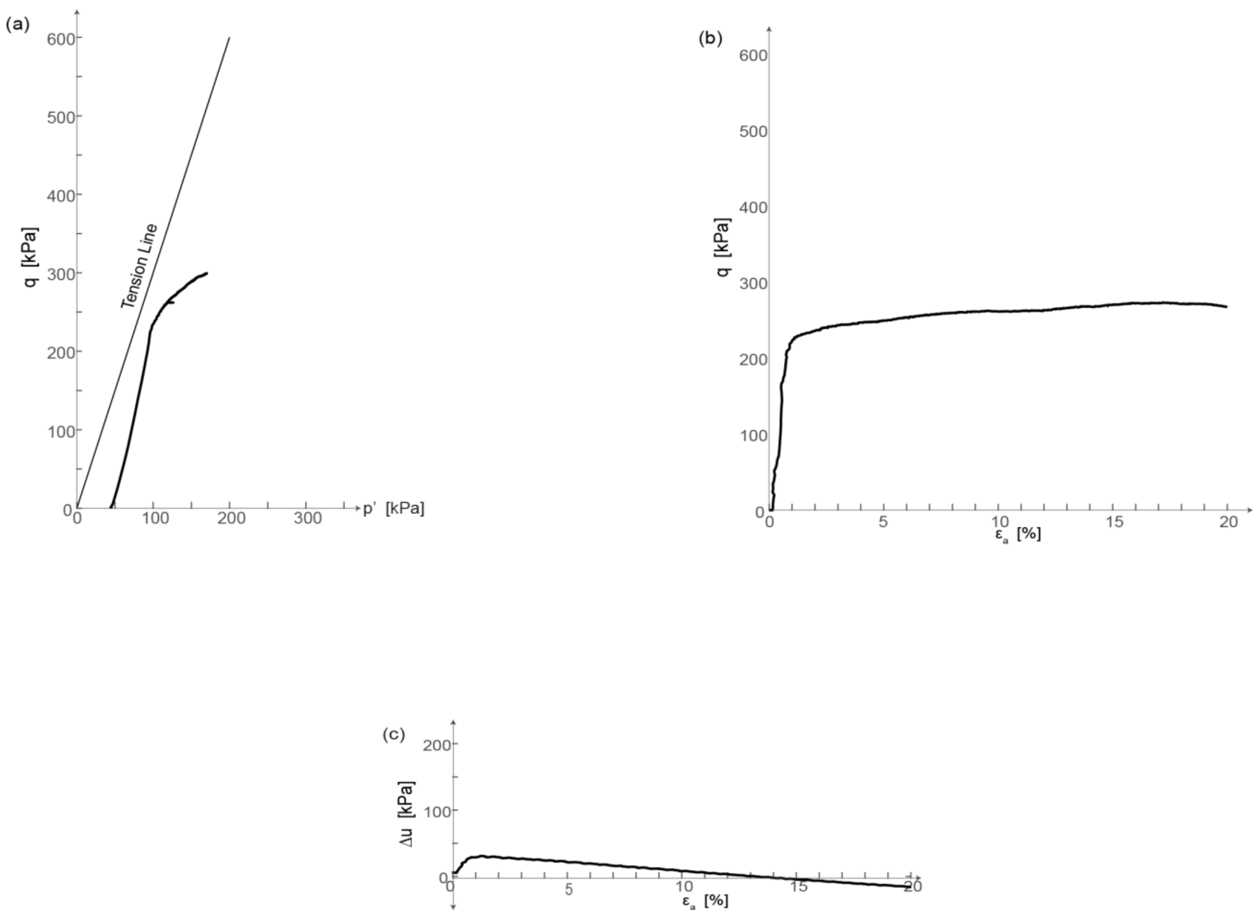

CU triaxial compression testing of fiber-reinforced kaolinite clay specimen at a p_o' of 100 kPa

<u>CU Testing</u>
Specimen type: Reconstituted - compacted
Fiber Content: 2%
Fiber length: 6 mm
Fiber type: PP
Trimmed specimen length: 95.01 mm
Specimen diameter: 51.1 mm
Water content: 28.7 %
Dry density: 1.75 g/cm^3

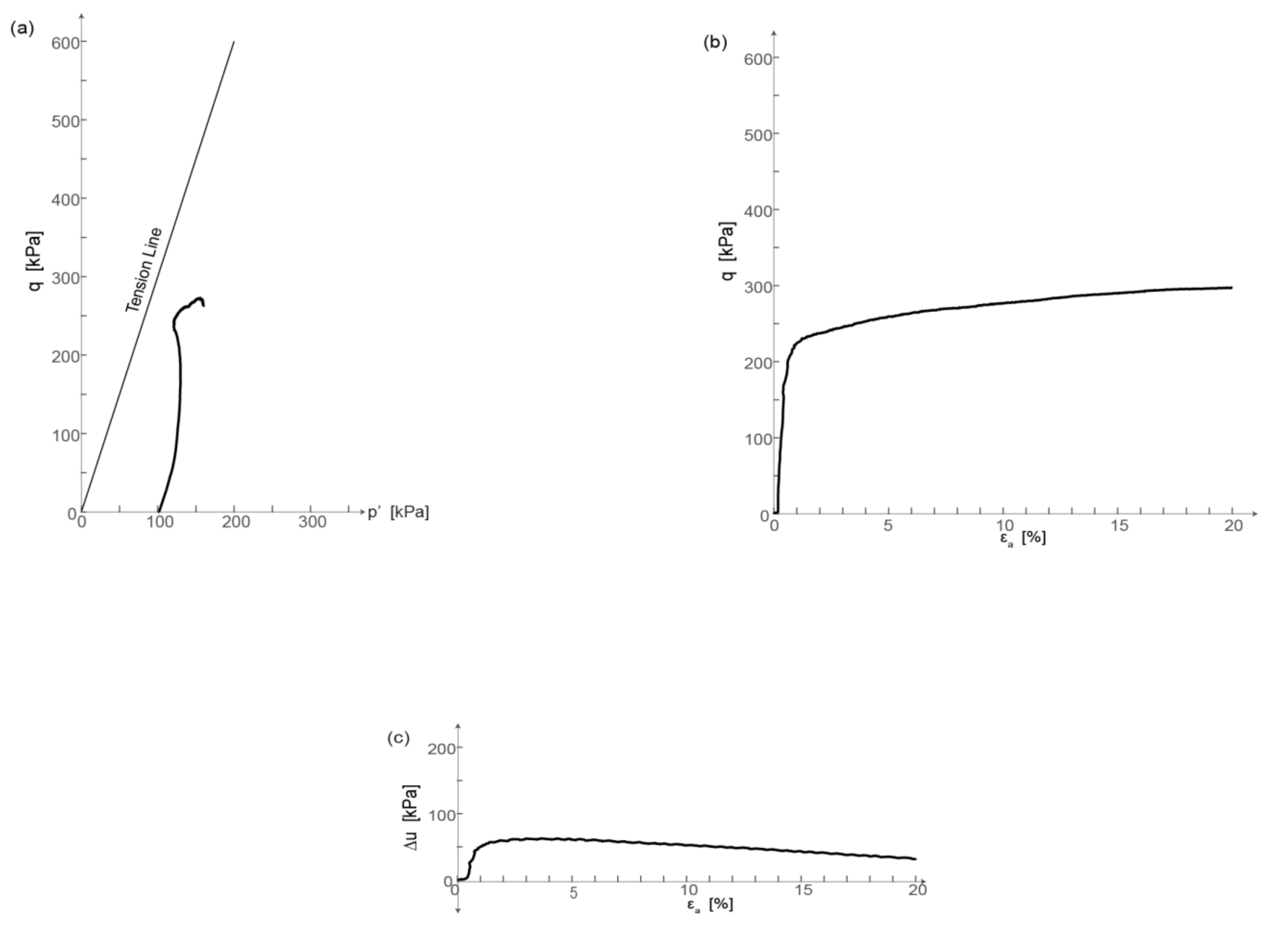

CU triaxial compression testing of fiber-reinforced kaolinite clay specimen at a p'_o of 200 kPa

<u>CU Testing</u>
Specimen type: Reconstituted - compacted
Fiber Content: 2%
Fiber length: 6 mm
Fiber type: PP
Trimmed specimen length: 99.3 mm
Specimen diameter: 50.63 mm
Water content: 28.2 %
Dry density: 1.71 g/cm^3

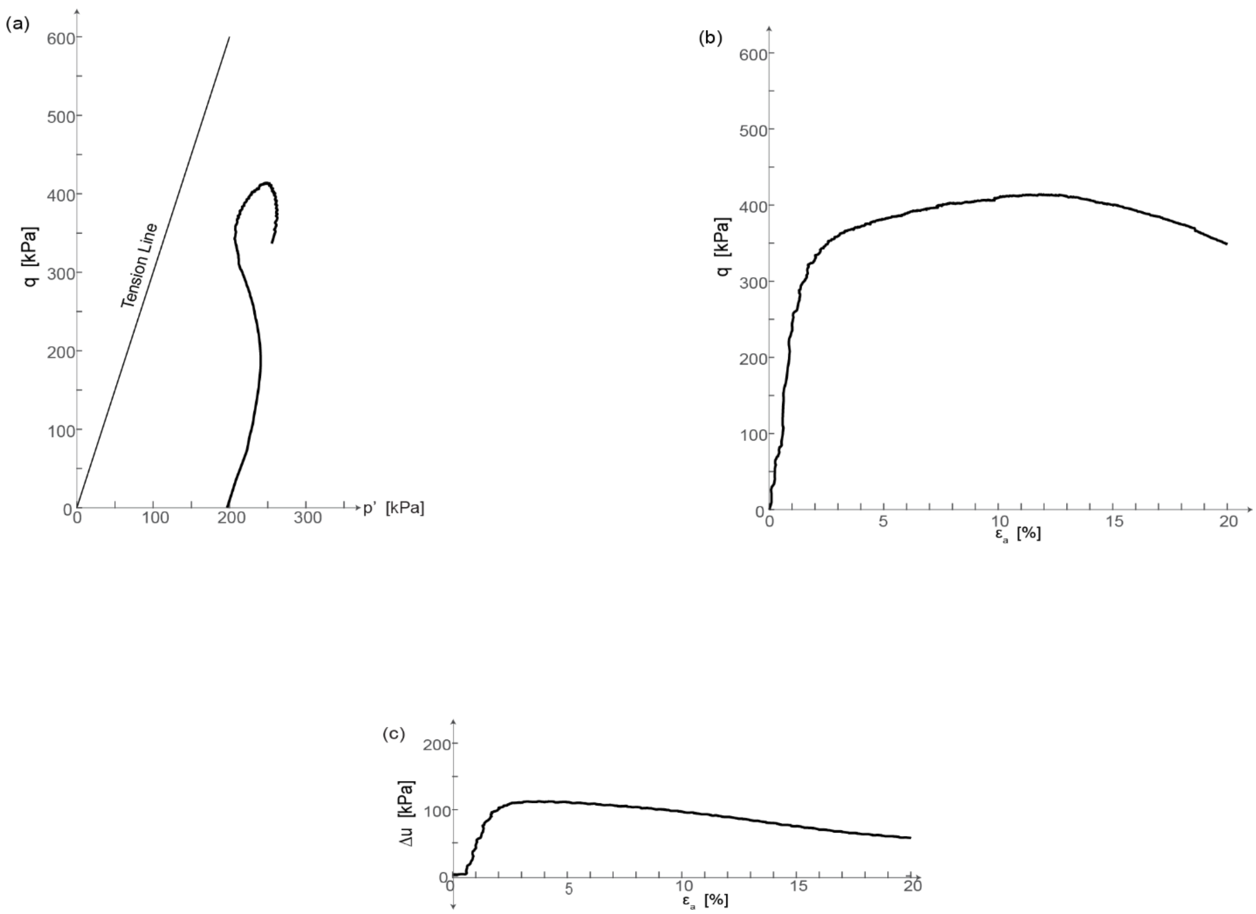

CU triaxial compression testing of fiber-reinforced kaolinite clay specimen at a p'_o of 50 kPa

<u>CU Testing</u>
Specimen type: Reconstituted - compacted
Fiber Content: 2%
Fiber length: 48 mm
Fiber type: PP
Trimmed specimen length: 94.96 mm
Specimen diameter: 50.19 mm
Water content: 28.6 %
Dry density: 1.76 g/cm^3

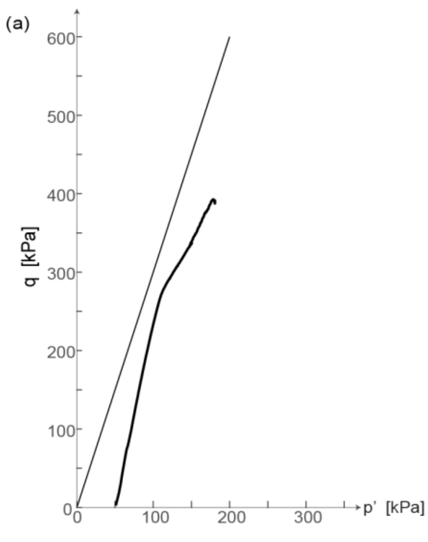

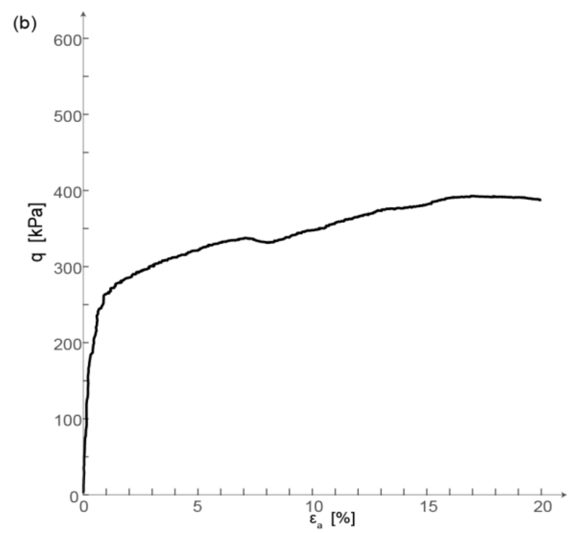

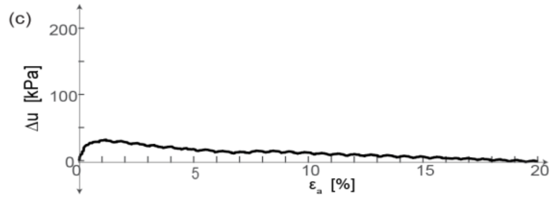

CU triaxial compression testing of fiber-reinforced kaolinite clay specimen at a p'_o of 100 kPa

<u>CU Testing</u>
Specimen type: Reconstituted - compacted
Fiber Content: 2%
Fiber length: 48 mm
Fiber type: PP
Trimmed specimen length: 98.36 mm
Specimen diameter: 50.69 mm
Water content: 28.4 %
Dry density: 1.74 g/cm^3

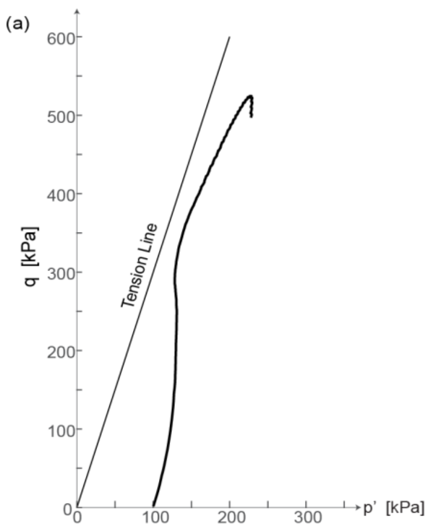

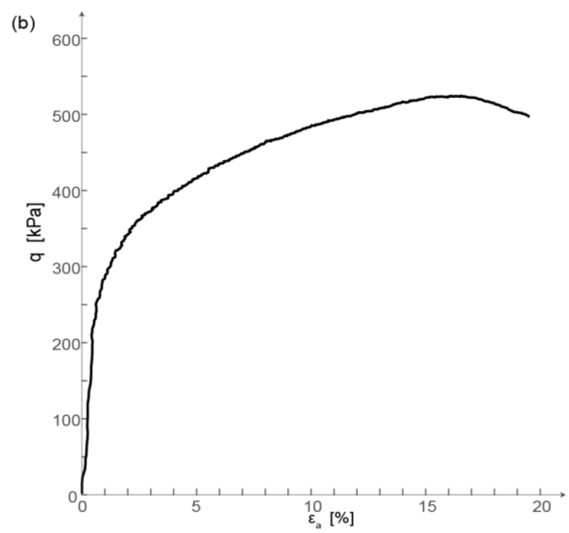

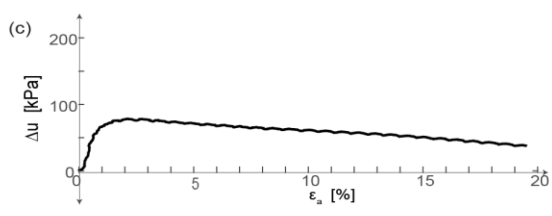

CU triaxial compression testing of fiber-reinforced kaolinite clay specimen at a p'_o of 200 kPa

<u>CU Testing</u>
Specimen type: Reconstituted - compacted
Fiber Content: 2%
Fiber length: 48 mm
Fiber type: PP
Trimmed specimen length: 96 mm
Specimen diameter: 50 mm
Water content: 28.3 %
Dry density: 1.76 g/cm^3

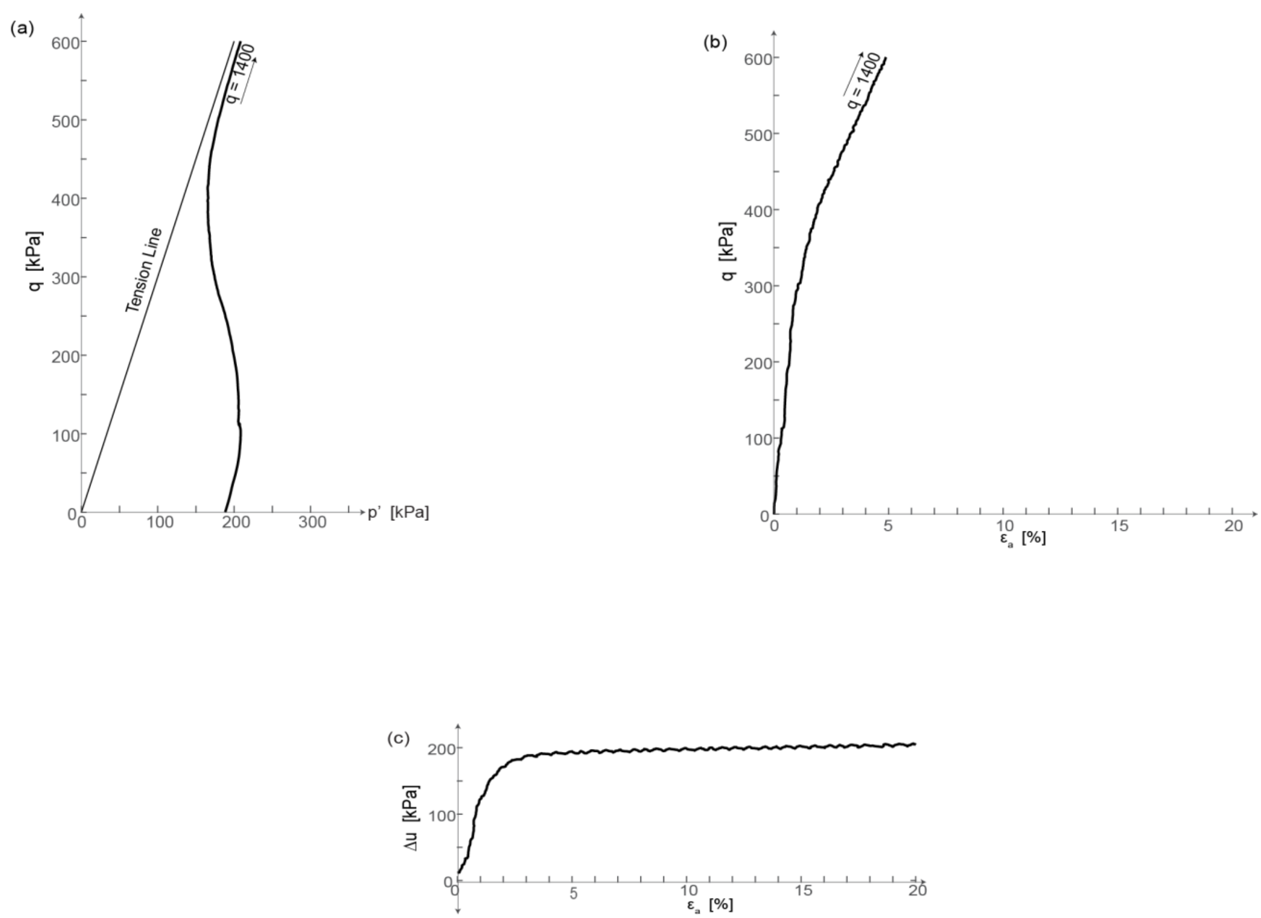

CU triaxial compression testing of fiber-reinforced kaolinite clay specimen at a p'_o of 50 kPa

<u>CU Testing</u>
Specimen type: Reconstituted - compacted
Fiber Content: 2%
Fiber length: 18 mm
Fiber type: PA
Trimmed specimen length: 96.2mm
Specimen diameter: 49.7 mm
Water content: 28.5 %
Dry density: 1.82 g/cm^3

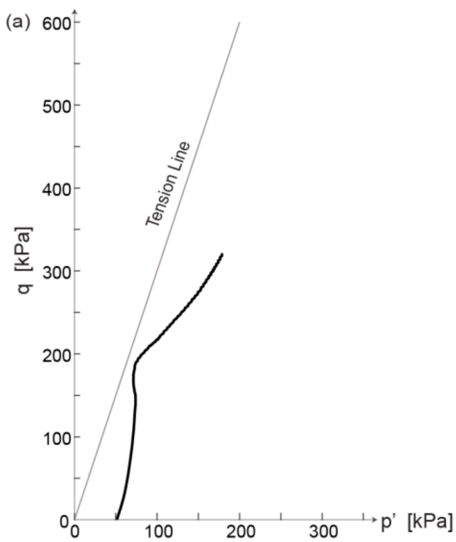

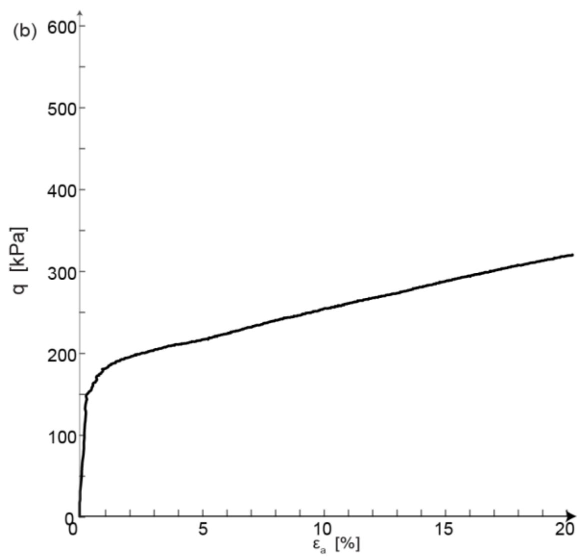

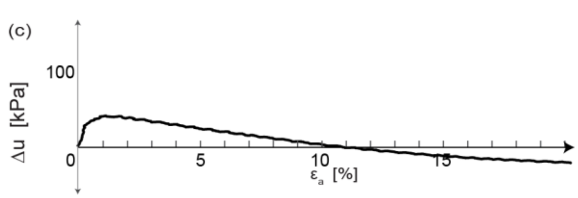

CU triaxial compression testing of fiber-reinforced kaolinite clay specimen at a p'_o of 100 kPa

<u>CU Testing</u>
Specimen type: Reconstituted - compacted
Fiber Content: 2%
Fiber length: 18 mm
Fiber type: PA
Trimmed specimen length: 97.4 mm
Specimen diameter: 49.9 mm
Water content: 28 %
Dry density: 1.8 g/cm^3

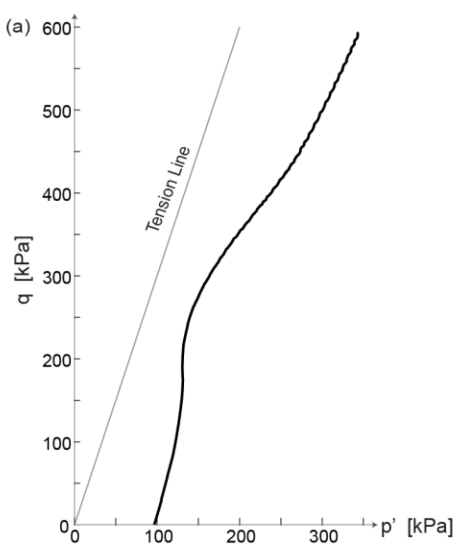

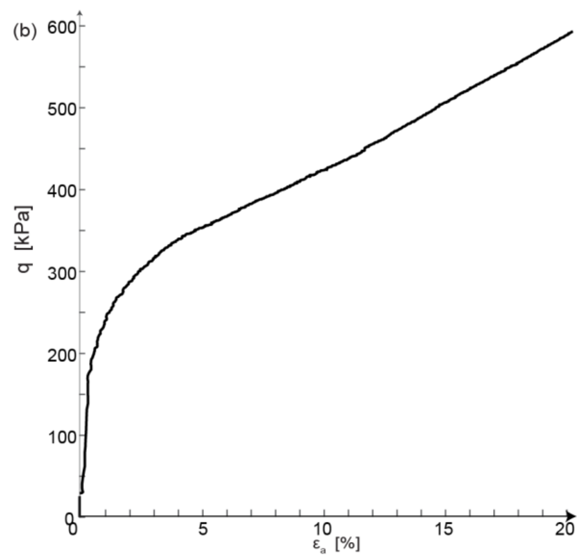

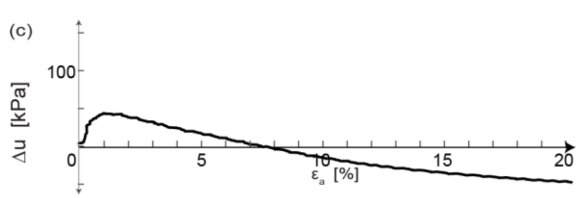

CU triaxial compression testing of fiber-reinforced kaolinite clay specimen at a p'_o of 200 kPa

<u>CU Testing</u>

Specimen type: Reconstituted - compacted
Fiber Content: 2%
Fiber length: 18 mm
Fiber type: PA
Trimmed specimen length: 96 mm
Specimen diameter: 48.4 mm
Water content: 28.2 %
Dry density: 1.81 g/cm^3

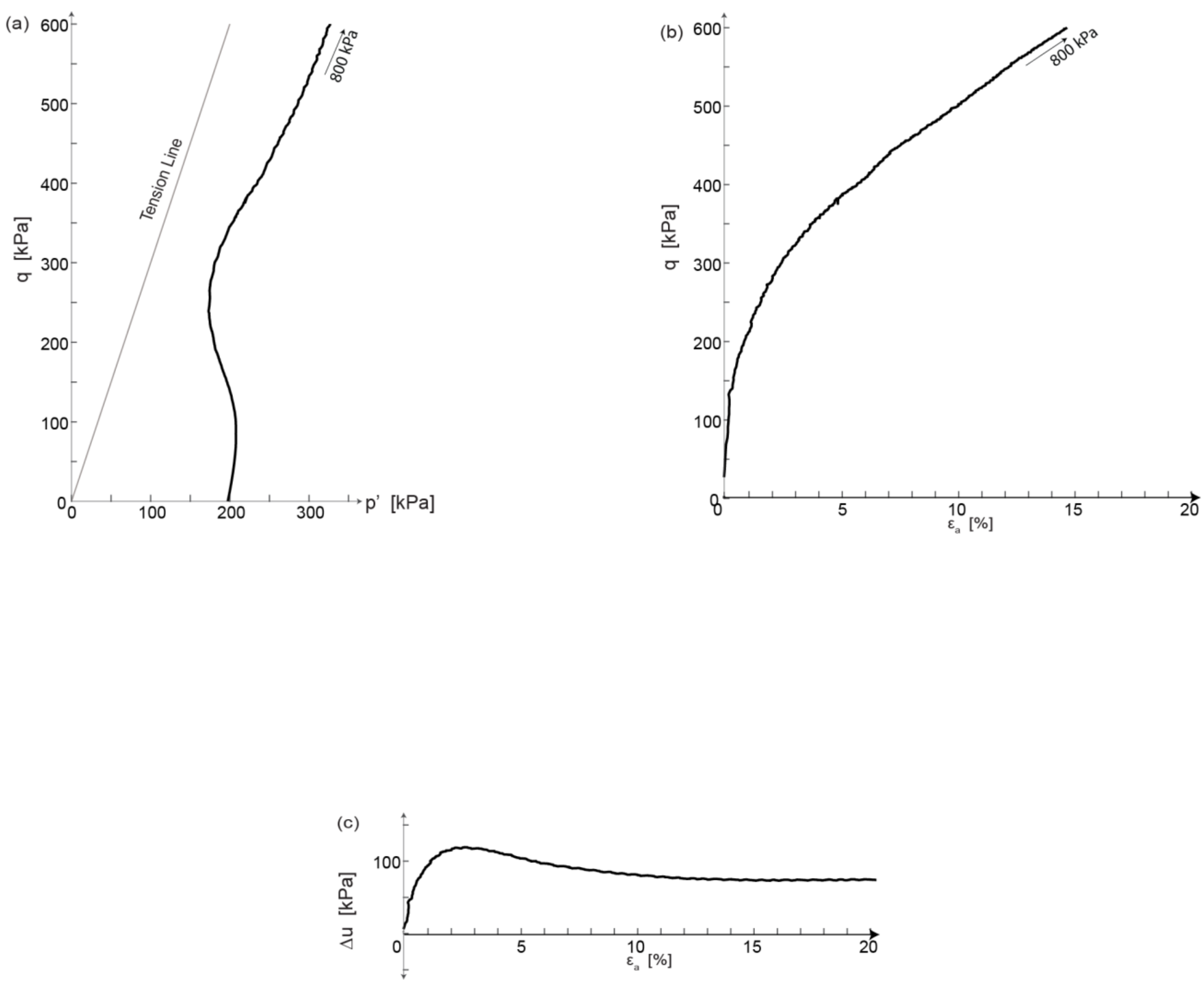

CU triaxial compression testing of unreinforced kaolinite clay specimen at a p'_o of 50 kPa

<u>CU Testing</u>
Specimen type: Reconstituted - slurry
Fiber Content: 0
Fiber length: NA
Fiber type: NA
Trimmed specimen length: 97.5 mm
Specimen diameter: 49.2 mm
Water content: 44.9 %
Dry density: 1.3 g/cm^3

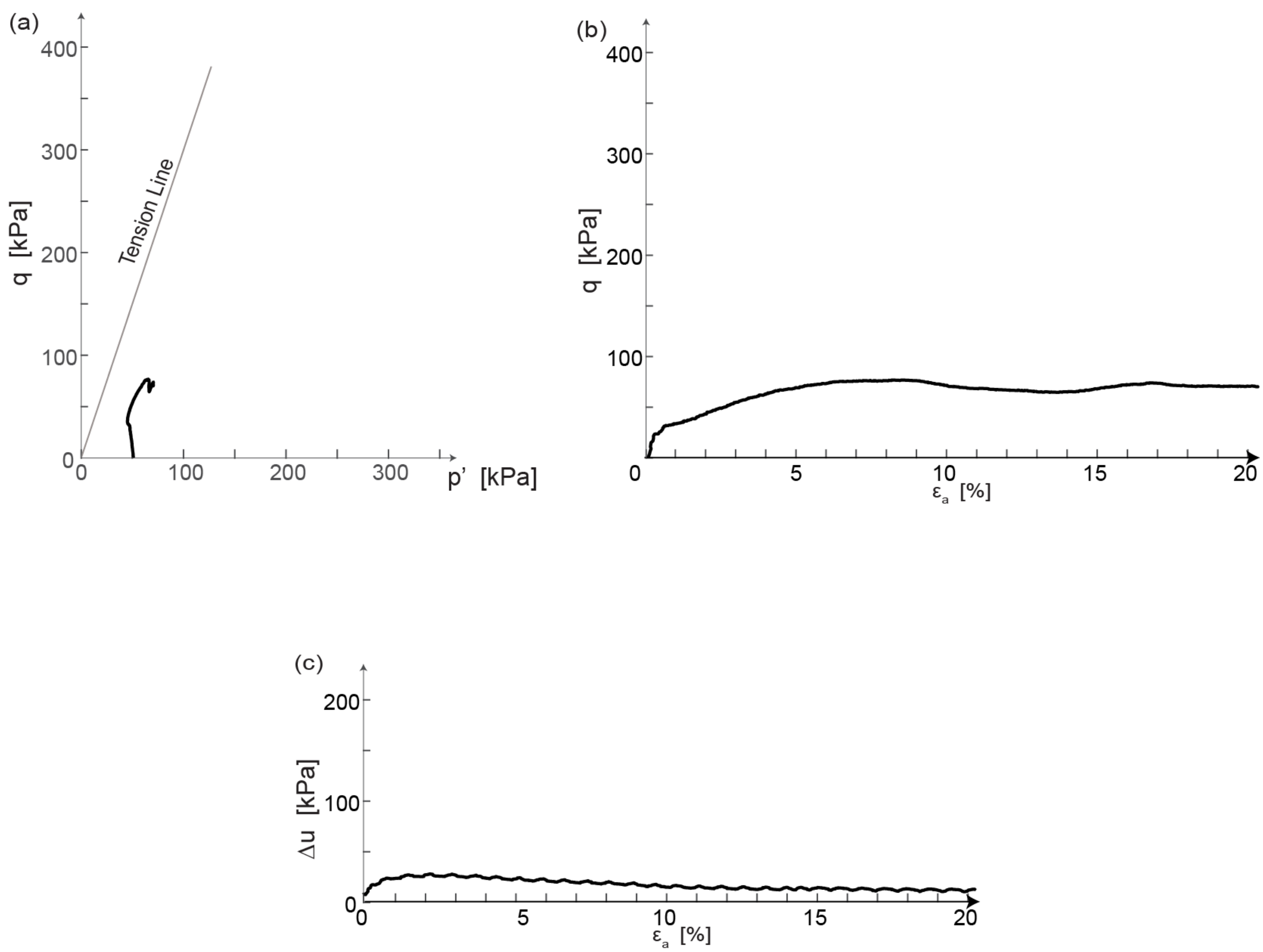

CU triaxial compression testing of unreinforced kaolinite clay specimen at a p_o' of 100 kPa

<u>CU Testing</u>
Specimen type: Reconstituted - slurry
Fiber Content: 0
Fiber length: NA
Fiber type: NA
Trimmed specimen length: 99.86 mm
Specimen diameter: 49 mm
Water content: 45%
Dry density: 1.34 g/cm^3

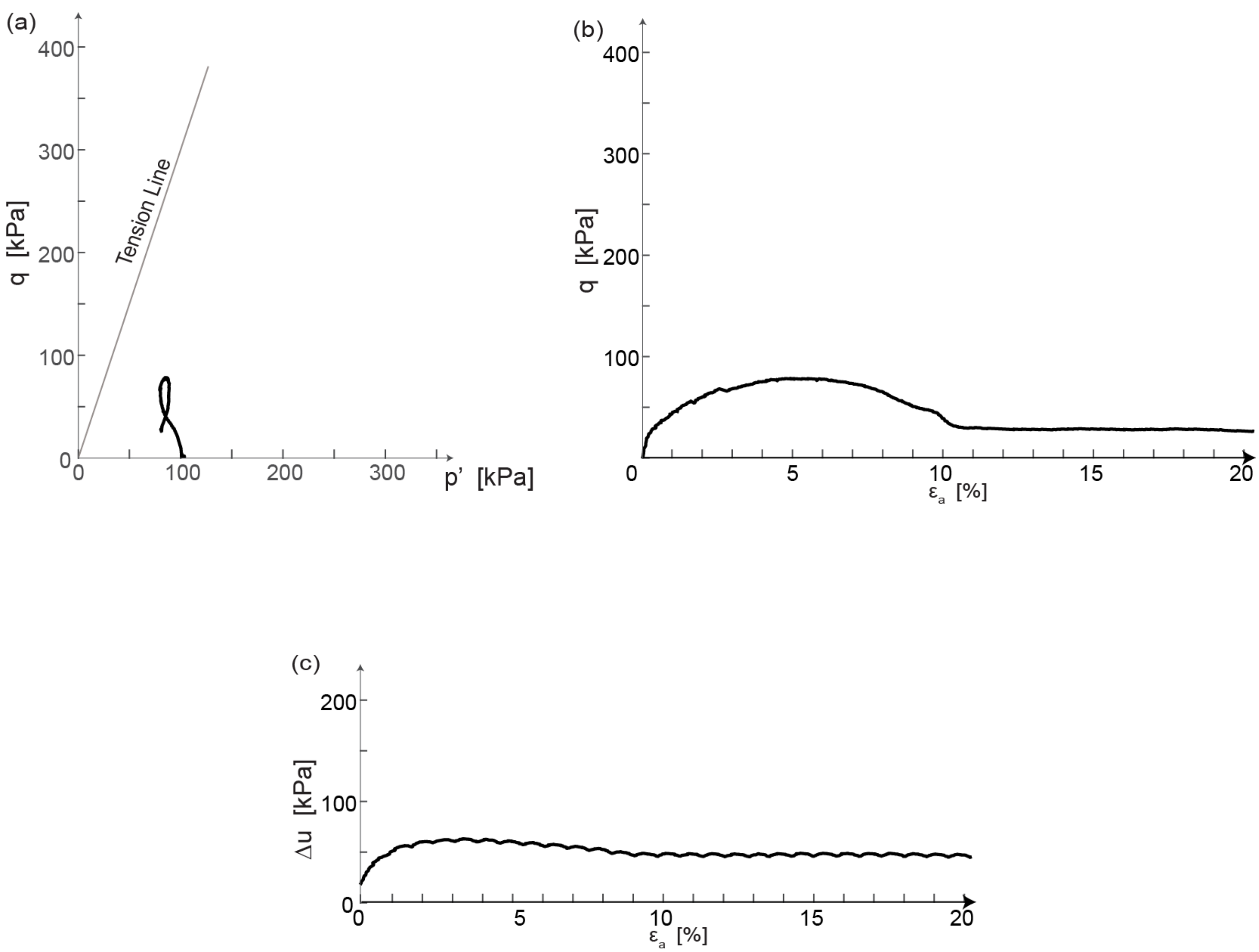

CU triaxial compression testing of unreinforced kaolinite clay specimen at a p'_o of 200 kPa

<u>CU Testing</u>
Specimen type: Reconstituted - slurry
Fiber Content: 0
Fiber length: NA
Fiber type: NA
Trimmed specimen length: 97.3 mm
Specimen diameter: 49.2 mm
Water content: 45.2 %
Dry density: 1.31 g/cm^3

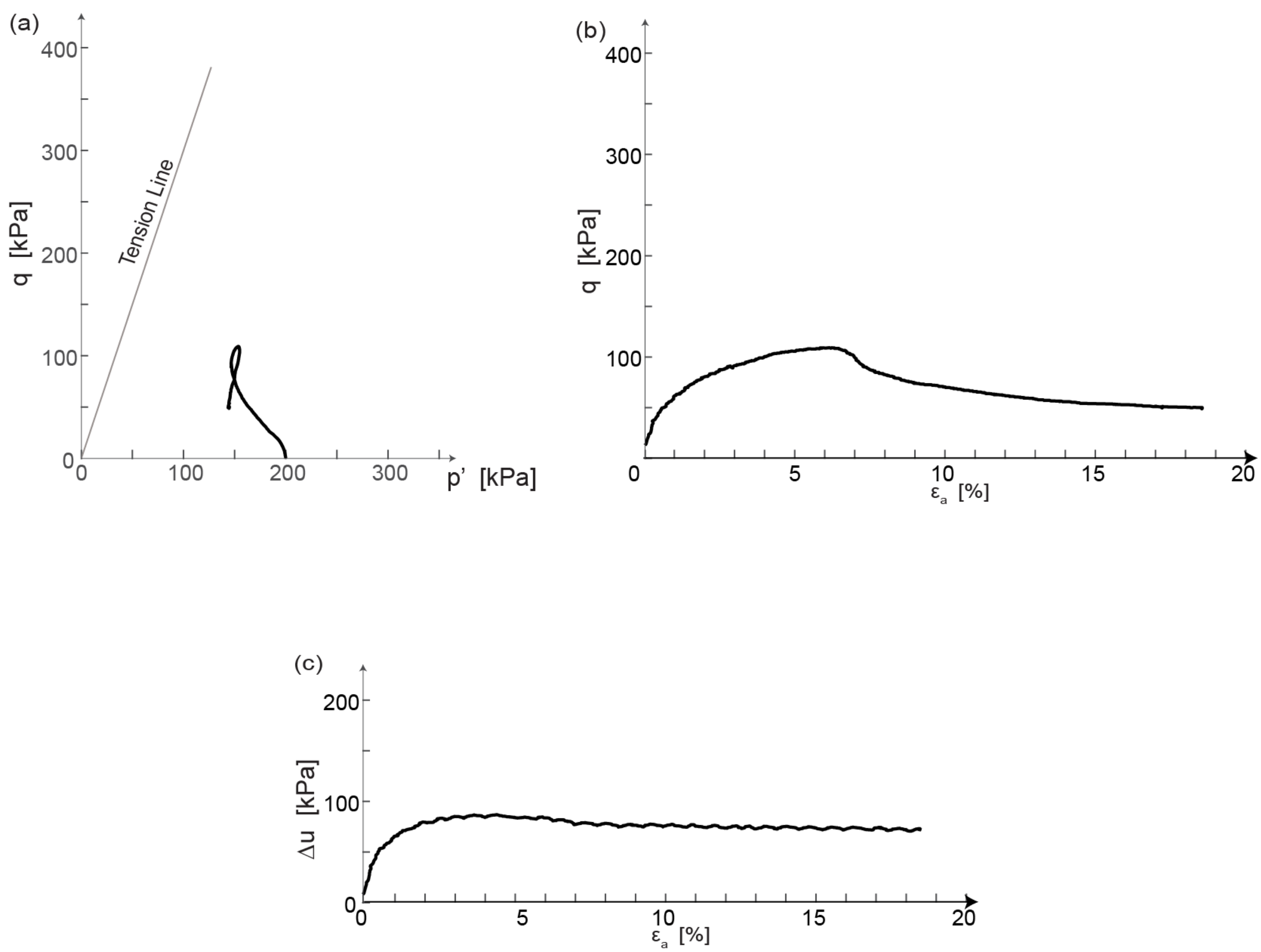

CU triaxial compression testing of fiber-reinforced kaolinite clay specimen at a p'_o of 50 kPa

<u>CU Testing</u>
Specimen type: Reconstituted slurry prepared
Fiber Content: 2%
Fiber length: 18 mm
Fiber type: PP
Trimmed specimen length: 95.8 mm
Specimen diameter: 49.5 mm
Water content: 46.5 %
Dry density: 1.59 g/cm^3

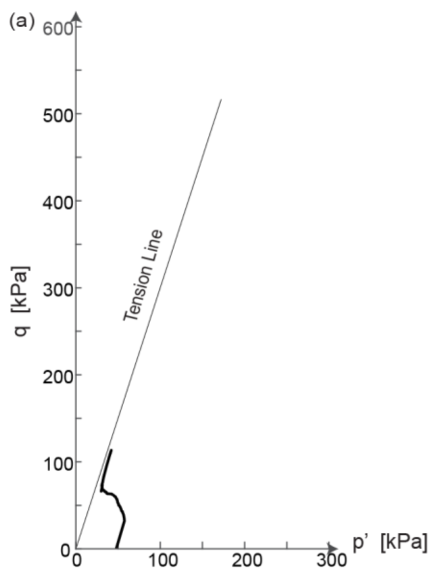

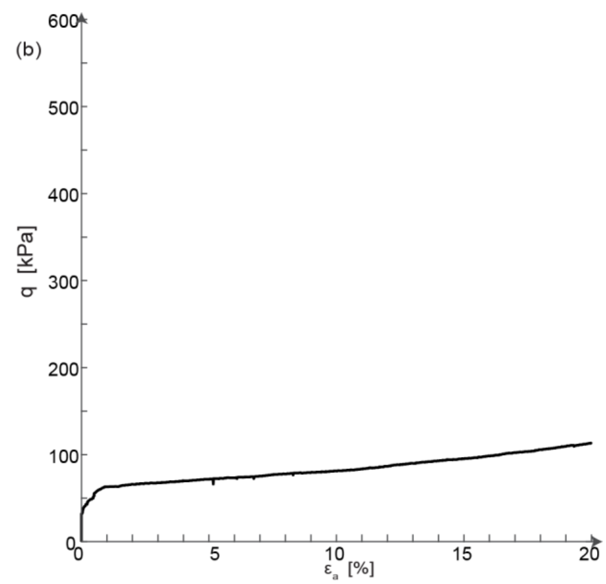

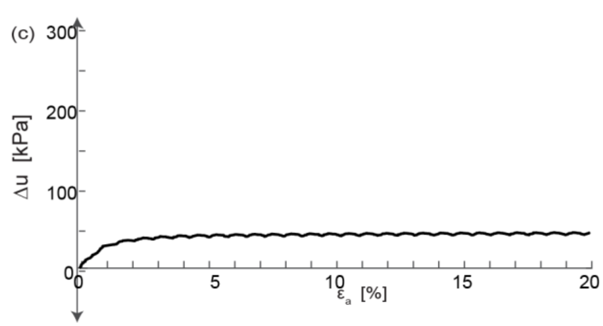

CU triaxial compression testing of fiber-reinforced kaolinite clay specimen at a p'_o of 100 kPa

<u>CU Testing</u>
Specimen type: Reconstituted slurry prepared
Fiber Content: 2%
Fiber length: 18 mm
Fiber type: PP
Trimmed specimen length: 99.2 mm
Specimen diameter: 49.1 mm
Water content: 46.4%
Dry density: 1.62 g/cm^3

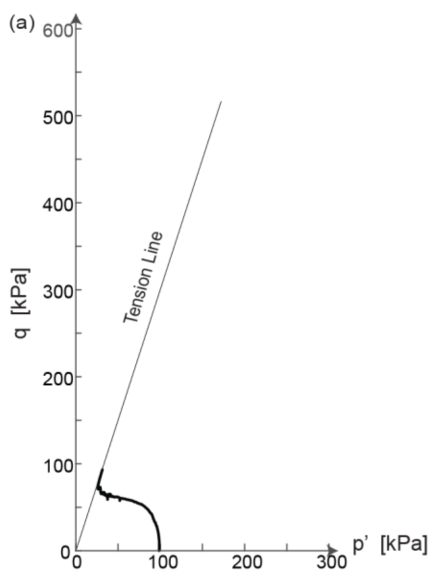

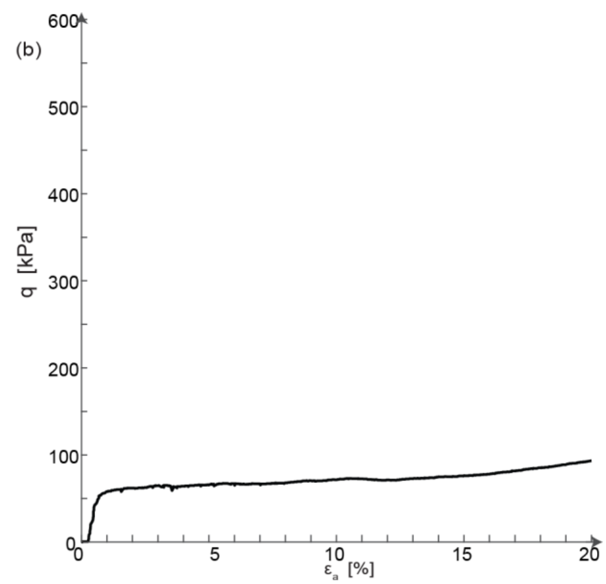

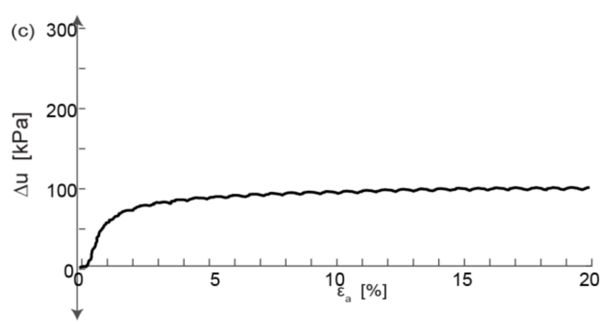

CU triaxial compression testing of fiber-reinforced kaolinite clay specimen at a p'_o of 200 kPa

<u>CU Testing</u>

Specimen type: Reconstituted slurry prepared
Fiber Content: 2%
Fiber length: 18 mm
Fiber type: PP
Trimmed specimen length: 98.3mm
Specimen diameter: 50 mm
Water content: 43.6%
Dry density: 1.57 g/cm^3

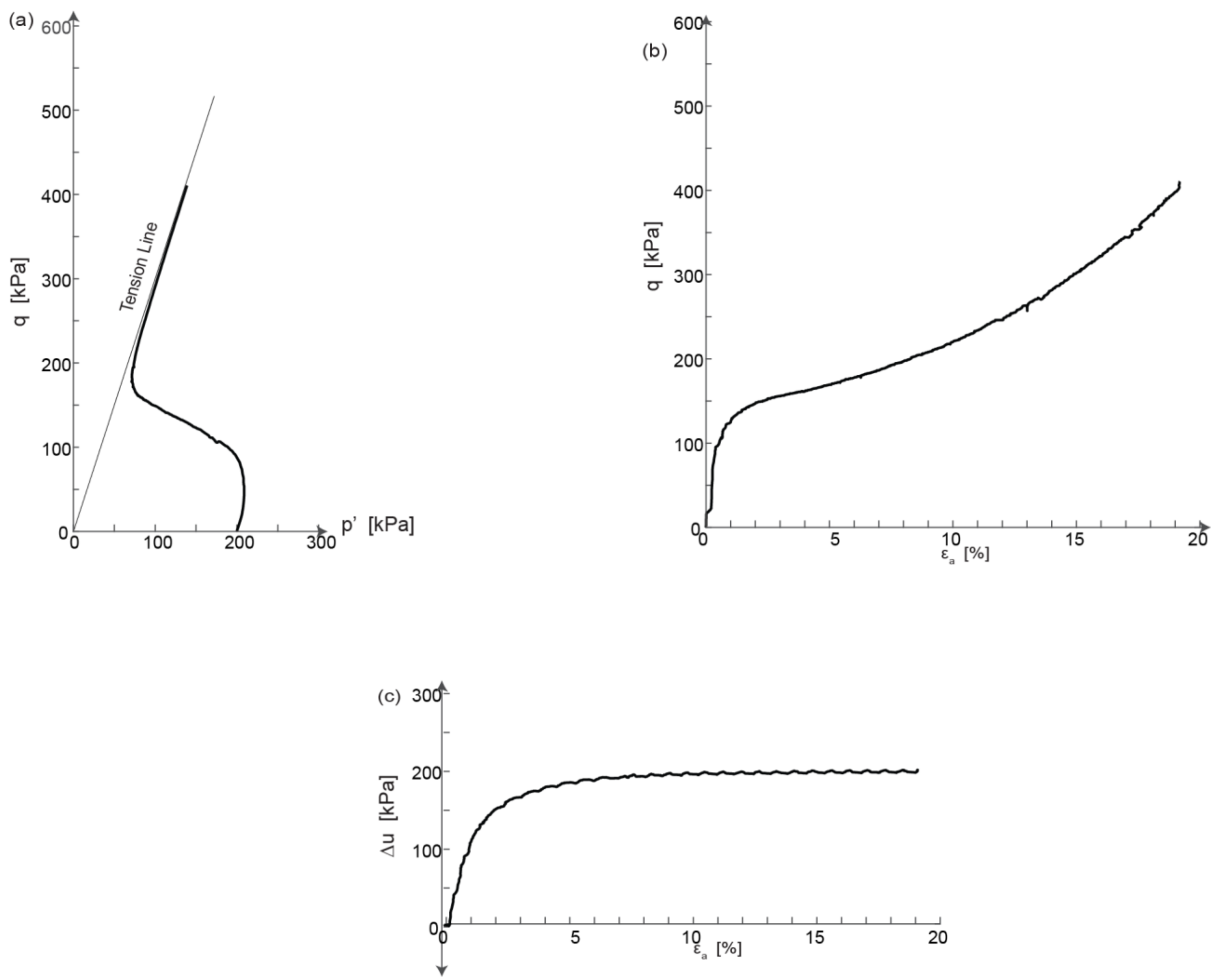

CU triaxial compression testing of fiber-reinforced kaolinite clay specimen at a p'_o of 50 kPa

<u>CU Testing</u>
Specimen type: Reconstituted slurry prepared
Fiber Content: 2%
Fiber length: 18 mm
Fiber type: PA
Trimmed specimen length: 104.8 mm
Specimen diameter: 50.9 mm
Water content: 46.7 %
Dry density: 1.47 g/cm^3

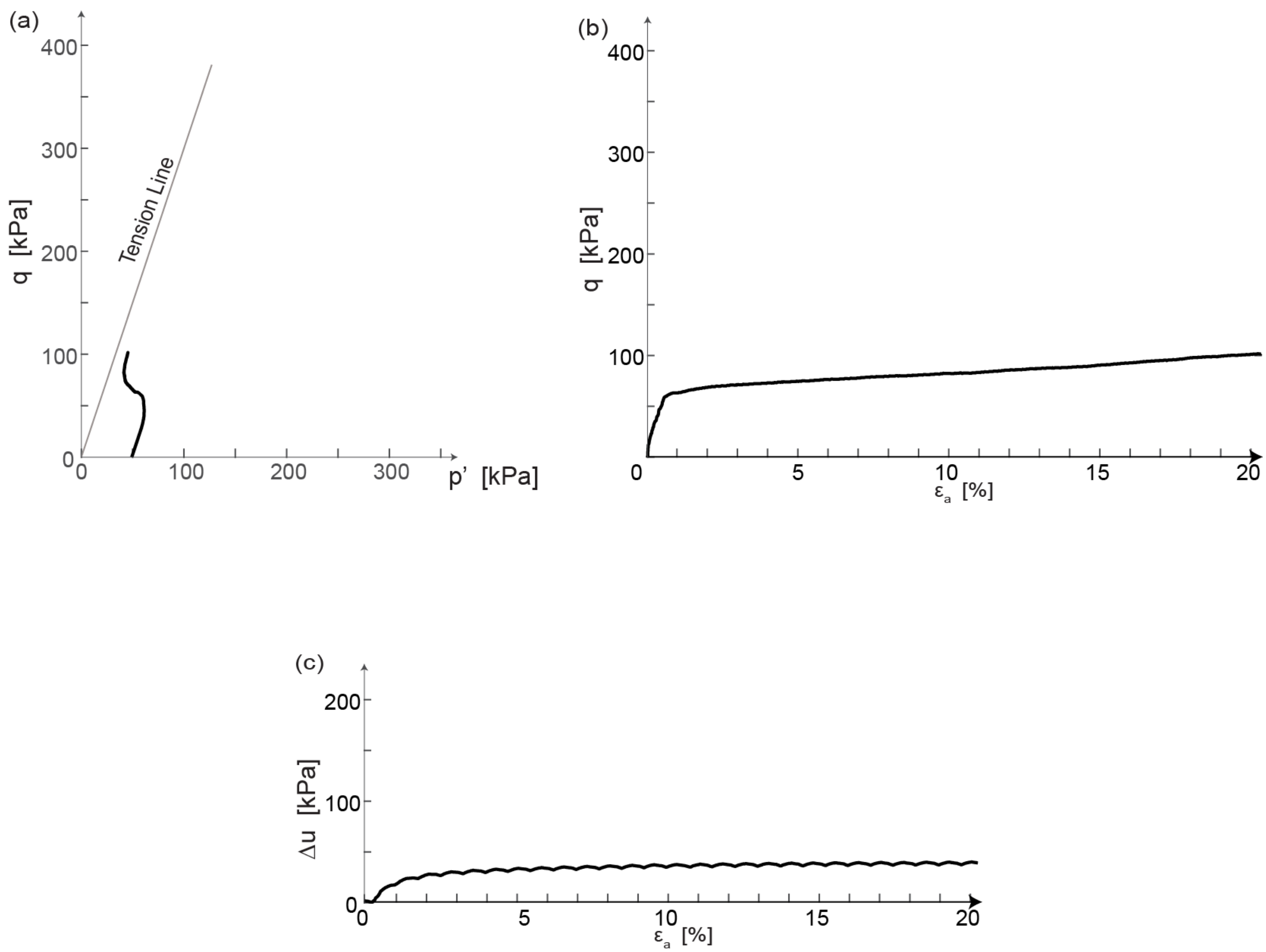

CU triaxial compression testing of fiber-reinforced kaolinite clay specimen at a p'_o of 100 kPa

<u>CU Testing</u>

Specimen type: Reconstituted slurry prepared
Fiber Content: 2%
Fiber length: 18 mm
Fiber type: PA
Trimmed specimen length: 100.2 mm
Specimen diameter: 49.7 mm
Water content: 46.2%
Dry density: 1.4 g/cm^3

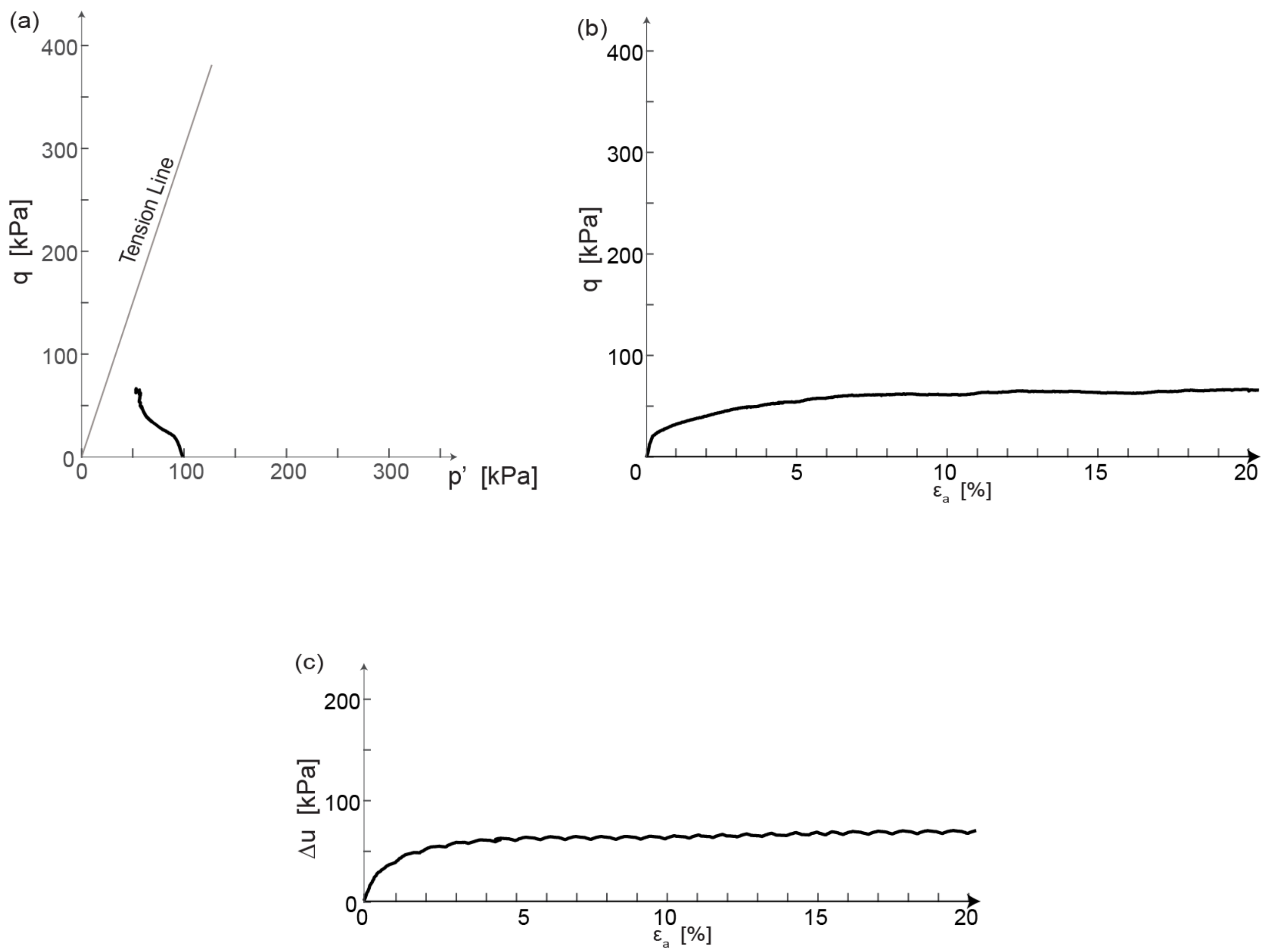

CU triaxial compression testing of fiber-reinforced kaolinite clay specimen at a p'_o of 200 kPa

<u>CU Testing</u>
Specimen type: Reconstituted slurry prepared
Fiber Content: 2%
Fiber length: 18 mm
Fiber type: PA
Trimmed specimen length: 99.2 mm
Specimen diameter: 48.5 mm
Water content: 46 %
Dry density: 1.49 g/cm^3

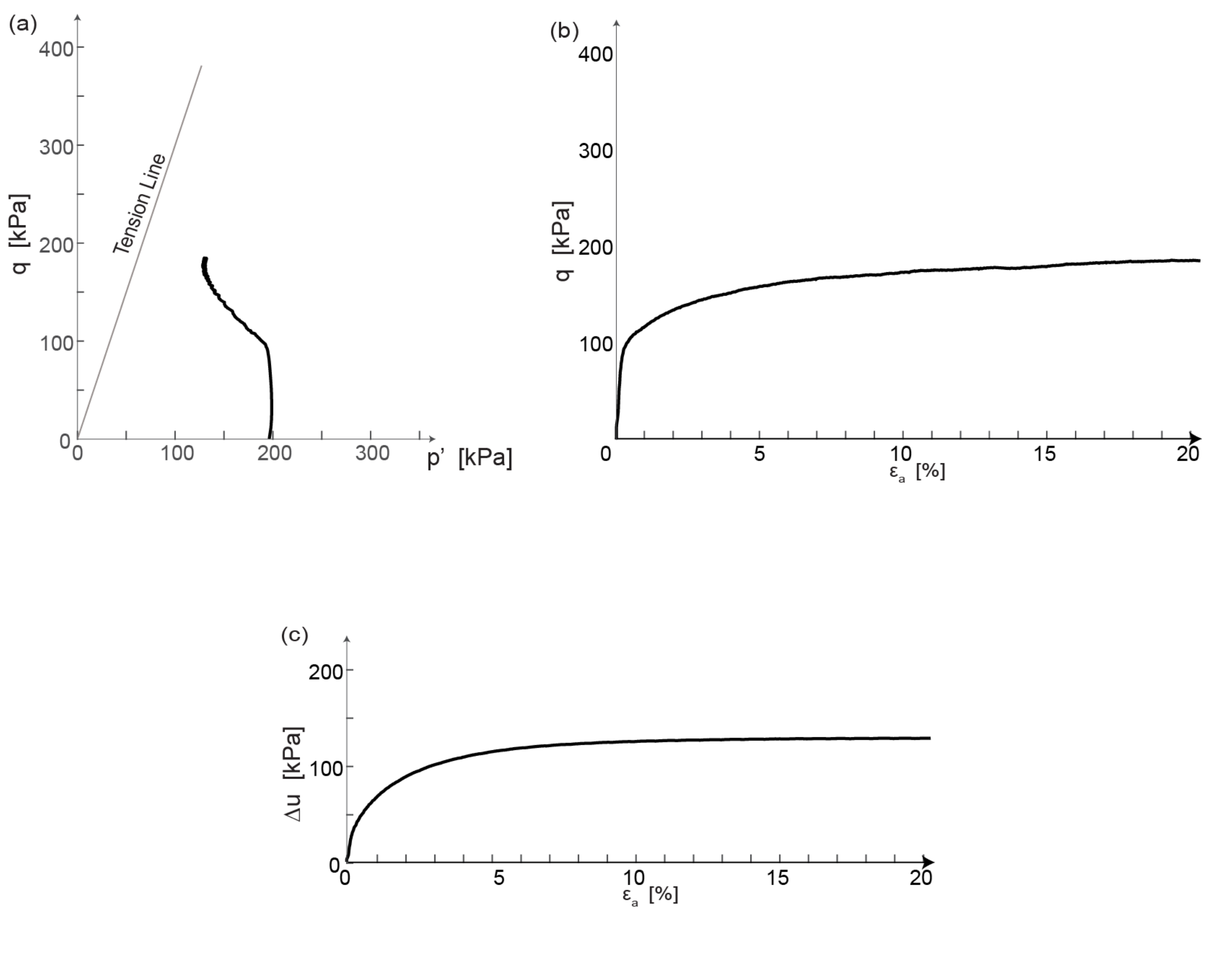

CU triaxial compression testing of fiber-reinforced kaolinite clay specimen at a p'_o of 50 kPa

<u>CU Testing</u>
Specimen type: Reconstituted slurry prepared
Fiber Content: 2%
Fiber length: 48 mm
Fiber type: PP
Trimmed specimen length: 96.8 mm
Specimen diameter: 47.8 mm
Water content: 44.39 %
Dry density: 1.42 g/cm^3

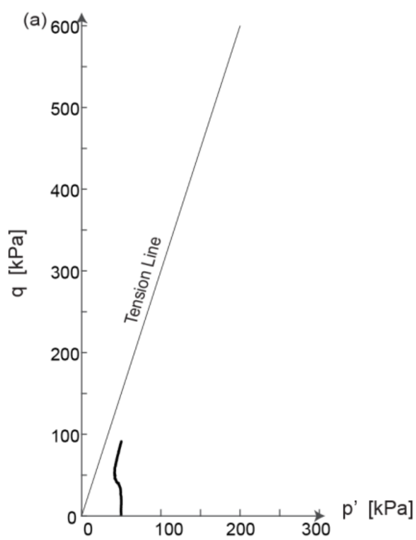

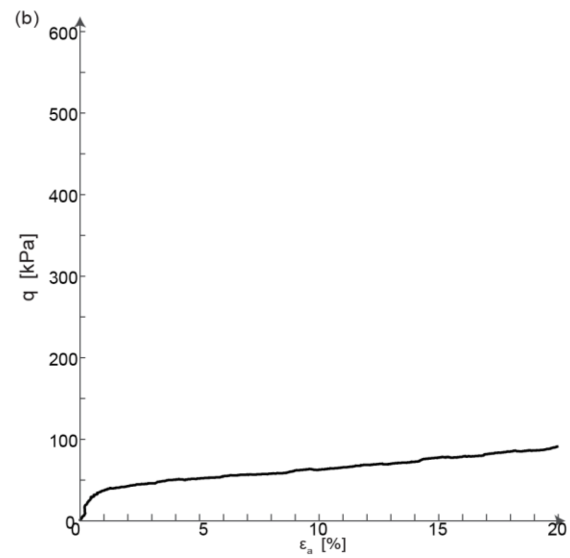

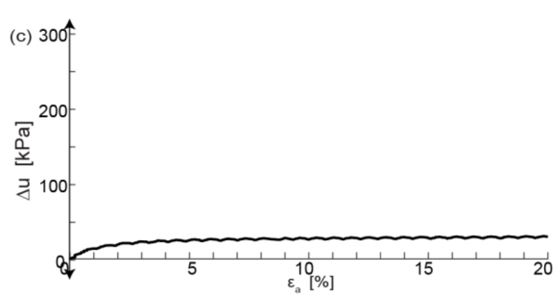

CU triaxial compression testing of fiber-reinforced kaolinite clay specimen at a p'_o of 100 kPa

<u>CU Testing</u>
Specimen type: Reconstituted slurry prepared
Fiber Content: 2%
Fiber length: 48 mm
Fiber type: PP
Trimmed specimen length: 98.7 mm
Specimen diameter: 50 mm
Water content: 44.5 %
Dry density: 1.47 g/cm^3

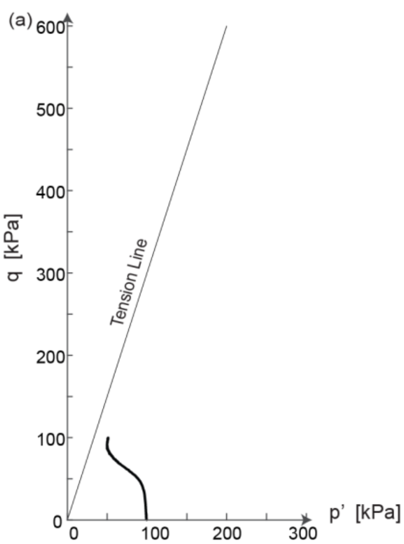

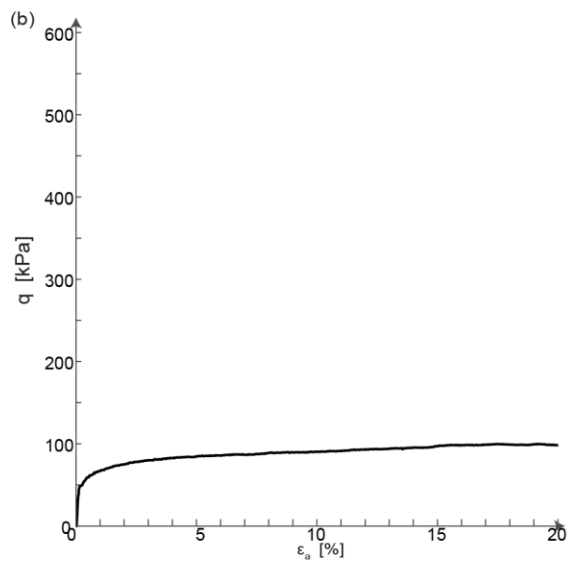

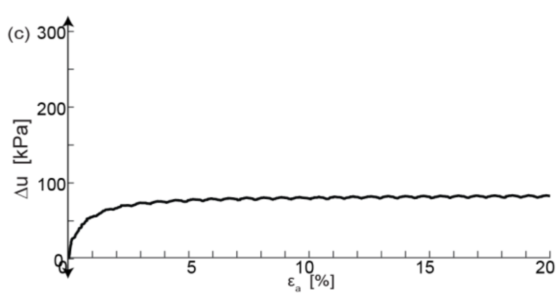

CU triaxial compression testing of fiber-reinforced kaolinite clay specimen at a p_o' of 200 kPa

<u>CU Testing</u>
Specimen type: Reconstituted slurry prepared
Fiber Content: 2%
Fiber length: 48 mm
Fiber type: PP
Trimmed specimen length: 97.5 mm
Specimen diameter: 49.5 mm
Water content: 43.9 %
Dry density: 1.44 g/cm^3

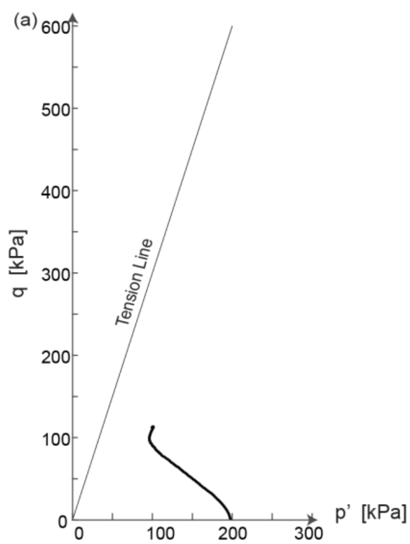

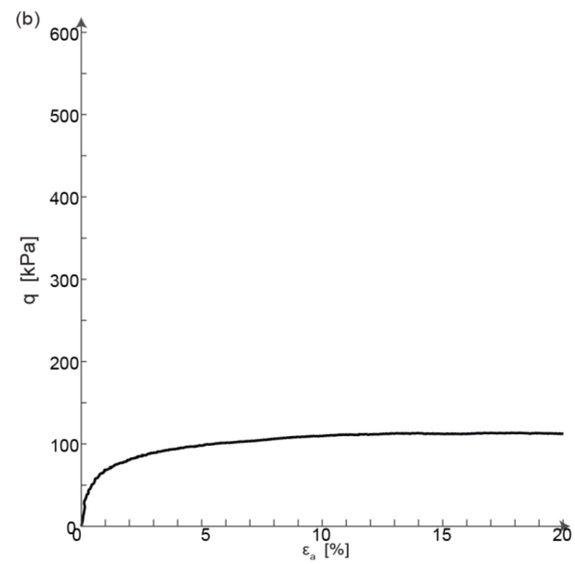

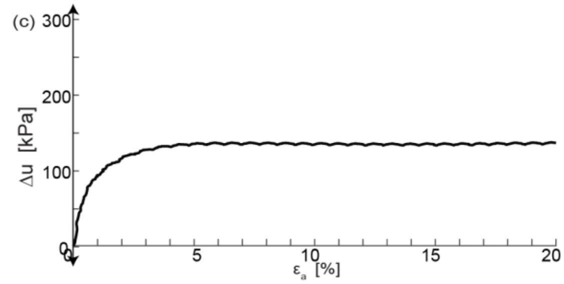

CU triaxial extension testing of fiber-reinforced kaolinite clay specimen at a p'_o of 50 kPa

CU Testing
Specimen type: Reconstituted slurry prepared
Fiber orientation: Horizontal
Fiber Content: 2%
Fiber length: 18 mm
Fiber type: PP
Trimmed specimen length: 95.2mm
Specimen diameter: 49.8 mm
Water content: 45.2 %
Dry density: 1.6 g/cm^3

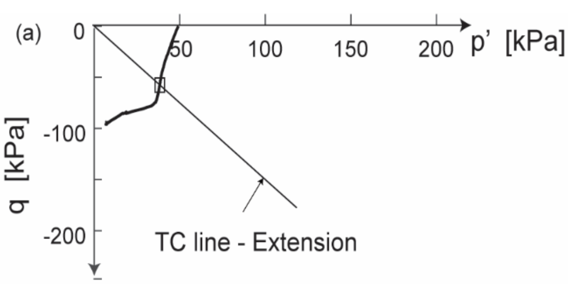

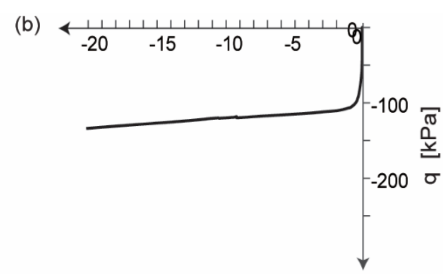

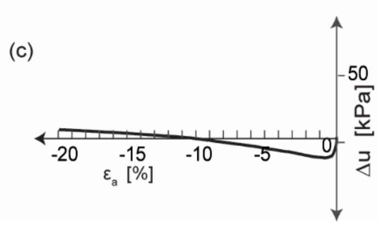

CU triaxial extension testing of fiber-reinforced kaolinite clay specimen at a p'_o of 100 kPa

<u>CU Testing</u>
Specimen type: Reconstituted slurry prepared
Fiber orientation: Horizontal
Fiber Content: 2%
Fiber length: 18 mm
Fiber type: PP
Trimmed specimen length: 98.5mm
Specimen diameter: 49.6 mm
Water content: 45.9%
Dry density: 1.61 g/cm^3

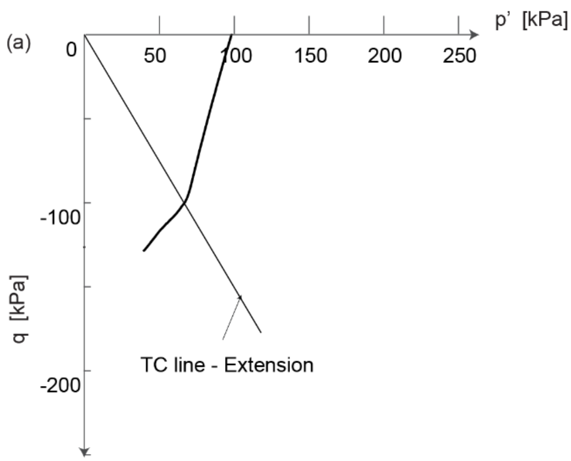

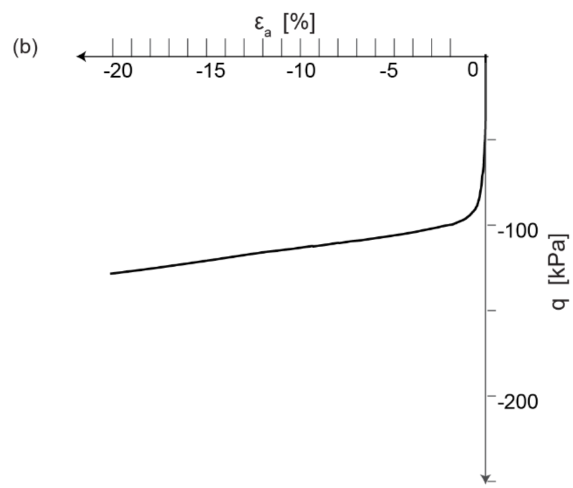

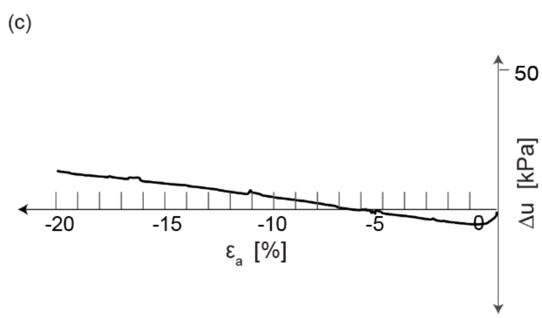

CU triaxial extension testing of fiber-reinforced kaolinite clay specimen at a p'_o of 200 kPa

<u>CU Testing</u>
Specimen type: Reconstituted slurry prepared
Fiber orientation: Horizontal
Fiber Content: 2%
Fiber length: 18 mm
Fiber type: PP
Trimmed specimen length: 97.9 mm
Specimen diameter: 49.4 mm
Water content: 46.5 %
Dry density: 1.55 g/cm^3

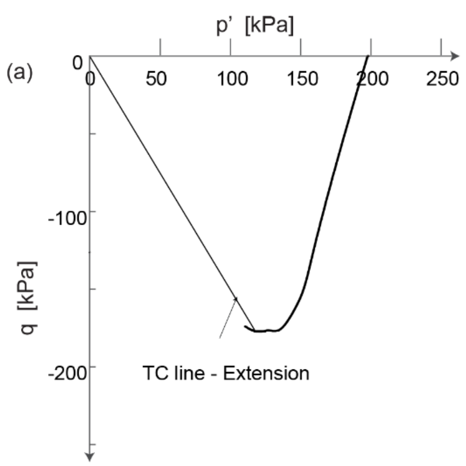

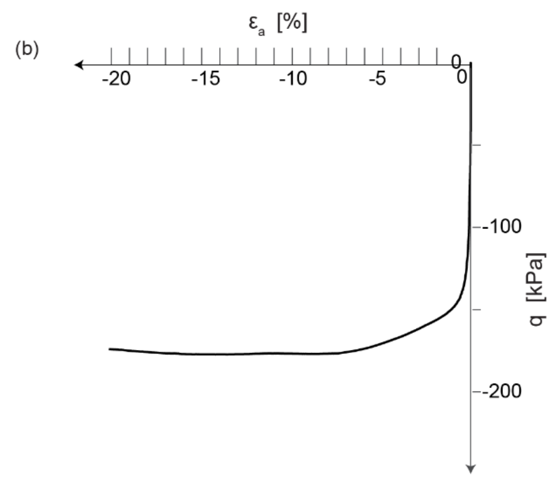

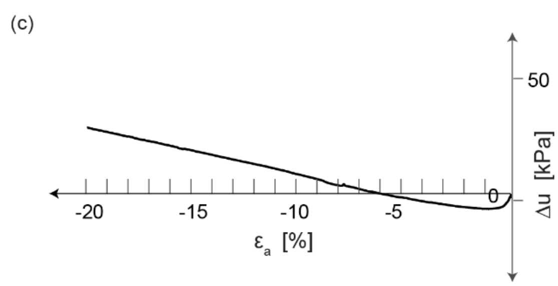

CU triaxial extension testing of fiber-reinforced kaolinite clay specimen at a p'_o of 50 kPa

<u>CU Testing</u>
Specimen type: Reconstituted slurry prepared
Fiber orientation: Horizontal
Fiber Content: 2%
Fiber length: 48 mm
Fiber type: PP
Trimmed specimen length: 98.7 mm
Specimen diameter: 48.2 mm
Water content: 46.2 %
Dry density: 1.52 g/cm^3

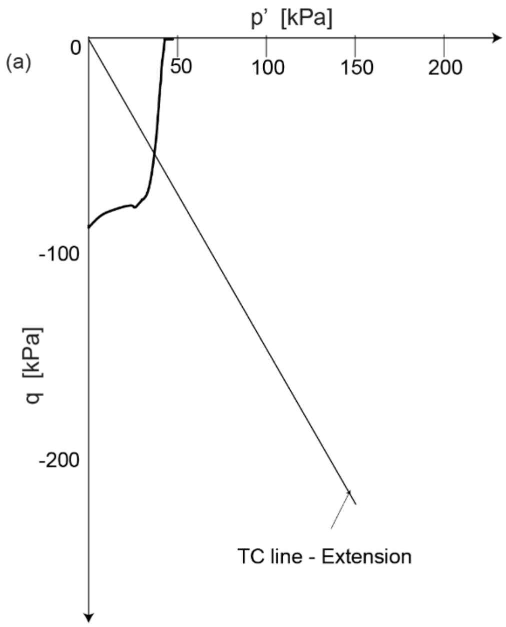

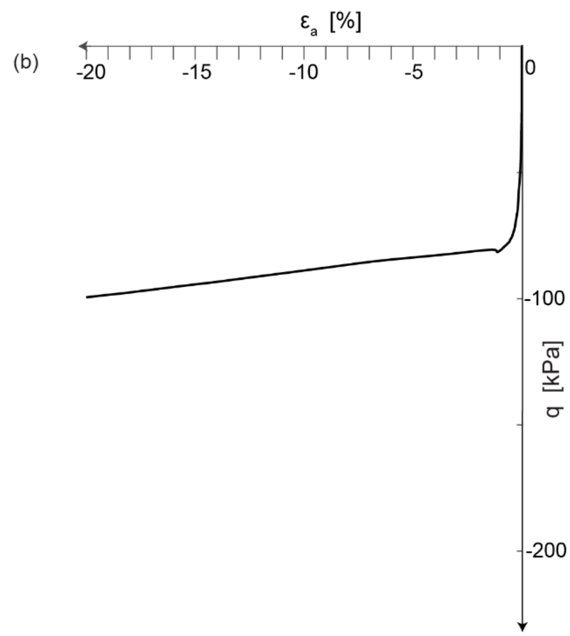

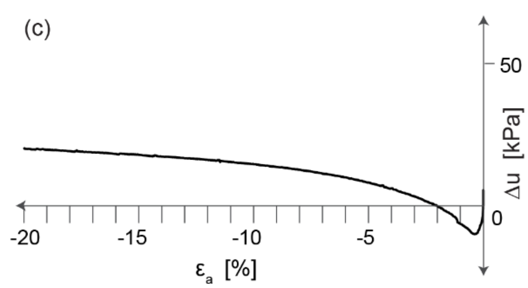

CU triaxial extension testing of fiber-reinforced kaolinite clay specimen at a p'_o of 100 kPa

<u>CU Testing</u>
Specimen type: Reconstituted slurry prepared
Fiber orientation: Horizontal
Fiber Content: 2%
Fiber length: 48 mm
Fiber type: PP
Trimmed specimen length: 99.2 mm
Specimen diameter: 48.6 mm
Water content: 45.9 %
Dry density: 1.57 g/cm^3

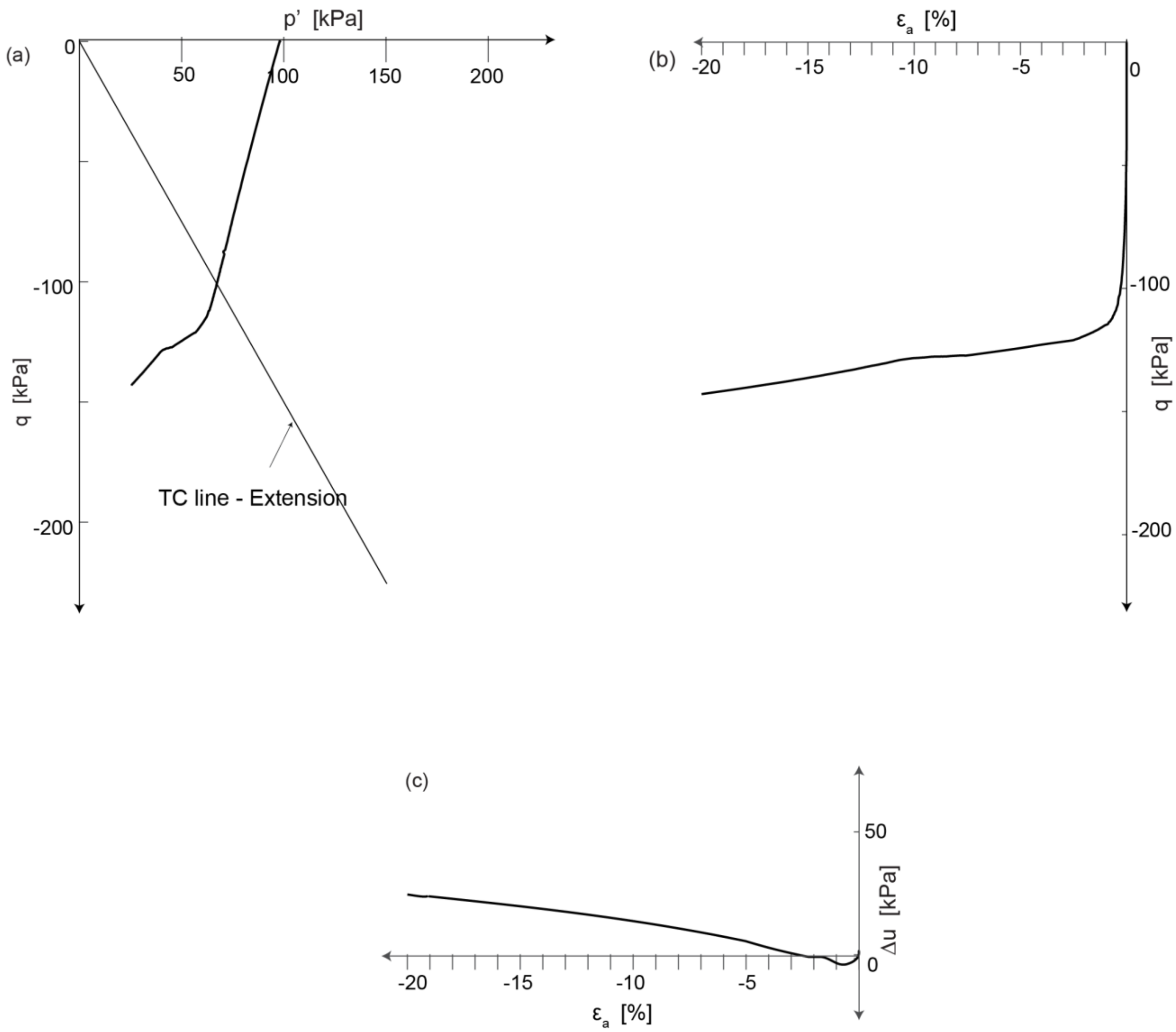

CU triaxial extension testing of fiber-reinforced kaolinite clay specimen at a p'_o of 200 kPa

<u>CU Testing</u>
Specimen type: Reconstituted slurry prepared
Fiber orientation: Horizontal
Fiber Content: 2%
Fiber length: 48 mm
Fiber type: PP
Trimmed specimen length: 99.8 mm
Specimen diameter: 50 mm
Water content: 45.9 %
Dry density: 1.59 g/cm^3

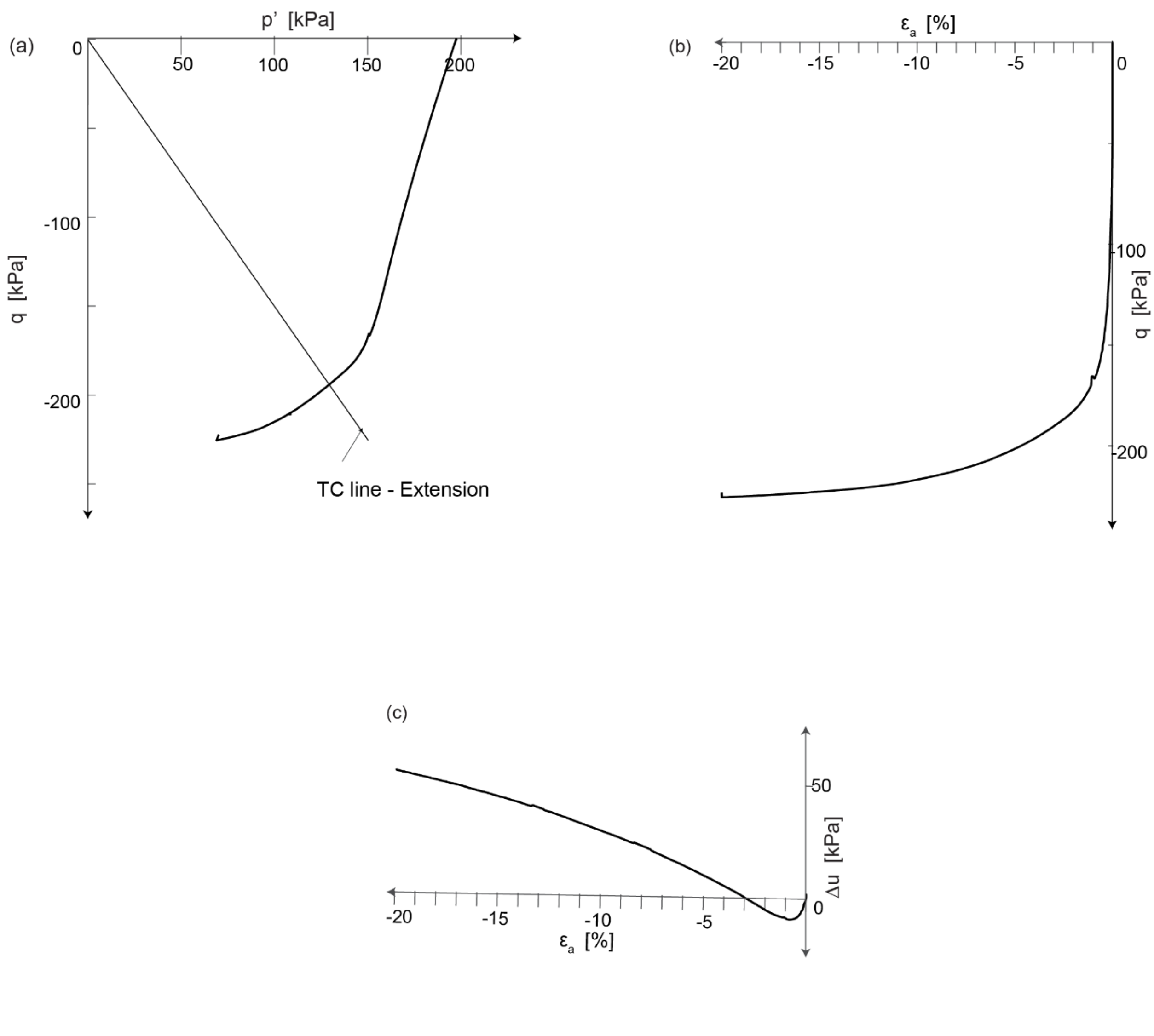

CU triaxial extension testing of fiber-reinforced kaolinite clay specimen at a p_o' of 50 kPa

<u>CU Testing</u>
Specimen type: Reconstituted slurry prepared
Fiber orientation: Vertical
Fiber Content: 2%
Fiber length: 48 mm
Fiber type: PP
Trimmed specimen length: 98.7 mm
Specimen diameter: 48.8 mm
Water content: 46.2 %
Dry density: 1.52 g/cm^3

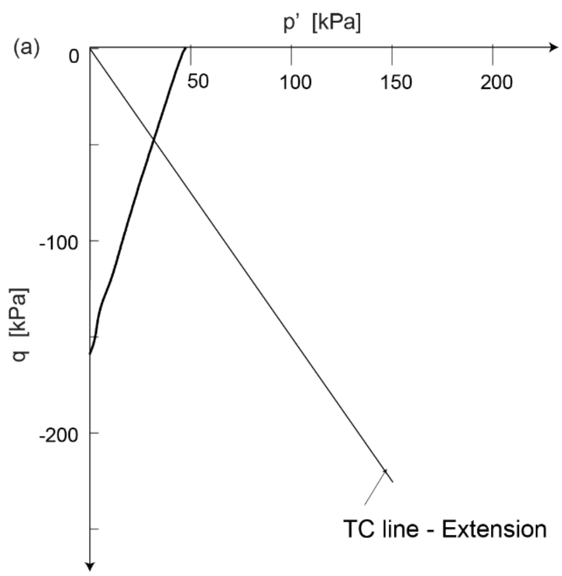

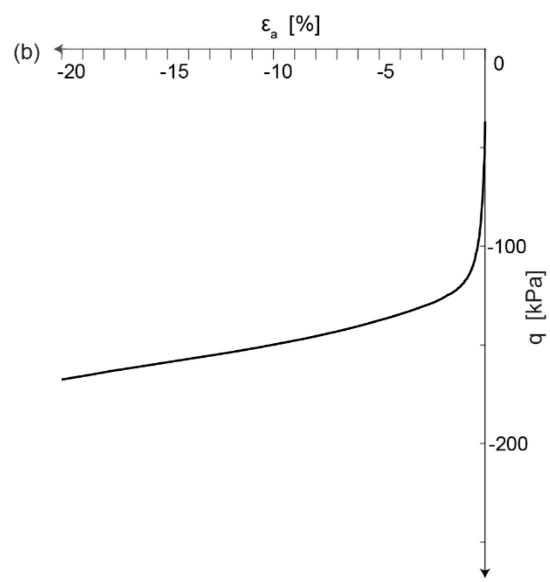

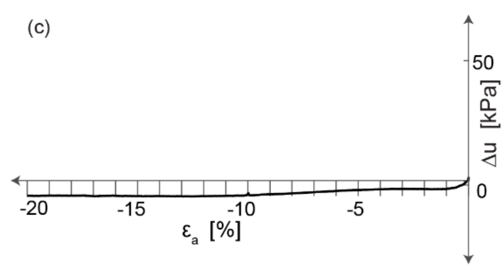

CU triaxial extension testing of fiber-reinforced kaolinite clay specimen at a p'_o of 100 kPa

<u>CU Testing</u>
Specimen type: Reconstituted slurry prepared
Fiber orientation: Vertical
Fiber Content: 2%
Fiber length: 48 mm
Fiber type: PP
Trimmed specimen length: 100.2 mm
Specimen diameter: 48.1 mm
Water content: 45.6 %
Dry density: 1.59 g/cm^3

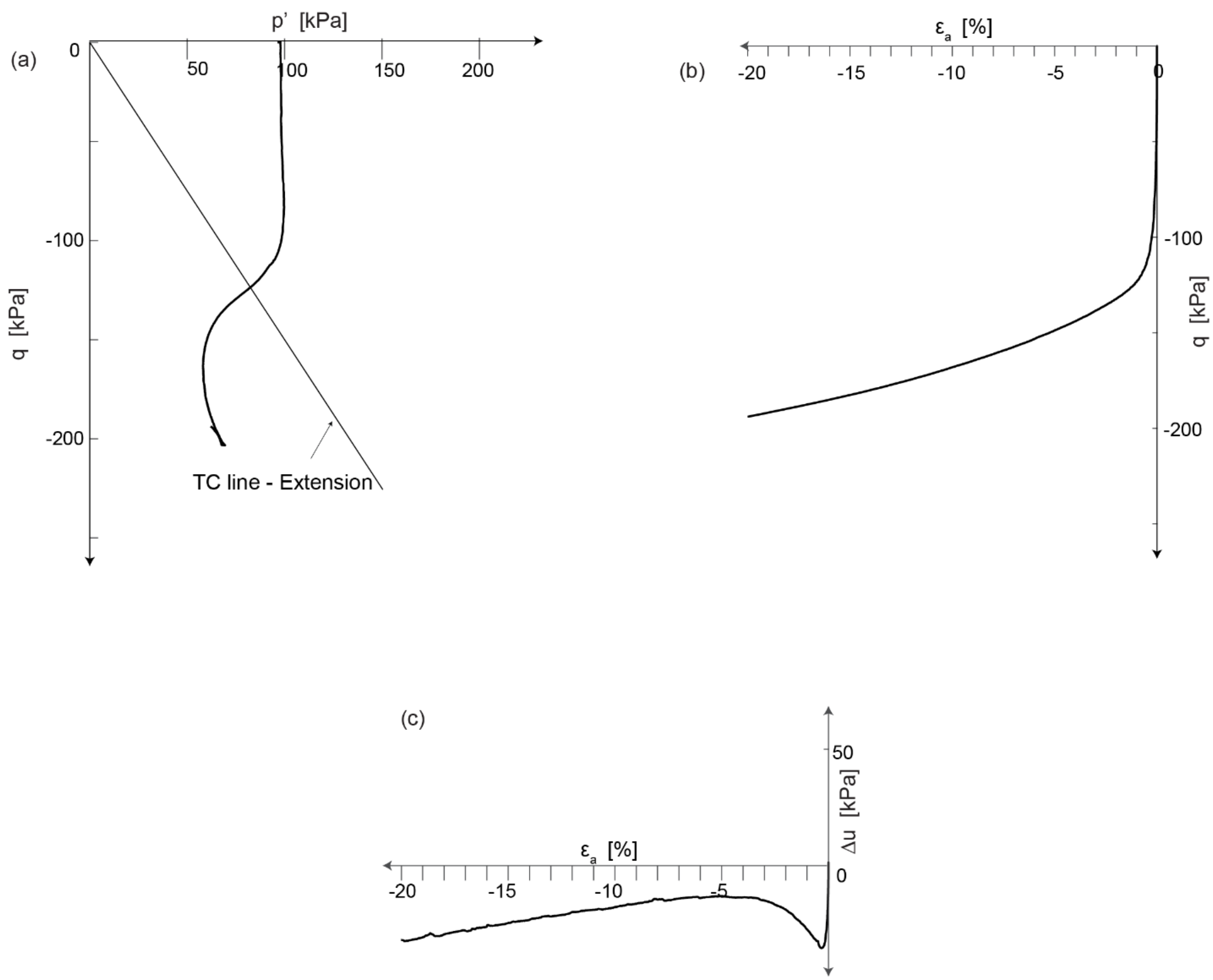

CU triaxial extension testing of fiber-reinforced kaolinite clay specimen at a p'_o of 200 kPa

<u>CU Testing</u>
Specimen type: Reconstituted slurry prepared
Fiber orientation: Vertical
Fiber Content: 2%
Fiber length: 48 mm
Fiber type: PP
Trimmed specimen length: 98.9 mm
Specimen diameter: 50.2 mm
Water content: 46.2 %
Dry density: 1.6 g/cm^3

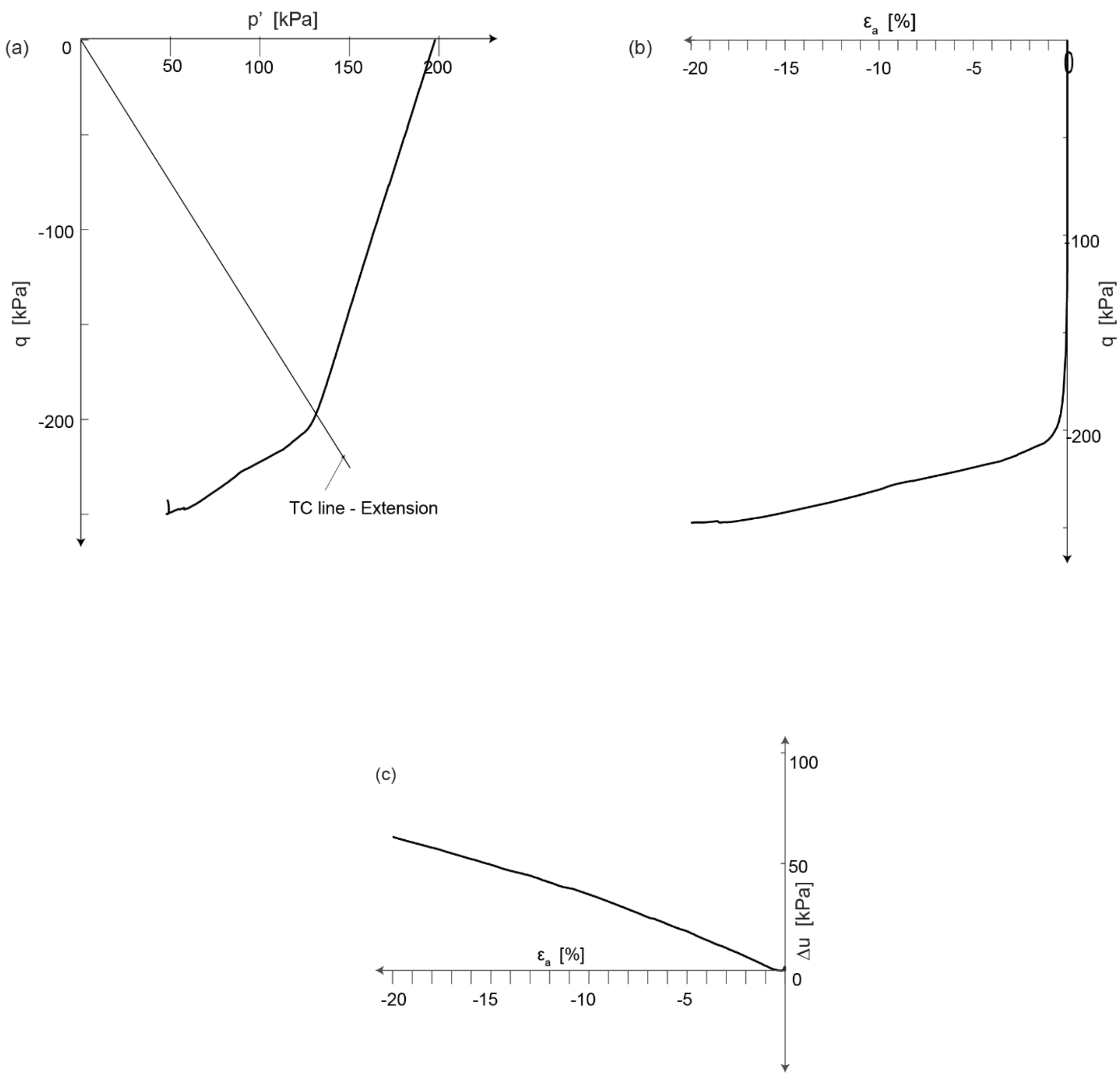

Appendix B: Results from direct shear testing of unreinforced and fiber-reinforced clay soil

This appendix provides a record of the direct shear testing results for unreinforced and fiber-reinforced specimens as presented in Chapter 5 (Manuscripts #3).

Direct shear testing of unreinforced kaolinite clay specimen at a σ'_N of 50 kPa

Properties of clay soil
Specimen type: Reconstituted - slurry
Water content: 45 %
Dry density: 1.35 g/cm^3

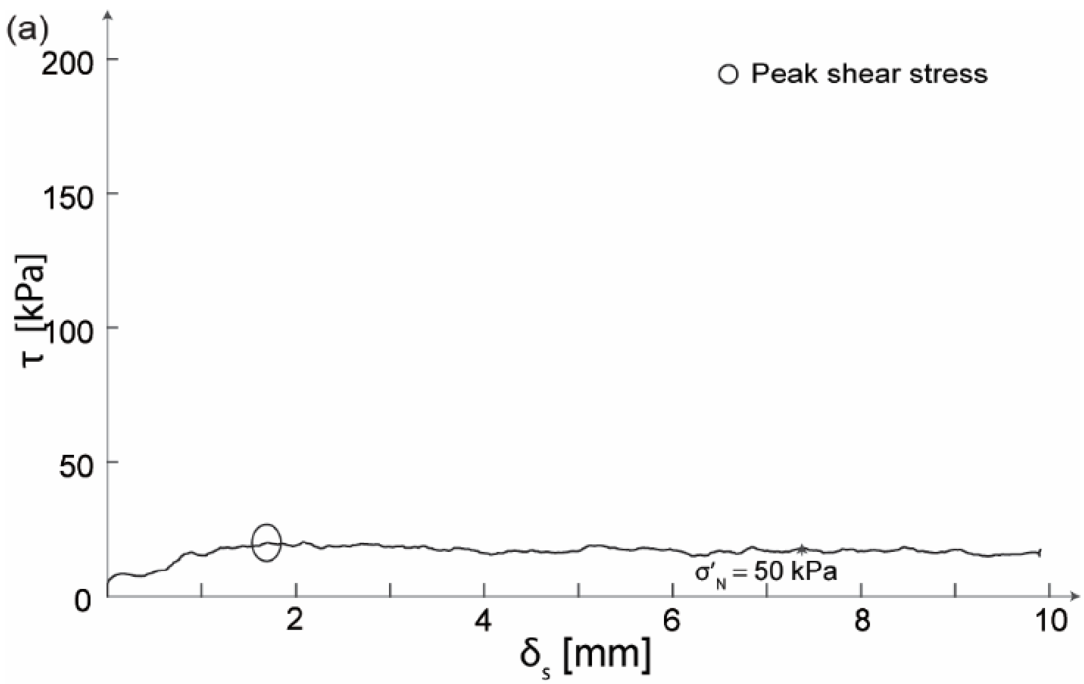

Direct shear testing of unreinforced kaolinite clay specimen at a σ'_N of 100 kPa

Properties of clay soil
Specimen type: Reconstituted - slurry
Water content: 45 %
Dry density: 1.32 g/cm^3

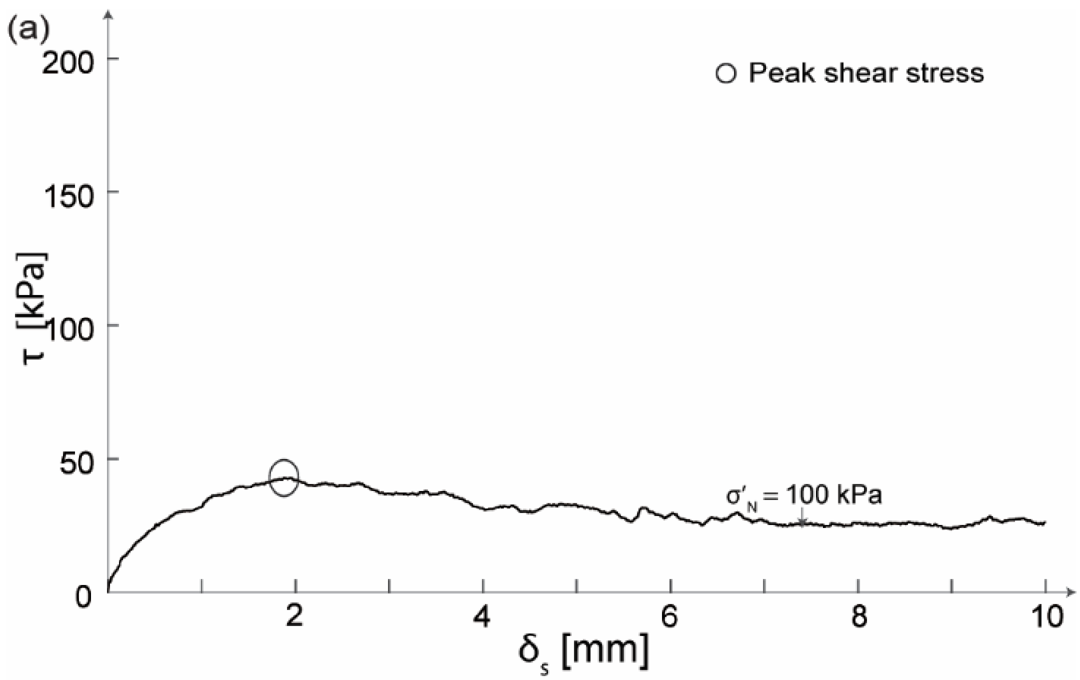

Direct shear testing of unreinforced kaolinite clay specimen at a σ'_N of 200 kPa

Properties of clay soil
Specimen type: Reconstituted - slurry
Water content: 45 %
Dry density: 1.3 g/cm^3

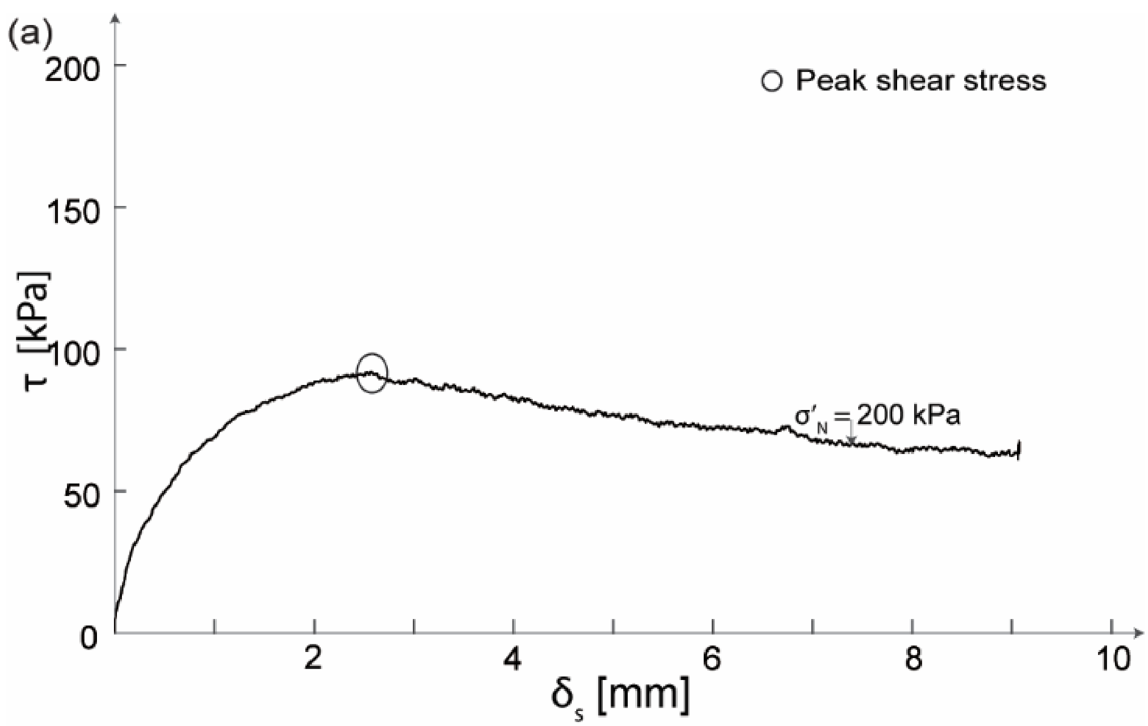

Direct shear testing of unreinforced kaolinite clay specimen at a σ'_N of 300 kPa

<u>Properties of clay soil</u>
Specimen type: Reconstituted - slurry
Water content: 44.5 %
Dry density: 1.34 g/cm^3

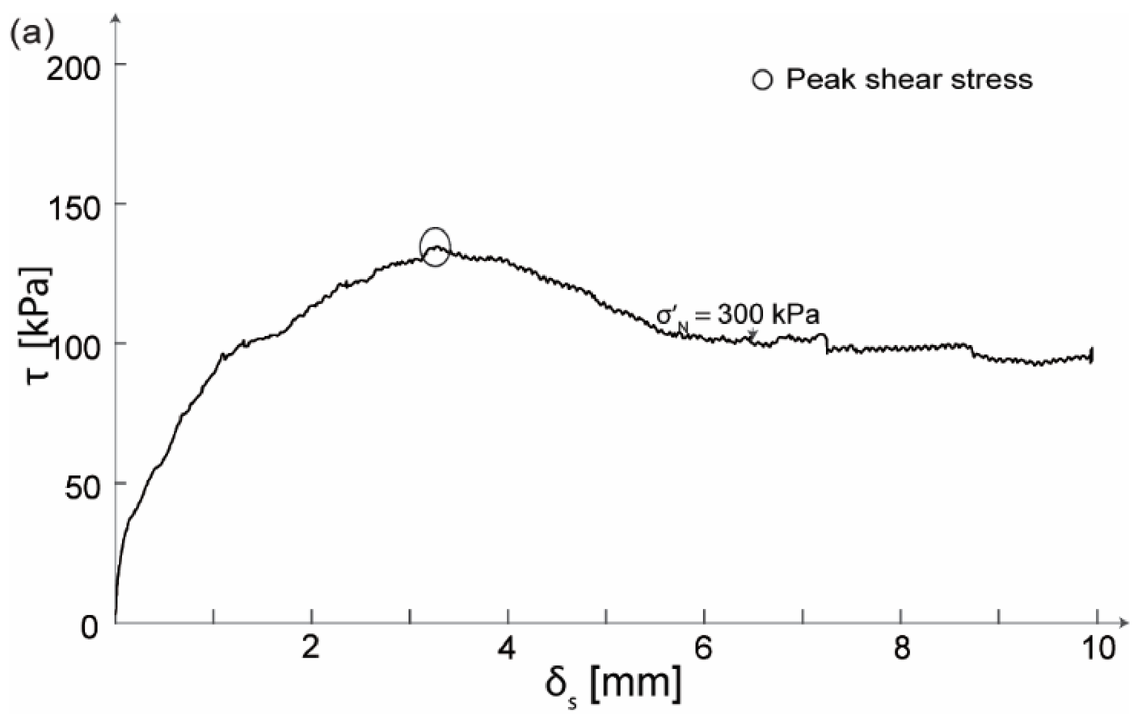

Direct shear testing of unreinforced kaolinite clay specimen at a σ'_N of 400 kPa

Properties of clay soil
Specimen type: Reconstituted - slurry
Water content: 45 %
Dry density: 1.3 g/cm^3

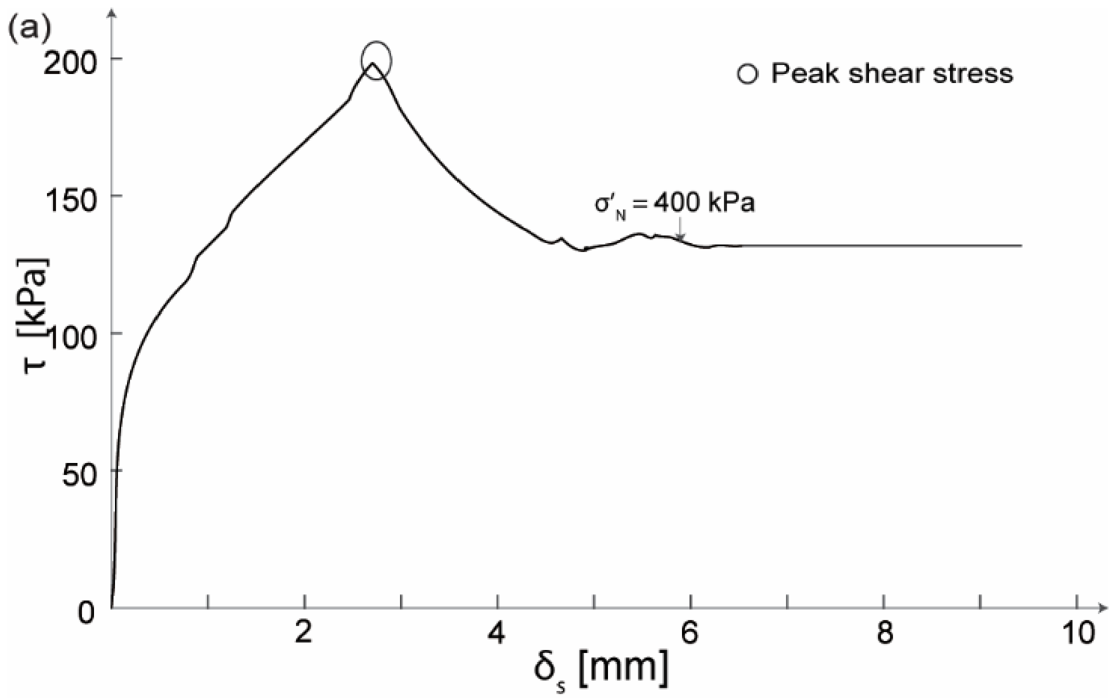

Direct shear testing of fiber-reinforced kaolinite clay specimen at a σ'_N of 50 kPa

Properties of clay soil
Specimen type: Reconstituted - slurry
Water content: 44.5 %
Dry density: 1.34 g/cm^3

Properties of fibers
Fiber type: PP
Thickness: 0.035 mm
Specific gravity: 0.91
Moisture Absorption< 1%

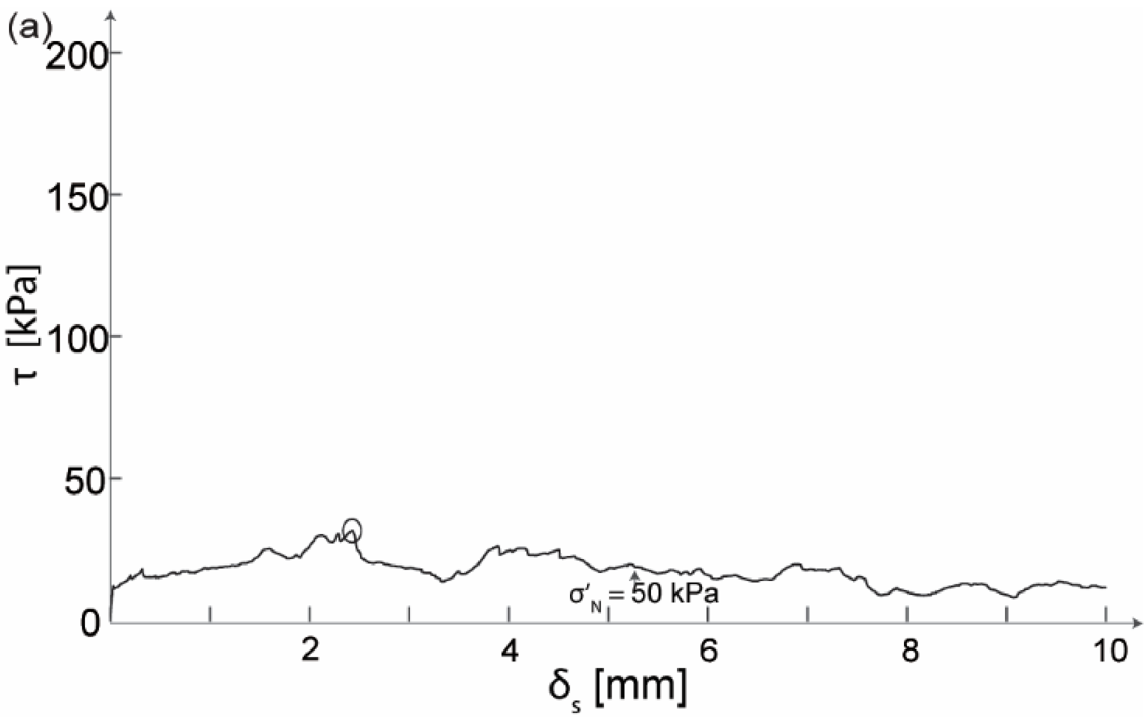

Direct shear testing of fiber-reinforced kaolinite clay specimen at a σ'_N of 100 kPa

<u>Properties of clay soil</u>
Specimen type: Reconstituted - slurry
Water content: 44 %
Dry density: 1.3 g/cm^3

<u>Properties of fibers</u>
Fiber type: PP
Thickness: 0.035 mm
Specific gravity: 0.91
Moisture Absorption< 1%

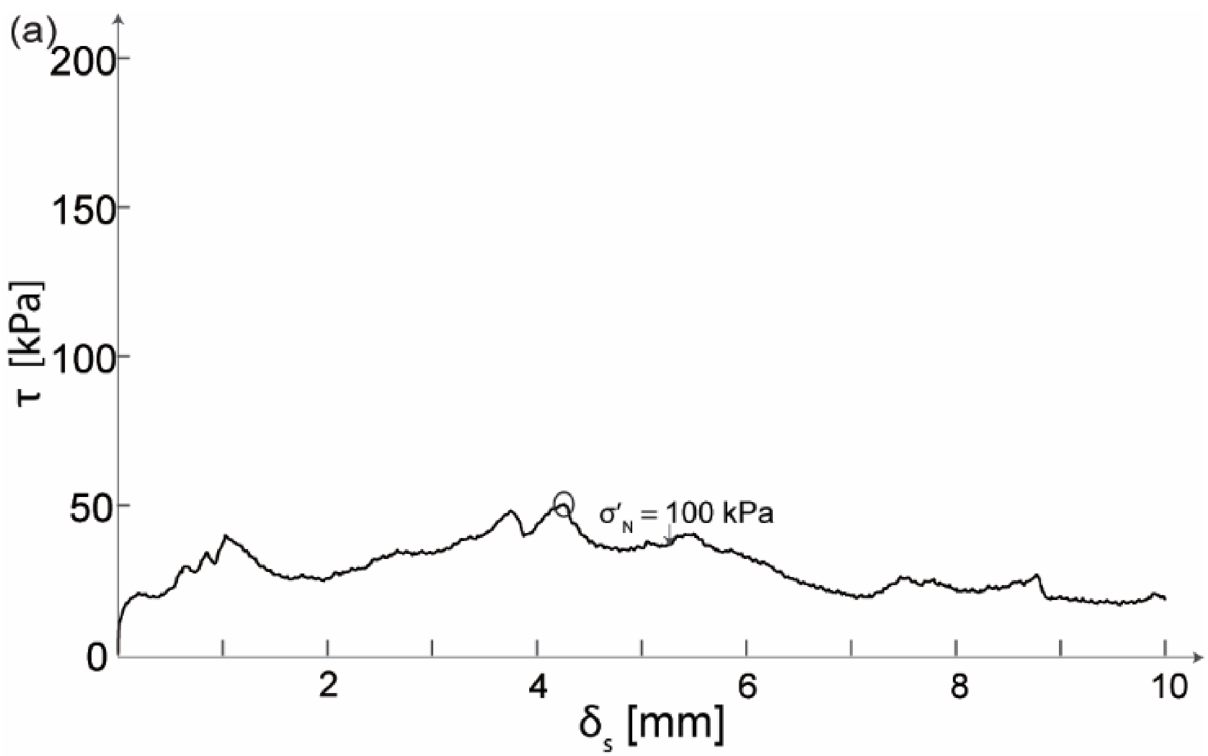

Direct shear testing of fiber-reinforced kaolinite clay specimen at a σ'_N of 200 kPa

Properties of clay soil
Specimen type: Reconstituted - slurry
Water content: 44.5 %
Dry density: 1.32 g/cm^3

Properties of fibers
Fiber type: PP
Thickness: 0.035 mm
Specific gravity: 0.91
Moisture Absorption< 1%

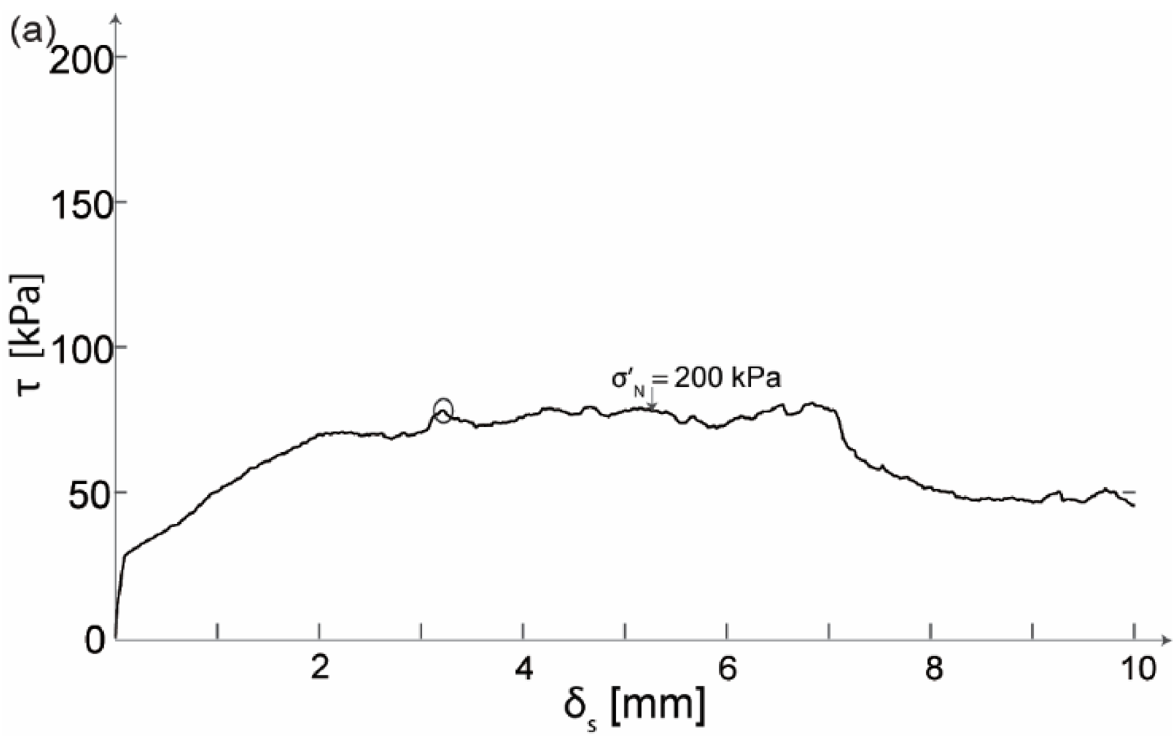

Direct shear testing of fiber-reinforced kaolinite clay specimen at a σ'_N of 300 kPa

<u>Properties of clay soil</u>
Specimen type: Reconstituted - slurry
Water content: 45 %
Dry density: 1.3 g/cm^3

<u>Properties of fibers</u>
Fiber type: PP
Thickness: 0.035 mm
Specific gravity: 0.91
Moisture Absorption< 1%

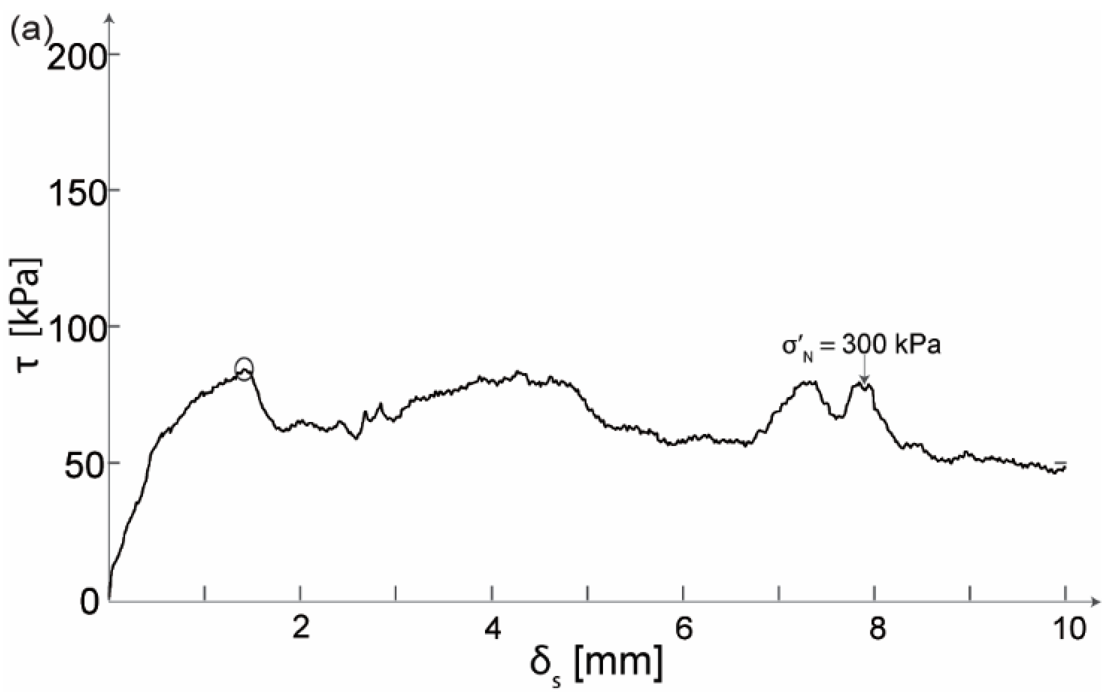

Direct shear testing of fiber-reinforced kaolinite clay specimen at a σ'_N of 400 kPa

<u>Properties of clay soil</u>
Specimen type: Reconstituted - slurry
Water content: 45 %
Dry density: 1.35 g/cm^3

<u>Properties of fibers</u>
Fiber type: PP
Thickness: 0.035 mm
Specific gravity: 0.91
Moisture Absorption< 1%

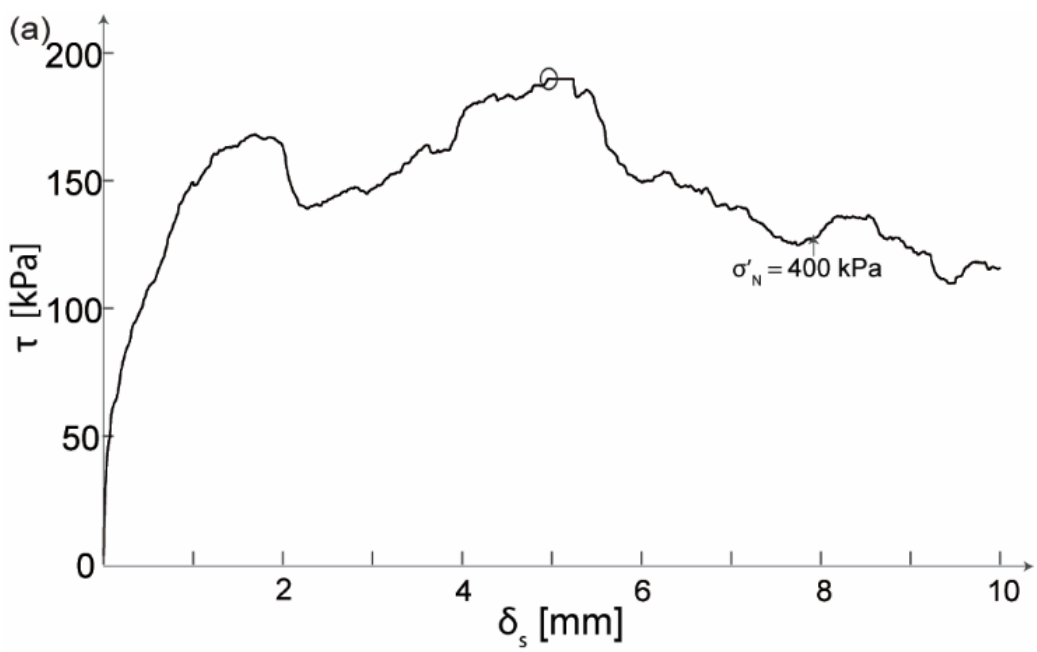

Direct shear testing of fiber-reinforced kaolinite clay specimen at a σ'_N of 50 kPa

<u>Properties of clay soil</u>
Specimen type: Reconstituted - slurry
Water content: 44.5 %
Dry density: 1.3 g/cm^3

<u>Properties of fibers</u>
Fiber type: PA
Thickness: 0.035 mm
Specific gravity: 1.14
Moisture Absorption = 3.5-5%

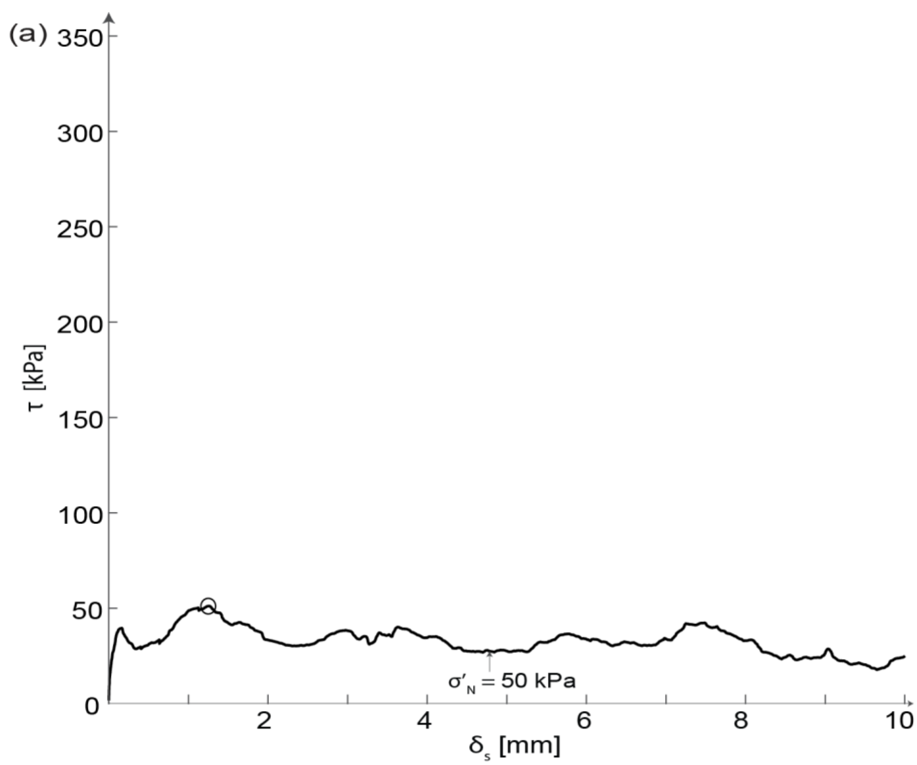

Direct shear testing of fiber-reinforced kaolinite clay specimen at a σ'_N of 100 kPa

<u>Properties of clay soil</u>
Specimen type: Reconstituted - slurry
Water content: 44 %
Dry density: 1.31 g/cm^3

<u>Properties of fibers</u>
Fiber type: PA
Thickness: 0.035 mm
Specific gravity: 1.14
Moisture Absorption = 3.5-5%

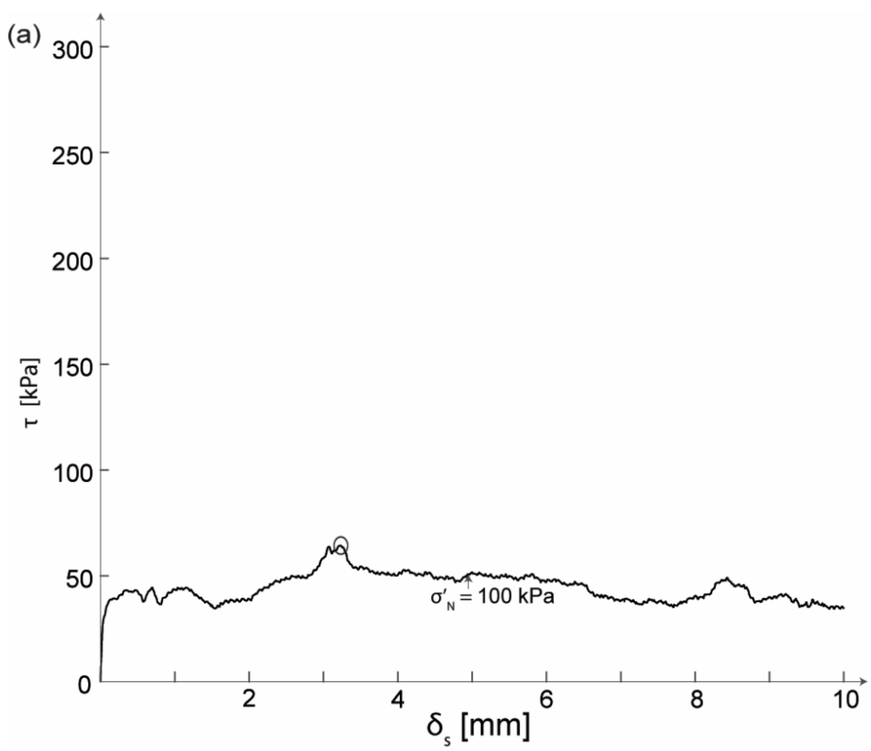

Direct shear testing of fiber-reinforced kaolinite clay specimen at a σ'_N of 200 kPa

<u>Properties of clay soil</u>
Specimen type: Reconstituted - slurry
Water content: 45 %
Dry density: 1.35 g/cm^3

<u>Properties of fibers</u>
Fiber type: PA
Thickness: 0.035 mm
Specific gravity: 1.14
Moisture Absorption = 3.5-5%

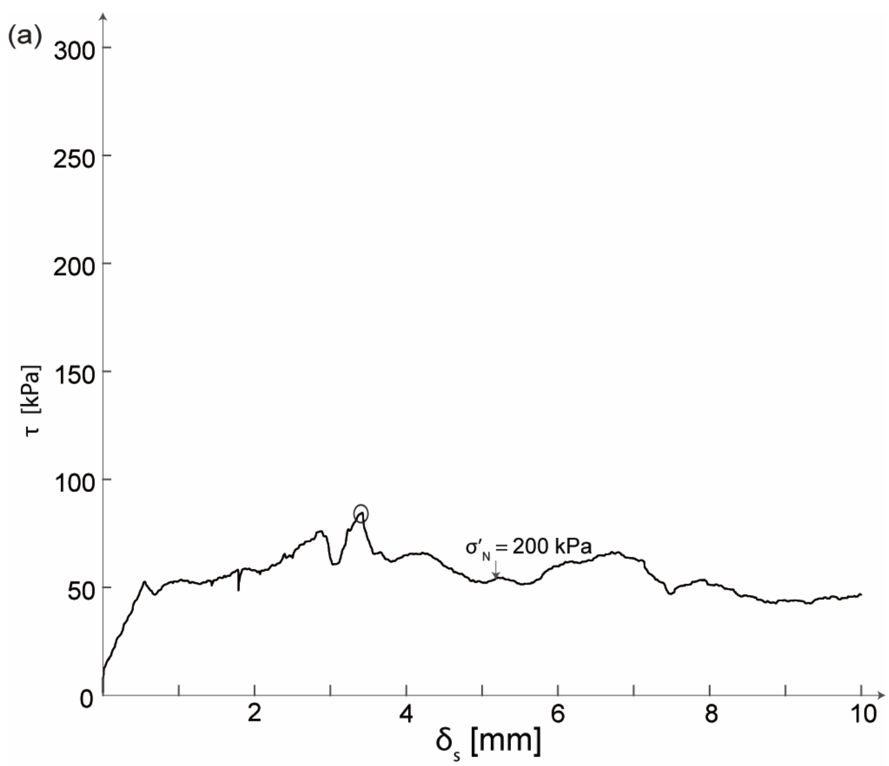

Direct shear testing of fiber-reinforced kaolinite clay specimen at a σ'_N of 300 kPa

Properties of clay soil
Specimen type: Reconstituted - slurry
Water content: 44.5 %
Dry density: 1.3 g/cm^3

Properties of fibers
Fiber type: PA
Thickness: 0.035 mm
Specific gravity: 1.14
Moisture Absorption = 3.5-5%

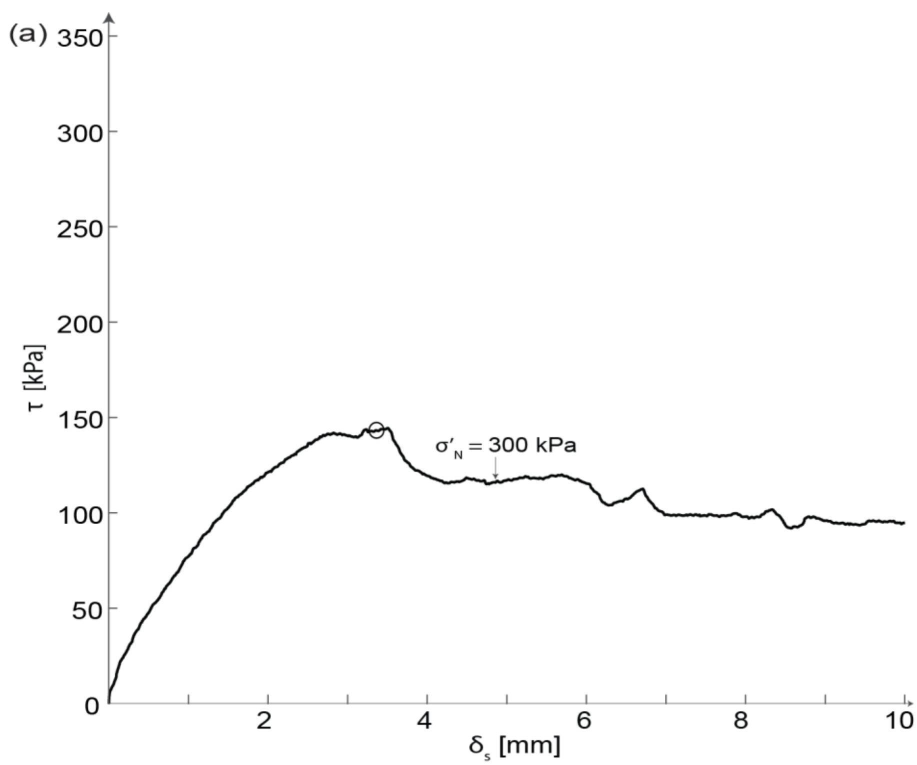

Direct shear testing of fiber-reinforced kaolinite clay specimen at a σ'_N of 400 kPa

<u>Properties of clay soil</u>
Specimen type: Reconstituted - slurry
Water content: 44.5 %
Dry density: 1.32 g/cm^3

<u>Properties of fibers</u>
Fiber type: PA
Thickness: 0.035 mm
Specific gravity: 1.14
Moisture Absorption = 3.5-5%

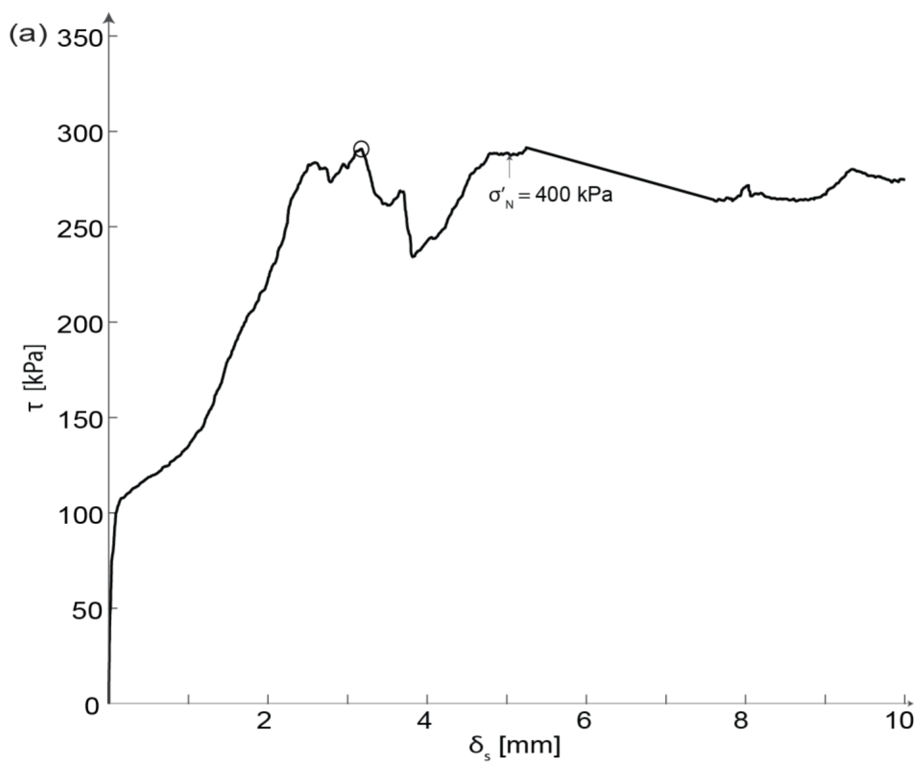

Appendix C: Additional images from laboratory testing

This appendix provides a record of the additional pictures from CU triaxial tests on fiber-reinforced samples presented in *Chapters 3, 4, 5, and 6* (Manuscripts #1, #2, #3, and #4).

Fig. C1: Apparatus used for preparing compacted fiber- reinforced samples including arbor press, 2-part compaction mold and hammer

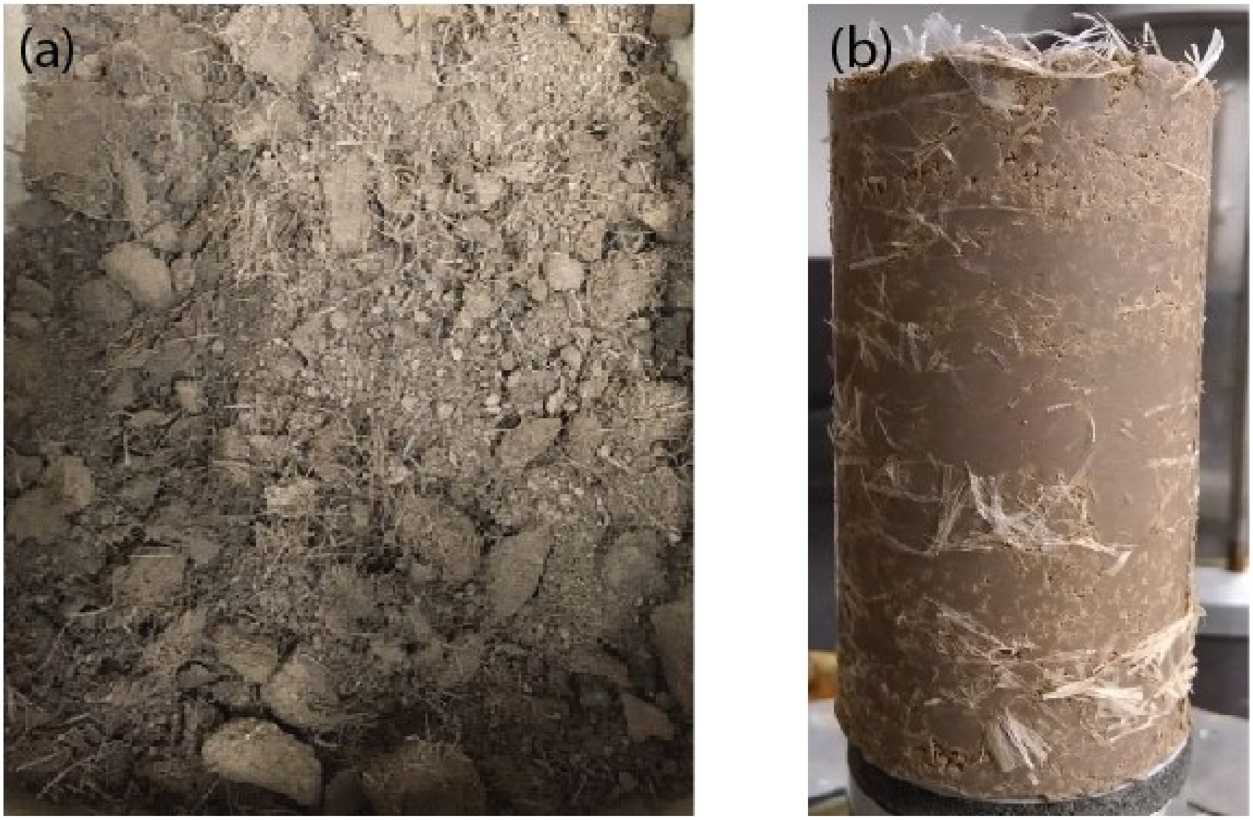

Fig. C2: (a) Prepared fiber-reinforced soil lot (b) Compacted fiber -reinforced sample used for testing

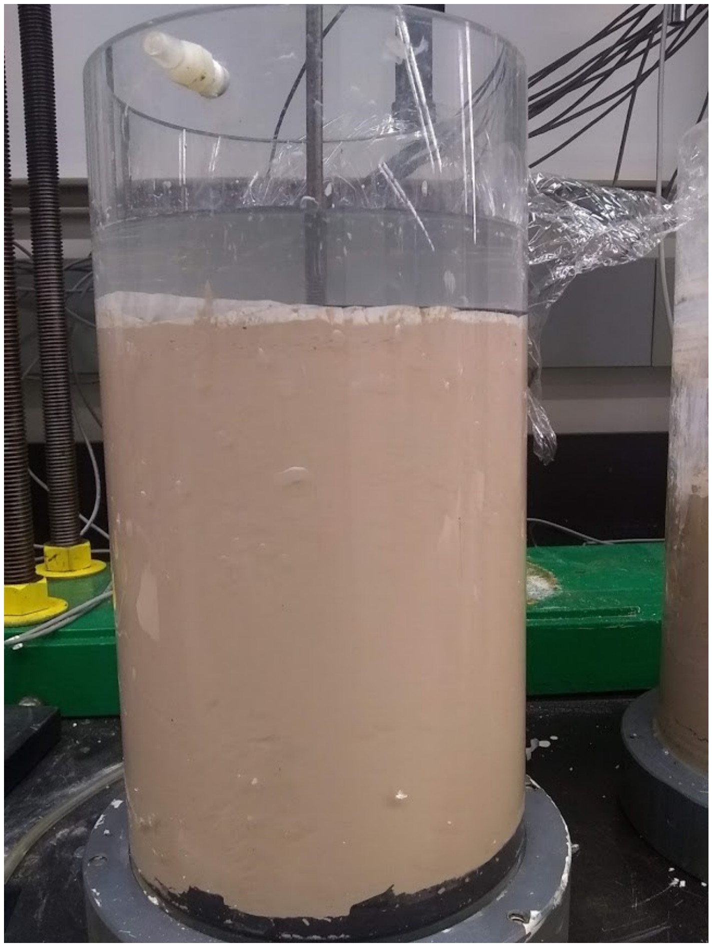

Fig. C3: Slurry fiber-reinforced sample left for consolidation

Fig. C4: Procedure used for obtaining cylindrical fiber-reinforced samples from the slurry for triaxial testing

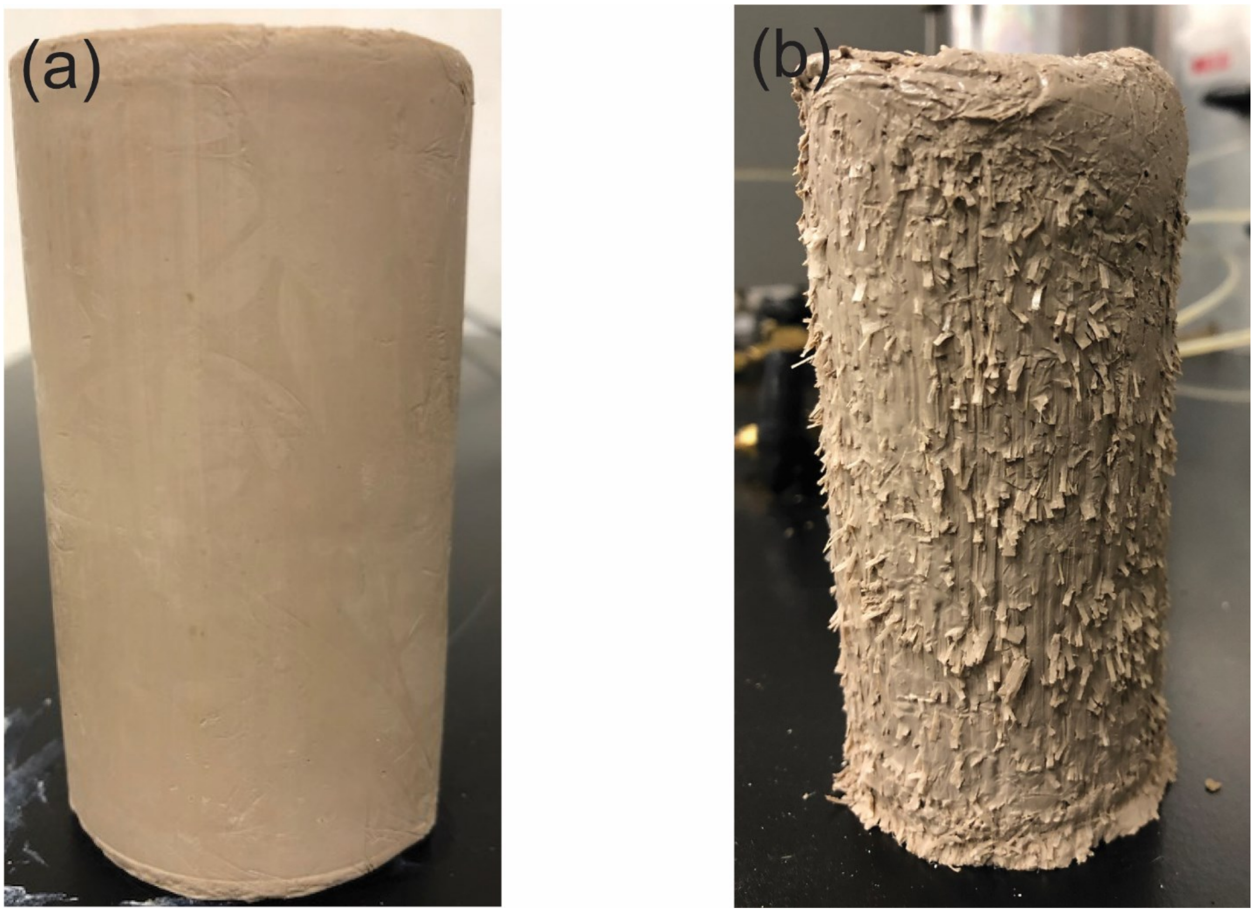

Fig. C5: (a) Slurry prepared unreinforced soil (b) Slurry prepared fiber-reinforced soil

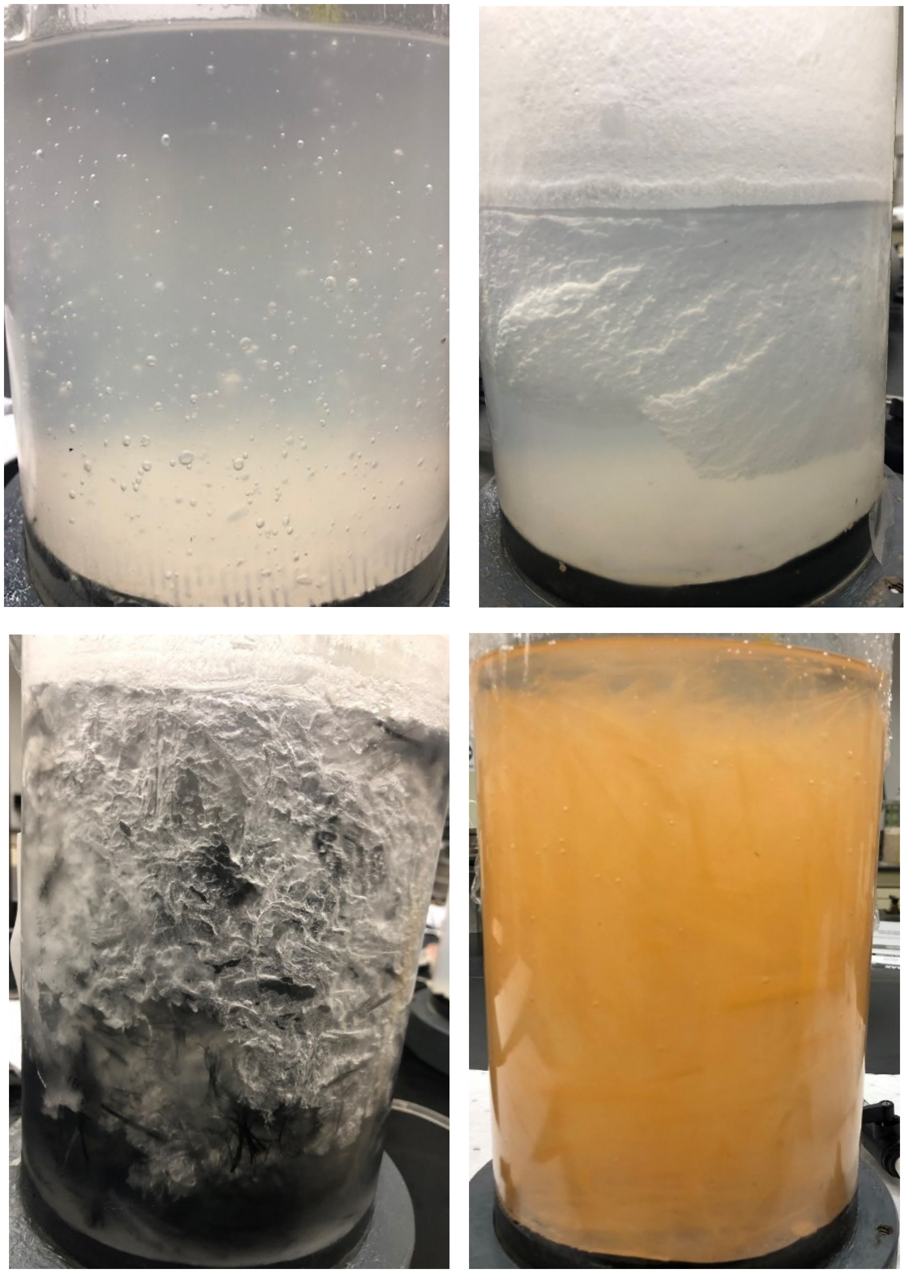

Fig. C6: Challenges faced during the preparation of transparent soil (intrusion of air bubbles and color from synthetic fibers mixing with the transparent clay)

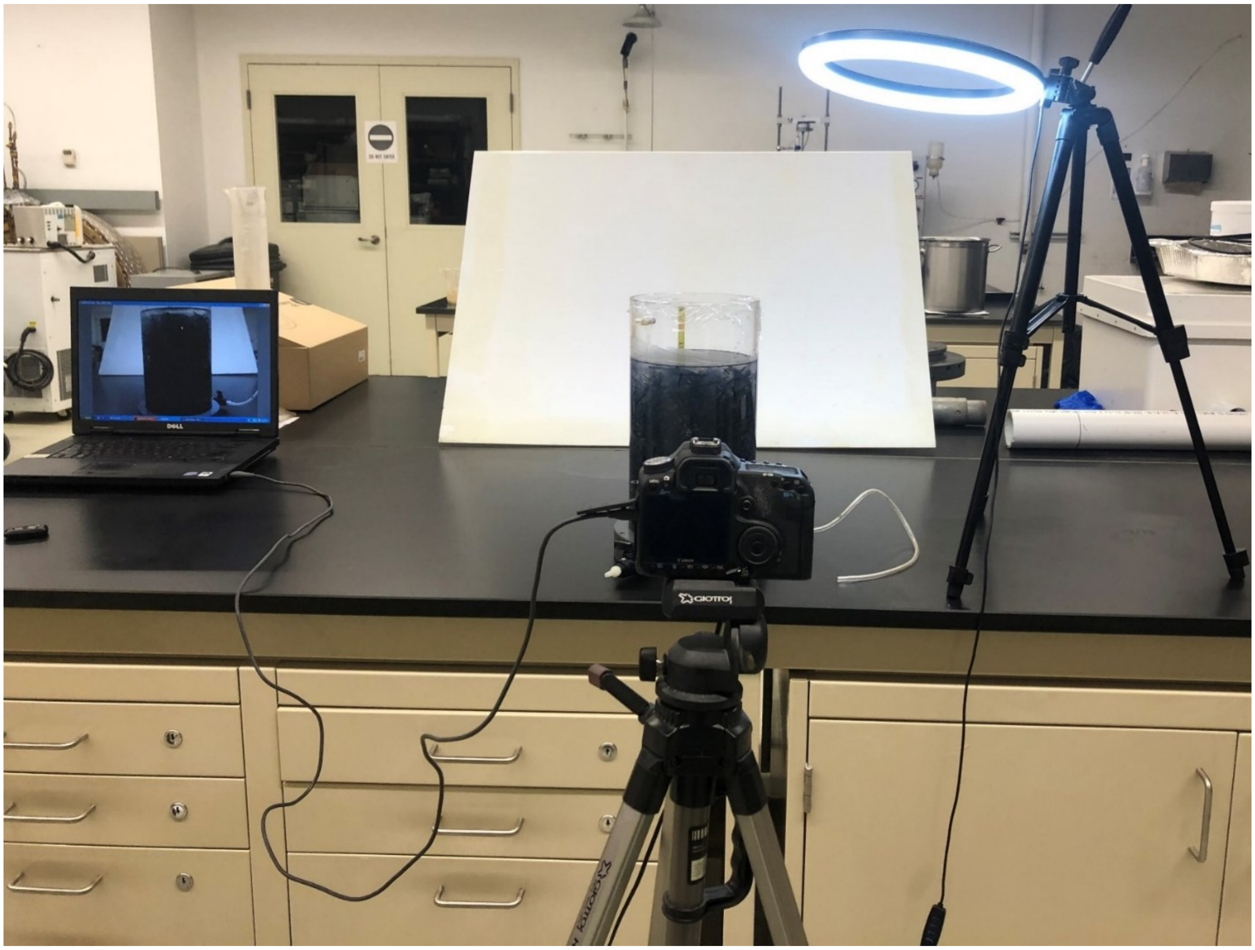

Fig. C7: Set up used for obtaining continuous images of fiber-reinforced transparent soil to track fiber orientation during soil consolidation

Appendix D: Visual examination of the fiber-reinforced clay soil

This appendix provides a record of the techniques attempted to determine the interaction of fibers with the soil and analyse the fiber orientation within clay. These studies were not successful in quantifying the orientation of fibers and hence not included in the dissertation.

Examination of the interaction of fibers with clay

The interaction between fibers and clay was analysed using the Optical Microscope Zeiss AXIO Lab.A1 (W1-040) available at the Nanofab lab within the University of Alberta.

Apparatus used: Zeiss AXIO Lab.A1 (W1-040)

Method of Sample preparation: Compaction method

Fiber content: 2%

Fiber length: 6 mm

Fiber type: PP

Fig. D1: A section of the prepared fiber-reinforced specimen observed using the optical microscope Zeiss AXIO Lab.A1

Visual examination of the soil

The samples were initially sheared to failure followed by the visual examination by cutting a plane through the specimen. Figures below show the wet and dry images of a fiber-reinforced soil sample after subjecting to failure.

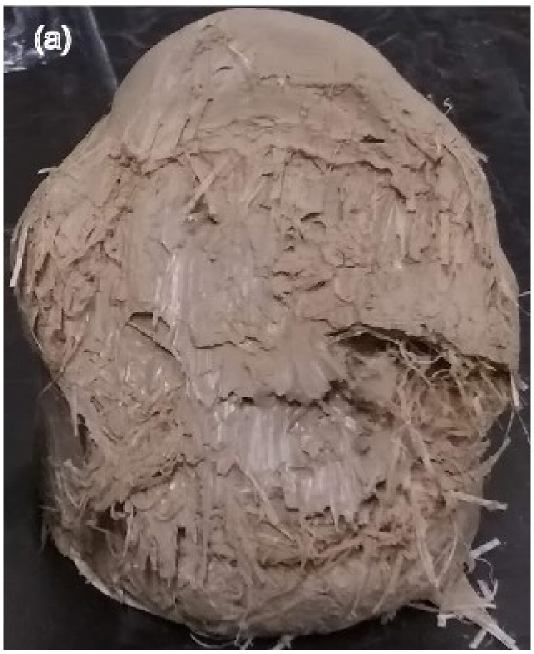

Fig. D2: Visual examination of the fiber-reinforced sample (a) Wet specimen; (b) Dry specimen

Limitation of the method: Fibers developed a tendency to realign in the horizontal direction due to the pressure imparted to the sample while cutting. Additionally, visually counting the number of fibers intersecting a plane is not feasible due to the lower diameter of polypropylene fibers and the optimum fiber content used in the sample preparation (2%) is a way higher than the maximum adoptable fiber content (0.25%) specified in the previous studies. (Diambra et.al, 2007, Ibrahim et.al, 2012).

Computed tomography (CT) Scan

Section 7.2.2 discusses the non-destructive computerized tomography (CT) scanning technique applied on the prepared fiber-reinforced samples prior to development of transparent fiber-reinforced soil (*Chapter Four*, Manuscript #2). This section in the Appendix discusses the four stages of Canny Edge detection applied on the DICOM slice to retrieve the lines from the image.

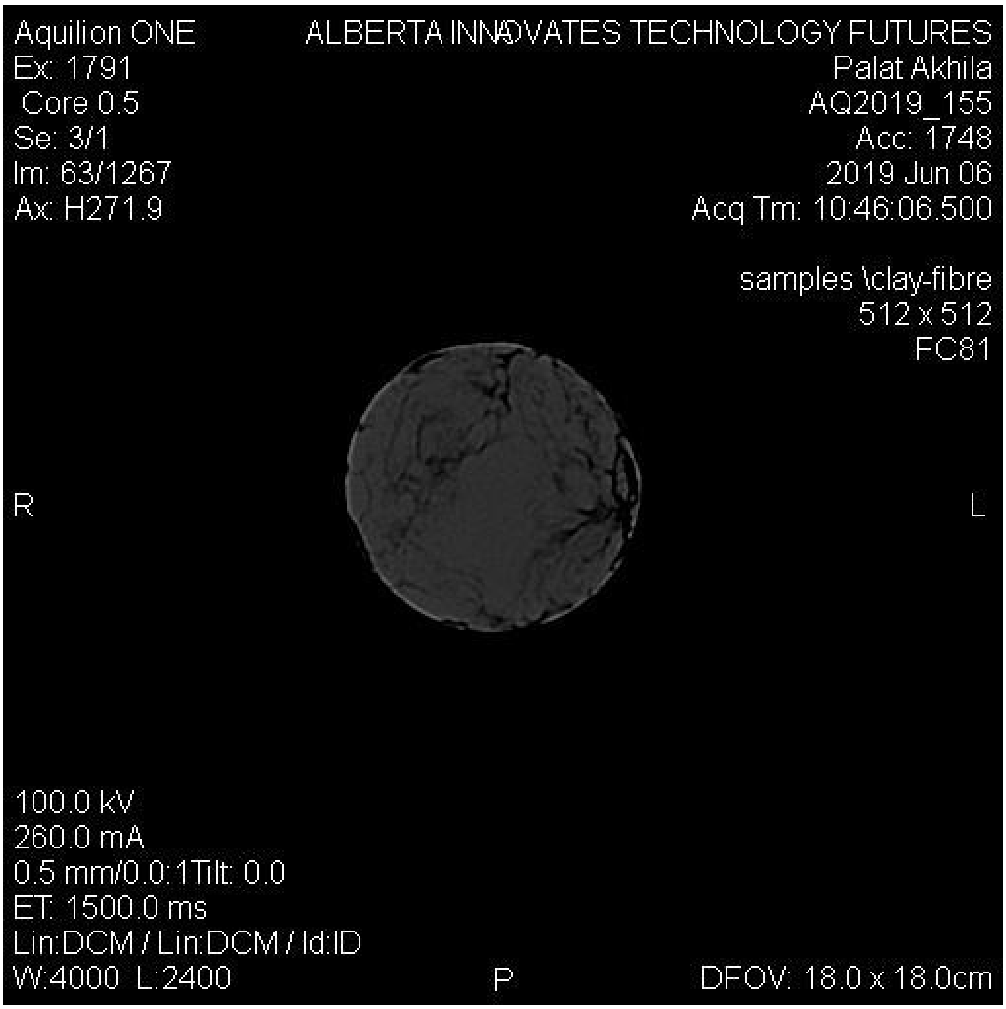

Fig. D3: Digital Imaging and Communications in Medicine (DICOM) image representing a slice of thickness 300 µm as retrieved from a CT Scan

Stage 1: Input image

The original image is trimmed and called in Matlab prior to the application of canny edge detection.

Source code (Copyright Hypermedia image processing reference © 2000 Robert Fisher, Simon Perkins, Ashley Walker and Erik Wolfart):

```
clc;
%Input image
img = imread ('soilfib.jpg');
%Show input image
figure, imshow(img);
img = rgb2gray(img);
img = double (img);
```

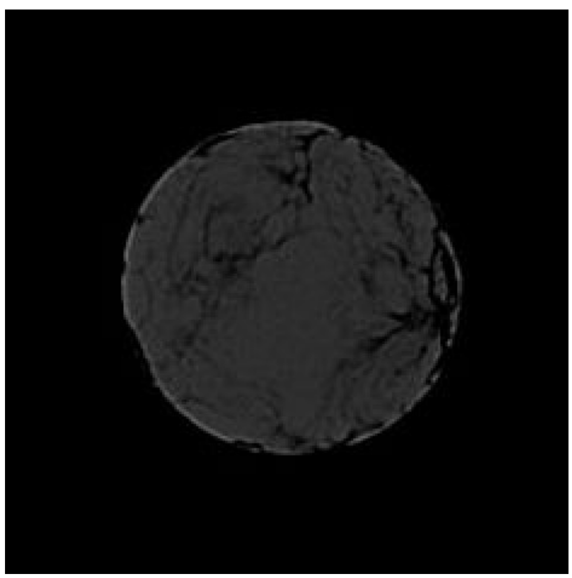

Fig. D4: Trimmed DICOM image used for applying the principle of canny edge detection

Stage 2: Smoothen the image by using Gaussian convolution

This stage reduces the noise in the image and smoothen the image by applying a Gaussian filter. Canny algorithm is then applied to detect the vertical, horizontal and diagonal edges in the blurred image. The data in the array is then displayed as an image that uses the full range of colors in the color map. The color bar represents the current color map.

Source code (Copyright Hypermedia image processing reference © 2000 Robert Fisher, Simon Perkins, Ashley Walker and Erik Wolfart):

```
%Value for Thresholding
T_Low = 0.075;
T_High = 0.175;
%Gaussian Filter Coefficient
B = [2, 4, 5, 4, 2; 4, 9, 12, 9, 4;5, 12, 15, 12, 5;4, 9, 12, 9, 4;2, 4, 5, 4, 2 ];
B = 1/159.* B;

%Convolution of image by Gaussian Coefficient
A=conv2(img, B, 'same');

%Filter for horizontal and vertical direction
KGx = [-1, 0, 1; -2, 0, 2; -1, 0, 1];
KGy = [1, 2, 1; 0, 0, 0; -1, -2, -1];

%Convolution by image by horizontal and vertical filter
Filtered_X = conv2(A, KGx, 'same');
Filtered_Y = conv2(A, KGy, 'same');

%Calculate directions/orientations
arah = atan2 (Filtered_Y, Filtered_X);
arah = arah*180/pi;
pan=size(A,1);
leb=size(A,2);

%Adjustment for negative directions, making all directions positive
for i=1:pan
    for j=1:leb
        if (arah(i,j)<0)
            arah(i,j)=360+arah(i,j);
        end;
    end;
```

```
end;
arah2=zeros(pan, leb);

%Adjusting directions to nearest 0, 45, 90, or 135 degree
for i = 1  : pan
   for j = 1 : leb
      if ((arah(i, j) >= 0 ) && (arah(i, j) < 22.5) || (arah(i, j) >= 157.5) && (arah(i, j) < 202.5)
|| (arah(i, j) >= 337.5) && (arah(i, j) <= 360))
         arah2(i, j) = 0;
      elseif ((arah(i, j) >= 22.5) && (arah(i, j) < 67.5) || (arah(i, j) >= 202.5) && (arah(i, j) <
247.5))
         arah2(i, j) = 45;
      elseif ((arah(i, j) >= 67.5 && arah(i, j) < 112.5) || (arah(i, j) >= 247.5 && arah(i, j) <
292.5))
         arah2(i, j) = 90;
      elseif ((arah(i, j) >= 112.5 && arah(i, j) < 157.5) || (arah(i, j) >= 292.5 && arah(i, j) <
337.5))
         arah2(i, j) = 135;
      end;
   end;
end;
figure, imagesc(arah2); colorbar;
```

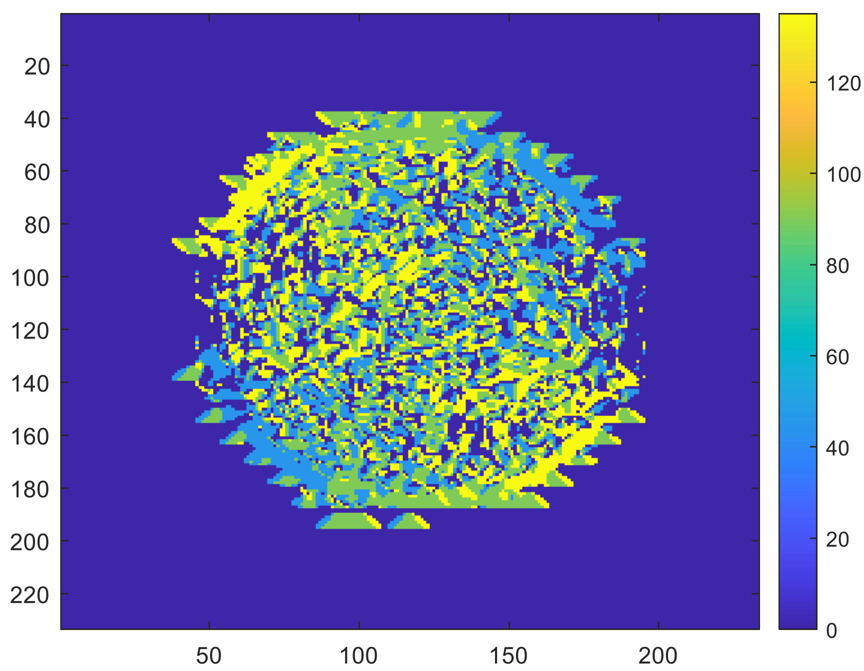

Fig. D5: Image smoothened by applying Gaussian convolution

Stage 3: Non-Maximum Suppression

An edge thinning technique used to find out the local maxima and suppresses all other gradient values. This stage is used to indicate locations with sharpest change in the intensity and provides a more accurate representations of the real edges in the image.

Source code (Copyright Hypermedia image processing reference © 2000 Robert Fisher, Simon Perkins, Ashley Walker and Erik Wolfart):

```
%Calculate magnitude
magnitude = (Filtered_X.^2) + (Filtered_Y.^2);
magnitude2 = sqrt(magnitude);
BW = zeros (pan, leb);

%Non-Maximum Suppression
for i=2:pan-1
  for j=2:leb-1
    if (arah2(i,j)==0)
      BW(i,j) = (magnitude2(i,j) == max([magnitude2(i,j), magnitude2(i,j+1), magnitude2(i,j-
1)]));
    elseif (arah2(i,j)==45)
      BW(i,j) = (magnitude2(i,j) == max([magnitude2(i,j), magnitude2(i+1,j-1), magnitude2(i-
1,j+1)]));
    elseif (arah2(i,j)==90)
      BW(i,j) = (magnitude2(i,j) == max([magnitude2(i,j), magnitude2(i+1,j), magnitude2(i-
1,j)]));
    elseif (arah2(i,j)==135)
      BW(i,j) = (magnitude2(i,j) == max([magnitude2(i,j), magnitude2(i+1,j+1),
magnitude2(i-1,j-1)]));
    end;
  end;
end;
BW = BW.*magnitude2;
figure, imshow(BW);
```

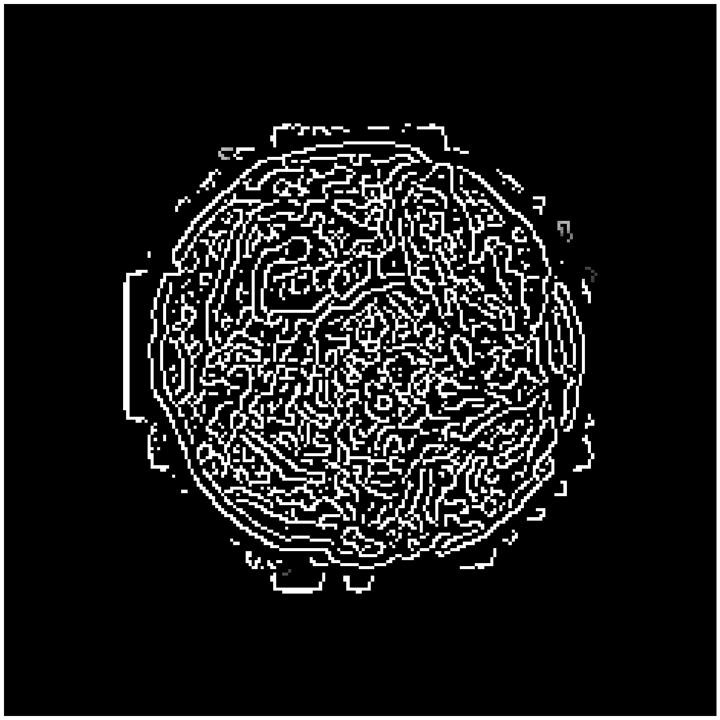

Fig. D6: A representation of the edges in the image

Stage 4: Hysteresis Thresholding

The initial threshold values for the image are modified depending maximum values obtained after non-maximal suppression. This stage only preserves the edge pixels that are higher than the high threshold value and displays the final edge detection result.

Source code (Copyright Hypermedia image processing reference © 2000 Robert Fisher, Simon Perkins, Ashley Walker and Erik Wolfart):

```
%Hysteresis Thresholding
T_Low = T_Low * max(max(BW));
T_High = T_High * max(max(BW));
T_res = zeros (pan, leb);
for i = 1  : pan
    for j = 1 : leb
        if (BW(i, j) < T_Low)
```

```
        T_res(i, j) = 0;
      elseif (BW(i, j) > T_High)
        T_res(i, j) = 1;

 %Using 8-connected components
      elseif ( BW(i+1,j)>T_High || BW(i-1,j)>T_High || BW(i,j+1)>T_High || BW(i,j-1)>T_High
|| BW(i-1, j-1)>T_High || BW(i-1, j+1)>T_High || BW(i+1, j+1)>T_High || BW(i+1, j-
1)>T_High)
        T_res(i,j) = 1;
      end;
   end;
end;
edge_final = uint8(T_res.*255);

%Show final edge detection result
figure, imshow(edge_final);
```

Fig. D7: The final edge detection result

<u>Limitations of this method:</u> The PP fibers used for reinforcing clay had a difficulty in interacting with the X-ray energy making them not visible in the images. Additionally, the clay acted as an effective shield against X-ray photons, and so very little signal penetrated the samples for detection.